DOCTOR OF PHILOSOPHY

The performance of pipeline ploughs

Lauder, Keith

Award date:
2010

DOCTOR OF PHILOSOPHY

The performance of pipeline ploughs

Keith Lauder

2010

University of Dundee

College of Art, Science & Engineering
School of Engineering, Physics and Mathematics
Department of Civil Engineering

The performance of pipeline ploughs

Keith Lauder

A dissertation submitted for the
degree of Doctor of Philosophy
to the University of Dundee
October 2010

Declaration

This is to certify that, the candidate is the author of the thesis; that, unless otherwise stated, all references cited have been consulted by the candidate; that the work of which the thesis is a record has been done by the candidate, and that it has not been previously accepted for a higher degree.

Keith Lauder (candidate), Dundee 27/10/2010

Dr. Michael Brown (supervisor), Dundee, 27/10/2010

Acknowledgements

This work is funded by CTC marine projects Ltd and student support was provided by an EPSRC project grant. I am grateful to my supervisors Dr. Michael Brown and Dr. Fraser Bransby for their direction and support. I would like to thank Peter Hudacsek and Rene Sonnenberg who helped me settle into the Geotechnical Research Group at the University of Dundee and the rest of the group all of whom helped me with my research in some way.

Thanks to Dr. Jim Pyrah and Dr. Julian Steward both formerly of CTC marine Projects Ltd, Dr. David Cathie of Cathie Associates and Dr. Neil Morgan formerly of Cathie Associates for technical assistance and feed back from initial test results which helped direct the research programme.

I would like to thank the technical staff within the Department of Civil Engineering at the University of Dundee. I would like to thank in particular David Ritchie for his guidance with apparatus development, Mike M^{c}Kernie for help with instrumentation, William Truswell for all his help in the soils lab and John Anderson, Alec Anderson and Willie Henderson for their help in the workshop. Last but not least I would like to take this opportunity to thank my family for their continued moral support over the last few years and I couldn't have done this without them.

Abstract

Pipeline ploughs are commonly used to bury offshore pipelines for their protection from loading by currents, damage from fishing trawler vessels and to provide thermal insulation to the line allowing the product to flow more efficiently. The rate of progress of pipeline ploughs in sand is complicated by a rate effect which causes the required tow force to increase drastically with velocity. In this research plough performance in sand is investigated by means of physical scale model tests. Scale model tests are the most practical method by which to conduct a parametric study on plough behaviour as full sized testing would be prohibitively expensive. Scale model tests also provide accurate control of sand conditions which allows investigation of the effect of soil parameters on plough behaviour.

Model ploughs were manufactured at 50^{th}, 25^{th} and 10^{th} scale so that scale effects could be explored. Each of the model ploughs had a detachable forecutter to allow its effect on plough performance to be observed. The forecutter was found to reduce the rate effect but increase the non-velocity dependant resistance of the plough. Ploughing tests were conducted at various relative densities in three sands of different permeability. The effects of ploughing rate on model plough behaviour under these various conditions was explored using an instrumented model plough, with particular attention paid to the resulting tow force.

Results from the model ploughing tests were interpreted to determine the effect of permeability, relative density and plough depth on the tow forces generated during ploughing. The rate effect was found to increase strongly with reduction in permeability of the sand. Increasing the relative density of the sand was found to increase the rate effect but had little influence on the passive resistance of the plough. The test results were compared to an empirical model developed by Cathie and Wintgens (2001). New coefficients (C_w, C_s and C_d) have been proposed and therefore design procedures modified which may allow trenching contractors to make better predictions of plough performance in sands.

Keywords: Pipeline ploughs, plough performance, trenching, rate effects, partial drainage of sands, forecutter.

Table of Contents

List of Figures

Chapter 2 Literature review

Chapter 3 Methodology

Chapter 4 Results and discussion from tests in dry sand

Chapter 5 Rate effects during ploughing

Chapter 6 Implications for industrial practice

List of Tables

Notation

A	area
C_d	coefficient of dynamic resistance
C_s	coefficient of passive resistance
C_u	coefficient of uniformity
C_w	coefficient of frictional resistance
C_z	coefficient of curvature
c_v	coefficient of consolidation
D	plough depth
D_r	relative density
D_t	trench depth
d_{10}, d_{60}, etc…	particle size characteristics
E_0'	one-dimensional modulus of elasticity
e_c	critical state void ratio
e_{max}	maximum void ratio
e_{min}	minimum void ratio
e_0	initial void ratio
F	tow force
F_f	frictional component of the tow force
F_h	Force acting on the heel
F_p	passive component of the tow force
F_s	Force acting on the share
$F_{v=0}$	non-rate dependant tow force ($=F_f + F_p$)
G_s	specific gravity of soil particles
K_p	coefficient of passive earth pressure
k	permeability
q_{st}	Quasi-stationary cone resistance
R_s	Krumbein roundness
r	radius
S	dilation potential
t	time
v	velocity
v_f	velocity of pore fluid
W	weight
x	horizontal displacement, horizontal axis
y	vertical displacement, vertical axis
α	rake angle, angle of the underside of share to horizontal in the transverse direction
α_t	angle of the trench walls to the horizontal
β	arm angle
γ'	effective submerged unit weight
γ_d	dry unit weight
γ_{sat}	saturated unit weight
γ_w	unit weight of water (= 9.81 kN/m^3)

δ	interface angle of friction
ε	linear (normal) strain
θ	angle between a failure plane and the horizontal; pitch of the plough
ρ	bulk density
σ_n	normal total stress
σ_n'	normal effective stress
τ	shear stress
φ'	angle of internal friction
φ'_{crit}	critical state angle of internal friction
φ'_{peak}	peak angle of internal friction
ψ	dilation angle

Chapter 1. Introduction

1.1. *Preface*

The oil and gas industry buries offshore pipelines under the sea bed as a means of protection from natural processes and human activity. Ploughing is a common method used to create a trench which pipelines are laid into and is favoured by the industry due to its effectiveness in various soil conditions. The force required to tow the plough is affected by the rate of ploughing which is particularly predominant when ploughing in sands and silts. The tow force will ultimately affect the rate of ploughing as the support vessels which tow the plough have a limited capacity.

Prior to the commencement of any ploughing operation it is necessary to estimate the time required to complete the work. This often involves the calculation of the required tow force to pull the plough at a particular depth and velocity through specific soil conditions. Currently much of the industry uses empirical equations to predict tow forces. The form of the equations developed has been based partially on the principles of passive soil mechanics and influenced by experience of real ploughing operations. Unfortunately, where data is used from real ploughing operations there is potential for significant variation in seabed soil conditions and topography encountered. This may be a result of the sporadic nature of site investigation where investigation points are usually over 1 km apart due to the significant lengths of pipeline to be buried. This leads to inaccurate development of soil dependant parameters where the exact soil type and state are potentially unknown. In contrast to the use of field data from real operations, ploughing tests in a laboratory environment allow both plough and soil variables to be accurately controlled and measured. Results from these tests may be used to refine the existing empirical models.

Full scale ploughing tests are impractical as they would be excessively time consuming, labour intensive and ultimately prohibitively expensive to conduct. Reduced scale model plough tests are a common method of overcoming testing impracticalities and were conducted at the University of Dundee in order to better understand pipeline plough behaviour. Controlled laboratory conditions allow highly

accurate measurements of tow force and plough depth to be made which would not be possible to achieve during offshore ploughing operations.

1.2. *Scale model ploughing tests*

Reduced scale model ploughing tests were carried out in three sands of different particle size distributions, at various relative densities and at three different plough depths. This allowed the effect of permeability, relative density and plough depth on plough performance to be investigated. Tests were conducted at three scales (50^{th}, 25^{th}, and 10^{th}) to allow scale effects to be investigated. The increase in tow force with plough velocity, known as the rate effect, is caused by an increase in effective stresses due to the reduction in pore water pressure during the shearing and therefore dilation of saturated sands. Tests were conducted in both dry and saturated sand which allowed for the rate effect to be studied separately from the other components of tow force. Results were also compared to the Cathie and Wintgens (2001) analysis and used to suggest new values for their empirical coefficients.

1.3. *Aim and Objectives*

The overall aim of this project is to (1) understand the soil mechanics phenomena occurring during ploughing and (2) Improve the existing techniques used by industry for plough performance prediction in granular material.

To achieve these aims the following objectives were devised.

1. Conduct a series of tests where the deformation of sand around the cutting blade of the plough, known as a share can, be observed so that the failure mechanism can be defined.

2. Conduct a parametric study using a model plough involving the following parameters: trench depth, plough velocity, particle size and the relative density of the soil.

3. Use the data gathered during the parametric study to draw relationships between physical parameters (both plough geometry and soil characteristics) and plough performance.

4. Compare the model data with full scale plough performance with a view to increasing the accuracy of performance predictions.

1.4. *Structure of thesis*

The thesis is presented in 7 Chapters:

Chapter 2 consists of a review of the current literature relevant to this study. Attention is focussed on: previous ploughing research, rate effects in sands and scaling effects. The end of the literature review summarises the information important to directing this research by highlighting areas where there are gaps in knowledge.

A description of the experimental methods used to conduct the study is contained in Chapter 3. Three types of ploughing test are explained along with the justification of the adopted approach to testing. Materials test results include: shear box tests, permeability tests and oedometer tests are included within this chapter.

Results and discussion of the ploughing tests are contained within Chapters 4, 5 and 6. Chapter 4 considers the non rate dependant component of tow force by means of examining dry ploughing tests. Chapter 5 focuses on the rate effect and the parameters which influence it, particularly permeability and relative density of the sand as they have been highlighted as key parameters found in the review of previous research on this topic. The influence of plough depth and drainage path lengths on the rate effect is also described and analysed. Chapter 6 presents the results from the various ploughing tests in a format which is readily understood and useable by the offshore industry. The Cathie and Wintgens (2001) analysis technique is applied to the test data and modifications to their equations suggested.

Chapter 7 summarises the main findings of the research, highlights how these are important and shows their potential applicability to the offshore industry. During the course of this research numerous avenues of potential investigation were uncovered, however time constraints prevented the exploration of many of these and they are instead presented as recommendations for future research.

Chapter 2. Literature review

2.1. *Introduction*

As pipeline ploughing literature available in the public domain is limited, this review consists mainly of previous research involving various shaped cutting objects being dragged or pushed through cohesionless material. These tests are similar to offshore ploughing as they are large strain events occurring at shallow depth with resulting low effective stresses. Particular attention is given to: mechanics of plough behaviour, current performance prediction methods, scaling issues and rate effects. The rate effect is the increase in the force required to move the cutting object through saturated sands and silts with a relatively small increase in its velocity. The rate effect has plagued numerous ploughing operations in the North Sea and beyond because its accurate prediction has so far eluded industry. Scale model tests are intended to investigate pipeline plough performance and as such scaling issues are important in determining if the behaviour of a full size plough with the capacity to create a 2 m deep trench can be successfully modelled by a plough only $1/10^{th}$ or even $1/50^{th}$ of its size.

2.2. *Trenching and pipeline burial*

The purpose of trenching is to provide protection to offshore pipelines from natural forces such as: tidal currents, turbidity currents (down seabed slopes) and wave generated flow (in shallow water) along the sea bed. Human activities such as: trawler fishing, mooring ships by means of drag anchors and dumping of solid waste can also be hazardous to pipelines on the sea floor and trenching is often required as a means of protecting pipelines from these activities.

Over 70% of all offshore cable faults are caused by human activity and almost 70% of these are due to fishing activities, (Featherstone *et al*.; 2001). Anchors for very large ships (up to 100,000 tonnes) can penetrate the sea bed to depths of 6 metres or more, (Hoshina & Featherstone; 2001). These mammoth anchors (which can weigh upwards 200 kN) are however, unlikely to come into contact with a pipeline outside known anchorage areas.

The presence of a pipeline on the sea bed causes a local increase of flow rate of water around the pipeline due to the continuity equation and increases turbulence due to the shedding of vortices. Both of these mechanisms will increase the likelihood of net loss of sand (scour) around in the vicinity of a pipeline. Scour of material from beneath a pipeline laid in a trench is reduced since the trench reduces the water velocity close to it. This is important in preventing the development of unsupported spans of pipeline which are subject to bending stresses caused by the pipeline's self weight.

During the operation of a pipeline axial compression forces may be induced because operating temperatures and pressures are greater than those when the pipeline was laid which in turn may cause buckling. However the trench should restrain the pipeline in the lateral direction and if the trench is backfilled forming a spoil heap on top of the pipeline this will physically restrain the pipeline and prevent upward buckling (see Figure 2-1) and also provides thermal insulation, (Palmer; 1999).

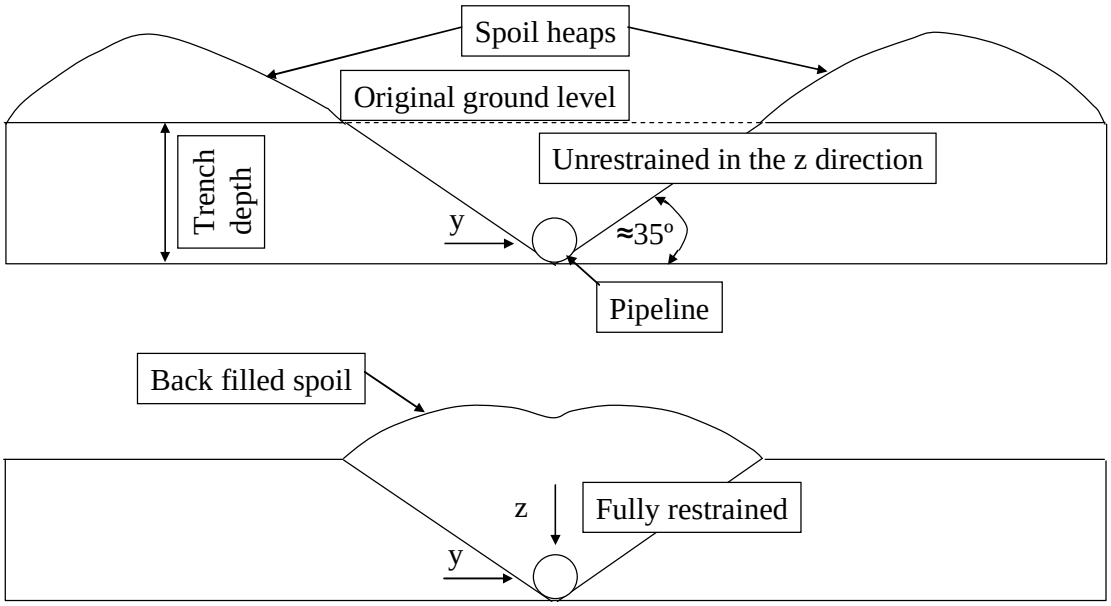

Figure 2-1: Pipeline trench cross section shown pre and post backfilling (Modified from Cathie *et al*; 1998)

Due to the high construction cost of pipelines and the potential for huge losses in profit when the pipeline is not running, it is important that the method of trenching will achieve the required protection from the dangers discussed above.

2.3. *Trenching method and selection*

Ploughing and jetting are the two main methods of pipeline installation and each has associated advantages and disadvantages, which are discussed below. There are other methods of pipeline burial, however their application is limited and some of these methods are only briefly discussed below.

2.3.1. Jetting

Modern jetting may involve lowering a jetting trencher from its support vessel down to the sea bed where it is aligned with the pipeline or cable, which is already in position along the sea bed ready for burial. Once in position the jetting trencher will lower its two jet-swords into the soil either side of the pipeline where it will start to pump water under high pressure through nozzles in the jet-swords, (Figure 2-2). In granular soil this fluidises the soil making it unable to support the pipeline's weight, allowing it to sink to the bottom of the fluidised zone.

Figure 2-2: Tracked sea bed jet trencher at dockyard, (a) jet swords, (b) rear view of trencher

A variation of this is the use of a jetting trencher that does not penetrate the ground with any solid part. The jetting nozzles sit just above the surface of the seabed and face towards the soil. These machines may be used for pre-laid or post-laid pipeline trenching and as they have no solid parts in contact with the pipeline are less likely to damage it during trenching. Their major drawback is that depending on the soil conditions they may leave the angle of trench walls too shallow, (Palmer; 1999) and

in clay the walls of the trench produced are not straight which may apply bending stresses to the pipeline, (Rockwell; 1981). The trench depth is usually specified as a measure of protection (Morrow & Larkin; 2007) but the angle of the trench walls and disturbance of sand in and around the trench during its creation are also important factors in determining the trench's ability to protect a pipeline and this must also be considered when jetting. Where the trench sides are left too shallow backfilling will then be required which will further delay operation of the pipeline and increase financial costs, (Chen *et al*.; 2001).

Jetting can be very slow, making it expensive and this can be exacerbated by the requirement for multiple passes in order to achieve the required depth which is often the case when jetting in stiff clay. A jet trencher may not be suitable for use in varying bed conditions as it will cut a deeper trench in soft/loose soil than for hard/dense material, (Ochtman & der Boer; 1980), which can lead to unsupported spans between shallow sections of the trench and induce stresses on the pipeline. Some of the modern remote operated vehicle (ROV) mounted jet trenchers can however produce trenches of similar out of straightness which would be expected from a pipeline plough. Jetting in sand works by fluidization of the particles which must remain in suspension for long enough for the pipeline to touch down onto the formed trench otherwise the sand will settle beneath the pipeline. Pipe flexibility and settlement velocity characteristics (i.e. particle size distribution, PSD) are therefore important considerations when jetting in sand. Jetting is reasonably effective in soft cohesive soils. In the dense sands and boulder clays of the North Sea, however, large pumps are required and even then the trenching rate can be extremely slow (Reece and Grinsted; 1986).

2.3.2. Ploughing

Ploughs are propelled along the seabed, at speeds up to 0.5 m/s via a long cable attached to support vessels on the surface. The share is used to cut the trench and its shape defines the walls of the trench, which are typically at 35º to the horizontal as this is the greatest angle which may be depended upon to ensure a stable trench, (Reece and Grinsted; 1986). Many ploughs have a smaller cutter in front of the main share, known as a forecutter, (Figure 2-3) which is used in an attempt to reduce

cutting forces and is discussed in Chapter 4 and Chapter 5. The skids are used to support the plough's weight and provide stability during ploughing, preventing the plough from rolling over. The skids are free to pivot about their midpoint during operations and can be raised and lowered on their connecting arm to adjust the depth of the trench.

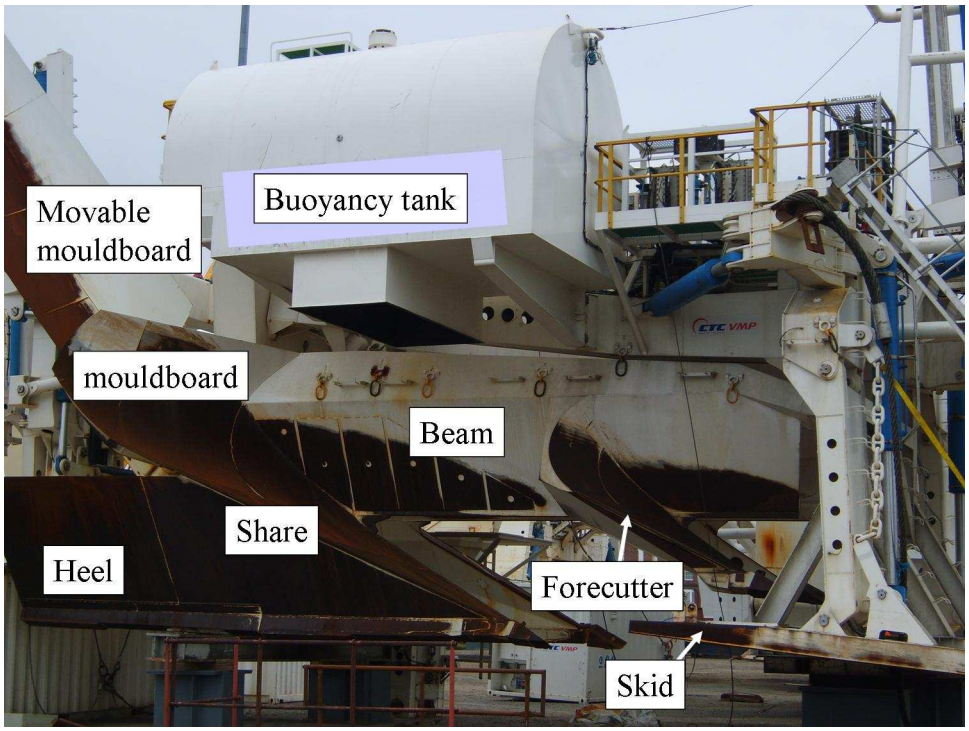

Figure 2-3: CTC VMP plough, awaiting mobilisation

Ploughing is more versatile than jetting and can be used to cut material from soft clay to weak or heavily fractured rock. That said jetting machines tend to be more successful in very weak material as they are lighter and apply less pressure to the supporting soil so do not tend to sink as much as a plough. Typical ROV mounted jetters weigh around 15 tonnes in air (Finch *et al.* 2000), which equates to around 13 tonnes in water. Even with large buoyancy tanks, the buoyant mass of a typical pipeline plough is somewhere in the region of 50 tonnes (www.tricomarine.com) and the AMP500 pipeline plough for instance is not recommended for use in soil of undrained shear strength less than 5 kPa (Cathie Associates report G031R01-01; 2006). This is because insufficient bearing capacity can lead to operational problems such as: over deep trenching, increased out of straightness and higher than predicted

tow forces as well as deployment problems (Cathie *et al.*; 2007). In very soft soils jetting is therefore the only reliable option.

Some ploughs (e.g. variable multi-pass plough, VMP 500) have built in jets which are intended to increase pore water pressures ahead of the share and "soften up" the soil prior to the share cutting it. These jets are therefore thought to reduce the rate effect during ploughing and have undergone some limited trials with mixed results. A caterpillar track fixed to the bottom of the share, known as a share track is also included on some ploughs. The track is designed to work actively and provide a forward force to the plough effectively providing extra capacity to the support vessel. The track can also work in a passive mode whereby it is not directly powered but instead reduces the interface friction for the component of the plough's weight it supports (Fugro report C312-78-02; 2005). Plough translation is an unsteady process due to: the catenary in the tow wire, currents applied to the plough and tow line, changing soil conditions and wind and wave loading on the support vessel. During the active mode, the speed of the share track must therefore be constantly altered to match that of the plough otherwise efficiency is reduced.

Both of these innovations require power from a vessel and this power requirement can out weigh their worth as a vessel providing them with power will have a reduced tow capacity. Furthermore there is uncertainty as to whether a jetting plough might adversely affect trench stability and therefore use of these two plough additions has been limited and their merits are not yet fully understood.

2.3.3. Other burial and protection methods

As an alternative to ploughing and trenching, draglines and clamshells (Figure 2-4a, b) are operated from the surface and may be used to form a trench in shallow waters where the operator has some ability to see the trench that they are forming. Forming a straight trench with an even base becomes a difficult task even in moderately deep waters and inevitably progress is very slow (Palmer *et al.*; 1979). The practical use of this equipment is limited to near shore operations. These techniques may be used where there are numerous crossings of existing infrastructure

which would require a plough or jetter to be lifted across crossings in order to prevent any damage to the infrastructure.

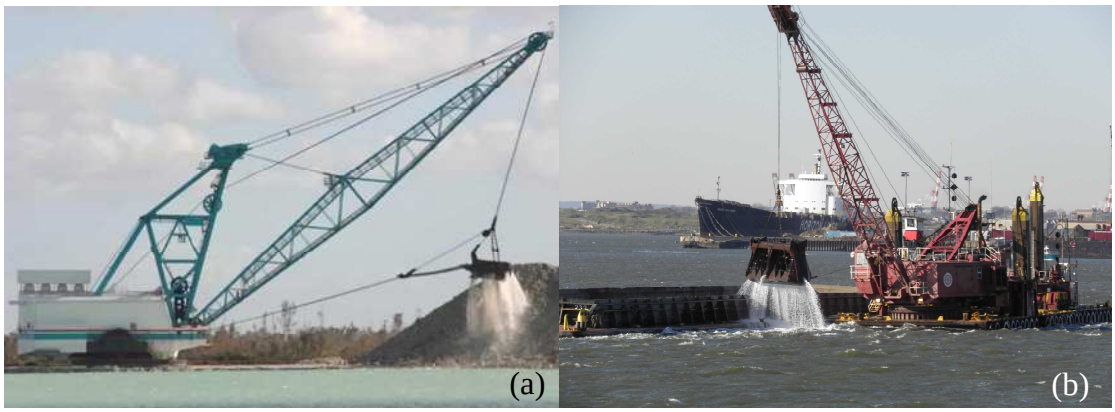

Figure 2-4: Surface operated excavators, (a) dragline excavator, (b) GLDD clamshell excavator (http://tugster.wordpress.com)

Cutting machines which feature a series of rotating teeth can be successful in rock but are not suitable for normal trenching operations as wear in the teeth is a problem in sands and high plasticity clay clogs the cutting mechanism. The performance of such machines is notoriously hard to predict and their use is best left to rock which is too strong to plough.

Rock dumping can be a viable alternative to trenching. This involves placing rock directly onto the pipeline by rock dumping vessels. Rock dumping can be useful in instances where the sea bed profile is particularly dynamic and there are concerns that the soil cover layer may be swept from a trenched pipeline. Another good application of rock dumping is where only a thin veneer of soil exists above solid bedrock and it is impossible to create a trench deep enough to protect the pipeline. Rock dump is also used for uplift prevention, however it is usually much cheaper and quicker to plough and backfill rather than rock dump.

2.4. *Mechanics of plough behaviour and stability*

Pipeline ploughs must be able to cut a trench without sinking into the seabed and without excessive pitching or rolling (rotation about the longitudinal and transverse axes). This is critical to producing a straight trench, which is necessary in ensuring the pipeline's integrity.

Palmer *et al.* (1979) designed an offshore pipeline plough which maintained a stable trenching depth by a method known as the long-beam principle which had previously been employed by forestry and agricultural ploughs. Modern offshore ploughs still maintain the trench depth they are set at by the long beam principle. During operation it is assumed that there is rotation of the plough about the skids (where there is no moment restraint) in order to maintain the desired depth. A plough is generally considered to be working properly when the underside of the share (known as its heel) is parallel with the direction of movement, during which the major soil forces act on the front of the share with only a small heel force, F_h. If the share starts to dig in too deep it will do so by pivoting (clockwise in Figure 2-5) about the pin connection between the skids and the arm connecting the skids with the plough. This tilts the heel backwards so that its back is deeper than the tip (aft pitching) and increases the force acting on the heel, F_h in Figure 2-5a. This causes the plough to pivot anti clockwise and thus correct its depth.

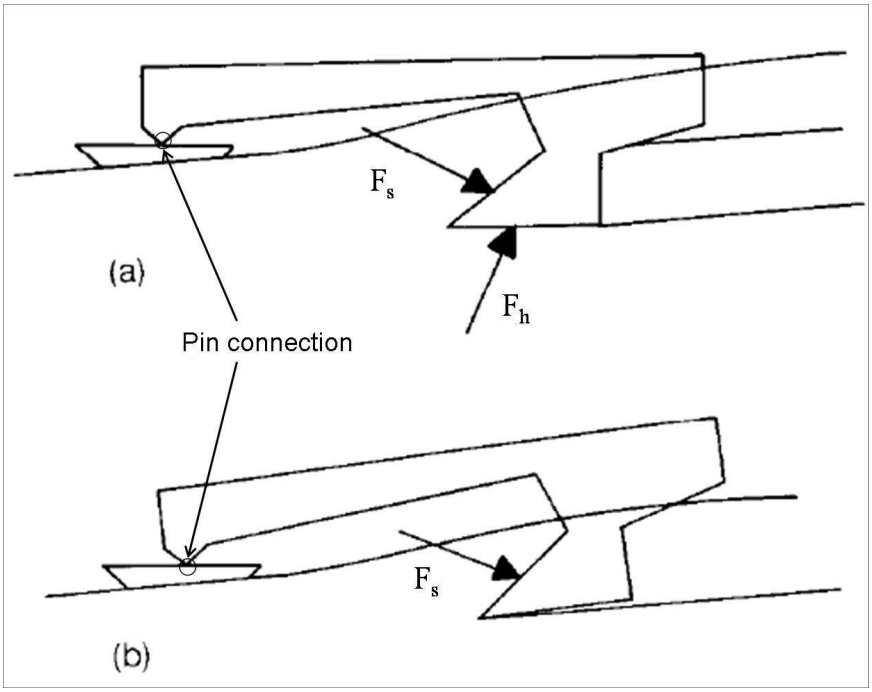

Figure 2-5: Stability and depth control of a long beam plough; (a) Plough cutting deeper than its design depth; (b) Plough cutting less deep than its design depth. (Palmer *et al.*; 1979)

Figure 2-5b shows that if the plough starts to pull out of the soil it again must rotate about the skids but this time in the opposite direction. This will cause the plough to forward pitch and the back of the heel to lose contact with the base of the trench. The reaction force, F_h then drops to nothing allowing the force on the front of the share to

push the share back into the soil. Note that the angles required to increase and reduce F_h to zero are small. Typically the angles will be of the order of a 1º or so, therefore not large enough to have a significant influence on the magnitude of the share reaction force, F_s (Figure 2-9 and Figure 2-10). It is clear that if the plough is unstable and the share rotates too far forward, F_h will equal zero and the reaction F_s may have rotated far enough so as to cause the share to lift out from the soil.

2.5. *Influence of share geometry on forces and failure planes*

Chisel ploughs are commonly used in the agricultural industry to break up hard ground and consist of a series of shanks spaced about 300 mm apart mounted to a frame. Although they are dissimilar to a pipeline plough in that they do not maintain their depth of cut by moment equilibrium they are still a metal object being translated through the soil. Forces measured on instrumented chisel ploughs are comparable to forces on the top of the share of a pipeline plough. Observed failure patterns within the soil during translation of a chisel plough also offer insights into soil failure around the share of a pipeline plough.

Figure 2-6: Curved chisel blade (www.ag.ndsu.nodak.edu)

The difference in form between chisel ploughs and mouldboard ploughs is clearly seen by comparing Figure 2-6 and Figure 2-7 which show a single chisel plough blade and a mouldboard pipeline plough respectively. The chisel plough is designed to loosen and aerate hard ground and has no requirement to create a trench whereas creating a trench is the function of the pipeline plough.

Figure 2-7: Mouldboard share as featured on a pipeline plough

Tanner (1960) conducted experiments using simple flat plates to investigate how the rake angle affected the performance of the simple chisel-type ploughs. Defining the rake angle as the angle from the back of the chisel to the horizontal he found that as the rake angle decreased so did the resulting draft (horizontal force) for constant depth tests. The lowest rake angle he tested was 20º as reducing the angle too much caused the chisel to become very long in order to achieve the desired depth. Tanner (1960) also found that if the rake angle was greater than around 60º then the vertical component of force applied to the chisel was upward (pushing it out of the soil) and was downwards for rake angles less than 60º. Hata (1979) conducted experiments using similar simple blades (Figure 2-8) and also found that the horizontal component of force during testing varied with rake angle.

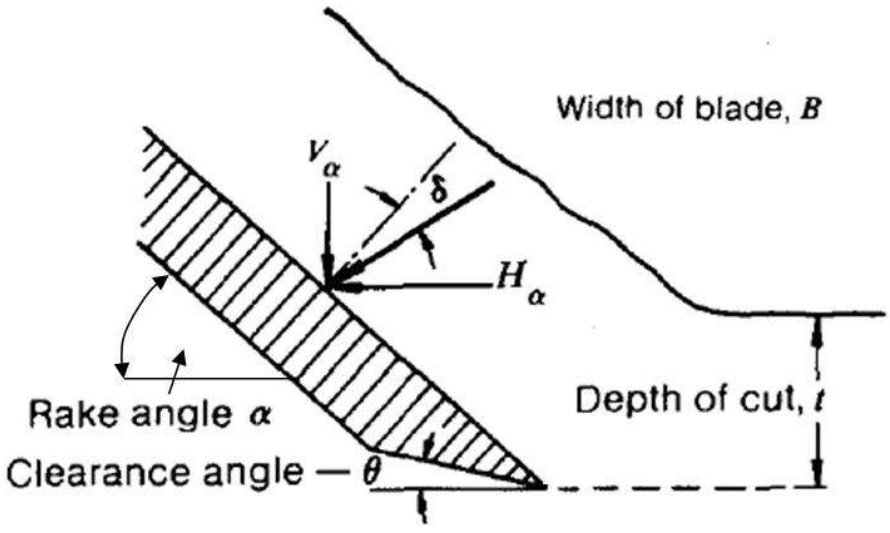

Figure 2-8: Resultant force acting on the cutting blade during testing (Hata; 1979, modified)

Results showing the effect of blade angle on cutting resistance from tests by: Tanner (1960), Hata (1979), Hettiaratchi & Reece (1975) and Godwin & O'Dogherty (2006) are presented in Figure 2-9. $H_\alpha/H_{\alpha=90}$ is defined as the horizontal component of force for inclined blades normalised by the horizontal component of force for the vertical blade. Although tests were conducted using different soils and different shaped blades of different surface finishes, the data in Figure 2-9 all show that horizontal force increases with blade angle. Typical rake angles found on pipeline ploughs are around 35º indicating that they are likely to perform fairly well in this respect based on the findings of Figure 2-9.

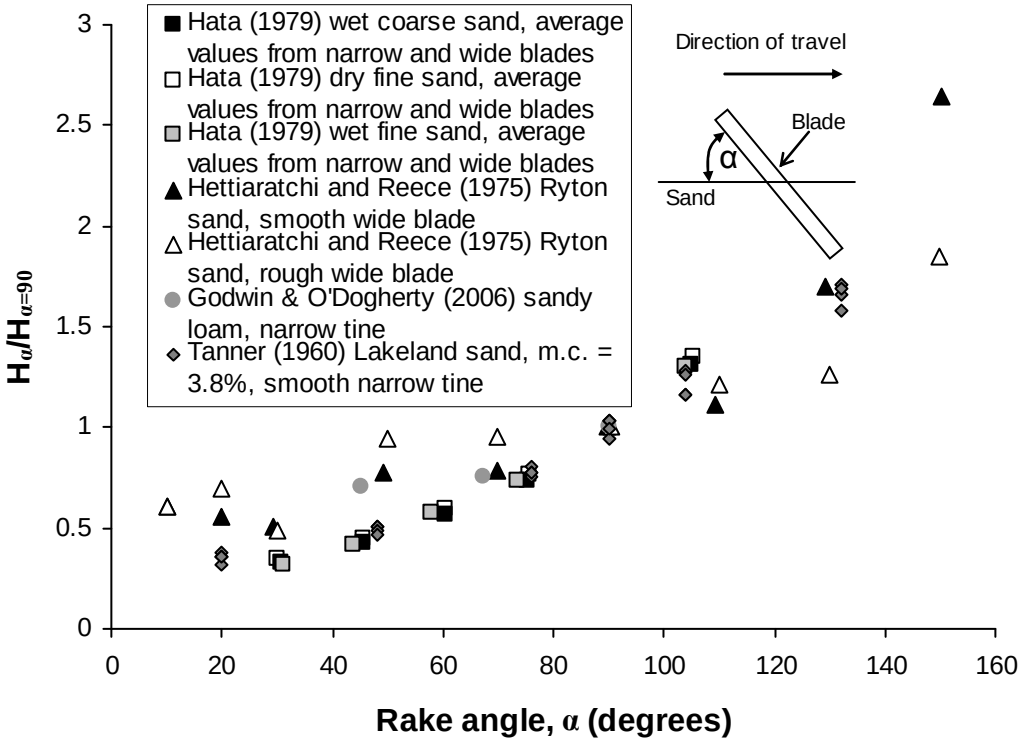

Figure 2-9: Effect of rake angle on cutting resistance

Results showing the effect of blade angle on cutting resistance from tests by: Tanner (1960), Hettiaratchi & Reece (1975) and Godwin & O'Dogherty (2006) are presented in Figure 2-10. $V_\alpha/V_{\alpha=90}$ is defined as the vertical component of force for inclined blades normalised by the vertical component of force for the vertical blade. For all tests the vertical component of force applied to a vertical blade is upward. The vertical force measured during the tests by Hettiaratchi and Reece (1975) using a smooth blade is very small since the interface angle δ will be small for a smooth blade and has the effect of increasing the magnitude of normalised vertical forces for this data series. The ratio $V_\alpha/V_{\alpha=90}$ increases with increasing rake angle and is positive

(upward) for rake angles greather than 70º and negative (downward) for rake angles less than 70º.

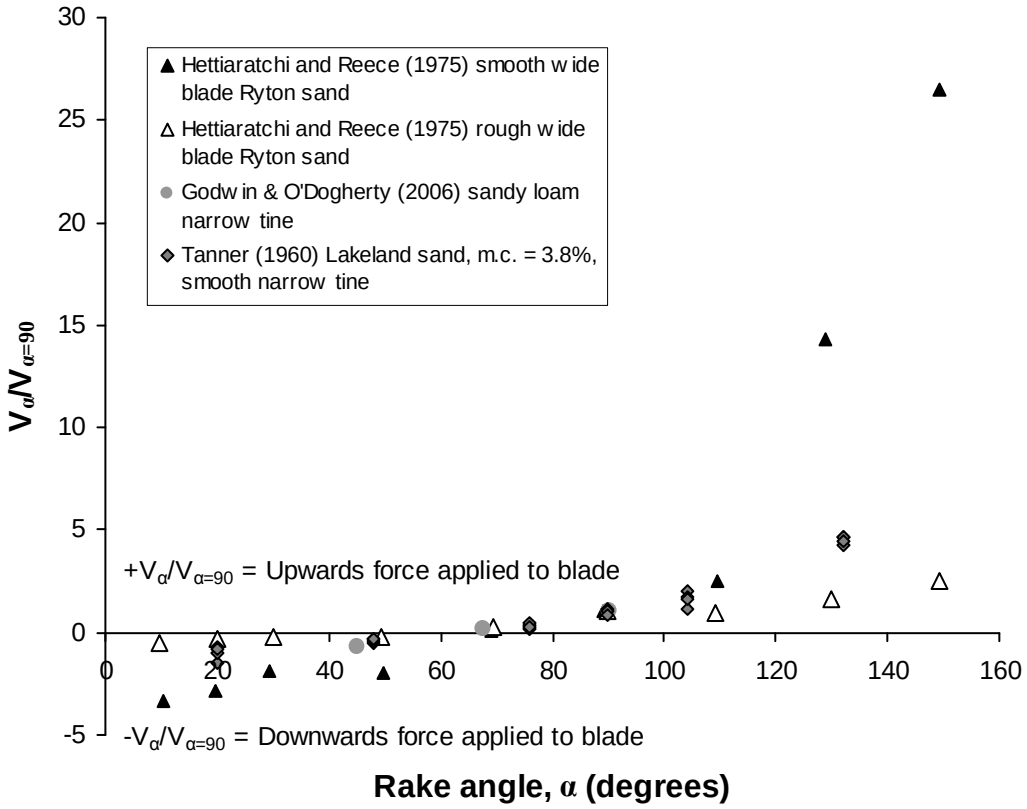

Figure 2-10: Vertical force data from translation of blades in sand with both a polished blade and a rough blade (Hettiaratchi and Reece; 1975)

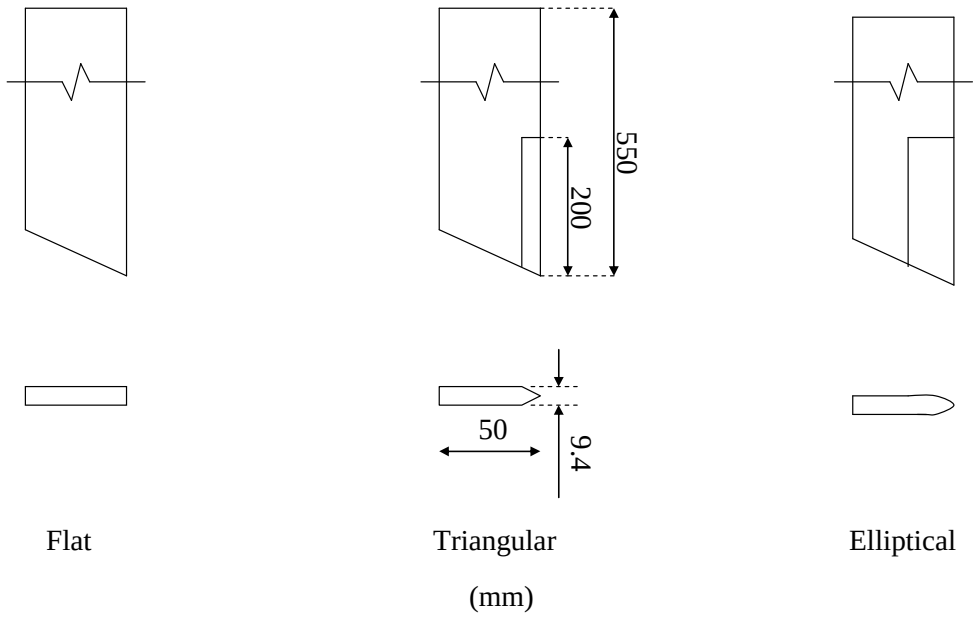

Figure 2-11: Different leading edge shapes of chisel tools (Rosa; 1997)

Rosa (1997) conducted a series of tests using three simple chisel type cutting tools each with a different shape of leading edge. Figure 2-11 shows the profiles of each of the leading edges of the tools tested.

The effect of leading edge profile on the tow force (draft), during tests over a range of cutting speeds in a silty clay-loam, compacted to a unit weight of 11.3 kN/m^3 and with a water content of 12.6% is shown in Figure 2-12. The cutting tool with the elliptical leading edge was shown to produce the lowest draft whilst the flat surface produced the highest draft. Note that Figure 2-12 shows that draft increases with velocity for all tests and is a commonly seen phenomenon in tillage research, which is often attributed to inertia. Typically a pipeline plough will be trenching at rates less than 0.5 m/s and still display larger rate effects than shown in Figure 2-12.

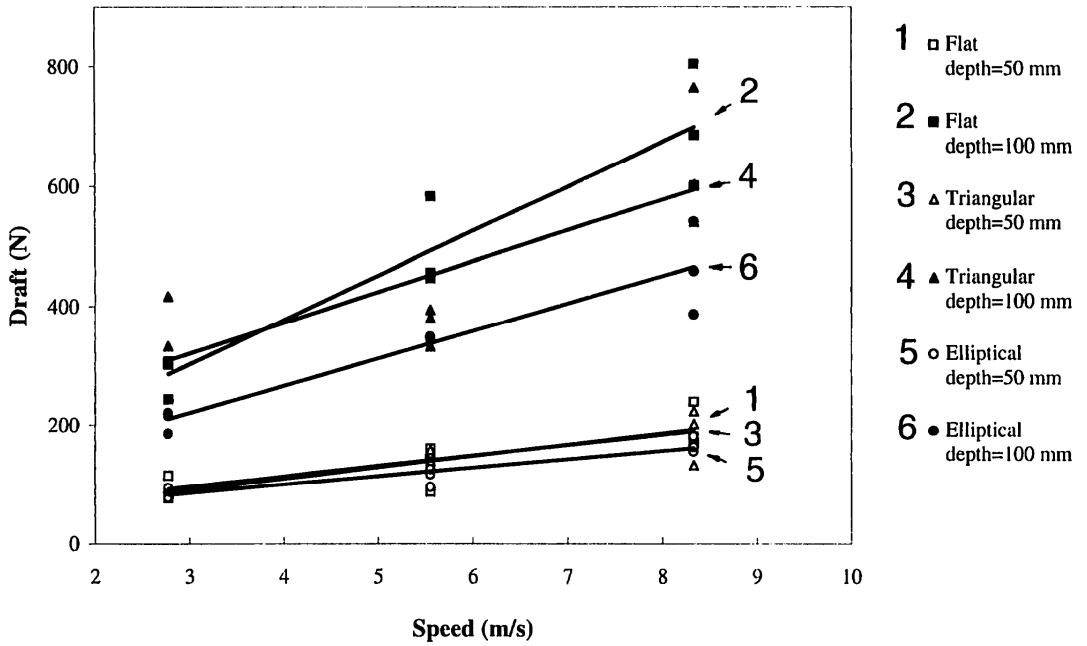

Figure 2-12: Tool draft in soft compacted soil (Rosa; 1997)

Van Leussen and Nieuwenhuis (1984) present plane strain cutting tests performed behind a glass plate so that soil displacements could be observed during the tests. Tests were conducted using two different blades: one with a sharp leading edge and one with a blunt leading edge. Figure 2-13 shows the blunt edge causes the failure plane to dip at the tip of the blade and extend the failure plane. The result of extending the failure plane is that forces are likely to increase.

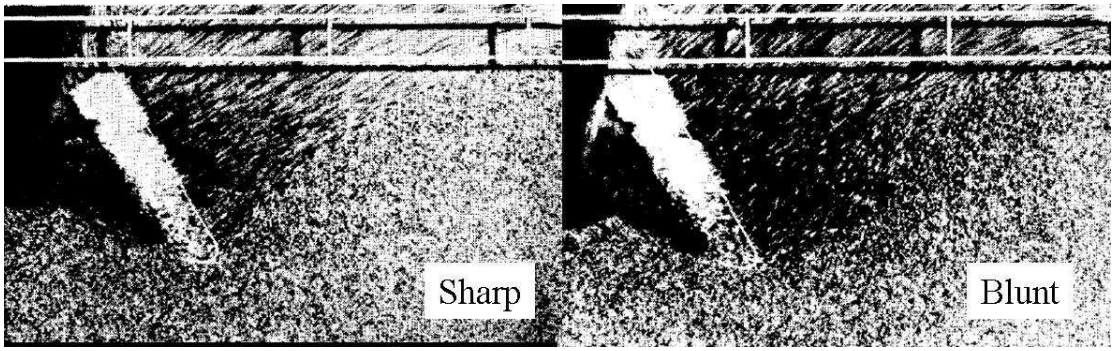

Figure 2-13: Effect of edge profile beneath the cutting blade on the shear plane (Van Leussen & Nieuwenhuis; 1984)

The share shape would appear to have clear implications on failure planes, tow forces generated and plough stability. Although present pipeline plough share geometry will no doubt be designed with these points in mind this appears to be an area which could be researched further and has clear potential benefits.

2.6. *Rate effects*

The tow force during ploughing increases with plough velocity and is known as a rate effect. The rate effect is not caused by inertia (Palmer; 1999) and is instead a soil response to shearing at velocity. Through a set of empirical equations, Reece and Grinsted (1986) found that ploughing forces in dry sand were completely independent of speed, for speeds up to 3000 m/h which is greater than practical ploughing speeds which tend not to be more than 1800 m/h, Cathie and Wintgens (2001). Any rate effect observed during ploughing is therefore for all intents and purposes unaffected by inertia. Rate effects during ploughing occur in both sand and clay, however they are far more pronounced in sand and frequently cause problematically high tow forces (Reece and Grinsted; 1986).

Miedema and Yi (2001) described the cutting process in 5 stages with respect to speed in saturated granular media as: (i) very low cutting velocities, (ii) cutting forces dominated by dilatancy properties of sand, (iii) Local cavitation, (iv) complete cavitation around the blade and no further increase in cutting forces due to sand's dilatant properties, (v) very high cutting velocities where inertia forces become significant. The first stage assumes pore pressure changes are negligible and is equivalent to cutting dry material. Stages 2-4 are highly applicable to pipeline

ploughing and are discussed below. As explained above, stage 5 is unlikely to occur during pipeline ploughing operations and is not discussed any further.

The majority of seabed soils in their natural state are on the dry side of critical state and will therefore dilate when sheared. This causes a local reduction in density within the dilating zone. In underwater ploughing operations the soil is saturated and during dilation pore water from surrounding soil flows with an associated simultaneous decrease in pressure into the dilating zone to fill the increased void volume. During ploughing operations an increase in tow force is generated by this reduction in pore pressure as it increases the mean normal effective stress, $\sigma_n' = \sigma_n - u$, which in turn increases the shear stress developed in the soil during shear deformation (Palmer; 1999).

Increasing the amount of dilation causes lower pore water pressures and therefore amplifies cutting forces, (Van Leussen & Nieuwenhuis; 1984). It is well known that reducing the particle size and hence permeability of the sand increases the resistance to the flow of water through the sand (Whitlow; 2001). Reducing particle size should therefore require greater pore pressure reductions to drive a given flow. Since dilation band dimensions are related to particle size (Roscoe; 1970) reducing particle size will also decrease the volume of water required to fill a void created by dilating sand. The pressure gradient required to drive the flow of pore water (degree of drainage) also increases with the rate of shearing and hence ploughing speed as this determines the velocity at which the water must flow to fill the voids created during dilation.

The volume of sand deforming in front of the share and the length of the drainage path(s) will influence the rate effect as they also contribute to the resistance to the flow of water. Therefore the size and cutting depth of the plough may also influence the rate effect, (Palmer; 1999). Hata (1979) found a strong rate effect during tests dragging simple share like blades through saturated sand and his results for a 150 mm wide by 150 mm deep blade are plotted in Figure 2-14.

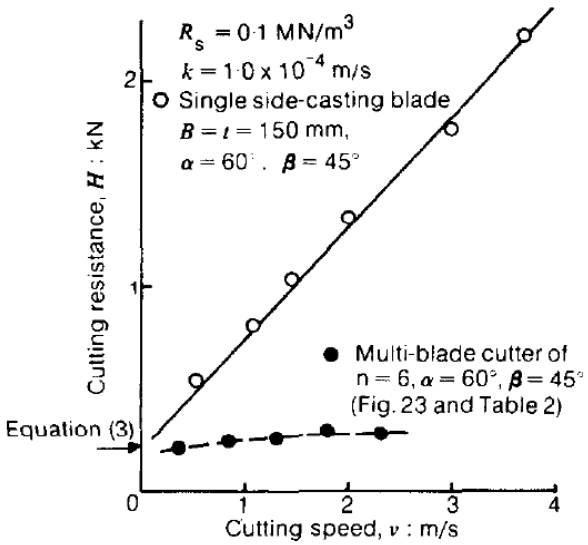

Figure 2-14: Cutting resistance and cutting speed for submerged sand (Hata; 1979)

In pulling a multiple blade model plough of similar projected width and depth through the same material, Hata (1979) found the rate effect was much less significant. Hata (1979) had already established during earlier tests that the cutting resistance of a rectangular blade increased with the square of its depth. He recognised that if a series of overlaid cuts into sand were made whereby each successive cut was slightly deeper than the previous one the total force required to do this may be less than for a single cut to the same depth as that of the final pass of shallow cuts. He developed a multi-blade plough to do this which allowed for a deep trench to be cut by six blades mounted on a beam one behind the other. The reason why this may affect the rate effect is that the length of drainage path and hence resistance to flow of pore water might be reduced if water from the free surface is required to fill the void created by dilation.

Rate effects arise in ploughing operations as speeds are typically great enough to prevent complete drainage of the soil being sheared, the faster the ploughing the less drainage and the greater the forces. Clays and silts act fully undrained even at very slow cutting speeds and therefore increasing the speed of ploughing will generally not cause any drainage related rate effects. Reece and Grinsted (1986) did however did find some although, much less marked rate effect when cutting clay, which may be due to viscosity. The rate effect Reece and Grinsted (1986) found was the same for dry and submerged clay. They could not provide an explanation for it but did however

note that it was not observed in normally consolidated weak clay. In the case of sands and gravels rate effects have been found by Grinsted (1985) to occur at lower ploughing speeds in fine, dense sand that is comparatively less permeable and compressible than in loose course sand.

Kutter and Voss (1995) analysed experiments on cable plough resistance in dense sand reported by Cable *et al*. (1993) and Girard and Taylor (1994) where the sand's resistance to the plough was found to steeply increase linearly with plough velocity up until the onset of cavitation. Grinsted (1985) found the same effect in both course sand and in fine silty sand and showed that tow force increased more rapidly with cutting speed for the fine silty sand. Van Os and Van Leussen (1987) studied the effects of dilatancy and cavitation of pore fluid. They derived a theoretical model to estimate the reduction of pore pressure during cutting. This allowed for the calculation of cutting forces using limit equilibrium analysis for which plane strain conditions were assumed. The results compared well with the measured cutting forces during plane strain tests and are shown in Figure 2-15. Both the data and the calculated cutting forces show that the rate effect appears to increase in a linear manner with velocity. Cutting forces are shown to be limited by cavitation which will onset at greater velocity as the equivalent water depth (they used a hypobaric chamber to simulate large water depths) is increased.

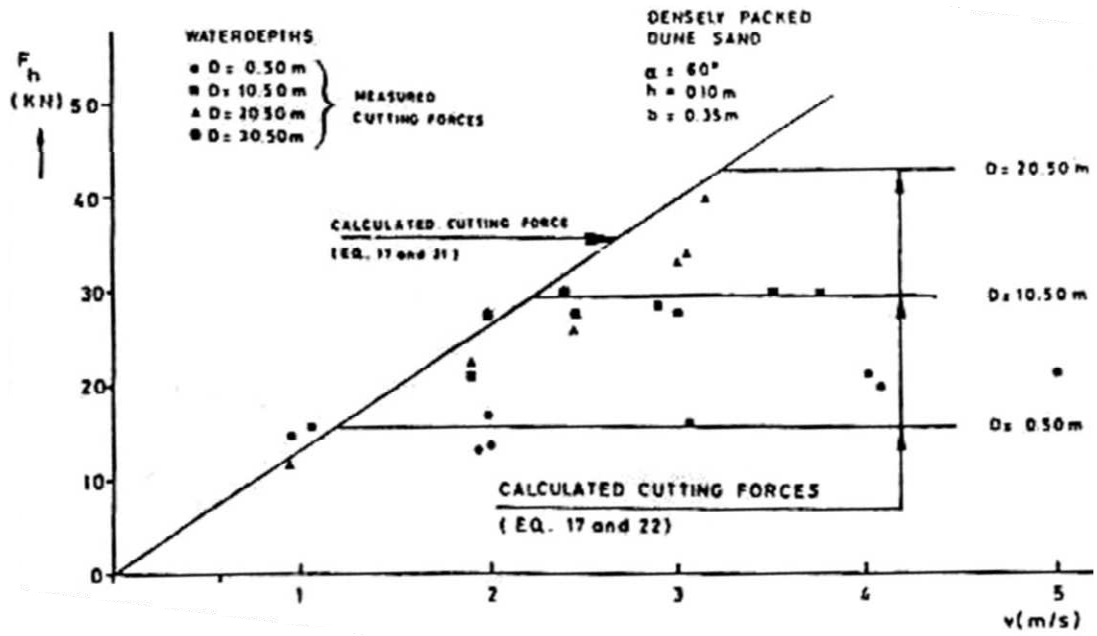

Figure 2-15: Comparison of measured and calculated cutting forces (Van Os and Van Leussen; 1987)

Cavitation results from the continued reduction of water pressure during shearing which reduces the solubility of dissolved gases within the pore fluid. This eventually leads to these gases coming out of solution in the form of bubbles. This vaporization results in incomplete saturation of the soil. As gasses are highly compressible and will readily flow under small pressure gradients, their presence reduces the rate effect. Kutter and Voss (1995) also show that this phenomenon can be adequately described by two straight lines. Figure 2-16 shows the relationship they formulated, through means of experimental observation for limiting rate effects due to cavitation. The solid black line in Figure 2-16 represents the true tow force-velocity relationship and curves towards the horizontal at velocities where vaporization commences. The rate effect will continue to reduce as more of these gases come out of solution until pressures around the share tip are low enough to cause local cavitation of pore fluid, followed by cavitation of all the pore fluid along the share at which point, no further increase in tow force can be expected for increase in plough velocity due to dilation, (shown as Q_{max} on Figure 2-16). Cavitation occurs at zero absolute pressure and as hydrostatic pressure in water increases linearly with depth the magnitude of decrease in pressure before absolute zero is reached and hence onset of cavitation will also increase linearly with the depth of water above the dilating sand. Cavitation of pore fluid is not likely to occur during ploughing operations in deep water and will not be investigated within this thesis.

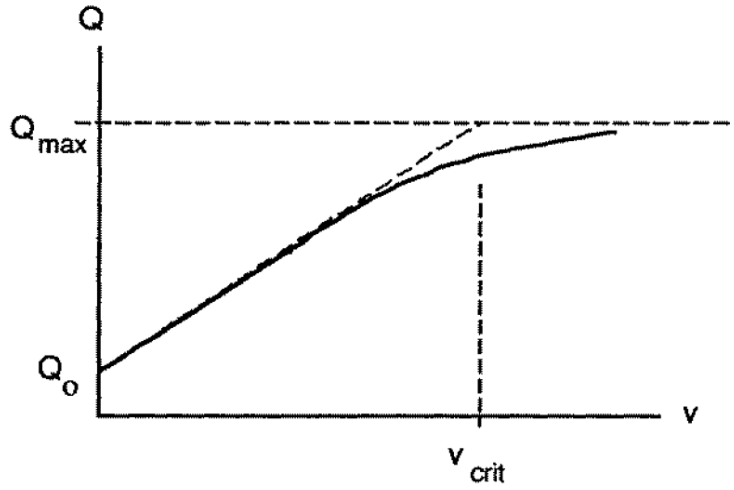

Figure 2-16: Plausible relationship between plough resistance and velocity (Kutter and Voss; 1995)

Grinsted (1985) defines a limit to the increase in cutting force with velocity due to the suppression of dilation. This limit is reached when the suctions caused by dilation

increase effective stresses to a point which prevents any further dilation from occurring and results in dilation approaching zero. As the dilation limit is dependant on normal effective stresses and cavitation is dependent on pore water pressure it is clear that water depth is key in determining which of these phenomena will occur at the lowest velocity.

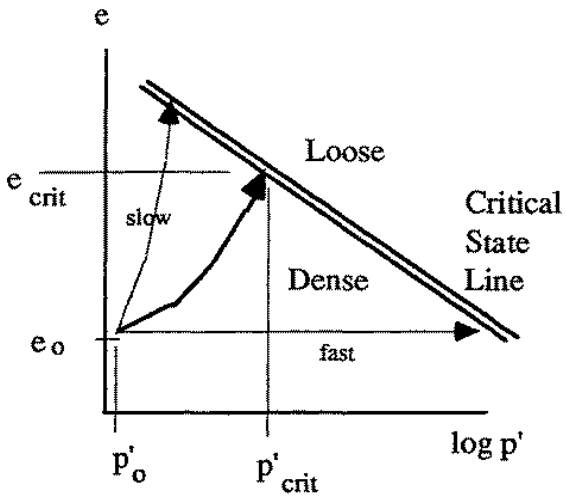

Figure 2-17: Possible stress paths for soil around the plough in dilative sand without cavitation (Kutter & Voss; 1995)

Kutter and Voss (1995) propose possible stress paths of sand initially on the dry side of critical state around the plough as it trenches through and Figure 2-17 plots these along with the critical state line (CSL) in the *e*-log *p'* plane. The stress path (marked slow) where the plough is travelling at the slowest rate results in a minimal increase in normal effective stress and therefore the sand dilates a large amount to reach the critical state void ratio, e_{crit}. The stress path marked fast shows the normal effective stress increasing (presumably due to reductions in pore water pressure) and no change in void ratio as the sand heads towards the CSL and is consistent with the theory of Grinsted (1985). The cause of this is due to the critical state void ratio reducing with increasing normal effective stress.

2.7. *The importance of characterisation of soils for offshore ploughing operations*

The selection of the most appropriate tool and estimation of the speed of progress require accurate soil characterisation (Puech *et al*. 1994). Ploughs tend to be the best option in medium to dense sands, hard clay and weak rock, whereas jet trenchers

perform best in soft mud and loose sands (Finch and Machin 2001). As the client will often provide soil test data to the contractor, adequate characterisation of the soil along the pipeline route helps prevent legal disputes which can result if the contractor's progress is not what they had predicted.

Bathymetry and stratigraphy are mapped by geophysical means such as multibeam echo sounders and ultra high-resolution seismics, which provide continuous measurement. Physical properties tend to be derived from cone penetrometer test (CPT) data and vibrocore (in sand) or drop core (in clay) samples taken at discrete points along the pipeline route. Vibrocores are disturbed samples and therefore cannot be used to describe the insitu state of cohesionless material. They are instead used to classify particle sizes and can be used to identify stratifications, however, plunging, compaction and core loss during sampling will adversely affect results. Cone penetrometer tests are favoured by the offshore industry as they allow fast data acquisition relative to sampling and laboratory testing (Puech & Foray; 2002) and careful evaluation of CPT data can reliably provide the density and friction angle of cohesionless material.

Puech *et al*. (1994) show that high resolution seismic profiling can be used to determine the nature and thickness of stratifications of soil in the first 3-5 m to an interface accuracy of 300 mm, which is still low resolution in terms of depths associated with ploughing. Offshore soil investigation guidelines (2004) suggest that soil samples and probing should be taken at a spacing of 0.5-1 km along the pipeline route and to a depth of 1 m below the proposed trench depth. Spacing is dependent on: the pipeline route, bed features and soil conditions and should be reduced with increasing heterogeneity.

Puech and Foray (2002) show that the conventional approach to CPT analysis is not suitable for pipeline route surveying as it ignores shallow failure mechanisms. They present a refined model for determining friction angle and relative density CPT results. Puech and Foray (2002) find that at shallow penetration depths in uniform soil conditions the cone resistance increases to a quasi-stationary value at some critical depth whereby a constant resistance is shown for increasing penetration depth. Table 2-1 shows the relationship between the quasi-stationary cone resistance and relative

density. The critical depth increases with relative density and ranges from around 0.8-1.8 m from loose to dense sand.

Table 2-1: Correlation between relative density, D_r and quasi-stationary cone resistance q_{st} at shallow penetration for fine to coarse silica sands (Puech and Foray; 2002)

Description	Relative Density, D_r (%)	Cone Resistance, q_{st} (MPa)
Very loose	<15	<0.6
Loose	15-25	0.6-1.5
Medium dense	35-65	1.5-7.0
Dense	65-85	7.0-16.0
Very dense	85-100	>16.0

At shallow depths, less than the critical depth Puech & Foray (2002) find the density of the soil is based upon the rate of increase in cone resistance with depth and on the critical depth itself. This may allow for accurate characterisation of relative density in uniform soil conditions, however is likely to be not very applicable in sea bed soils which have been laid down in layers where relative density is likely to differ between the layers. As the critical depth is of similar magnitude to a typical pipeline trench the relative density of the majority of the depth of the trench would be hard to define.

An alternative and less used method of surveying the geotechnical characteristics of the route may be by grapnel survey. A grapnels consists of a fluke (narrow, hook-like share) mounted on wheels. Conventionally these tools are used to retrieve buried cables in order to repair faults. The concept is that the grapnel penetrates the soil to the depth of the desired trench and is towed along the proposed route. As the fluke is very narrow, the forces measured during towing are relatively small compared to ploughing and allow for rapid progress at little cost. The forces can then be used to indicate expected plough tow forces. The frequency of use of this survey technique is considered rare and there is only evidence of it being used on a small number of occasions (Damian Morrow, personal comm., 2010).

2.8. *Current performance prediction methods*

2.8.1. Importance of performance prediction

Plough performance includes plough stability and tow force requirements, however it is the latter which often involves the greatest uncertainty. Good pipeline plough performance prediction reduces the likelihood of unforeseen circumstances during trenching and allows the trenching operation to be priced appropriately. Past site experience can be a great indicator for performance on that particular site, however for ploughing projects in new territory performance prediction must be made by other means. Use of empirical equations which allow input of soil data are the most common method of performance prediction employed.

2.8.2. Background

Reece (1965) proposed what he termed the fundamental equation of earth moving mechanics (Equation 2-1). The simple equation is similar to Terzaghi's civil engineers' bearing capacity equation. The equation contains four terms representing the forces due to the effects of the soil's cohesion, self weight, surcharge and adhesion between the soil and the earth moving machine. Where: c is cohesion, b is a characteristic length, q is any surcharge, c_α is soil to metal adhesion and N_c, N_γ, N_q and N_α are independent dimensionless factors depending on the shape of the soil failure surface.

$$F = cb^2 N_c + \gamma b^3 N_\gamma + qb^2 N_q + c_\alpha b^2 N_\alpha \tag{2-1}$$

Reece and Grinsted (1986) showed that Equation 2-1 can be simplified when cutting saturated submerged soil and for cutting in sand they added a rate term which accounts for the increase in effective stress resulting from dilating sand drawing water into the shear plane (see Equation 2-2). Where K_3 is a constant dependant on the interface friction angle between the plough and sand, W is the weight of the plough. K_4 is a constant which depends on plough shape, the sand's unit weight and soil friction angle and D is the depth of cut. K_7 is a function of plough size and shape, v is the velocity of the plough, R is the dilation ratio of the sand and k its permeability.

$$F = K_3 W + K_4 D^3 + K_7 v R/k \quad (2\text{-}2)$$

2.8.3. Cathie and Wintgens (2001)

Cathie and Wintgens (2001) formulated a pipeline plough performance prediction model based Equation 2-2 where the rate dependant component of tow force was modified to give Equation 2-3, which predicts tow forces in cohesionless soils. The coefficients were optimised based on the back analysis of data from pipeline ploughing operations at over 30 sites. This appears to have become an industry standard way by which a ploughing contractor will try to predict tow forces encountered during ploughing and hence predict the length of time required to complete any ploughing operation.

$$F = C_w W' + C_s \gamma' D^3 + C_d v D^2 \quad (2\text{-}3)$$

where,

F is tow force, C_w is a dimensionless friction coefficient, W' is the submerged buoyant plough weight, C_s is a dimensionless passive pressure coefficient, γ' is the submerged unit weight of the soil, D is the depth from the origonal sand surface to the heel of the share, C_d (t/m^3/hr) is a dynamic coefficient and v is the plough velocity.

The model was calibrated using data from actual ploughing operations. The values used for the three coefficients were therefore selected from data obtained from variable natural soil conditions in an environment where accurate and precise observations are very difficult. C_w was selected by looking at force-velocity data from numerous ploughing operations when the depth of the share was thought to be low and the speed of the plough known to be slow. C_w appears to vary little with soil type and condition and is the most well defined of the Cathie and Wintgens (2001) coefficients. With the friction term in the equation known, the C_s coefficient was determined in a similar manner, by looking at forces during transition regions of embedment as the plough achieved its natural depth and by examining forces during starts and stops while embedded (i.e. when velocity is very small).

The dynamic force coefficient, C_d was then found by the difference between the measured tow force and the static component of tow force as deduced by the first two terms in Equation 2-3 including the previously established C_w and C_s values. Table 2-2 shows the values of C_w and C_s coefficients which Cathie and Wintgens (2001) propose. C_w is shown to be unaffected by relative density whereas C_s increases with relative density. C_s increases with relative density much in the same way as K_p (which Cathie and Wintgens (2001) compare C_s to) increases with friction angle.

Table 2-2: Tow force coefficients C_w and C_s for cohesionless soils (Cathie and Wintgens; 2001)

Tow force coefficient	Relative density, D_r (%)	Value
C_w	All	0.4
C_s	Loose	5
	Medium Dense	10
	Dense	15
	Very Dense	20

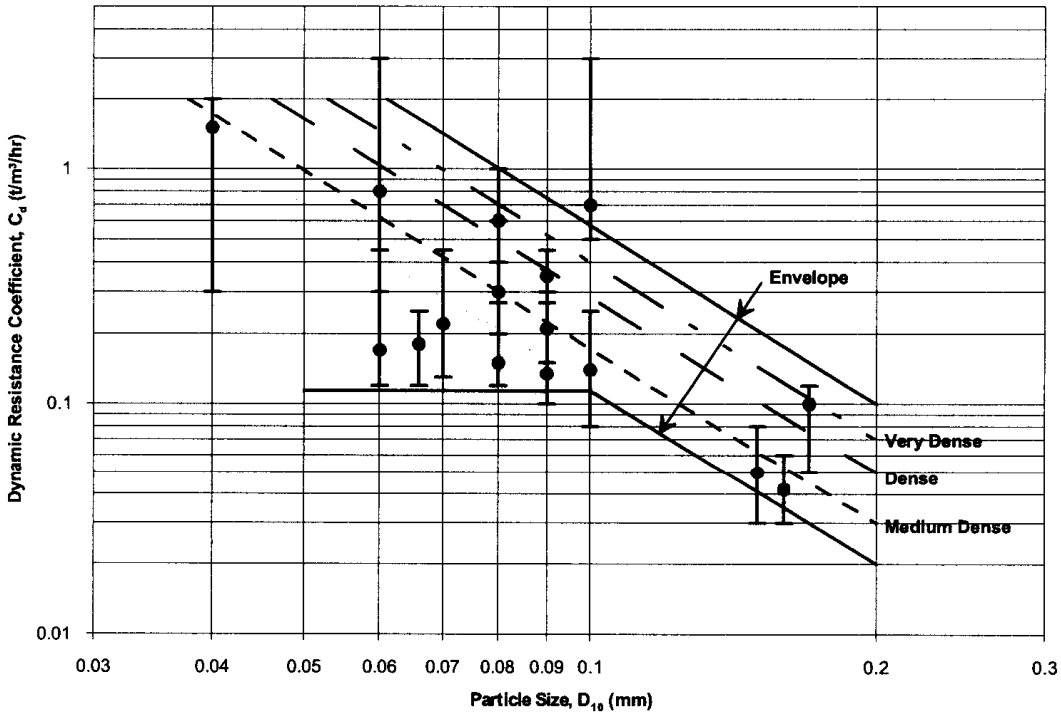

Figure 2-18: Ploughing resistance coefficient, C_d – Field data and interpretation (Cathie and Wintgens; 2001)

Cathie and wintgens (2001) present a chart for determining C_d. The chart plots a series of lines which show C_d to increase with increasing relative density and with reducing particle size, D_{10}, which was used as a measure of permeability (Figure 2-18).

As Equation 2-3 is constructed in a stepwise manner (i.e. the value given to C_d depends on that of C_s which in turn depends on C_w) it is important that the values for C_w and C_s are accurate when trying to determine C_d. Accurate values are difficult to achieve for data derived from real ploughing operations as there are far too many uncontrollable variables. Cathie and Wintgens (2001) use the skid height corrected by plough pitch as a means of determining plough depth but note that it is difficult to differentiate plough pitch from sea bed slope, which can cause inaccuracy. D_{10} is used as a measure of permeability in their work as this was the data available to them however, this is not as accurate as direct measurement. Empirical correlations between CPT resistance and relative density were used to determine the relative density of sand for their work which adds another layer of uncertainty since direct measurement would be ideal however this is not practically feasible.

The accuracy of the three coefficients: C_w, C_s and C_d could be greatly increased if their values were determined from a controlled set of laboratory tests. This is because control of sand density and particle size, for instance allows isolation of critical state angle of friction (φ'_{crit}), peak angle of friction (φ'_{peak}), unit weight (γ) and permeability (k) and hence their effect on the three coefficients and also the equation as a whole.

As full scale laboratory testing would be prohibitively expensive and time consuming, reduced scale testing seems a logical method of investigation. The extrapolation of data from reduced scale model tests to full scale plough behaviour can however be a complicated procedure. Particle size effects and normal effective stress differences between prototype and model scale can affect results and must be accounted for.

2.9. *Scaling issues*

Deriving results applicable to the ploughing industry from reduced scale model tests requires some form of scaling. The depth of soil displaced during ploughing is usually less than 2 m and therefore the normal effective stresses of the soil at the base of the trench would be expected to be at a maximum of 20 kPa for a soil with a normal submerged unit weight, γ'=10 kN/m^3. During scale model tests conducted in the same material, lengths and hence normal effective stresses will be reduced by the scale factor which can alter soil response in subtle ways.

Wood (2005) presents scale factors which can be used to extrapolate full scale behaviour from reduced scale model results. Table 2-3 shows the scale factors selected from Wood (2005) which are used to scale the test results presented in Chapters 4-6.

Table 2-3: Scale factors (modified from Wood; 2005)

Quantity	Scale Factor
length	1/N
stress	1/N
mass	1/N^3
force	1/N^3
pore fluid viscosity	1
permeability	1

Wood (2005) also describes subtle issues regarding the use of these scale factors which must be taken into account. The behaviour of sand subjected to shearing has been found to be dependant on effective stress (Bolton; 1986), which is reduced during model scale. Scaling effects due to particle size have been observed by numerous researchers including Bolton & Lau (1989) and should also be accounted for.

2.9.1. Effective stress issues

For the majority of applications in soil mechanics a linear relationship between shear stress, τ and normal effective stress, σ_n' is perfectly acceptable. This is the case when

the range of effective stresses considered is low enough so that the failure envelope is approximately linear. The most common linear approximation used to describe a failure envelope is to take a tangent to the failure envelope where the failure envelope becomes described by Mohr-Coulomb, Equation 2-4.

$$\tau_f = \sigma_n' \tan \varphi' + c' \quad (2\text{-}4)$$

where τ_f is the shear stress at failure, σ_n' is the normal effective stress, tan φ' defines the slope of the envelope and c' the shear stress intercept. The cohesion intercept on the shear stress axis of the Mohr-Coulomb plot exists for an uncemented soil, solely to define the Mohr-Coulomb equation, (Atkinson; 1993) and its origin may be a result of investigation over an inadequate range of stresses during testing (Maksimovic; 1996).

At high normal effective stresses various researchers have found the angle of internal friction, φ' to vary with normal effective stress. Vesic and Clough (1968) demonstrate for dense sand that secant φ' varies linearly with log mean normal stress from 100 kPa to 10,000 kPa at which point particle crushing becomes evident. Note that crushing pressure will also be dependant on mineralogy, particle angularity and size.

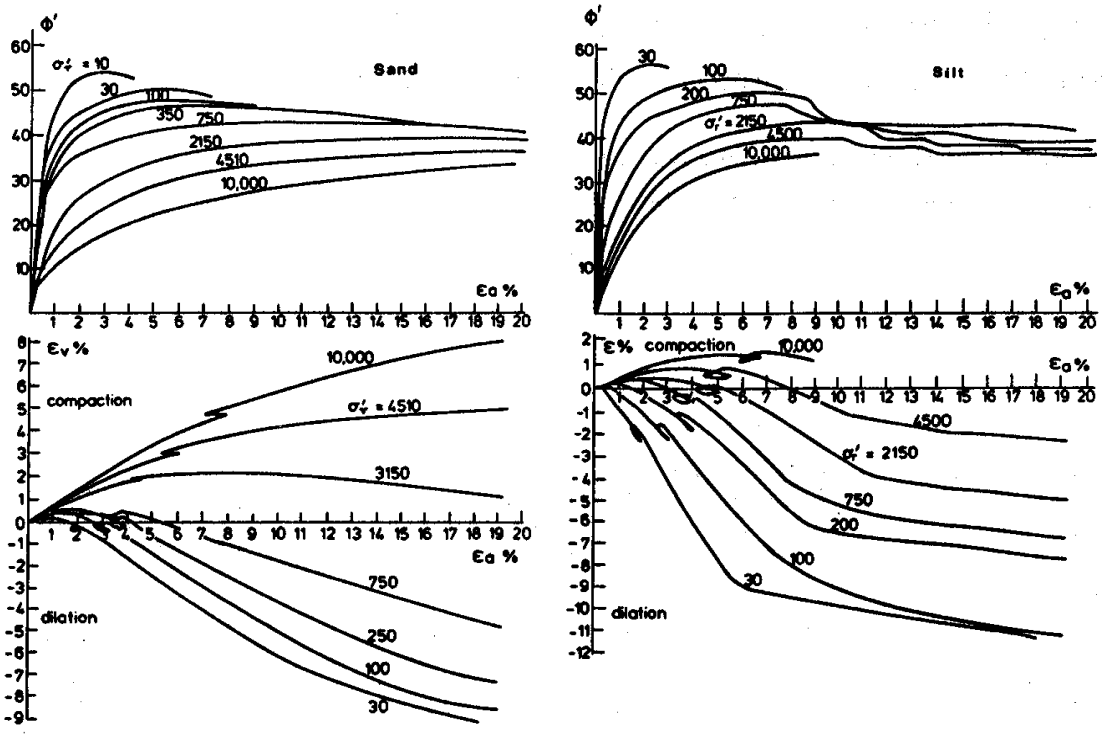

Figure 2-19: Drained triaxial compression tests (Bolton & Lau; 1989)

Numerous researchers have found maximum secant angle of shearing resistance (φ'_{sec}) to increase with reducing normal stress and attributed this to reduced suppression of dilation. Figure 2-19 taken from Bolton & Lau (1989) shows an increase in stiffness, maximum angle of shearing resistance and dilation with reduction in effective cell pressure from 10 MPa down to 10 kPa. Importantly, the rate of increase in φ'_{sec} with reducing effective stress level is at its greatest for the lowest normal effective stresses.

At normal effective stresses less than approximately 50 kPa the failure envelope is less well understood, however its form would be expected to be a convex line heading towards the origin in τ-σ_n' space. The influence of normal stress on dilation angles is best observed in granular material on the dry side of critical state which will dilate when sheared. Ponce and Bell (1971) conducted triaxial tests on quartz sand at two states of relative density, 5% and 95% over a range of confining pressures from 1.44-241 kPa. They found that for the dense samples, larger dilation angles at lower normal stresses increased the principal stress ratio at failure. They also found that at very low stresses even the very loose specimens tended to dilate. Fannin *et al*. (2005) found through direct shear tests that for all sands tested peak friction angle, φ'_{peak} decreased from around 71-54º with increasing normal effective stress over a range of 5-17 kPa. Chen *et al*. (2003), tested granular soils of different particle shapes in a triaxial cell at cell pressures from 30-100 kPa and also found that for most soils tested the peak stress ratio decreased as the confining pressure increased. Sture *et al*. (1998) conducted triaxial tests on board a Space Shuttle orbiting the earth, where gravity induced stresses were low which allowed for very low effective stress tests to be conducted without having a large stress gradient within the sample which would influence failure. They tested samples at normal stresses from 0.05-1.3 kPa and found peak friction angles up to 70º in dense and very dense Ottawa sand.

Bolton (1986) compiled plane strain data of numerous researchers at various relative densities and normal effective stress levels. Bolton (1986) defines a relative density index, I_r which is dependant on effective stress and relative density (Equation 2-5).

$$I_r = D_r(10 - \ln p') - 1 \qquad (2\text{-}5)$$

$$\varphi'_{peak} - \varphi'_{crit} = 0.8\psi_{\max} = 5I_r \quad (2\text{-}6)$$

Equation 2-6 related I_r to φ' and dilation angle, ψ_{max} and coupled with Equation 2-5 allows for the prediction of dilation angles for known effective stress and relative density conditions. Figure 2-20 shows how his empirical relations match plane strain test data.

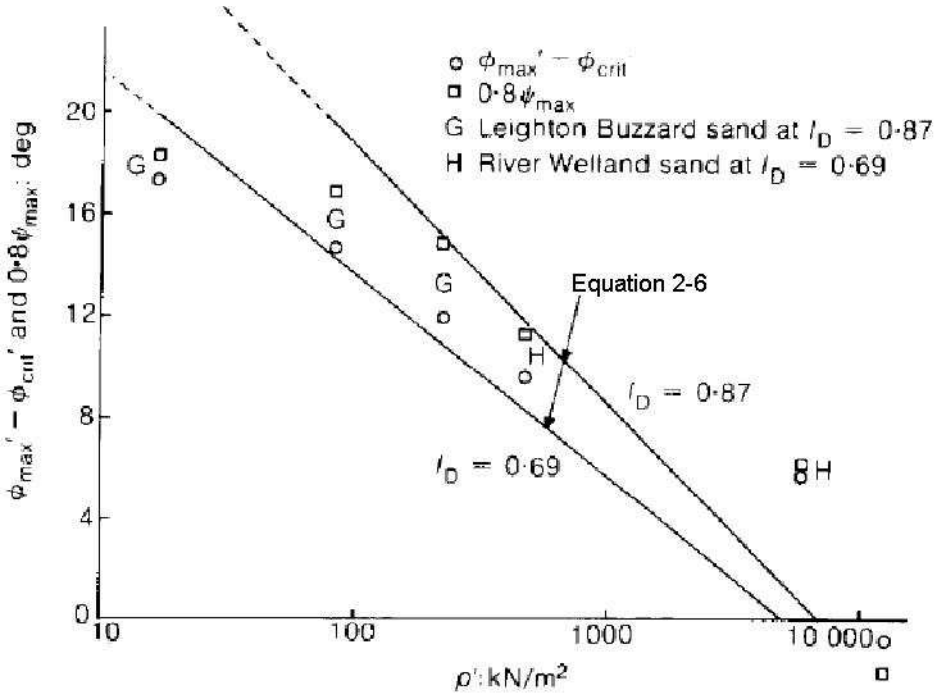

Figure 2-20: Plane strain data for sands failing at various mean effective stresses (Bolton; 1986)

Bolton (1986) suggests that Equation 2-6 is only valid for $0 < I_r < 4$ due to a lack of reliable data at low stress levels. Bolton (1987) shows for Toyoura sand (a sub-angular quartz sand, d_{50} = 0.16 mm) that at very low effective stresses ($\sigma_3' < 50$ kPa), peak friction angle and maximum dilation angle do not continue to increase with further reductions in effective stress. Fannin *et al* (2006) show that the same may be true for well-graded gravelly-sands of angular particles. This may imply that stress induced scale effects are negligible if the minor principal stress at prototype scale is less than 50 kPa, such as could be the case during offshore pipeline ploughing.

Stone and Wood (1992) suggest that the rate of change in dilation angle, ψ_{max} with the increase in I_r may reduce at these low stress levels. Stone and Wood (1992) calculate

a value of I_r = 7.1 (using Equation 2-5) for a series of faulting tests conducted at single gravity. They therefore use the limiting value of I_r = 4 to determine ψ_{max} by Equation 2-6. ψ_{max} is found it to correspond with the direction of the initial shear band observed during the tests. They do however point out that the values of normal stress and relative density which they use to calculate I_r are based on the initial at rest values which will change during the test. Applying Equation 2-5 and Equation 2-6 to the Ottawa sand (φ'_{crit} = 36º) at 0.05 kPa, a peak friction angle of 80º is found which is 10º higher than measured by Sture *et al*. (1998) during triaxial tests which also points towards there being a possible limit to the increase in dilation with reducing effective stress.

It would seem that accurate characterisation of sand at the low effective stresses applicable to reduced scale model tests would be helpful. This would allow the potential magnitude of the difference in dilation angle between reduced scale model stresses and prototype stresses to be found. If dilation angles are greater at low effective stresses the reduced scale test results could be extrapolated to full scale by comparing them with full scale tests at a greater relative density to allow ψ_{max} to be consistent between the two scales.

2.9.2. Particle size and shear band dimensions

Model tests using silts and clays at full scale stress levels (in the centrifuge) may reliably be extrapolated to full scale behaviour. Stone and Wood (1992) suggest that the same should be true for course grained materials provided they behave in a continuous fashion, where the sand will deform fairly uniformly without any large strain localisations. However due to the exceptionally large strains involved during ploughing, the soil response will inevitably involve numerous bifurcations. Therefore the ability to extrapolate full scale plough behaviour from reduced scale tests depends on a fundamental understanding of the formation and progression of shear bands. As shear band dimensions are linked with particle size, therefore particle size effects should be considered in the interpretation of model tests (Stone and Wood; 1992).

Shear bands are strain localizations which may occur due to the application of shear stress to soil, the blocks of soil on either side of the shear band tend to stay fairly

intact and move relative to each other. Oda and Kazama (1998) provide good evidence that shear bands form at around peak shear stress and that non-recoverable strain is concentrated within the shear band(s) as soon as it starts to develop.

Roscoe (1970) examined radiographs (which picked up density variations in the form of dilation bands which in turn were assumed to be shear bands) of coarse grained sand samples following simple shear tests and found the thickness of a shear band to be approximately 10 soil grains thick. Numerous researchers since then have published data that links the thickness of a shear band to the mean grain diameter, d_{50}. Mühlhaus and Vardoulakis (1987) performed biaxial tests on medium and fine grained sands and found through radiographs that the thickness of a shear band was equal to 16 times d_{50}. They also state that the thickness of a shear band varies along its length and may gradually change post failure, however Oda and Kazama (1998) point out that this change in thickness along the length of the shear band may have been caused by the edge effects at top and bottom rigid platens. Finno *et al*. (1997) performed plane strain tests on fine grained sand in a loose state and found dilation bands to form and band thickness varied from 10 to 25 times the mean grain diameter. Table 2-4, extracted from Wood (2002) shows experimentally derived values of shear band thickness for a range of mean particle diameters by various researchers. Wood (2002) states that the tests reffered to in Table 2-4 were conducted on poorly graded sand where d_{50} was a good measure of the size of the majority of grains and that tests on well graded sands may not yield entirely similar results.

Table 2-4: Radiographic observations of shear band thickness (Wood; 2002)

Test type	Sand grading	Particle size d_{50} (mm)	Rupture thickness t_z (mm)	t_z/d_{50}	Reference
Long shear box	100/170	0.12	1.7	14.2	Hartley (1982)
	30/52	0.40	3.8	9.5	
	14/25	0.90	9.0	10.0	
Long shear box	30/52	0.40	Up to 5.5	Up to 13.75	Scarpelli (1981)
Rotating blade	25/52	0.4	4–5	10–12.5	Stone (1985)
	14/25	0.85	9–15	10.5–17.6	
	7/14	1.5	11–20	7.3–13.3	
Biaxial test	Fine	0.2	3.7	18.5	Mühlhaus and Vardoulakis (1987)
	Medium	0.33	4.3	13	

As previously stated pipeline ploughs typically form trenches around 2 m deep in the sea bed. A 50th scale model plough would therefore create a trench of around 40 mm deep. Model tests in sand of d_{50} = 0.2 mm would give rise to shear bands 2 mm thick which is 1/20th the depth of the plough. Their thickness in relation to plough dimensions may be considered small enough to be negligible.

The near tip domain at the leading end of a shear band is the length over which the values of ψ drop from a maximum at the leading tip towards zero at critical state away from the tip (Figure 2-21).

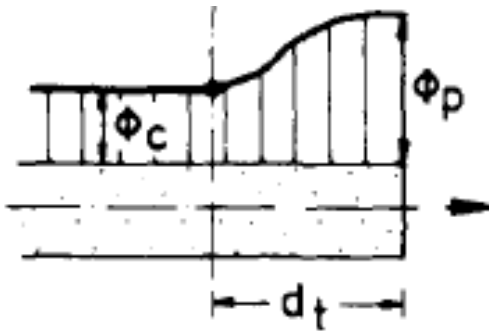

Figure 2-21: Shear band including the change in φ' along its length (Vardoulakis *et al.*; 1981)

Vardoulakis *et al*. (1981) conducted active and passive trapdoor tests in medium grained Karlsruhe sand. They found the near tip domain to be less than 40 mm. Stone and Wood (1992) suggest that this length is related to particle size and from rotating blade experiments find the near tip domain to be around 176 d_{50}. They show that this is consistent with Vardoulakis *et al*. (1981) who show a near tip domain for 0.33 mm Karlsruhe sand to be 40 mm which is equivalent to 121 d_{50}.

A potential scaling issue may arise if the same material is used during reduced scale model tests as for prototype scale since the reduced length of the shear plane at model scale will mean a higher proportion of the shear plane will be composed of the tip with associated increased friction angle (Wood; 2002). Scaling of results could then cause an over estimation of forces.

A 50th scale model plough is trenching at 40 mm depth. The major principal stress is in the horizontal direction and therefore shear planes may be expected to rise from the plough at 45º-φ'/2 from the horizontal. For a friction angle of 30º this would result in

a shear plane of around 80 mm long. Assuming the length of the near tip domain is 176 d_{50} and considering a sand of d_{50} = 0.2 mm the near tip domain could be expected to extend as far as 36 mm which is a significant proportion of the length of the shear band and scaling effects may arise as a consequence. This implies that reducing the particle size of the soil by the model scale factor may provide more accurate results, as post peak softening will be closer to full scale. The resulting reduction in particle size would likely change the soils response to loading. An associated reduction the soil's permeability would occur which is necessary to match to full scale to observe realistic rate effects. Particle sizes should therefore not be scaled during reduced scale model tests.

2.9.3. Scaling rate effects

Palmer (1999) suggests that due to the reduced length of drainage paths and volumes of sheared sand when dealing with model scale when compared with full scale ploughing, greater speeds may be required at model scale to achieve the same proportion of draft increase as for full scale. Through dimensional analysis he found that if model scale plough behaviour is to be compared to that of full scale ploughs cutting the same soil of the exact same conditions, then the velocity × depth of the model should be the same as for the full scale plough. Bransby *et al*. (2005) and Brown *et al.* (2006) conducted 1/50th scale model plough tests in saturated sand at 1g and found their results to compare best with full scale ploughing where model velocity equalled that of the full scale plough. Palmer (1999) assumed continuum behaviour (i.e. no shear banding) of the sand in his dimensional analysis which may account for the difference between his findings and those of Bransby *et al*. (2005) since there is already a hidden scale factor in shear band thickness.

It is clear that the normal effective stress changes produced during model ploughing at 50th scale are less than during prototype scale ploughing. This will increase the velocity during scale model tests at which dilation suppression affects the rate effect and it is likely that the dilation limit will never be reached during the model ploughing tests. This should not cause any scaling issues as the dilation limit is likely never reached during the field as there are no recorded cases evidencing its occurrence.

2.10. *Important findings and areas for further investigation*

This review of previous ploughing research can be summarised as follows:

1. The general mechanics of plough stability appear to be well understood.

2. Numerous researchers have performed ploughing-like tests using simple cutting tools, the results of which may have influenced the design of the share of a modern pipeline plough.

3. Current performance predictions appear to be based on the Cathie and Wintgens (2001) model.

4. Either verification of existing coefficients C_w, C_s and C_d or proposal of new coefficients would seem to be of use to pipeline ploughing contractors. Accuracy of the Cathie and Wintgens (2001) model would be greatly increased if a controlled set of laboratory tests were used to provide values for the three coefficients. This is because control of sand density and particle size allows isolation of the two parameters and their effect on the three coefficients and also the model as a whole.

5. As performance predictions are made based on the unit weight, friction angle, interface angle, relative density and D_{10} (permeability) of the soil, the industry would benefit from a more accurate method of sand characterisation which is just as quick and efficient as current practice.

6. Innovations in ploughing which appear to be in their infancy (i.e. jet assisted ploughing and share track) are potentially worth investigation.

7. Interpretation of reduced scale model ploughing results must take into account the issues highlighted in section 2.9 if they are to be extrapolated to full scale.

8. As rate effects are dependent on permeability and relative density, selection of appropriate materials to test in will be informed by the most problematic conditions pipeline trenching contractors meet, namely dense, fine sands.

Chapter 3. Methodology

3.1. *Introduction*

Reduced scale ploughing tests were conducted in order to study the behaviour of offshore pipeline ploughs under controlled laboratory conditions. Reduced scale ploughs were designed and manufactured as were two soil tanks with associated testing equipment. Two different types of ploughing arrangements were used. The first was the towed test which was designed to emulate offshore ploughing and the second was the fixed ploughing test which involved forcing the plough through the test bed at a predetermined pitch and depth. The towed ploughing tests alone allow insight into how different parameters influence plough performance. The objective of the fixed ploughing tests was to try and break down the components of force acting on the plough during trenching, thus providing more detailed and fundamental information on the mechanics of ploughing.

In addition to the two arrangements involving accurately designed and manufactured model ploughs, plane strain tests involving simple triangular prisms which represented the plough's share were conducted. Standard materials tests were also undertaken which included: the constant head test to derive permeability and direct shear testing to determine soil frictional behaviour. Material properties could then be related to plough behaviour and ultimately used in a performance prediction method.

3.2. *Reduced scale model ploughs*

Simplified, reduced scale models based on the full scale CTC advanced pipeline plough (APP) were used to perform various ploughing tests. The APP weighs around 190 tonnes is 17.5 m long, 10 m wide and 8.5 m high. It has the capacity to lay pipelines of up to 1200 mm in diameter at a depth of 1.8 m at the invert, in a single pass, which can be increased to 2.5 m by a second pass. The APP is stable up to velocities of 500 m/h and at pitches up to 6º. It features buoyancy tanks of 90 tonne uplift capacity which allow the submerged plough weight to be reduced both in soft soils to prevent sinking and to reduce tow forces. One of the attributes of the APP (although not exclusive to it) is its forecutter which sits ahead of the main share and is

designed to reduce tow forces. The affect of the forecutter on plough performance is however not well understood.

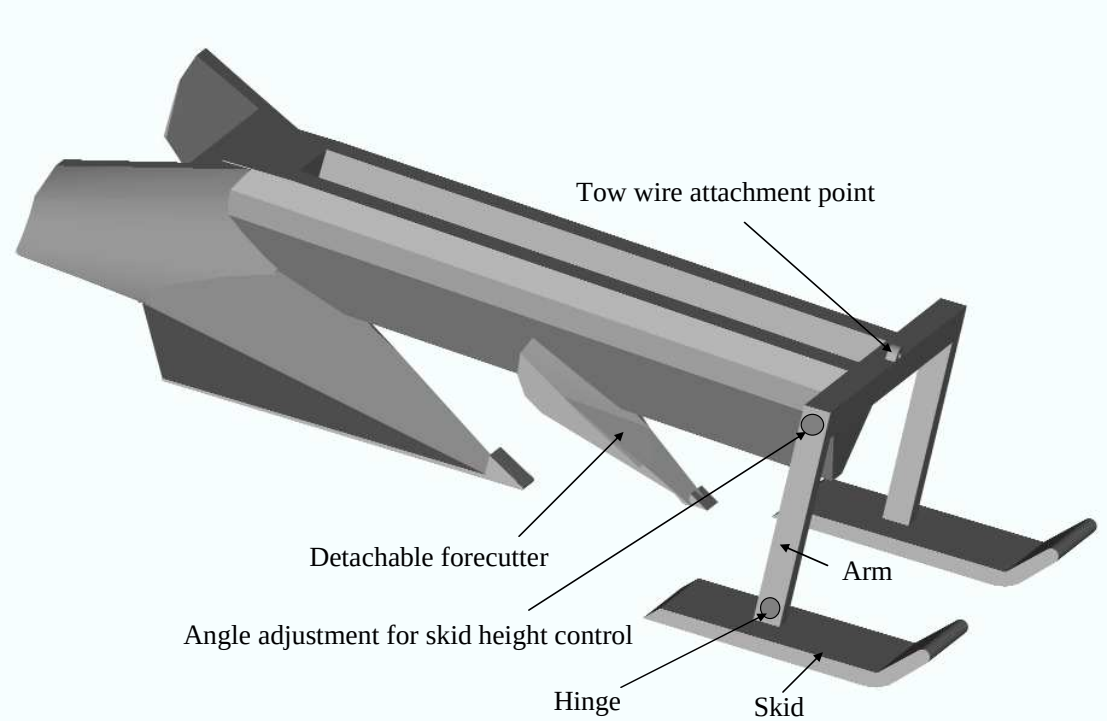

Figure 3-1: Schematic of simplified APP for model manufacture

Autocad drawings of the APP were provided courtesy of CTC Marine Projects Ltd, Darlington, England. These were simplified by removing much of the infrastructure, such as hydraulics, pipeline grabs, buoyancy tanks and surveillance equipment which were not required for the model tests and that made fabrication of the models simpler. Figure 3-1 shows a 3 dimensional simplified drawing of the APP. Houstons of Coupar was selected to manufacture the scale model ploughs and minor modifications were made at the University of Dundee.

Table 3-1: Numbered skid settings and resulting typical plough depth at 50th scale

Skid setting	Arm angle, β (º)	Resulting plough depth, D (mm)
1	67	19
2	50	26
3	44	30
4	30	36
5	17	41

Scale models were made at 50th, 25th and 10th scale and each had the capability of depth control via skid height control. The scale models were manufactured lighter than their required scale weight and ballast was added to provide the correct weight. Expected plough depths at 50th scale for a range of skid settings are shown in Table 3-1 where arm angle is the angle between the arm and the heel of the share.

A hinge between the skids and arms of the plough allow the skids to remain in contact with and parallel to the soil's surface as the plough's pitch changes. The forecutter was made as a separate removable piece which bolted onto the beam of each model. This allowed the forecutter's effect on plough performance to be studied in detail, which is not practical in the field. Figure 3-2 shows the 50th scale and 10th scale model ploughs.

Figure 3-2: 50th and 10th scale model pipeline ploughs with thesis author for scale

The 50th scale plough was easy to handle as its mass was only 1.6 kg and was 250 mm long with the capacity to form a trench 36 mm deep. The 10th scale plough by

comparison weighed 200 kg and was 1.25 m long with the capacity to cut a 180 mm deep trench. This is because the scaling laws shown in Table 2-3 were used to scale both the mass and length of the model ploughs. The majority of the ploughing tests were therefore carried out using the 50th scale plough: with a small number of tests carried out using the 25th and 10th scale ploughs to investigate scaling issues.

3.3. *50th scale ploughing methodology*

3.3.1. Rationale behind tests

50th scale ploughing tests were conducted to provide a large data set to form a parametric study. This was possible because the small size of the tests made them reasonably quick and easy to set up and conduct. Relative density, permeability, ploughing depth and the presence of a forecutter were investigated and their affect on tow force and plough pitch and resulting trench depth and shape examined.

3.3.2. Apparatus and experimental setup

The apparatus and experimental setup used to conduct the 50th scale ploughing tests was influenced by previous research conducted at the University of Dundee. The test tank was 2 m long, 500 mm wide and 400 mm deep and was used previously for the pipeline ploughing work of Bransby *et al*. (2005) and Brown *et al*. (2006).

Figure 3-3 shows the experimental setup used by Brown *et al*. (2006) for their ploughing tests. A high torque 12v DC, geared electric motor with a 40 mm diameter winding reel was used to create a winch and provide linear actuation for the plough. A motor controller was used for speed control. The winch was mounted to a supporting frame (above the starting position of the plough) which surrounded the tank and the tow wire was passed through a pulley at the far end of the tank and back towards the plough. The tow wire was passed through an eye at the front of the plough and connected to a load cell located at the plough's centre of mass, which was used to measure the required tow force to pull the plough. A draw wire displacement transducer (DWT) mounted above the sand bed was connected to the plough and used

to measure its horizontal translation. The plough depth was inferred by post test trench depth measurement.

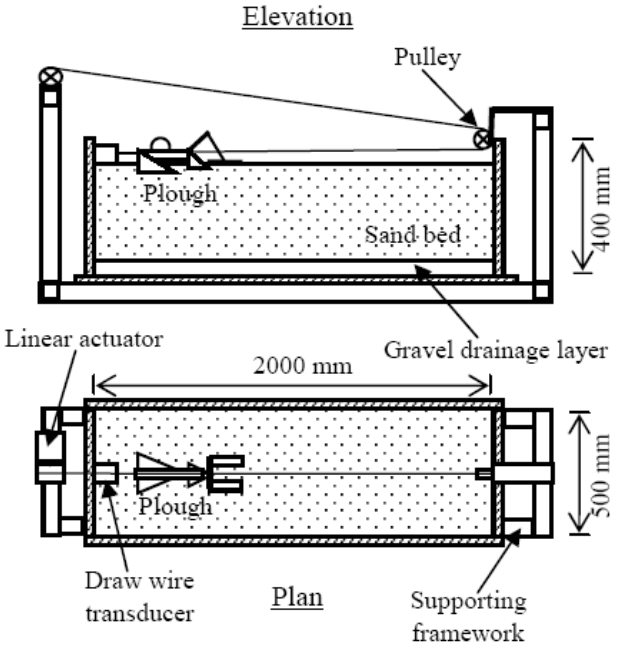

Figure 3-3: Schematic of 1/50th scale experimental setup (Brown *et al.*; 2006)

Figure 3-4 shows the improved experimental setup developed for the 50th scale ploughing tests conducted as part of the current study. The plough is connected via a tow line to a load cell, which is mounted on a trolley that is free to translate horizontally along tracks on top of the test tank. A motor and winch arrangement is used to actuate the trolley at a constant velocity. During the tests of Brown *et al.* (2006) the tow angle increased as the plough moved closer to the pulley at the far end of the tank.

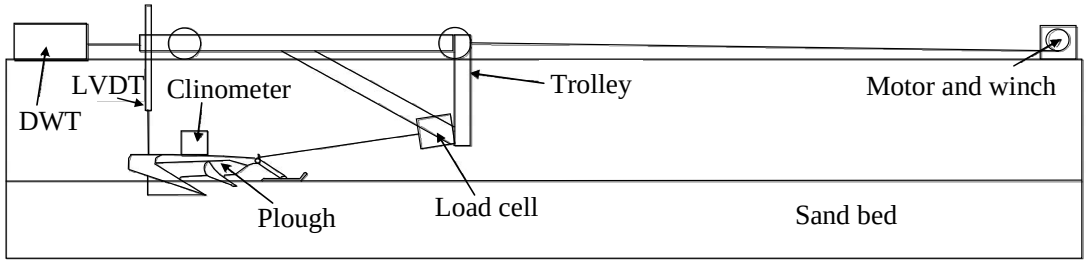

Figure 3-4: 50th scale apparatus and experimental setup

The improved setup (Figure 3-4) allows the tow angle to remain constant throughout the test and provides a reference platform for continuous measurement of plough

depth during testing. This also provides a better representation of a support vessel towing a plough in constant depth water. The draw wire transducer applies a constant load to whatever it is attached to, which in the case of Brown *et al*. (2006) was the plough and their load cell readings therefore had to be corrected for this. The load from the DWT would also alter plough kinematics as it applied a force to a different point of the plough from the sand and could not be corrected for. In the setup shown in Figure 3-4 the DWT is connected to the trolley and therefore does not form part of the load chain nor does it alter plough kinematics.

A slot pluviator (Figure 3-5) was designed to prepare the test beds as the Brown *et al.* (2006) had prepared test beds by pluviation through a mesh which was hard to attain consistent density throughout the sample. The pluviator was 540 mm wide which allowed a sand curtain to fall the full width of the tank during pluviation. The hopper had an internal volume of 0.033 m^3 which allowed around 60 kg of sand to be filled into it. The test bed was usually between 100-150 mm deep which would require 3-5 hopper loads. This depth was chosen as it was great enough to prevent any boundary effects due to the rigid base of the tank but still allowed for a water depth of 100-150 mm above the surface of the sand during the saturated tests ensuring the plough was fully submerged.

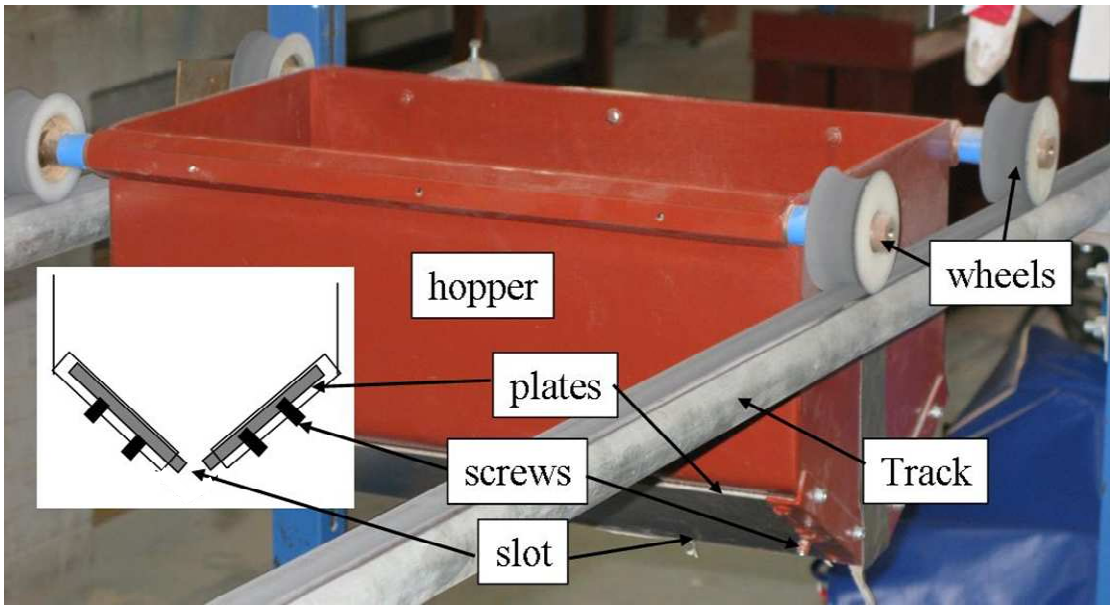

Figure 3-5: Slot pluviator for preparing test beds for the 50th scale ploughing tests. Inset schematic showing cross section through pluviator

The pluviator was mounted on four wheels which ran along two tracks, one either side of the tank. The tracks could be raised and lowered on the supporting frame and a fall height greater than 800 mm was typically maintained, which allowed the sand particles to reach terminal velocity. The slot width could be varied by sliding the plates up and down the inclined sides of the hopper and each was secured in position by four screws. Typical slot widths used were 0.5-4 mm, with relative density increasing with reducing slot width and associated flow rate. The relative density of the sand was sensitive to the speed the pluviator was moved back and forth along the rails at. This was done manually at around 150 mm/s.

The relative density of pluviated sand increases with the energy applied by the sand falling from the pluviator to the surface layers of sand which have already landed. This energy increases with reducing intensity of deposition rate and is often controlled by fall height, slot width or hopper displacement rate. Figure 3-6 shows how the relative density of a test bed can be controlled by the width of the slot and by the displacement rate of the pluviator.

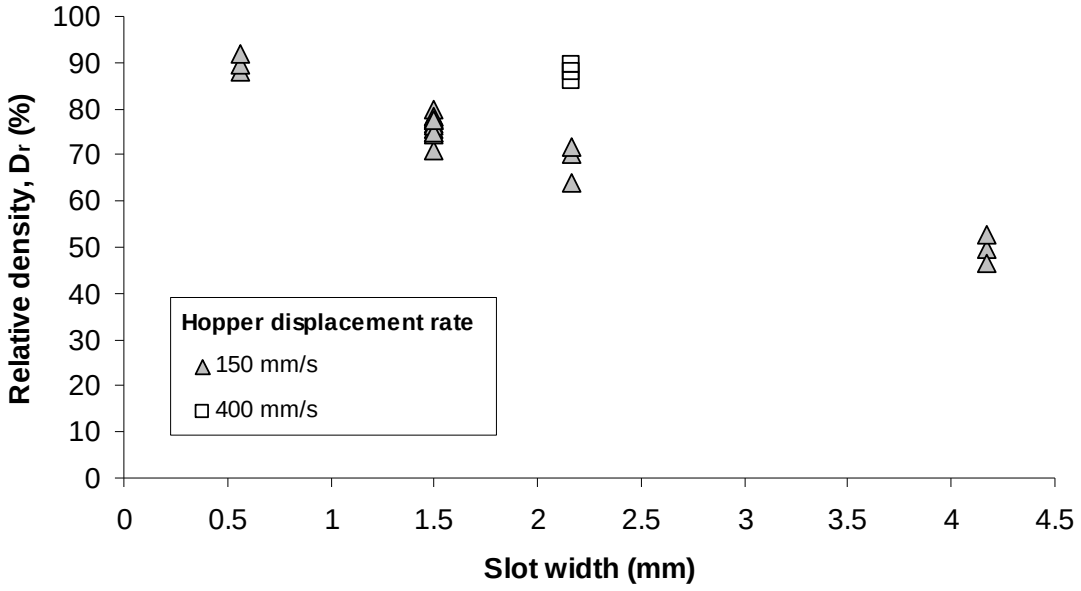

Figure 3-6: The relationship between relative density and slot width for fine silica sand (HST95), with the fall height of the sand kept above 800 mm to ensure terminal velocity of the sand particles is reached

3.3.3. Plough and sand bed instrumentation

The 200 mm stroke, linear variable differential transformer (LVDT) at the back of the trolley (Figure 3-4) was used to measure the plough depth during a test, which is another improvement over the Brown *et al*. (2006) setup. It was also used to measure the sand level prior to ploughing and the trench depth post ploughing. The (RDP) draw wire transducer (DWT) had a 2 m long cable and was used to measure the position of the LVDT during the ploughing tests. A Schaevitz Accustar electronic clinometer mounted to the beam of the plough measured the plough's pitch. The tow force during ploughing was measured using a 20 kg, RLT tension load cell mounted to the trolley and connected to the plough via a tow line. During some of the tests two mini Druck, PDCR81 pore pressure transducers were inserted into the sand beneath share depth and along the centreline of the where the plough would travel. This provided information about how the reduction in pore water pressure was influencd by plough velocity and on the special variation of pore water pressure around the share. Further information on the tests which featured pore water pressure transducers is described in Section 5.2.8. All instruments were logged on a 16 bit, National Instruments card, NI USB-6211 at typical logging rates of 1 sample per second. The logging device was capable of logging up to 8 differential analogue input channels at once. The logger had a built in amplifier whereby the gain is determined by the input range, which is helpful when logging small signal devices such as the load cells and pore pressure transducers. The software used to log the data was National Instruments LabVIEW version 8.2 graphical programming environment.

3.3.4. Test preparation

The test tank contained a 30 mm thick, fine to medium gravel base layer which was used during the saturation of the sand prior to saturated tests. The gravel was covered by a porous membrane to prevent sand mixing with it. The ploughing tests conducted in dense sand were prepared by dry pluviation using the purpose built slot pluviater (Figure 3-5) described above. Once in place the sand was carefully levelled by scraping the surface with a flat edge. Saturated tests then required the addition of water which was done via a hose connected to the bottom of the tank. Water would

flow through the gravel layer from the bottom up until at a depth of around 100 mm above the surface of the sand to ensure the plough was fully submerged during testing.

Although the width of the slot on the pluviator could be altered to change the flow rate of the sand and resulting density of the sand bed attaining a relative density of below around 50% was not possible. In order to achieve the very loose sand beds, sand was carefully poured through a funnel with its tip very close to the sand's surface so that the sand was carefully placed. The resulting bed was then levelled and saturated in the same manner as for the pluviated beds.

It was found that stirring the saturated HST95 produced beds of around 53% relative density which was independent of the sand's initial density. The sand was then levelled using the same method as mentioned above. This preparation allowed multiple tests to be conducted in a day whereas the other methods only allowed 1 test per day. This is because pluviation and saturation prior to testing were not required and neither was draining of the water and emptying of the sand post test. It also reduced the amount of sand which needed to be dried per test and so saved many hours labour in the laboratory. Ploughing tests in dry sand were also conducted in dry stirred test beds however it was found that dry stirring gave a relative density of 17% which was less than attained by saturated stirring. This may be due to the difference in sand weight in water and air.

3.3.5. Test procedure

Prior to each test the depth to the sand surface was measured from the reference trolley along the length of the tank. This was done by attaching a sled to the trolley via a tow line and placing it on the surface of the sand. The shaft of the LVDT was then dropped onto the sled and the DWT attached to the trolley. The logging equipment was then started and the motor switched on and the depth to the sand along the centreline of the tank was measured.

The plough was then placed onto the sand, aligned with and connected to the tow wire. The shaft of LVDT was subsequently lowered onto the beam of the plough in the position shown in Figure 3-4. The instrumentation was then checked and the

motor started to translate the trolley system and plough. The logging system was started at the same time as the motor. Once the trolley reached the end of the tank the motor and the logging programme were stopped.

The depth of the excavated trench was measured along the length of the tank which allowed trench development to be examined. Trench cross sections (including spoil heaps) were measured at 1000 mm and 1200 mm from the inside face of the tank closest to where the plough started. This provided trench profiles at plough displacements which gave steady state conditions (see section 4.2.1 for a description of steady state). The sand was cleaned out of the tank after each test and air dried for future use.

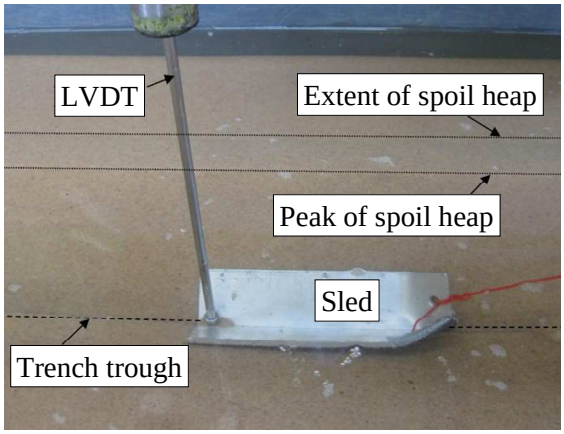

Figure 3-7: Continuous measurement of trench depth (shown submerged)

Figure 3-7 shows the LVDT attached to an aluminium sled which was placed in the trench and pulled along its length so that the depth could be measured. If the whole of the base of the sled was in contact with the trench then the measured depth at any instant was the minimum depth under the sled. The sled was designed so that its sides rested against the side walls of the trench as it was pulled forwards. The LVDT was attached to the back of the sled which allowed the sled to tilt upwards towards the towline with its rear end in contact with the sand. This meant that the recorded trench depth at any instant was more accurate than if the whole of the sled was in contact with the sand.

3.3.6. 1/50 scale experimental programme

The dry ploughing test programme outlined in Table 3-2 involved 45 tests. It was devised in order to find how plough depth, relative density and the presence of a forecutter affect non-rate dependant tow forces resulting during ploughing. The tests were conducted in two different sands HST95 and HST50, the respective characteristics of which and of a third sand (Redhill 110) used during the saturated tests are shown in section 3.7. Dry ploughing tests were unaffected by ploughing rate and all tests reported were conducted at roughly 50 m/h. Plough depth is the average steady state depth of the plough's heel relative to the original ground level. Within each test series, shown in Table 3-2 different skid settings are used for each test to provide a relationship between plough depth and the resulting tow force and plough pitch in each of the four sand conditions. Each individual test has its own steady state plough depth resulting from the skid setting used during the test and the moment equilibrium of the forces acting on the plough.

Table 3-2: Summary of dry 50th scale test programme

D_r (%)	Number of tests	Forecutter present	Sand type	Skid setting	Plough depth (mm)
90	5	Yes	HST50	5	38.0
				4	35.5
				3	27.4
				2	25.0
				1	20.6
90	4	No	HST50	5	40.0
				4	25.0
				3	28.6
				1	17.5
25	9	Yes	HST50	5	40.7
				5	39.3
				4	34.0
				3	30.4
				3	29.8
				3	29.5
				2	26.3
				1	21.0

				1	17.9
25	8	No	HST50	5	42.0
				4	34.5
				4	32.5
				3	30.6
				3	28.0
				2	27.0
				1	18.2
				1	17.9
75	3	Yes	HST95	5	39.5
				4	34.0
				2	25.3
75	3	No	HST95	5	38.7
				4	33.1
				2	25.7
17	5	Yes	HST95	5	41.0
				5	40.3
				4	35.3
				3	29.6
				2	25.8
17	8	No	HST95	5	41.4
				5	41.1
				4	36.1
				4	35.7
				3	30.0
				2	27.0
				2	25.7
				1	19.1

The saturated 50th scale ploughing test programme involved 119 tests and was devised to provide information on how the plough behaved at different depths and under various sand conditions, with a focus on the rate dependant component of ploughing. A summary of the saturated tests conducted are outlined in Table 3-3. Each test was conducted at a single plough velocity and the range of velocities column in Table 3-3 shows the maximum and minimum velocity that tests were conducted at for each test series. The tests within each series were intended to be conducted at the same plough

depth however, there was some variability within each series and the value stated in Table 3-3 the average steady state value of the series.

Table 3-3: Summary of saturated 50th scale plough test programme

D_r (%)	Number of tests	Forecutter present	Range of velocities (m/h)	Sand type	Skid setting	Plough depth (mm)
75	9	No	36-472	HST95	1	40
75	8	Yes	24-940	HST95	1	39
53	14	No	29-383	HST95	1	39
53	11	Yes	30-326	HST95	1	37
0	3	No	41-191	HST95	1	43
0	3	Yes	40-191	HST95	1	41
53	9	No	21-190	HST95	2	34
53	10	Yes	31-189	HST95	2	31
0	3	No	60-192	HST95	2	38
53	9	No	13-197	HST95	3	28
90	7	Yes	10-175	HST50	1	36
90	6	No	12-183	HST50	1	36
61	8	Yes	19-180	HST50	1	38
61	8	No	18-187	HST50	1	39
45	7	No	26-187	Redhill 110	1	39

3.4. *Fixed ploughing tests*

The fixed ploughing tests were devised in order to gain more information about how the plough attracted sand reaction forces and find their direction and magnitude. Fixed tests also allowed the plough to be placed at specific depth and pitch conditions and maintain these throughout the test rather than relying on skid settings and moment equilibrium. The volume of sand used in a fixed test could be reduced as the transition length is smaller than for a towed test with stability maintained through rigid supports and not the long beam principle (see Chapter 2).

3.4.1. Fixed test rationale

The underlying principle behind the fixed tests was that the interaction between the share and the sand is exactly the same for a fixed test as during a towed test. There is a clear difference in that the plough is supported by the sand beneath the heel and the skids during a towed test whereas it is supported by a trolley during a fixed test. If the correct depth and pitch are matched for the sand conditions that would be expected during normal ploughing then there should be no difference in the measured tow force between the tests.

3.4.2. Development of the fixed test

The first fixed tests were conducted using a 50th scale plough in dry sand. The plough was mounted to two load cells which were in turn mounted to the end of a 500 mm stroke screw jack actuator (see Figure 3-8).

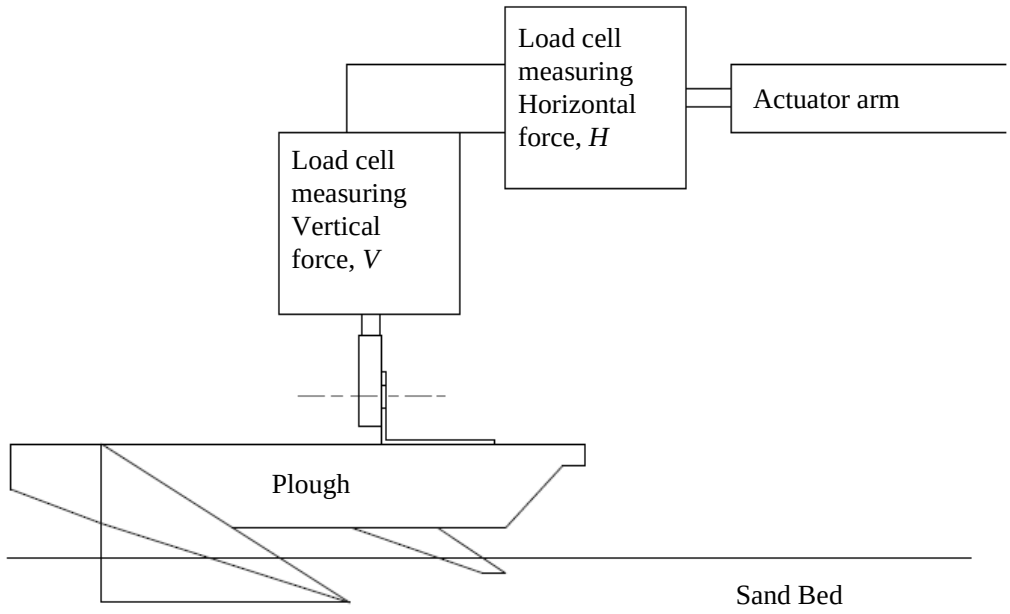

Figure 3-8: Mounting arrangement for initial fixed test apparatus

A series of tests was performed in HST95 Congleton sand at a relative density of 17% at a range of plough depths from 7-37 mm and at four different pitches from -3.5º to 1.5º. Negative values of pitch indicate forward pitching whereas positive angles indicate aft pitching of the plough. The four pitches investigated are shown in Figure

3-9 below. Pitches of -1.5º, 0º and 1.5º were chosen as they are typical of actual offshore pipeline plough pitches, the tests conducted at -3.5º were chosen to see if the heel reaction could be reduced to a negligible value and also represents a possible but more extreme offshore plough pitch. The plough depth, D is the depth from the original ground level to the back of the heel and is defined in Figure 3-9.

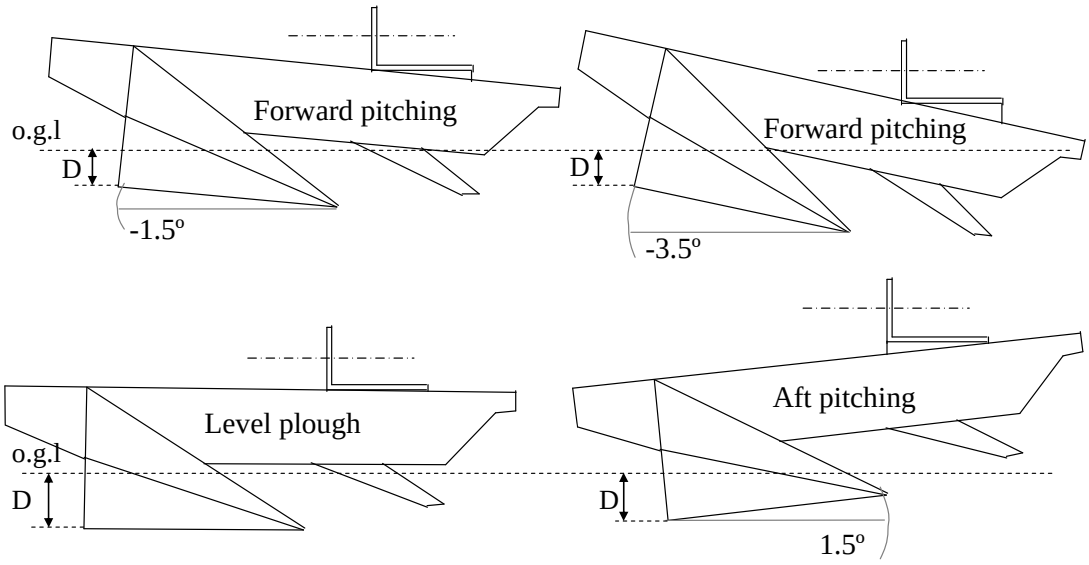

Figure 3-9: Schematic showing plough pitches investigated during initial fixed tests

The test programme of the preliminary fixed tests is shown in Table 3-4.

Table 3-4: Test programme for the preliminary fixed tests conducted in loose dry HST95 with a 50th scale plough

Pitch, θ (º)	1.5	0	-1.5	-3.5
Depth, D (mm)	12	10	7	8
	18	11	11	13
	20	17	17	14
	24	20	19	15
	29	24	19	16
	29	28	22	16
	37		25	

Some of the results from the preliminary fixed ploughing tests are shown in Figure 3-10. Negative values of force mean tension in the load cell and positive values show compression.

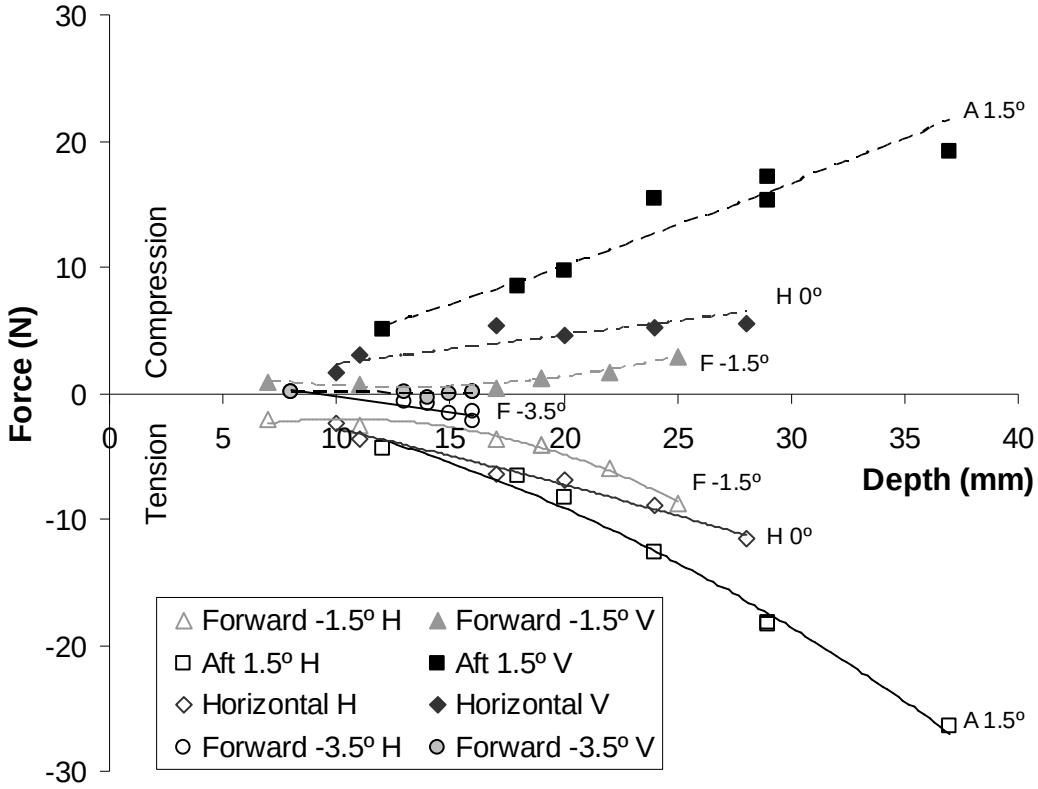

Figure 3-10: Steady state horizontal and vertical forces produced during 50th scale fixed ploughing tests in dry, fine, silica sand (HST95) at D_r = 17%

Tow forces were extracted from the horizontal forces, *H* and vertical forces, *V* by means of Equation 3-1.

$$F = H + \tan\delta \times (W - V) \tag{3-1}$$

Where, *F* is the tow force derived from fixed ploughing tests, *H* is the force measured in the horizontal load cell, *V* is the force measured in the vertical load cell, *W* is the weight of the plough and δ is the interface friction angle between the plough and HST95 (δ = 24º).

Equation 3-1 accounts for the fact that during the fixed tests the plough is supported not by the sand but by the arm of the actuator. In Figure 3-11 tow forces derived from fixed tests using the 50th scale plough by Equation 3-1 are compared to tow forces measured during towed/pull tests with the same plough.

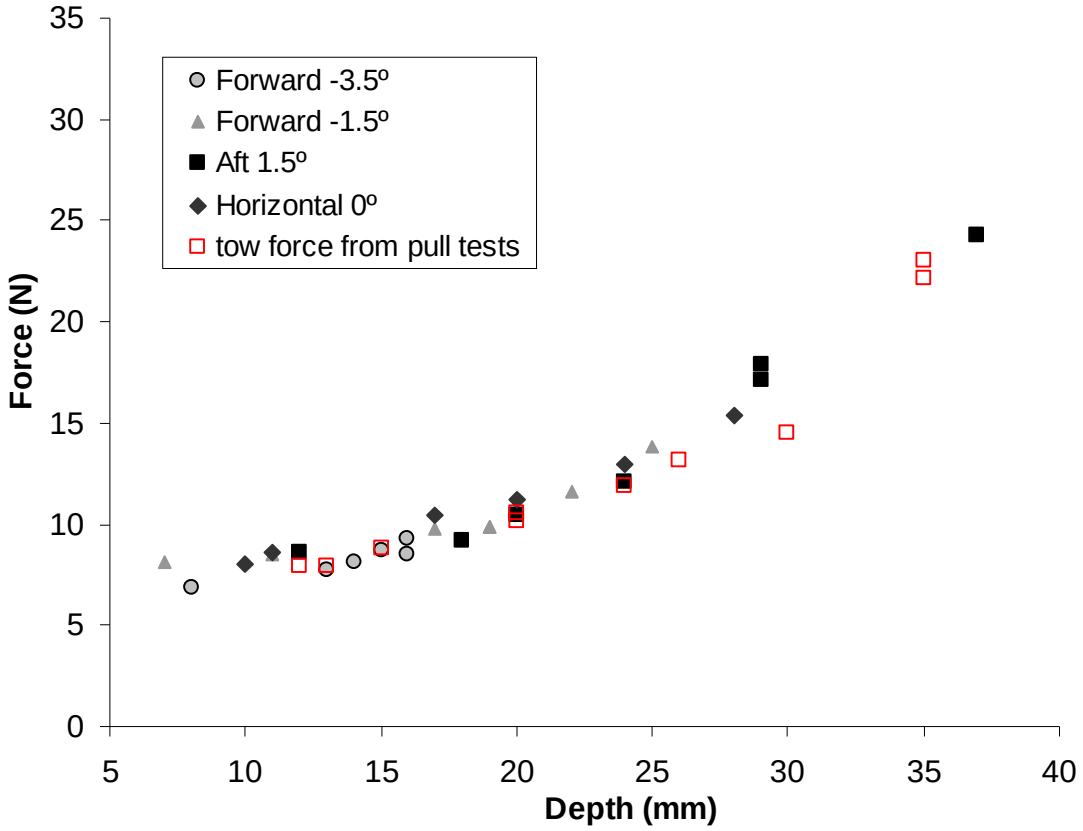

Figure 3-11: Steady state tow forces derived from fixed test data and compared to ploughing tests. All tests were conducted in loose, dry, fine silica sand (HST95)

Figure 3-11 presents the tow force derived from the fixed test results and the tow force measured during ploughing tests. During the towed tests the pitch of the plough reduced with plough depth so that the shallow tests had a positive pitch (2º at D = 15 mm) and the deepest tests had a negative pitch (-0.5º at D = 40 mm). Although the sand reaction beneath the share is strongly influenced by the pitch of the plough, Equation 3-1 corrects for this and fixed tests conducted at the same depth but at different pitches compare well. The fixed tests compare well with the pull tests which gives encouragement to the fixed test concept.

3.4.3. Fixed test apparatus

Based on the experience gained during the initial 1/50th scale fixed test trials a large (2.5 m×1.5 m×0.75 m) steel tank was constructed specifically for 1/25th and 1/10th fixed tests (Figure 3-12). A square hollow section (Celsius 355 80×80×4 SHS) was mounted at each corner of the box to a height of 1m above the top of the tank. These sections were used to support two 3 m long Celsius 355 100×60×5 RHS sections which spanned the length of the tank above each side.

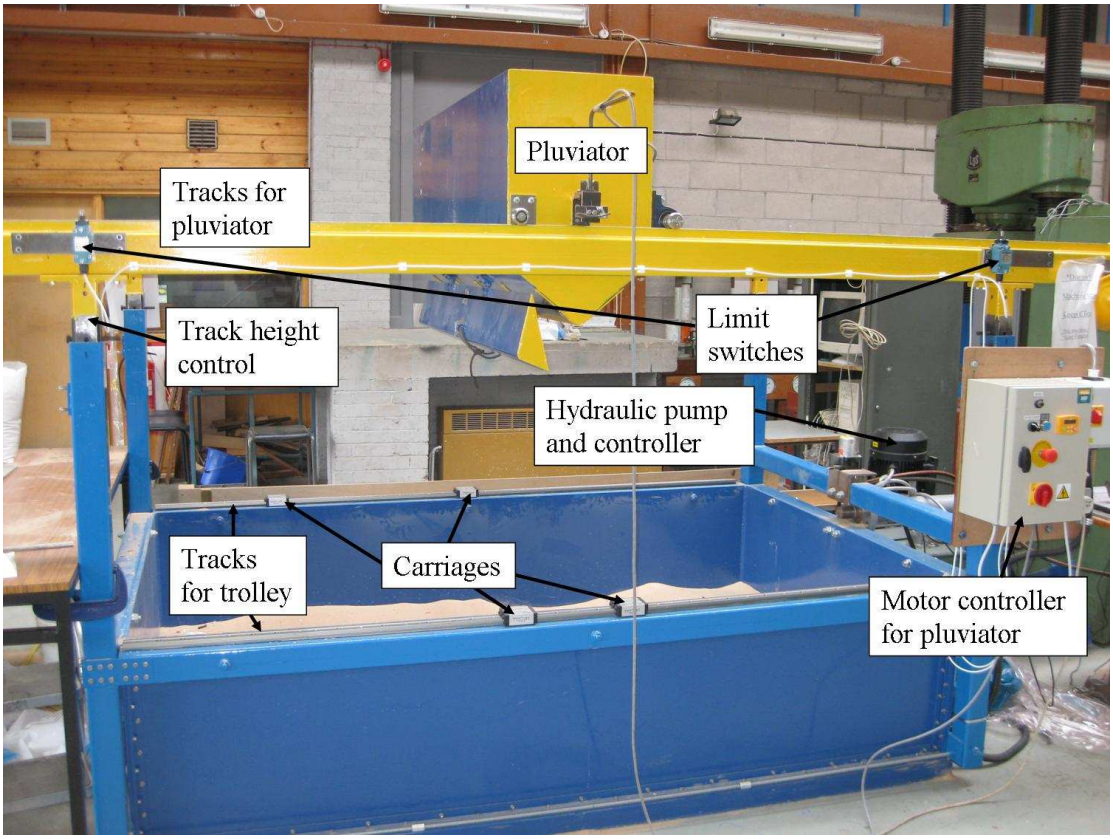

Figure 3-12: Fixed test apparatus used for 25th and 10th scale tests

The beams supported rails on which a pluviator designed to pour sand into the tank could run. The beams had 500 mm height adjustment which was designed to allow the distance between the sand and the pluviator to be kept constant as the sand height increased during pouring. A trolley system was used for supporting the plough during testing. This consisted of two universal beams 127×76×13 kg/m running parallel to each other separated by a distance of 0.3 m spanning the width of the tank and mounted on four independent carriages with dry linear bearings running on tracks. Two of the carriages were mounted on each track, one at either side of the box. This

arrangement supported an L-frame to which the plough was mounted (Figure 3-13). A 2 m long, 80 mm bore, hydraulic cylinder was mounted on the back end of the tank and used to actuate the trolley system.

The pluviator took the basic shape of the one designed for the 50th scale tests however some improvements were made in the design of the pluviator for the 25th and 10th scale test tank. These were necessary due to the large size and mass of the pluviator making the pluviator it harder to operate. An AC motor mounted to the front face of the pluviator drove a pair of wheels on the tracks, which ensured a constant velocity was maintained during pluviation. The pluviator would travel from one end of the tank to the other, tripping a limit switch at each end which changed the direction of the motor and thus the pluviator. A relative density of 75% was achieved in HST95 when using the pluviator with a 2 mm slot fitting, travelling at a velocity of 100 mm/s, at a height of 800 mm above the sand bed. Different gauged slot attachments allowed a change in the flow rate of the sand during pluviation which provided density control. The velocity of the motor could also be increased or reduced with a view to increasing or reducing respectively the relative density of the pluviated sand, however unless fairly slow velocities were used the sand bed would be unacceptably uneven and so this control was not an option.

3.4.4. Fixed test instrumentation

This fixed tests arrangement shown in Figure 3-8 was superseded by that shown in Figure 3-13 with three main developments. The pinned joints prevent moment being applied to the load cells during testing which may possibly cause spurious load readings. The loading frame is now far more rigid as are the attachments to the plough reducing any flexibility in the system. This new arrangement was designed to provide three components of force, including the horizontal and vertical components of the resulting force and the position at which that force acted on the plough.

The instrumentation used during the fixed ploughing tests consisted of a draw wire transducer which provided the position and checked the velocity of the plough, a clinometer which measured the plough's pitch to check that it was constant and three loadcells arranged as shown in Figure 3-13. The load cell marked as *H* in Figure 3-13

records the force in the horizontal direction and is of 500 N in capacity, while the vertical forces, V_f and V_b were measured using 200 N load cells. The moment acting on the plough about the share tip can be resolved by Equation 3-2.

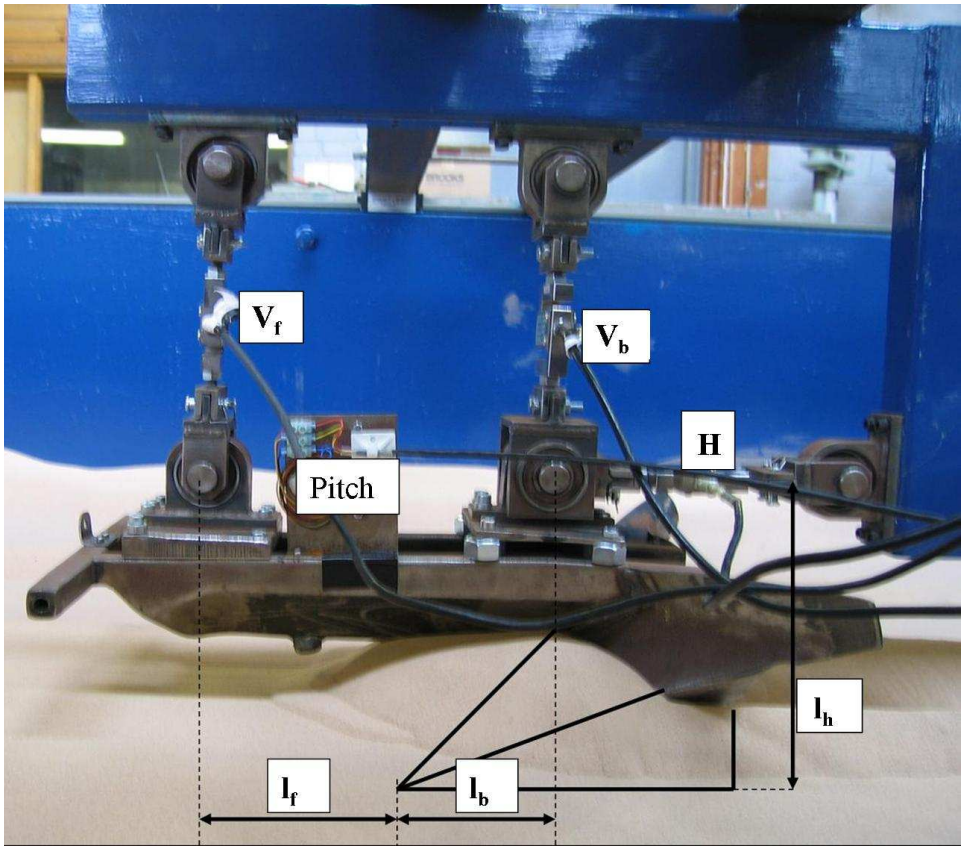

Figure 3-13: Load cell arrangement for fixed ploughing tests

$$M = V_b \times l_b - V_f \times l_f - H \times l_h \quad (3\text{-}2)$$

3.4.5. Validation of the fixed test load cell arrangement

To ensure that the load cell arrangement gave accurate readings of the force applied to the plough during the fixed ploughing tests validation tests were conducted. Figure 3-14 shows one of the validation test setups where a known mass was hung from the share tip of the plough. The magnitude of the applied force, its direction and the horizontal distance of application from the back of the heel (point *O* in Figure 3-14) were all calculated from the load cell readings.

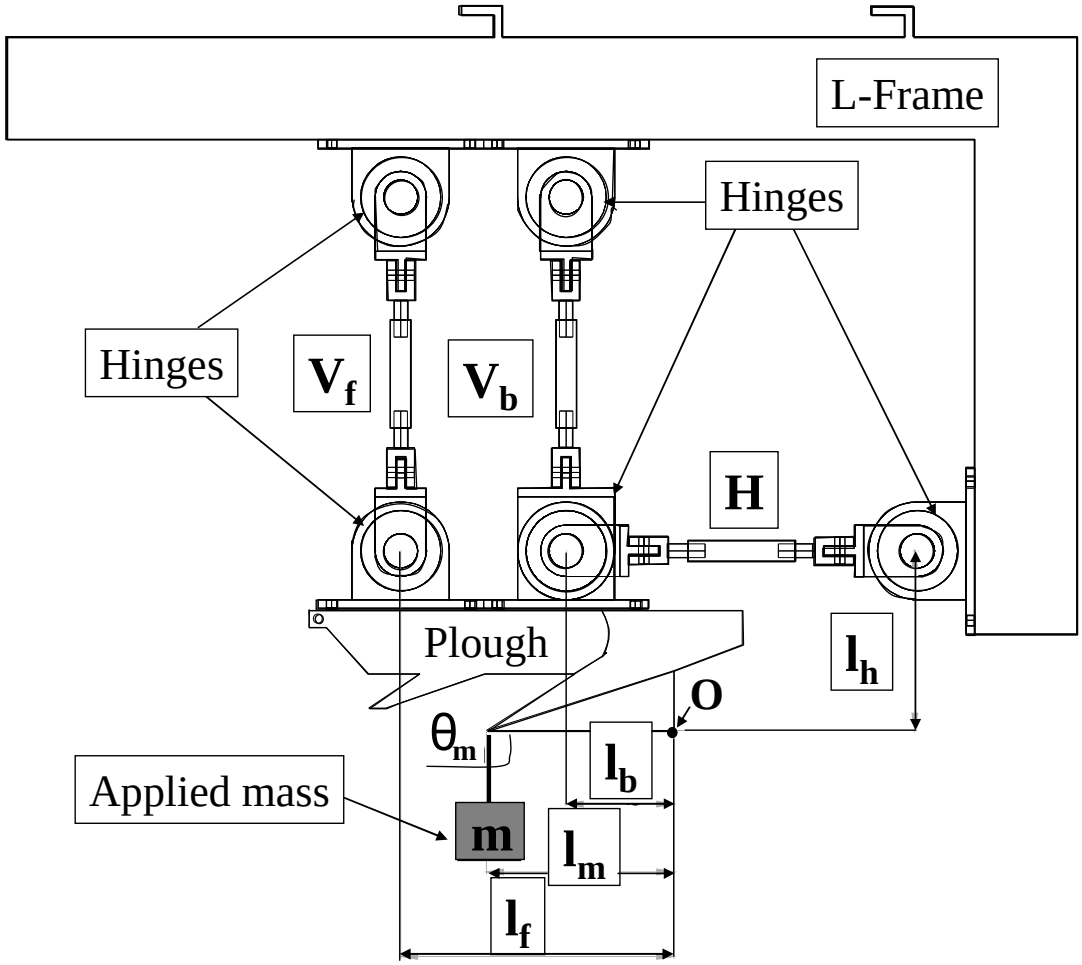

Figure 3-14: Schematic of load cell arrangement for fixed tests during validation

The following three Equations 3-3, 3-4 and 3-5 were used to find the position, l_m direction, θ_m and magnitude of the applied force, F:

$$l_m = \frac{(V_b \times l_b + V_f \times l_f + H \times l_h)}{V_b + V_f} \tag{3-3}$$

$$\theta_m = \tan^{-1}\left(\frac{V_b + V_f}{H}\right) \tag{3-4}$$

$$F = \frac{(V_b + V_f)}{\sin(\theta_m)} \tag{3-5}$$

The good agreement between the applied load and the values of position, direction and magnitude calculated from Equations 3-3, 3-4 and 3-5 (shown in Table 3-5)

provides confidence that the load cell arrangement works well. The hinges which connect the plough worked well and prevented moment loads from being carried through the load cells, as shown by the agreement of measured and calculated values of F, θ_m and l_m which would otherwise have caused an indeterminate system.

Table 3-5: Comparison between applied position, direction and magnitude to calculated values from Equations 3-3, 3-4 and 3-5

Applied vertical force at share tip			Calculated from load cell readings		
Force, F (N)	Direction, θ_m (degrees)	Position, l_m (mm)	Force, F (N)	Direction, θ_m (degrees)	Position, l_m (mm)
9.8	90	110	9.7	89	110
19.6	90	110	19.4	89	106
29.4	90	110	29.5	89	106
39.2	90	110	38.9	88	108

3.4.6. Test procedure

The I-beam trolley system was removed from the tank and the sand was prepared using one of the methods outlined in section 3.3.4 although at a larger scale. The plough was attached to the L-frame and then inserted into the even sand bed to the desired depth after which the sand around the plough was once again levelled. The pitch of the plough could be changed between tests by inserting spacers between the load cell attachments and the plough's beam. To make the plough aft pitch spacers were inserted at the rear load cell attachment (see, Figure 3-13) and to make the plough forward pitch spacers were inserted between the beam and front load cell. The I-beams were reattached to their carriages and the L-frame was bolted to them. The draw wire transducer (DWT) was connected to the L-frame and all of the instruments were checked to ensure they were working correctly and the hydraulic cylinder was activated. The plough was translated a distance of 2 m horizontally and loads, horizontal position and pitch were measured during the test. Post test, the trench profile was measured and the plough, L-frame and I-beams were removed. The sand was then excavated and the tank was ready for preparing the sand bed for the next test.

3.4.7. Experimental programme for 25th scale fixed tests

38 fixed tests at 25th scale were conducted at plough depths ranging from 11-80 mm at pitches of -4-6º. All tests were carried out in dry HST95 sand at a relative density of 17% and the results were compared with a series of ploughing (drag or towed) tests with the same plough under the same sand conditions.

3.5. *25th and 10th scale towed ploughing tests*

Figure 3-15 shows the setup used during the 25th and 10th scale towed tests. There was little difference in the test procedure between the 50th scale and the larger scale ploughing tests. Instrumentation was slightly different and a second LVDT of 100 mm stroke was used to measure the height of the front of the plough during ploughing, which in conjunction with the LVDT at the back of the plough allowed the pitch to be measured in place of the clinometer. A 0.5 kN load cell was used to measure tow forces during the 25th scale tests and a 5 kN load cell was used during the 10th scale tests. The tank used for the tests was the same as that used for the fixed ploughing tests and the experimental setup is shown in Figure 3-15.

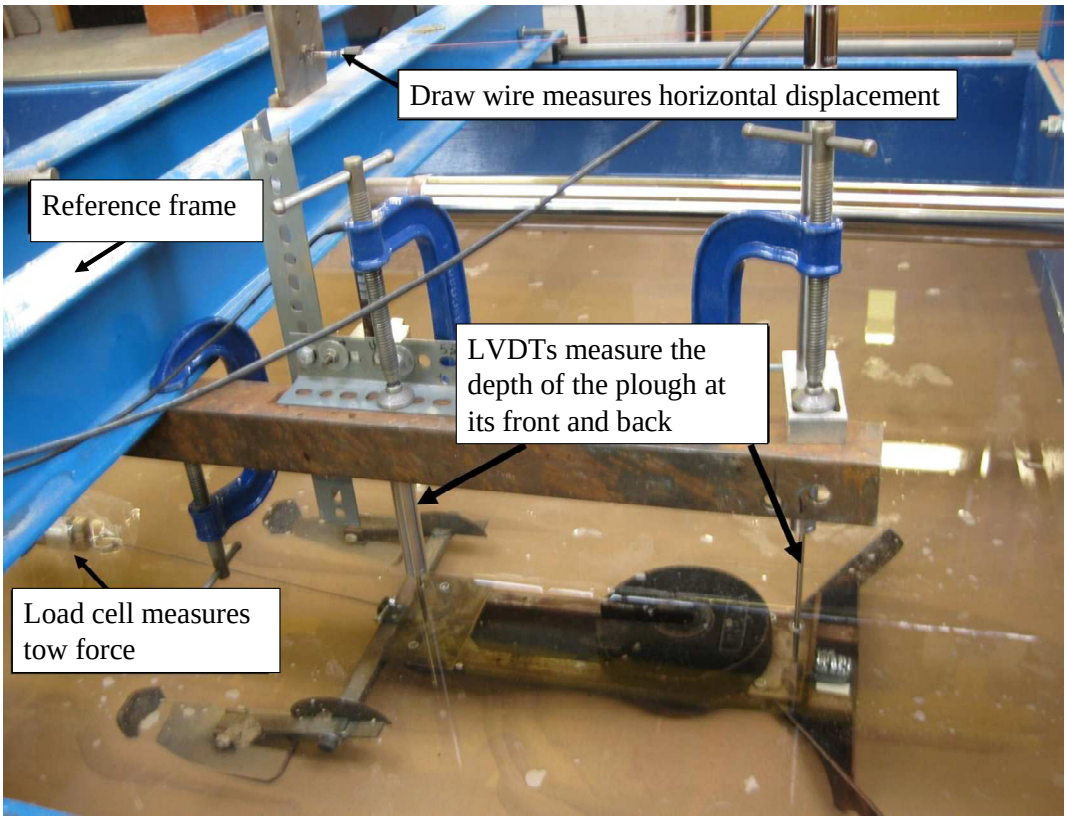

Figure 3-15: Towed test setup for the 25th and 10th scale ploughs

3.5.1. Experimental programme for 25th & 10th scale towed tests

The experimental test programmes for dry and saturated tests at 25th and 10th scale are shown in Table 3-6 and Table 3-7 respectively.

Table 3-6: Summary of dry towed test programme for 25th and 10th scale ploughs

Scale	Depth range (mm)	Number of tests	Sand type	Relative density (%)	Forecutter present
1/25	37-83	7	HST95	17	No
1/25	37-84	5	HST95	76	No
1/10	84-200	8	HST95	17	No

Table 3-7: Summary of saturated towed test programme for 25th scale plough

Depth (mm)	Velocity range (m/h)	Number of tests	Sand type	Relative density (%)	Forecutter present
65	1-334	4	HST95	76	No
65	5-334	8	HST95	53	No

3.6. *Plane strain tests*

A series of plane strain tests was devised in order to find how the pitch of the plough affects sand deformation. The plane strain tests were conducted by forcing a simplified share (triangular prism) to translate through sand in a transparent box through which sand deformation adjacent to the box walls could be viewed.

3.6.1. Apparatus

The plane strain apparatus consisted of a (500×250×250 mm) Perspex and steel box was designed specifically for the test series outlined herein and manufactured at the University of Dundee. The Perspex side walls were bolted onto the steel front and back walls and base. Figure 3-16 shows the box with built in screw jack and AC electric motor which were used to actuate the simplified share during testing.

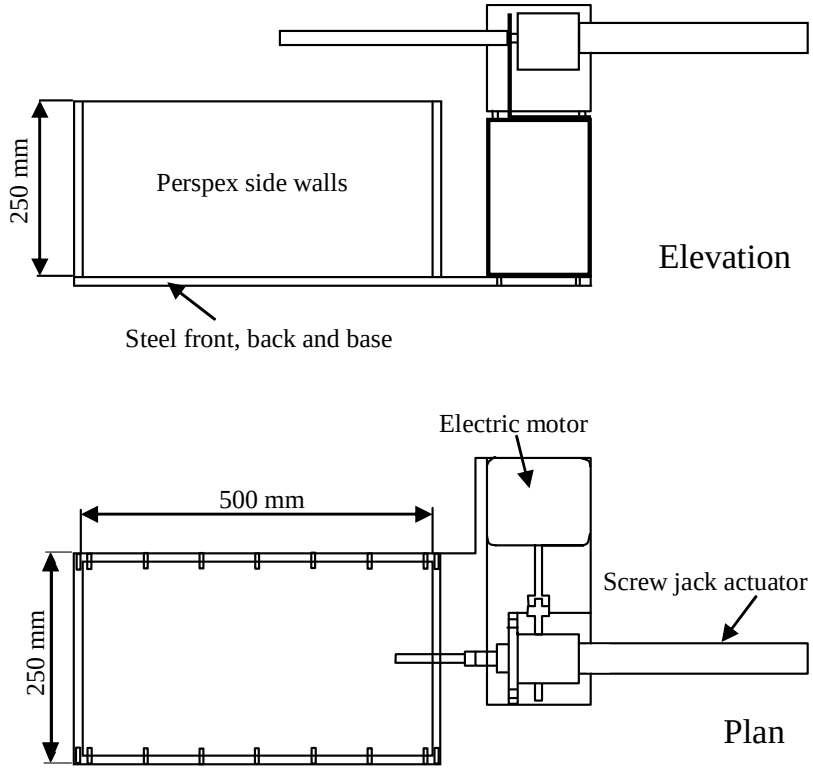

Figure 3-16: Plan and elevation of plane strain test box and rig

A simplified share (Figure 3-17) was constructed of steel and was 199 mm wide with a 70 mm long base and a 25º rake angle. This was used during the plane strain tests to allow sand deformations at share depth to be viewed during testing.

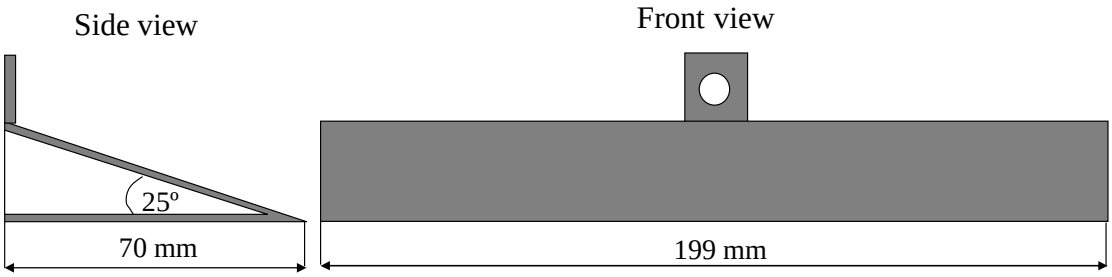

Figure 3-17: Simplified share for plane strain tests

3.6.2. Test preparation

All plane strain tests were conducted in dry HST95 at a relative density of 70%. The sand was prepared by dry pluviation through a mesh pluviator. Layers of sand were first pluviated into the box and the prism was placed onto the surface of the sand. More layers of sand were then pluviated on top of the prism which allowed the prism to be placed with minimal disturbance of the sand. As visualisation of shear planes

was important, thin layers of HST95 which had been coloured blue by permanent ink were poured at the viewing window at the side of the box at vertical spacing of between 5 and 8 mm apart. When the sand was sheared during testing a discontinuity was visible within the blue lines. Figure 3-18 shows how the experiments were set up. The two 200 N capacity load cells measure the force in the horizontal and vertical directions, while a draw wire transducer measures the horizontal translation of the simplified share. The simplified share is held in position by a rigid connection preventing changes in depth or rotation. This system allows the sand deformations to be viewed through the side walls of the box, showing the angle and frequency of shear planes and allowing a better understanding of the ploughing process. A camera connected to a PC was setup on a tripod facing a side wall of the box and was used to record photographs of the sand deformations during the test.

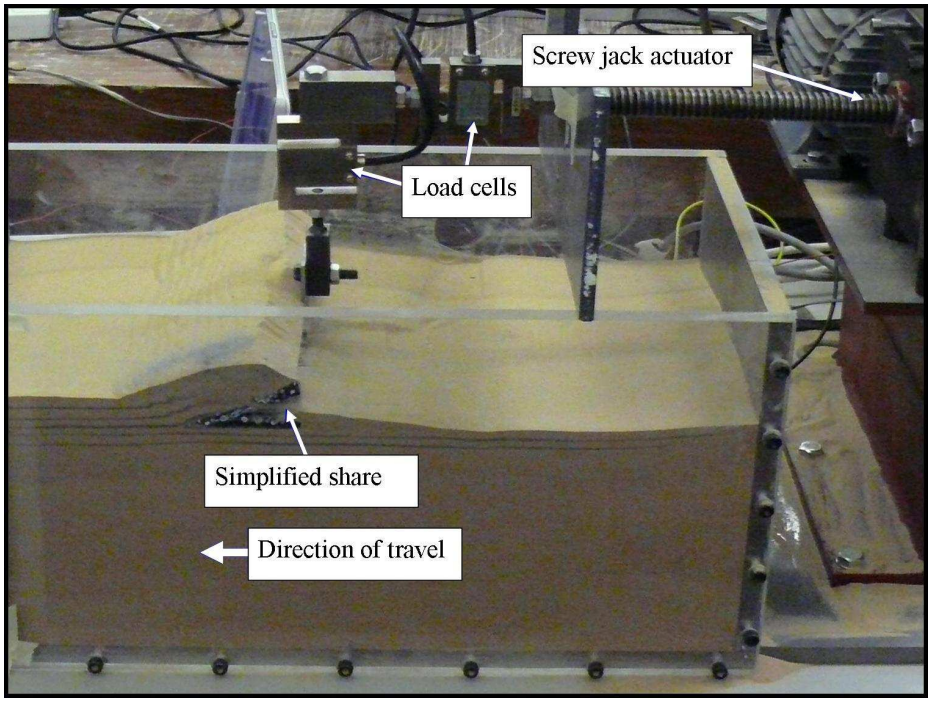

Figure 3-18: Experimental setup for the plane strain tests

3.6.3. Test procedure

Once the setup was complete, the logging system was started and the camera software set to instruct the camera to take a photograph at 20 second intervals. The AC electric motor which powered the screw jack actuator was then turned on and the simplified share was advanced through the sand at a rate of around 1 mm/minute until it had

travelled 250 mm when the test was stopped. The experiments concerned only the affect of pitch on sand deformations and tow force and tests were conducted at 2º, 0º and -2º pitch

3.7. *Material Characterisation*

Material characterisation through element testing is an essential part of the work to allow understanding of how sand state and material characteristics affect plough behaviour. The permeability and friction angles of the sands used during the ploughing tests were particularly important in understanding how sand properties influence the rate effect during ploughing. Two different sand fractions (HST95 and HST50) of the same source (Bent Farm in Congleton, Cheshire) were selected for testing. HST95 and HST50 are typically 94.5% and 97.0% quartz respectively and have respective 10% passing grain sizes, D_{10} of 0.1 mm and 0.19 mm. A third finer sand, (D_{10} = 80 μm) Redhill 100 was sourced from Redhill in Surrey. Redhill 110 is typically 98.8% quartz, has angular grains and specific gravity, G_s = 2.65 (Villalobos; 2007). Element tests undertaken consisted of direct shear box, oedometer compression, constant head permeameter and particle size determination (PSD) by sieving.

3.7.1. Direct Shear box

Shear box tests were conducted in order to characterise the shear characteristics of the sands used during the ploughing experiments. A rectangular prism of sand is prepared in the shear box and during testing is sheared horizontally along a plane induced mechanically by the box while simultaneously being subjected to a specific vertical pressure. Shear box tests were conducted at low normal effective stresses to provide representative angles of friction for the scale model ploughing tests. For example the normal effective stresses at share depth for the 50th scale plough are in the region of 1 kPa.

3.7.1.1. Shear box apparatus and procedure

The shear box used has a standard 60×60 mm in plan by 50 mm high split box which the sand was prepared and tested in. Dense sand samples were pluviated into the shear box and loose samples poured in and then stirred. The shear box tests were conducted in accordance with B.S. 1377, Part 7 (1990). The displacement rate was 0.031 mm/s, which gave drained behaviour of the sand and which was consistent for all tests.

3.7.1.2. Results from shear box tests

In Figure 3-19, Mohr-Coulomb failure envelopes are plotted through shear box data gathered during tests in dry HST95 (fine silica sand) at three different relative densities (75%, 40% and 17%). The Mohr-Coulomb envelopes shown have been forced through the origin to reflect the fact that apparent cohesion, *c'* should be equal to zero for dry sand.

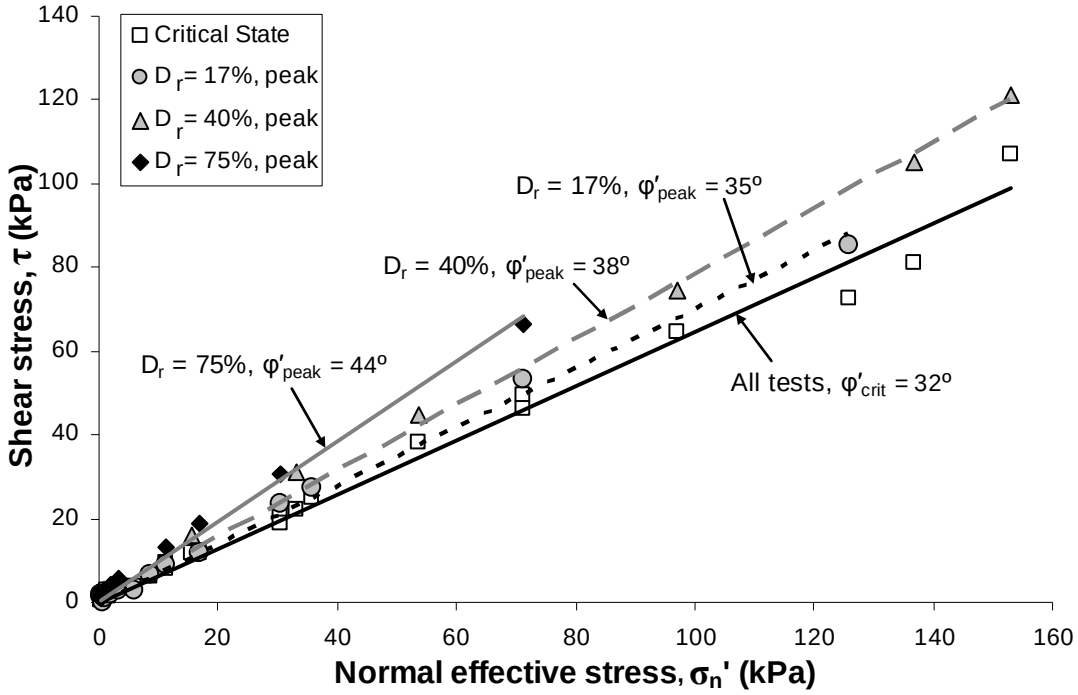

Figure 3-19: Mohr-Coulomb failure envelopes drawn from shear box tests in HST95 (fine silica sand) at relative densities of 75%, 40% and 17%

The angle of repose of this fine grained Congleton sand was measured by first pouring a loose heap of sand onto a flat surface and then excavating some material from the toe. The angle of the slope to the horizontal where the excavation had taken place was then measured by a protractor. The angle of repose was found to be 31º and compares

well with φ'_{crit} = 32º determined by shear box testing. Quartz grains tend to have a critical state angle of friction of around 33º ± 2º (Bolton; 1986) and is consistent with φ'_{crit} = 32º found during the shear box tests reported herein. The value of peak angles of friction presented here for the dense and medium dense tests are high for sand of this mineralogy, shape and size however, the peak angle is possibly high due to the low normal effective stresses which the tests were conducted at.

3.7.1.3. Effective stress issues found during shear box tests

Figure 3-20 shows peak and critical state shear stresses plotted against normal effective stress for 9 shear box tests. A curve in the data is observed which is most apparent at the lowest effective stresses. φ'_{peak} = 44º for dense HST95 (fine silica sand) at normal effective stresses of 10-70 kPa if *c'* is fixed at zero. This increased to φ'_{peak} = 60º over the normal effective stress range 1-5 kPa.

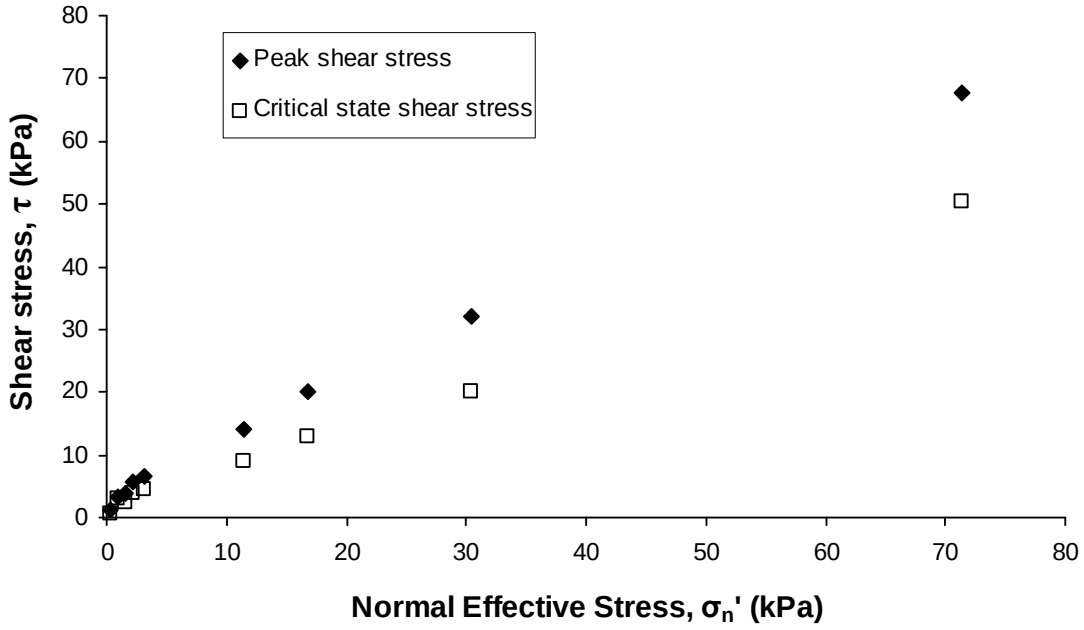

Figure 3-20: Results from shear box tests on fine Congleton sand (HST95) at D_r = 75%

Peak friction angles, shown in Figure 3-20 display a slight non linearity in shear stress/normal effective stress space. The influence of effective stress on dilation was therefore deemed important to the scaling of model ploughing tests to prototype scale, which are conducted at normal stresses of 50, 20 and 10 times smaller than prototype stresses respectively for the 50th, 20th and 10th scale model ploughs. Horizontal and

vertical box displacements measured during shear box tests in HST95 at a relative density of 75% are shown in Figure 3-21. The data from tests conducted at less than 1 kPa, from 1-5 kPa and greater than 5 kPa are marked with a star, square and triangle respectively. The tests conducted at the lowest effective stresses (stars) show most dilation whereas the tests conducted at the highest normal effective stresses (triangles) show least dilation. The samples were all prepared to a relative density of 75% ± 4%, however when the vertical pressure was applied a reduction in sample height was recorded. The test conducted at 75 kPa for example experienced a reduction in height of 0.6 mm from an initial height of 71.7 mm which corresponded to an increase in relative density from 72%-79%. Although not a huge increase, the results will be slightly skewed by this effect which will likely increase the dilation angles derived from tests at the higher effective stresses compared to the lower effective stresses.

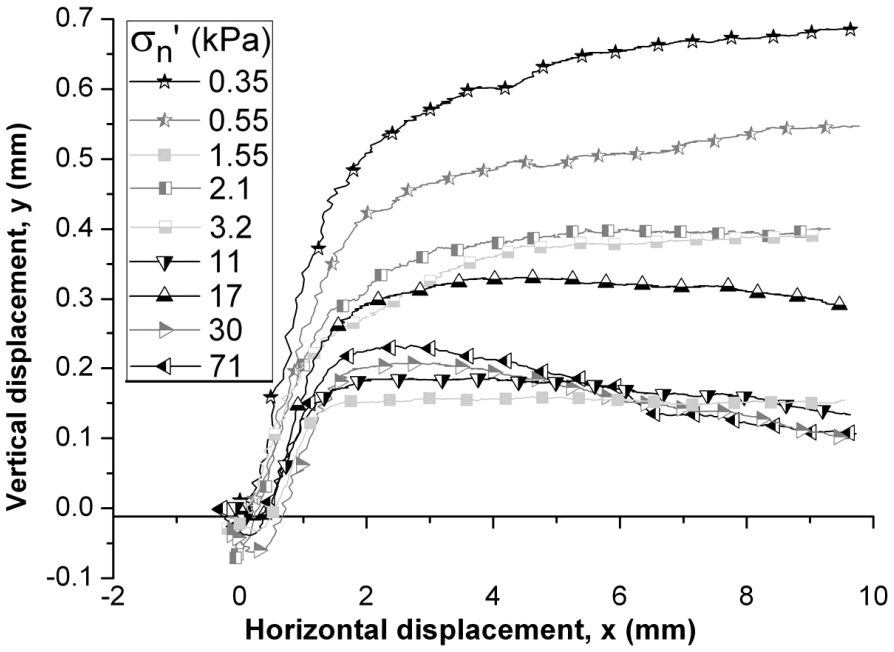

Figure 3-21: Horizontal and vertical displacements measured during a series of shear box tests in HST95 at D_r = 75%

The dilation angles derived from shear box tests conducted in HST95 at a relative density of 75% are shown in Figure 3-22. Dilation angles are shown to reduce linearly on a logarithmic scale as was found by Bolton (1986) during the examination of triaxial and plane strain tests on a number of different sands at p' ranging from 10-10,000 kPa. Bolton (1987), however, finds that at minor principal stresses less than

around 50 kPa both dilation angle and peak friction angle no longer increase with further reductions in effective stresses. The minor principal stress is less than 50 kPa for all of the tests shown in Figure 3-22 and the increase in dilation angle with reduction in effective stress is less than found at higher stress range by Bolton (1986) but not negligible as found by Bolton (1987) for tests at very low effective stresses.

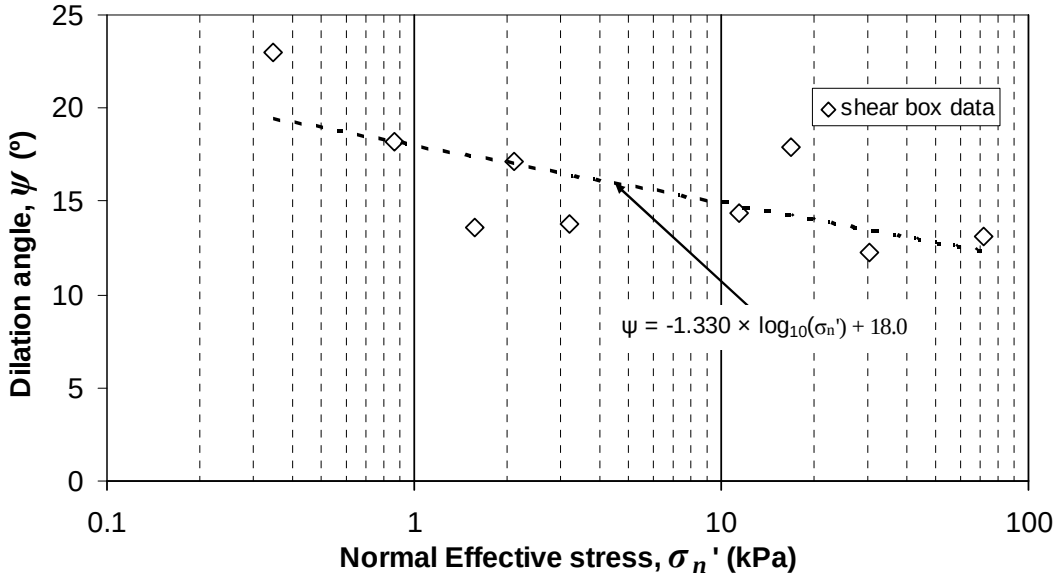

Figure 3-22: Dilation angles derived from shear box test results in HST95 at D_r = 75%

Figure 3-23 shows φ'_{peak} to vary between 68º and 42º with an increase in normal effective stress (σ_n') from 0.9-71 kPa at a relative density of 75%. This presents a problem when trying to define an appropriate friction angle to characterise the sand during the ploughing tests where the normal effective stress is unknown due to the unmeasured suctions involved and the complex effective stress regime close to the plough. Figure 3-23 gives unexpectedly high values of φ' which on first inspection appear erroneous and may well be. One might say that the very low effective stresses the sand was tested at during this study are beyond the limitations of the apparatus and that meaningful results are hard to attain. With this in mind, empirical curves derived by Bolton (1986), (Equation 2-5, $I_r = D_r(10\text{-}\ln p')\text{-}1$) and (Equation 2-6, $\varphi'_{peak} - \varphi'_{crit} = 5I_r$) in order to match dilatancy behaviour of sands over a range of stresses and relative densities were fitted to the data. D_r is the relative density of the sand, p' is the mean effective stress and I_r is the relative dilatancy index.

The peak angles of friction derived from tests in HST95 compare well with the Bolton (1986) equations. The peak friction angles of the four tests at normal stresses

greater than 10 kPa lie about 4º below and parallel to the Bolton (1986) equations (Equations 2-5 & 2-6). The corresponding critical state angles do not appear to change with normal stress. The five tests conducted at normal stresses below 10 kPa show more scatter and the peak angles of friction lie slightly above the extrapolated Bolton (1986) relationship. The critical state angles of friction for these tests also appear to increase with decreasing normal stress level. Since the reason φ'_{peak} increases with reducing normal effective stresses is because of increases in ψ_{max}, the value of φ'_{crit} should therefore be unaffected by normal effective stress. White and Cathie (2010) however, note that critical state friction angle may also increase with reduction in effective stress and it seems that there may be some conflict in the research in this matter.

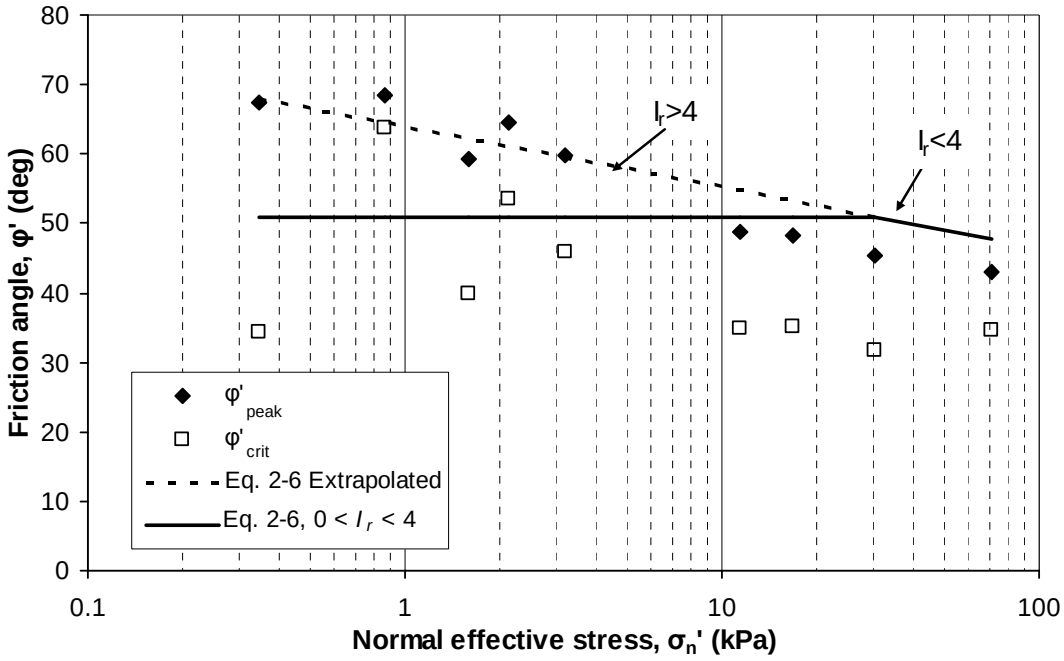

Figure 3-23: Increase in friction angle (φ′) with reduction in normal effective stress for HST95

It is worth noting however, that although the Bolton (1986) correlation agrees with the data fairly well that he stipulates that $0< I_r <4$ as he did not have access to data at very low effective stresses which he considered to be of sufficient quality and therefore could not verify if the same trend applied. The data in this study falls $3< I_r <8$ and is therefore mostly outside the range his correlation was developed for. Bolton (1986) notes that as effective stresses are reduced there may be some critical stress at which further reduction in stress beyond it will cause no further increase in dilation. Therefore his limit of I_r must not be greater than 4 also accounts for this.

The trend of peak angles of friction at very low effective stresses looks reasonable in Figure 3-23. The high degree of scatter at the very lowest normal effective stresses combined with critical state angles which are affected by stress complicates interpretation of the very low stress data. This presents a problem when examining model plough test data, especially for tests conducted at 50th scale where normal stresses are less than 1 kPa throughout the full depth of the share. As a measure of comparison between the tow forces generated during ploughing tests in different sands and the respective friction angles of those sands, friction angles have been attained from shear box tests over a range of normal effective stresses from 10-70 kPa.

Table 3-8 shows peak and critical state friction angles for HST95, HST50 and Redhill 110 during shear box tests conducted over a range of 10-70 kPa.

Table 3-8: peak and critical state angles of friction for HST95, HST50 and Redhill 110 (Friction angles determined over normal effective stress range 10-70 kPa)

Sand type	State		
	Dense	Medium dense	Loose
	φ'_{peak} (°)	φ'_{peak} (°)	φ'_{crit} (°)
HST95	44	38	32
HST50	41	39	34
Redhill 110	-	35	34

The critical state values shown here compare well with values calculated using an empirical equation (Equation 3-6) developed by Bareither *et al*. (2008):

$$\varphi'_{crit} = 1.89 + 20.56 \times D_{10} + 2.35 \times \gamma_{d\max} - 24.10 \times R_s \quad (3\text{-}6)$$

D_{10} is in mm, R_s is Krumbein roundness and γ_{dmax} is the maximum dry unit weight of the material in kN/m^3. φ'_{crit} calculated by Equation 3-6 for HST50 and HST95 are 35° and 32° respectively. D_{10} was found to be the main influencing factor causing the difference between the calculated values of φ'_{crit} for HST95 (D_{10} = 0.1 mm) and

HST50 (D_{10} = 0.19 mm). Redhill 110 was found to have φ'_{crit} = 35º calculated by Equation 3-6 which again agrees with the value measured during direct shear testing. Equation 3-6 shows that although the small particle size of Redhill 110 in comparison to HST95 and HST50 reduces its respective critical state friction angle, its greater angularity increased its friction angle.

3.7.1.4. Determination of critical state void ratio

The void ratio at critical state, e_{crit} is used in Chapter 5 as a means of normalising the data. e_{crit} was found during shear box tests by assuming that the sand inside the box sheared along a single band of thickness equal to $20D_{50}$. $20D_{50}$ was selected as it lies within the range of shear band thicknesses found in the literature (Finno *et al.*: 1997) and causes the best agreement between the values of e_{crit} found during initially dense and initially loose samples in the shear box. e_{crit} was therefore found through Equation 3-7.

$$e_{crit} = \left[\frac{H_f - H_0}{20D_{50}} \times 1 + e_0 \right] + e_0 \qquad (3\text{-}7)$$

where, H_f is the final sample height, H_0 id the initial sample height, D_{50} is the maximum size of the smallest 50% of HST95 and e_0 is the initial void ratio.

e_{crit} found during shear box tests in both initially loose (D_r = 17%) and initially dense (D_r = 75%) samples of HST95 are plotted in Figure 3-24 against the normal effective stress at which the tests were conducted. The data are fairly scattered, however the loose and the dense tests both provide similar values of e_{crit}. The void ratio of an HST95 sand sample prepared by dry stirring: e_0 = 0.717, D_r = 17% and subjected to one dimensional compression in an oedometer cell is also plotted in Figure 3-24. Comparing the values of e_{crit} found during shear box testing with the values of e found during oedometer tests in HST95 prepared at e_0 = 0.717 that over a range of normal effective stresses of 1 – 100 kPa, dry stirring gives a void ratio approximately equal to e_{crit}. This seams likely on an intuitive basis as the prossess of dry stirring effectively shears the sand to large strains which should take the sand to critical state.

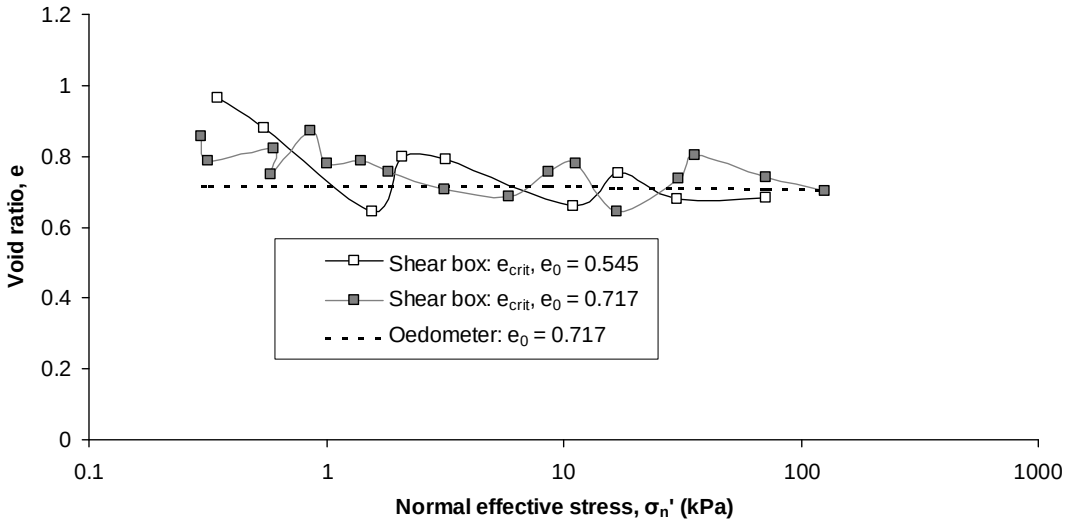

Figure 3-24: Estimation of e_{crit} from shear box tests at initial void ratios e_0, of 0.545 (D_r = 75%) and 0.717 (D_r = 17%) in HST95 compared to the measured void ratio during oedometer tests in HST95, e_0 = 0.717

Values of ecrit in HST50, HST95 and Redhill110 are shown in Table 3-9.

Table 3-9: values of e_{crit} for HST50, HST95 and Redhill 110

sand	e_{crit}
HST50	0.658
HST95	0.717
Redhill110	0.928

3.7.1.5. Interface tests

Interface friction between the plough and the sand constitutes a significant proportion of the tow force generated during ploughing. Quantification of this friction allows for the component of tow force generated to be separated from the total tow force. A series of tests were conducted in a standard shear box where the bottom of the shear box was filled with a rectangular prism of steel (designed to replicate share roughness) and sand prepared on top of the steel in the upper half of the box. Tests were conducted where a shear plane is induced along the interface between the sand and steel.

Figure 3-25 shows the interface friction angle δ from a series of shear box tests in HST95, providing δ_{peak} and δ_{crit} values of 27º and 26º respectively, taken over the

normal effective stress range 10-79 kPa. Although the sand is dense there is little difference between δ_{peak} and δ_{crit} which is likely to be due to the steel interface not being rough enough to allow significant interlocking of particles with it. The peak interface friction angles are 64% of the peak sand-sand friction, which agrees with $\delta = 0.67\varphi'$ commonly used by the offshore industry.

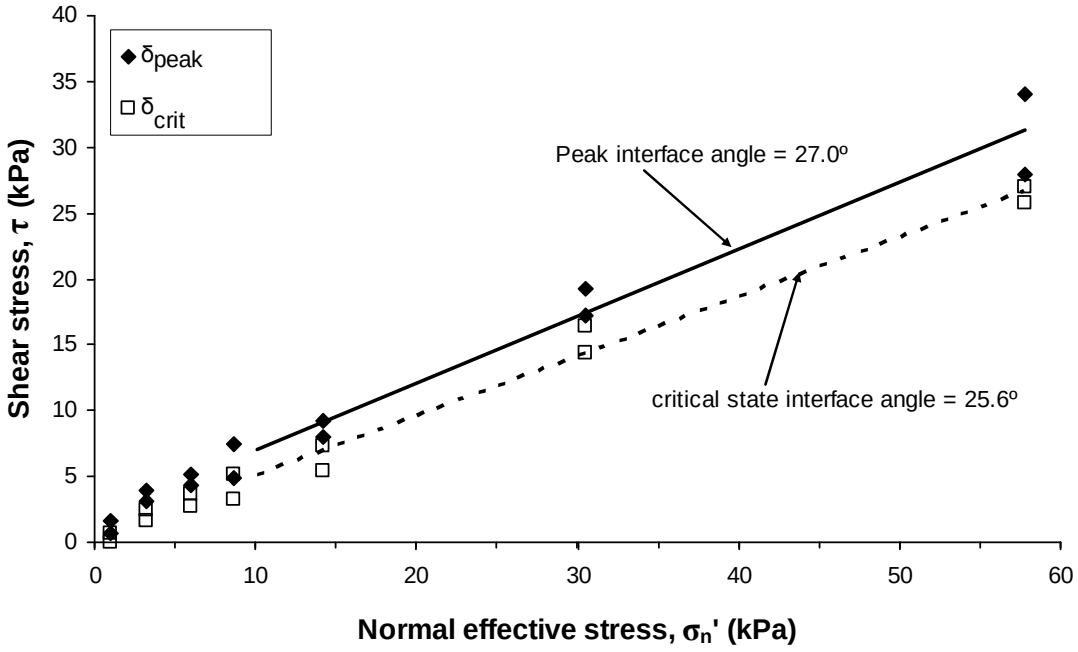

Figure 3-25: Sand-steel interface shear box test results for fine, dense (D_r = 75%) Congleton sand (HST95) showing the relationship between shear stress and normal effective stress

There is however variation of δ with σ_n' and this is shown in Figure 3-26. δ_{peak} ranges from 58º at 1 kPa to 27º at 60 kPa and δ_{crit} ranges from 35º at 1 kPa to 25º at 60 kPa. The data show a similar trend to Figure 3-23 whereby at normal effective stresses less than 10 kPa the friction angle increases more rapidly with reducing normal effective stresses than it does above 10 kPa. δ_{crit} also appears to increase at stresses below 10 kPa which would not be expected and therefore the same approach used in determining the representative values of φ'_{peak} and φ'_{crit} has been employed to find appropriate values of δ_{peak} and δ_{crit}.

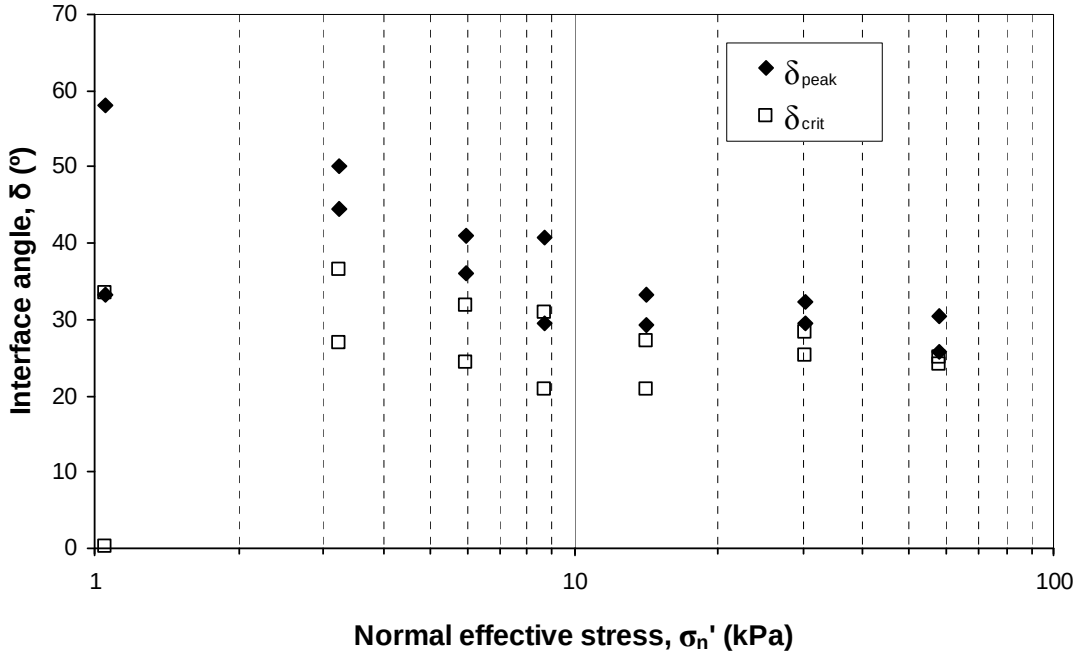

Figure 3-26: Variation of the interface angle, δ with normal effective stress in HST95 at D_r = 76%

Table 3-10 shows peak and critical state interface friction angles for HST95 and HST50 during shear box tests conducted over a range of 10-70 kPa.

Table 3-10: Interface angles of friction

Sand type	Peak interface angle, δ_{peak} (º)	Critical state interface angle, δ_{crit} (º)
HST95 (D_r = 75%)	27	24
HST50 (D_r = 90%)	29	27

3.7.2. Permeability determination from permeameter tests

Constant head permeability tests were conducted in accordance with B.S. 1377 part 5 (1990) using a permeameter cell. Loose samples were prepared by pouring sand into the cell and stirring it with a rod. Medium and dense samples were prepared by pouring sand into the cell and then vibrating the cell. It would have been desirable to pluviate into the cell to achieve the same densities used for the ploughing tests, however the top of the cell had a lip on it which prevented pluviation. A hydraulic gradient was applied to the saturated sand sample and the resulting flow of water

through the sand was measured. The results from the permeability tests are shown in Table 3-11.

Table 3-11: Permeability values derived from constant head tests on HST95, HST50 and Redhill 110

Sand type	Relative density, D_r (%)	Permeability, k (m/s)
HST 50	25	4.95×10^{-4}
HST 50	74	3.48×10^{-4}
HST 95	17	1.23×10^{-4}
Redhill 110	30	1.01×10^{-4}
HST 95	60	8.62×10^{-5}

3.7.3. One dimensional oedometer compression

Confined one-dimensional compression tests were conducted using a 76 mm diameter oedometer with the intention of defining the confined stiffness modulus $E_{0,}$' for Redhill 110, HST95 and HST50 in both loose (prepared by dry stirring) and dense (prepared by dry pluviation) states over a range of stress levels. E_0' can be used in conjunction with the permeability to find coefficient of consolidation, c_v which was used to normalise rate effects. Tests were conducted in accordance with B.S. 1377 part 5 (1990).

Figure 3-27 shows the confined stiffness modulus plotted against the normal effective stress for HST95, HST50 ad Redhill 110. The graph shows E_0' increasing steadily with increasing σ_n'. The data point at 175 kPa for HST95 is an outlier and may have been caused by disturbance of the sample during testing. On initial loading HST95 and HST50 appear to lose stiffness with increasing effective stress before showing an increase in stiffness with increasing stress at higher stress levels. Stamatopoulous and Kotzias (1978) show that this is the typical behaviour of overconsolidated soils prior to reaching their precosolidation pressure during the oedometer test. It is probable that accidental loading of the samples occurred during the lowering of the ball into the loading cap which prestressed the sample prior to testing and the high initial values of E_0' ignored.

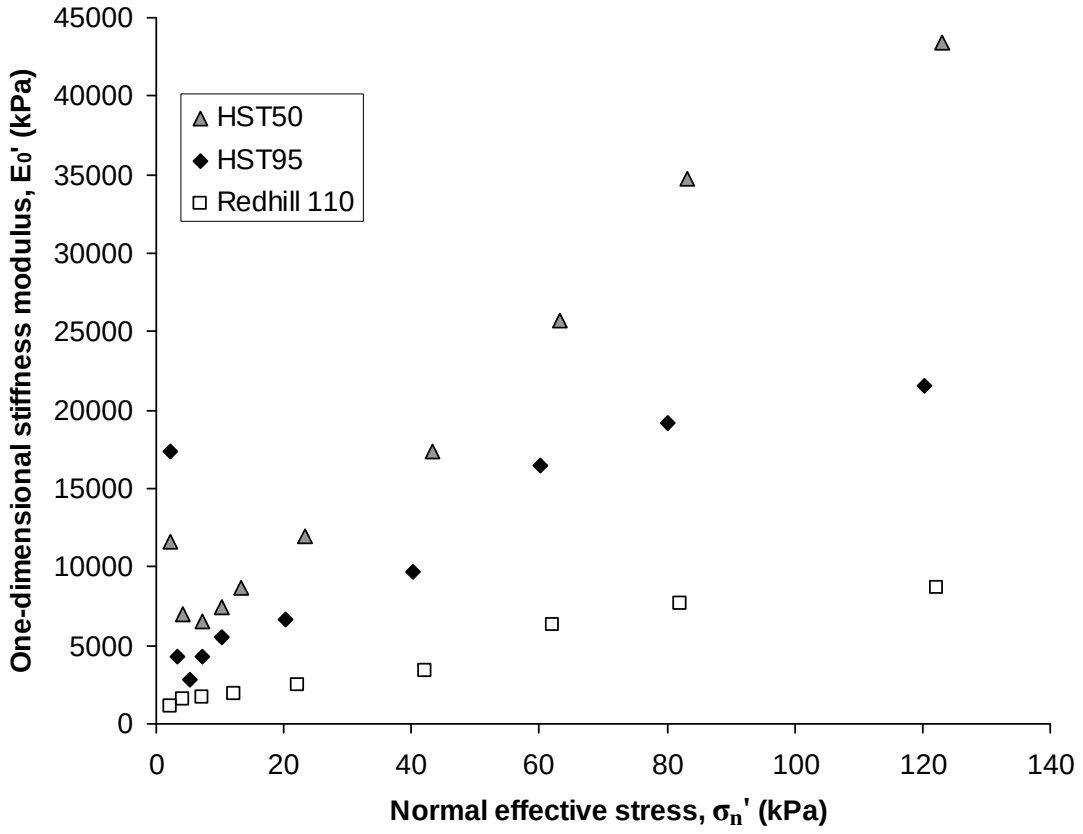

Figure 3-27: One-dimensional stiffness modulus, E_0' against normal effective stress, σ_n' for loose sands: HST95, HST50 and Redhill 110

The values of E_0' found over the stress range 5-10 kPa are shown in table Table 3-12 for HST50, HST95 and Redhill 110.

Table 3-12: One dimensional stiffness modulus values derived from oedometer tests on Redhill 110, HST95 and HST50, $\sigma_n' \approx$ 5-10 kPa

	Values of one dimensional stiffness modulus, E_0' (kPa)		
Condition	HST50	HST95	Redhill 110
Loose	6500	5000	1700
Dense	11500	8000	-

3.7.4. Particle size distribution by dry sieving

Sieving was conducted in accordance with B.S. 1377 part 1 (1990) in order to find the grading characteristics of the materials being tested. Figure 3-28 shows the particle size distribution (PSD) curves giving the relative proportions of different particle sizes

within samples of HST95, HST50 and Redhill 110 respectively. HST95, HST50 and Redhill 110 are found all to be fine sands with uniformity coefficients (C_u) of 1.5, 1.4 and 1.6 respectively, making them all uniform sands. Redhill 110 is the finest of the three sands and 4% by mass passes through a 63 micron sieve whereas HST95 and HST50 do not contain any silt sized particles.

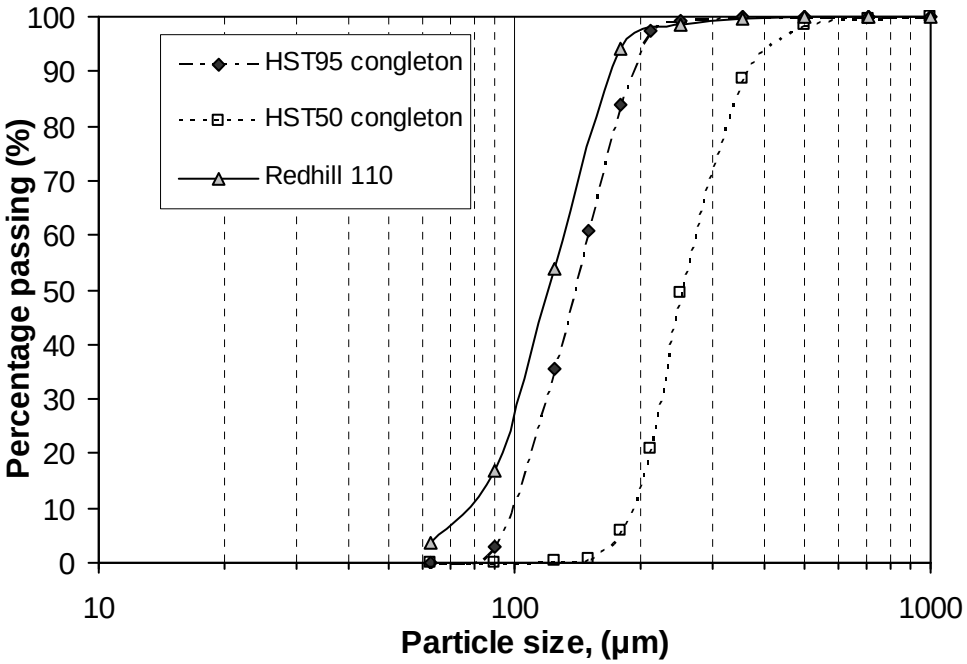

Figure 3-28: Particle size distribution curves for HST50, HST95 and Redhill 110

3.8. *Characteristics of HST50, HST95 and Redhill 110*

HST50, HST95 and Redhill 110 maximum void ratios were determined by the British standard method (BS 1377 part 4 1990) and minimum void ratios by pluviation at a very low flow rate. e_{max} and e_{min} for Redhill 110 were found to be 1.049 and 0.709 respectively. e_{max} and e_{min} for HST95 were found to be 0.769 and 0.467 respectively. e_{max} and e_{min} for HST50 were found to be 0.714 and 0.490 respectively. As these values are important in determining the relative density of the sands it was imperative that they were accurate and were therefore compared with correlations developed by Rouse *et al*. (2008) and Youd (1973).

These values provide reasonable agreement with values calculated using Rouse *et al*. (2008) Equations 3-8a and 3-8b applicable for soils with $C_u \leq 2.5$. The resulting

values of e_{max} and e_{min} for HST95 and HST50 determined by Equations 3.2a and 3.2b are shown in Table 3-13.

$$e_{max} = 0.615 + 0.107R^{-1} \quad (3\text{-}8a)$$

$$e_{min} = 0.433 + 0.051R^{-1} \quad (3\text{-}8b)$$

Where, R is particle roundness and is defined in Equation 3-9

Using the Youd (1973) chart (Figure 3-29) e_{max} and e_{min} 0.67 and 0.39 respectively are obtained for HST95 and 0.69 and 0.40 respectively for HST50.

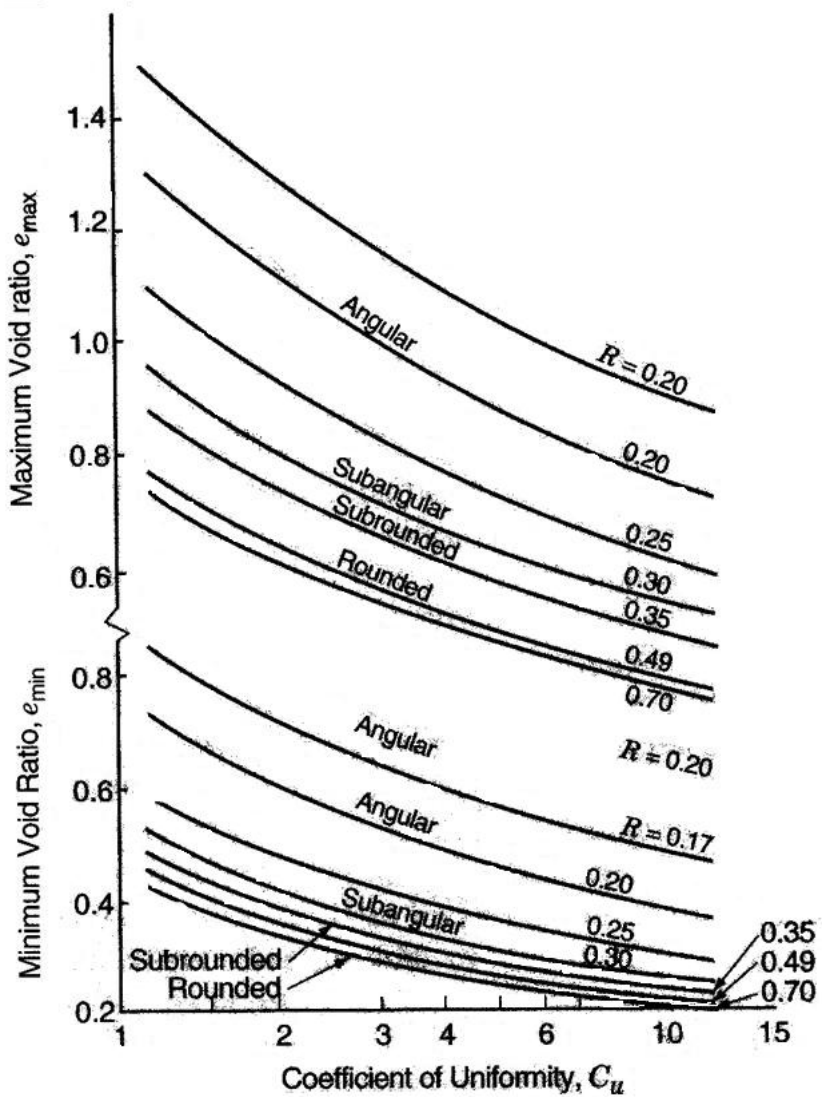

Figure 3-29: Maximum and minimum void ratios of sands as a function of roundness and the coefficient of uniformity (Youd:1973 referenced from Mitchell and Soga: 2005)

Table 3-13: Comparison of experimental determination of void ratio extents with Youd (1973) and Rouse *et al.* (2008) correlations

	HST 50		HST 95		Redhill 110	
Method	e_{max}	e_{min}	e_{max}	e_{min}	e_{max}	e_{min}
Experimental	0.714	0.49	0.769	0.467	1.045	0.627
Youd (1973)	0.69	0.4	0.67	0.39	1.2	6.8
Rouse *et al*. (2008)	0.81	0.526	0.817	0.529	1.150	0.688

Table 3-13 shows experimentally determined values of maximum and minimum void ratios generally agree with the values calculated by methods developed by Rouse *et al*. (2008) and Youd (1973). However as HST95 and HST50 are both rounded, their roundness does not hugely affect their e_{max} and e_{min} values and the difference between the particle sizes may be the cause of the different values. Bareither *et al*. (2008) found for a range of sands with $0.8 < D_{50} < 0.15$ that both e_{max} and e_{min} increase with reducing mean particle size. It may therefore be the difference in particle size which causes the change in e_{max} and e_{min} between the three sands.

3.9. *Particle shape analysis*

HST50 and HST95 sand grains were viewed through an electron microscope to see if the slight difference in shear characteristics and e_{max} and e_{min} was due to difference in shape. It is well documented that increasing roundness R reduces critical state angle of friction (Gye-Chun Cho *et al*. 2006). Youd (1973) relates e_{max} and e_{min} to uniformity coefficient and roundness and Rouse *et al*. (2008) show how roundness and particle size affect e_{max} and e_{min}.

The roundness of HST95 and HST50 was found by taking the images of each material captured under an electron microscope and inscribing circles which fit into the major features of a grain of sand along with inscribing the largest circle which wholly fits into the grain. The roundness of each grain is the average radius of the features found on the grain divided by the largest circle which fits inside the grain (Equation 3-9).

$$roundness = \frac{\sum (r_i / N)}{r_{max}} \tag{3-9}$$

Figure 3-30 shows an example of a grain of HST50 with features marked by circles of radii, r_1-r_5 and the circle of radius r_{max} shows the largest circle which fits inside the grain. 30 grains of each material were examined in this way to provide their respective roundness's of 0.55 for HST50 and 0.53 for HST95. The roundness values are very similar and therefore roundness is unlikely to be a source of difference in friction angles between HST50 and HST95. Redhill 110 is angular (Villalobos; 2007) and this is the likely reason why it has a higher critical state friction angle than HST95. Figure 3-29 shows that as roundness reduces e_{max} and e_{min} increase and is a probable cause as to why e_{max} and e_{min} are higher for Redhill 110 than HST50 and HST95.

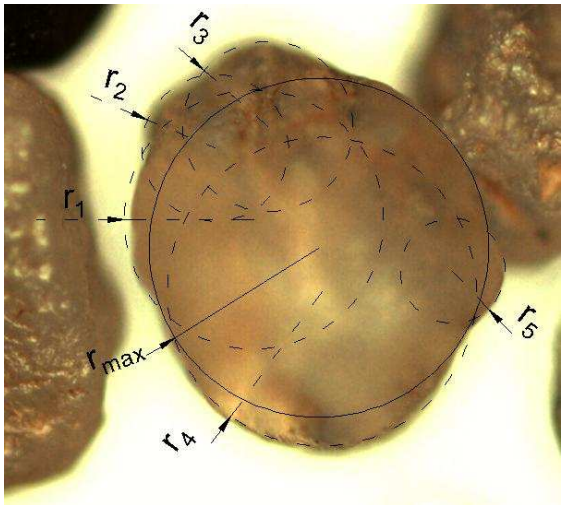

Figure 3-30: Image analysis of HST50 sand grain roundness

It was assumed on selection of the materials that HST95 and HST50 in particular would have similar e_{max} and e_{min} values and friction angles. It is important to ensure that e_{max} and e_{min} for all sands is as accurate as possible as they will determine the relative density of each sand, which is the best means of density comparison as it compensates for particle shape and grading effects (Bolton; 1986). The consequence of HST95 and HST50 having slightly different friction angles and e_{max} and e_{min} values is that they may have to be taken into account during analysis of rate effects.

3.10. *Summary of materials characterisation*

The material properties of HST50, HST95 and Redhill 110 are shown in Table 3-14. These properties are used to help with analysis of the ploughing tests discussed in Chapter 4 and Chapter 5.

Table 3-14: Summary of material properties of HST50, HST95 and Redhill 110 sands

	Sand		
Property	HST50	HST95	Redhill 110
D_{10} (mm)	0.19	0.10	0.08
D_{30} (mm)	0.22	0.12	0.10
D_{60} (mm)	0.26	0.14	0.12
C_u	1.4	1.4	1.5
C_z	1.0	1.0	1.0
G_s	2.63	2.63	2.65
$\gamma_{d\ min}$ (kN/m^3)	15.06	14.59	12.71
$\gamma_{d\ max}$ (kN/m^3)	17.32	17.58	15.98
e_{max}	0.714	0.769	1.045
e_{min}	0.490	0.467	0.627
ϕ_{crit} (°)	34	32	34
δ_{crit} (°)	27	24	-
Loose, k (m/s)	4.95×10^{-4}	1.23×10^{-4}	1.01×10^{-4}
Shape	rounded	rounded	angular
Loose, E_0' (kN/m^2)	6500	5000	1700
Dense, E_0' (kN/m^2)	11500	8000	-

Chapter 4. Results and discussion from plough tests in dry sand ('static' ploughing)

4.1. *Introduction*

Ploughing tests conducted in dry sand were used to provide information on plough performance in fully drained (known as 'static' type) conditions. In the dry condition it is reasonably assumed that the compressibility and low viscosity of air prevents rate effects from developing as a result of effective stress changes because fully drained conditions occur. These tests combined with the saturated ploughing tests were designed to allow complete separation of the rate effect from the static components of ploughing. This is not something that is possible for field derived data and may be a source of inaccuracy in Cathie and Wintgens (2001) data.

This Chapter contains results and discussion from ploughing tests where the plough is dragged through the sand on a tow line which were designed to mimic offshore ploughing operations. It also contains results and discussion of tests where the plough was fixed in place at a particular depth and pitched and forced through the sand. The plough was held in place by three load cells and the extra force information was used to try and break down the components of force acting on the plough. Simplified share plane strain tests results are also discussed which indicate the failure mechanism during ploughing.

4.2. *50^{th} scale towed ploughing tests*

A parametric study was conducted using the results from 50^{th} scale plough testing in dry sand. The 50^{th} scale plough was used to examine the effect of: depth of ploughing, use of a forecutter, variation of relative density and particle size of the sand on the plough's performance. The performance characteristics considered were: the required tow force, the pitch of the plough during trenching and trench collapse.

4.2.1. Derivation of results from raw data

During the setup for the 50th scale ploughing tests the plough was placed on the surface of the sand so that it rested on its skids at the front and the share at the back. On initiation of the test the plough was towed forward and due to the geometry of the share it started to penetrate the sand. This process, known as transition, continued until the plough reached a depth where the forces acting on the share were in balance and the plough simply maintained its depth as it translated forwards during the rest of the test.

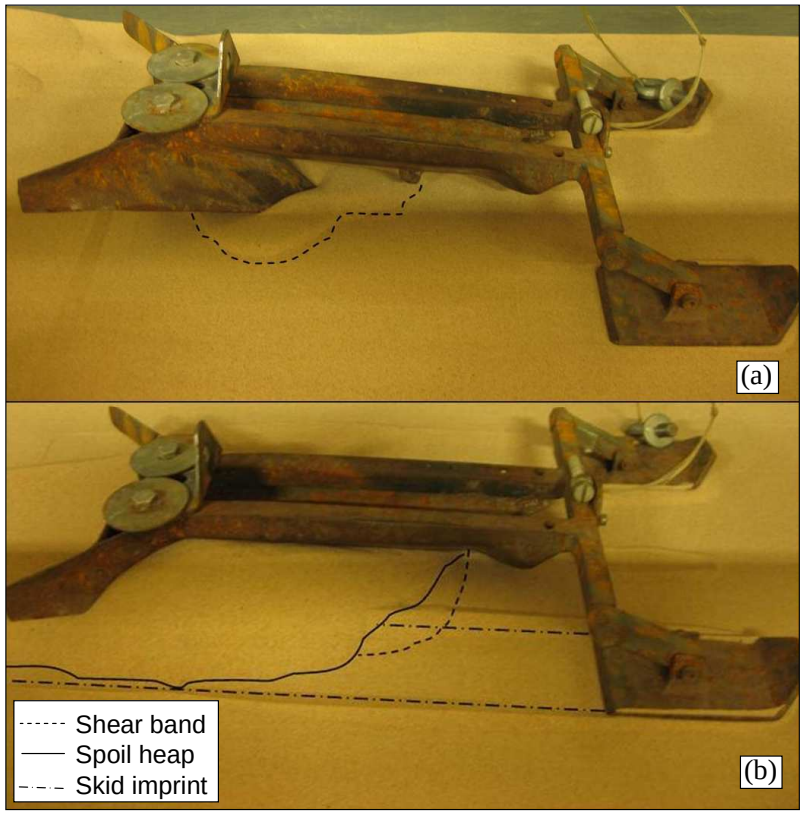

Figure 4-1: Photographs of the 50th scale model plough in the sand tank, (a) transition towards steady state, (b) steady state condition

Figure 4-1a and Figure 4-1b highlight the differences in plough orientation between transition (Figure 4-1a) and steady state ploughing (Figure 4-1b), whilst Figure 4-2 shows the differences seen in the recorded data between transition and steady state ploughing. Figure 4-1a shows the plough during the transition between the start of the test and attainment of steady state conditions. The plough is visibly forward pitched, (up to -12^{o} at the start of the test) whilst creating a shallow trench and the spoil heaps are undeveloped. A discontinuity in the surface of the sand (dashed line) indicates a shear plane which has formed due to the movement of the share through the sand and

as the plough continues to translate forward during transition spoil heaps are formed and the trench increases in size.

At steady state (Figure 4-1b) the pitch of the plough tends to be close to zero and the spoil heaps have formed around and in front of the share (continuous black line). The dashed line in front of the spoil heap shows the emergence of a shear plane which tends to reappear in advance of the share approximately every 20 mm of forward advance. The dash dot line highlights that the skids have embedded into the sand slightly due to the forces acting on the plough during trenching.

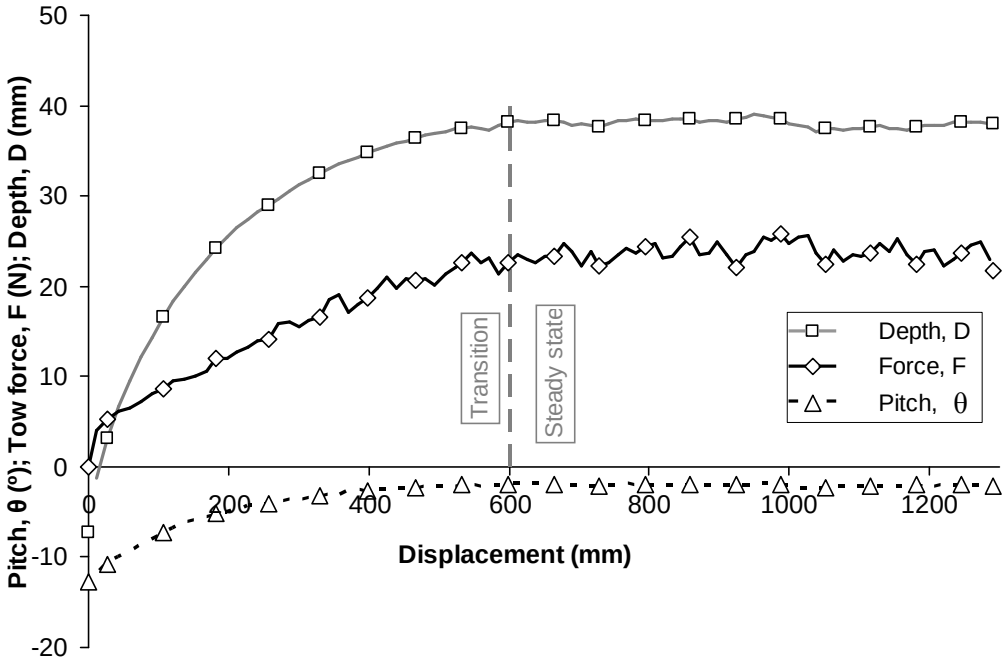

Figure 4-2: Development of the steady state ploughing conditions in dry HST50, D_r = 90%

Figure 4-2 shows the data collected during a 50th scale ploughing test. The pitch at the start of the test is around -12^o (forward pitching) which tends towards -1^o at steady state. The tow force starts at 0 N, then jumps to 4 N on commencement of the test and continues to steadily increase to a constant 20 N thereafter. The plough depth (depth from the sand surface prior to ploughing to the back of the heel) starts around zero depending on how the plough was placed on the sand and from the start of the test increases in a logarithmic fashion until the steady state condition is reached. At 50th scale the steady state condition is reached within 600 mm of plough translation and is highlighted on Figure 4-2 by a dashed grey line defining the end of transition state

and the beginning of steady state. The results displayed throughout this chapter and the rest of the thesis are steady state results taken as average values of depth, pitch and tow force from 600 mm displacement until the end of each respective test. Consequently, steady state values derived from the test shown in Figure 4-2 are: F = 20 N, D = 40 mm and θ = -1º. This ensures that results used are meaningful and helps with repeatability.

4.2.2. Influence of ploughing depth on plough performance

The plough depth here is defined as the depth from the surface of the sand to the back of the heel. Plough depth is controlled by the skid settings in combination with the balance of moments about the skids known as the long beam principle (Chapter 1). Clients of a trenching contractor will usually specify a minimum depth of cover for a pipeline. It is therefore important for the contractor to understand how the plough's performance is affected by its trenching depth and also how external factors such as sand density can in turn affect the plough's depth. The depth of cover specified often forces the plough to be used at the very limit of its depth specification and therefore large depth trenching of around 2 metres (40 mm at 50th scale) is of particular interest.

Table 4-1: Skid settings and corresponding ploughing depth

Skid setting	Arm angle, β (º)	Mean plough depth, D (mm)
1	67	19
2	50	26
3	44	30
4	30	36
5	17	41

Table 4-1 shows the plough depth achieved when trenching without a forecutter in loose (D_r = 25%), dry, sand (HST50), for a range of skid settings, also showing corresponding arm angles. Figure 4-3 defines the arm angle and shows that the skids are brought towards the plough as the arm angle (β) is increased, which causes the skids to attract more of the plough's self weight during ploughing. Looking at the simple case of the plough sitting on the surface of the sand with its weight supported by the skids at one end and assuming a reaction point under the share at the other the

effect of skid setting on the loading on the skids was examined using static analysis. The skids were found to attract 40% of the plough's weight with skid setting 5 and 45% of the plough's weight with skid setting 1. This however, does not represent the loading on the skids during ploughing very well as it is the balance of forces acting on the share along with the ploughs self weight which will determine the loading on the skids.

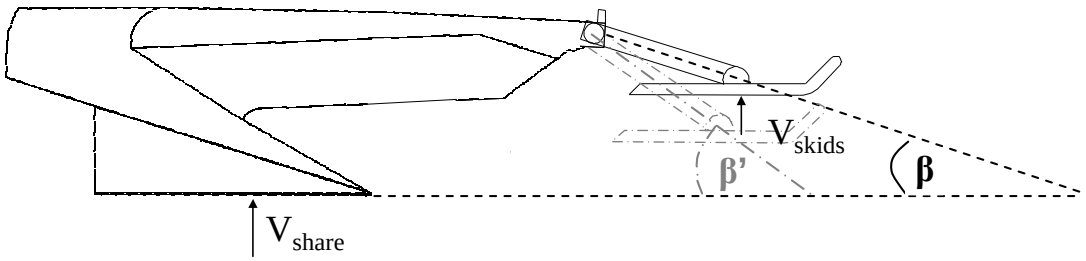

Figure 4-3: Depiction defining the arm angle, *β* as the angle of the arm relative to the share

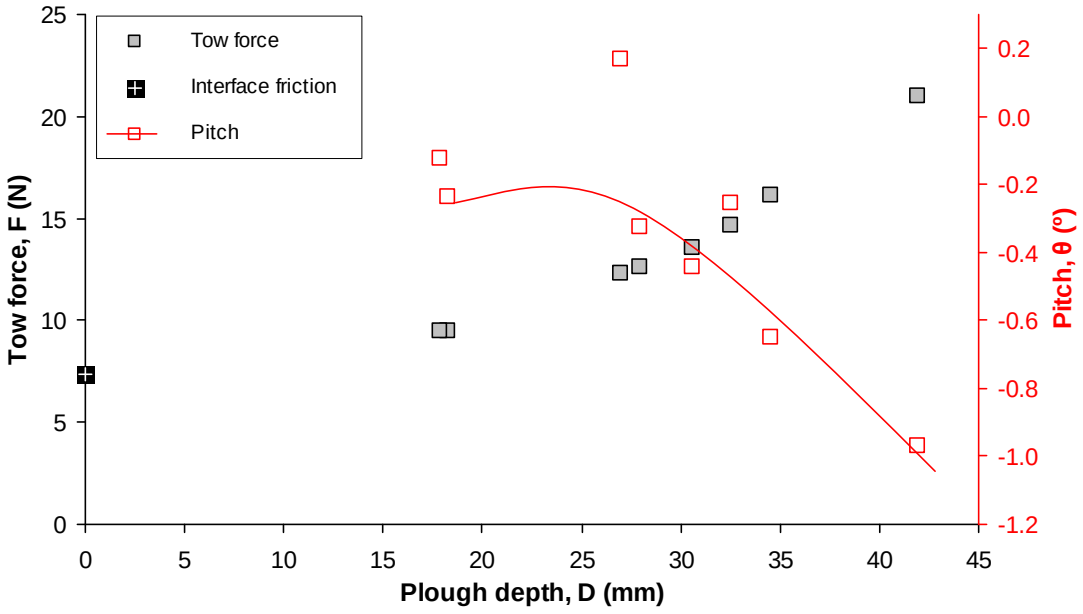

Figure 4-4: Effect of plough depth on tow force and pitch using a 1.8 kg plough without a forecutter in dry HST50 at D_r = 25%

Figure 4-4 presents steady state tow force and plough pitch with respect to plough depth for the 50th scale plough. The plough is without a forecutter and trenching in loose (D_r = 25%), dry, sand (HST50), and 8 test results are shown at 5 different skid settings. The pitch of the plough reduces (plough pitches further forward) with increasing depth and is a result of a shift in the position and magnitude of forces

acting on the share and the position of the skids relative to the share. At depths less than 26 mm the plough skids sink a couple of millimetres into the sand (possibly as a result of increased loading) so that the trend is obscured and the pitch is slightly reduced.

As expected, tow force increases with plough depth, which is in part due to normal effective stress being proportional with depth and also that the increased depth provides a larger projected area of sand in front of the plough. In order to allow the relationship to be projected to the sand surface or the equivalent of zero depth for the plough the force due to the weight of the plough acting on the sand, known as either base friction or interface friction was calculated. The interface friction point at zero depth is derived from the interface angle between HST50 and rusty steel measured in shear box interface tests (see chapter 3) multiplied by the plough's weight. It can be seen that this calculated data point for D = 0 mm appears to correspond to the relationship between tow force and depth measured with increasing depth.

Equation 4-1 describes the interface friction component of the tow force.

$$F_w = W \times \tan\delta \tag{4-1}$$

where W is the weight of the plough and δ is the interface friction angle between sand and steel.

The other component of the tow force in dry sand is due to the passive resistance of the sand and is thought to be some function of the ploughing depth cubed as shown in the Cathie & Wintgens (2001) and Reece and Grinsted (1986) models. Figure 4-5 and Equation 4-2 show mathematically why the passive pressure portion of the tow force is modelled as a function of the depth cubed. The triangular wedge shape in Figure 4-5 represents the share of a plough of width, w and depth, D and the passive resistance of the sand is F_p.

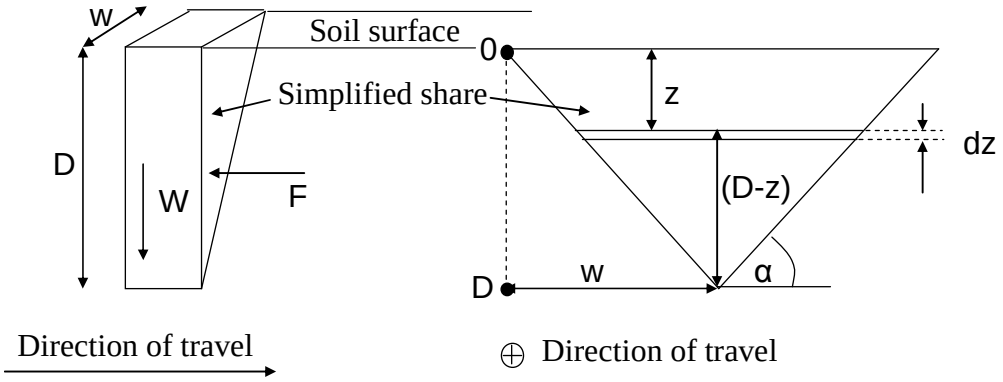

Figure 4-5: Simplified share and the force acting on it

Equation 4-2 attempts to quantify the force acting on the share and shows simply the horizontal passive pressure the sand is capable of resisting per unit width, $K_p\,\gamma' z$ at any depth z from 0 to D. The width of the share is defined by $(D\text{-}z)/\tan(\alpha)$ and ranges from 0 at depth = D to $2w$ at depth = 0.

$$F_p = \int_0^D K_p \gamma' z \times \frac{(D-z)}{\tan\alpha}\,dz$$

$$F_p = \frac{K_p \gamma'}{\tan\alpha}\int_0^D (Dz - z^2)\,dz$$

$$F_p = \frac{K_p \gamma'}{\tan\alpha}\left[\frac{Dz^2}{2} - \frac{Dz^3}{3}\right]_0^D$$

$$F_p = \frac{K_p \gamma'}{\tan\alpha}\left[\frac{D^3}{2} - \frac{D^3}{3}\right]$$

$$F_p = \frac{K_p \gamma'}{6\tan\alpha} \times D^3$$

Therefore, F_p is defined by Equation 4-2

$$F_p = \frac{K_p \gamma'}{6\tan\alpha} \times D^3 \qquad (4\text{-}2)$$

The static resistance to ploughing can therefore be defined by Equation 4-3

$$F_{v=0} = W\tan\delta + \frac{K_p \gamma'}{6\tan\alpha} \times D^3 \qquad (4\text{-}3)$$

Equation 2-3 can be simplified to give Equation 4-4 where rate effects are absent.

$$F_{v=0} = C_w W + C_s \gamma' D^3 \quad (4\text{-}4)$$

Equation 4-4 is the static tow force component of the Cathie & Wintgens (2001) model and is composed of two parts of similar form to Equation 4-3. The first term, C_wW is a base friction component, where C_w is the coefficient of friction between the sand and the plough and W is the plough's weight. This is in effect exactly the same as Equation 4-1. As stated in Chapter 3, the coefficient of friction was measured in a shear box and can reliably be taken as 0.40 in HST95 and 0.44 in HST50 which are close to 0.4 suggested by Cathie & Wintgens (2001).

The term $C_s\gamma D^3$ in Equation 4-4 describes the component of tow force generated by the passive resistance of the sand and therefore encompasses sand friction angle and weight. The unit weight of the sand γ' and the plough's depth D can be easily quantified and leaves only C_s as an unknown, but by comparing Equation 4-2 and Equation 4-3, C_s would appear to be equal to $K_p/6\tan(\alpha)$.

K_p was calculated using Coulomb's theory (Equation 4-5) which accounts for interface friction and the non-vertical rake angle of the share. Where, α is the rake angle of the plough (measured from the horizontal to the front face of the share), φ' is the friction angle, δ is the interface angle and θ is the angle failure plane and the horizontal. The theory assumes a two dimensional, planar failure mechanism within the soil and this is not the case during ploughing with a pipeline plough.

$$K_p = \frac{\sin^2(\alpha - \phi') \times \cos(\delta)}{\sin\alpha \times \sin(\alpha - \delta) \times \left[1 - \sqrt{\left(\frac{\sin(\phi' + \delta) \times \sin(\phi' + \theta)}{\sin(\alpha + \delta) \times \sin(\alpha + \theta)}\right)}\right]^2} \quad (4\text{-}5)$$

Figure 4-6 compares tow forces measured during 50th ploughing tests over a range of depths in dry HST50 with tow forces predicted by Equation 4-3 and Equation 4-4.

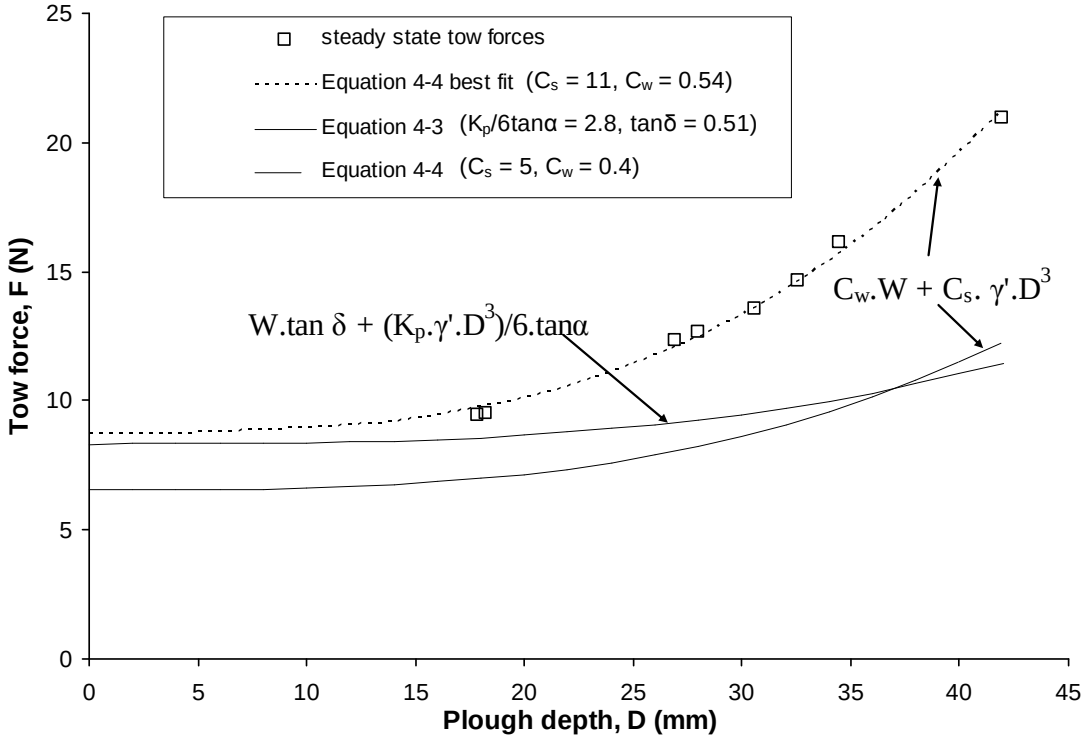

Figure 4-6: Prediction of tow force in dry HST50 at D_r = 25% when ploughing without a forecutter and comparing the suitability of Equation 4-3 and Equation 4-4

Cathie and Wintgens (2001) suggest that the passive pressure coefficient, C_s varies with relative density and that a value of 5 is appropriate in loose sand. They found the interface friction coefficient, C_w to be independent of relative density and that a value of 0.4 was appropriate when ploughing in sand. Equation 4-4 with C_s = 5 and C_w = 0.4 has been plotted as the long dashed line in Figure 4-6 and underpredicts both the interface friction component of tow force and the passive pressure component when compared to the 50th scale plough data. The reason why the Cathie and Wintgens (2001) data does not fit the small scale test data could lie in scaling issues which are discussed later in this chapter. It could equally be associated with the back analysis of sometimes dubious data that Cathie and Wintgens (2001) had to work with which may cause the discrepancy between their coefficients and the scale model test data presented here.

Equation 4-3 is a better fit to the shallow depth scale model data than Cathie and Wintgens (2001) but a worse fit to the tests at greater depth. The interface friction calculated by Equation 4-3 matches the data reasonably well which is why Equation 4-3 gives a reasonable fit to the shallow test data. The passive term however,

does not and is likely due to the assumption of two dimensional planar failure mechanism used for the calculation of K_p. The back calculated C_w or tanδ value of interface friction coefficient from the 50th scale plough test data in HST50 is 5.4 which is slightly higher than found duing the interface friction shear box tests in HST50 and 35% greater than the Cathie and Wintgens (2001) value. The C_s value back calculated from the test data is again greater than both the Cathie & Wintgens (2001) value and the value found analytically. The D^3 nature of the respective passive components of Equation 4-3 and Equation 4-4 do however appear to make a good fit with the data which provides confidence in their form. The problem is in finding the magnitude of effect of the simplifications made in Equation 4-3 and in correcting them.

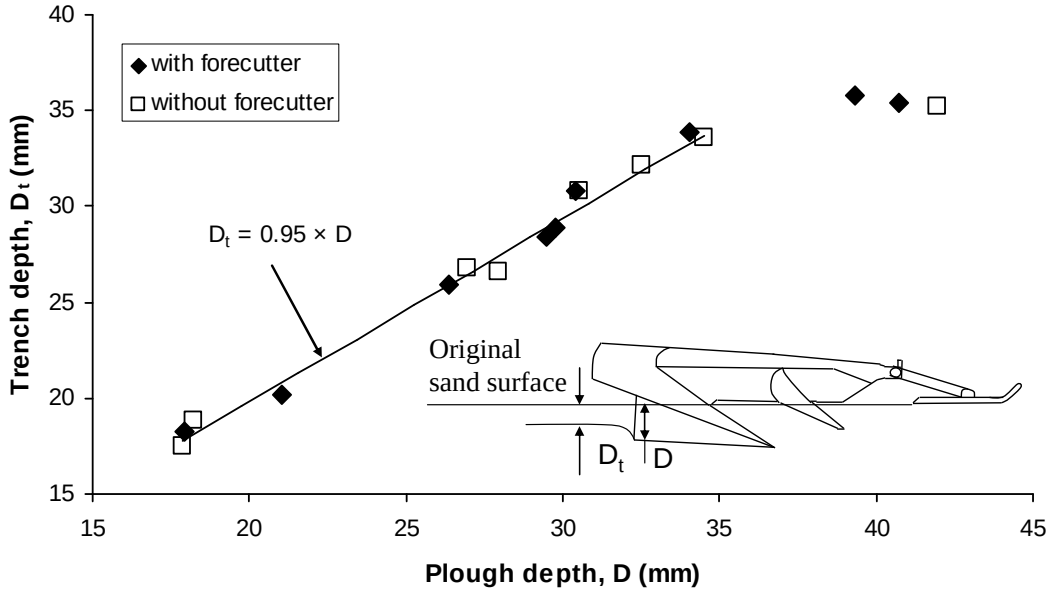

Figure 4-7: Comparison of 50th scale plough depth and trench depth in dry HST50 at D_r = 25%

The tow force associated with a given plough depth is of course of great interest to a trenching contractor. The other depth associated commercial interest is the relationship between plough depth and the depth of trench achieved. This relationship is governed by two phenomena, namely: trench collapse and over topping both of which reduce the trench depth for a given plough depth. This is important as there is little point in increasing the plough's depth (with an associated increase in tow force) if all that happens is all the extra spoil generated falls back into the trench below the

laid pipeline. Figure 4-7 shows the relationship between plough depth and trench depth for the 50th scale plough.

The final excavated trench depth is approximately 95% of the plough depth for plough depths up to 35 mm after which trench depth only increases very slightly with plough depth and by 39 mm no increase in trench depth is observed for an increase in plough depth. For tests where the plough depth was less than 35 mm there was very little to no fall back of spoil into the trench and any difference between plough depth and trench depth in this case was possibly due to measurement error but may have been due to the sand either relaxing after reduction in normal effective stress once the plough had passed or dilating during shearing.

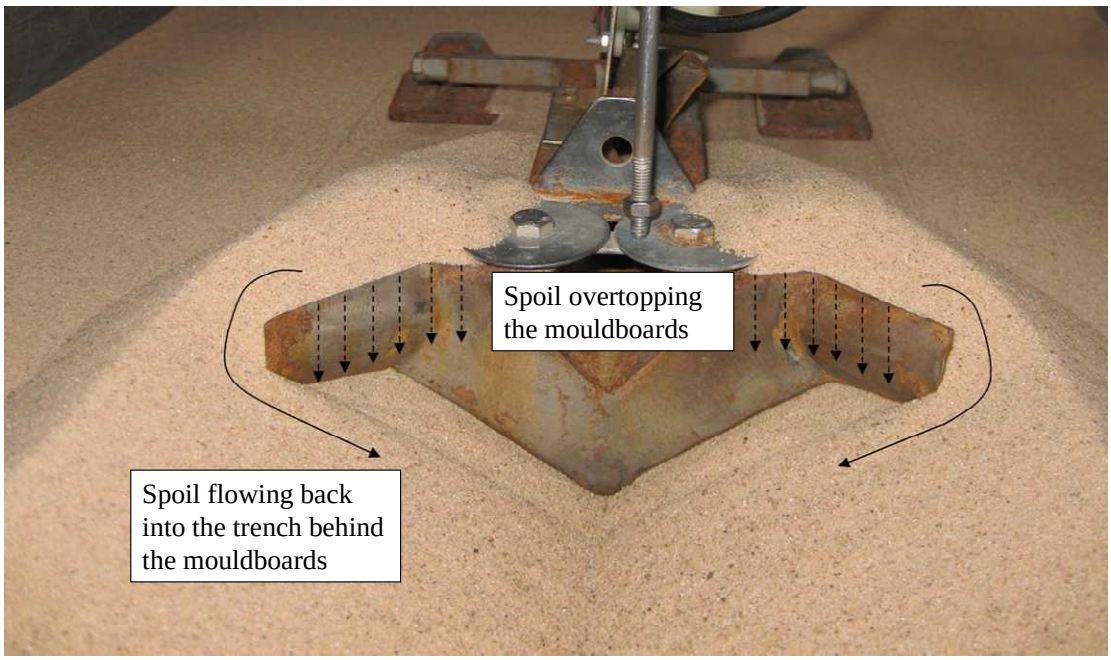

Figure 4-8: Spoil falling into trench during a test with plough depth = 41 mm

As the plough depth increased beyond 35 mm, sand started to flow around the sides of the mould boards (see Figure 4-8) and into the trench reducing its depth. Figure 4-8 shows the 50th scale plough, trenching in HST50 at 41 mm depth. The curved arrows at either side of the mouldboards indicate sand flowing around them and cause a step in the trench depth between the sand immediately behind the plough and the sand far behind the plough. The dashed arrows point out that a small amount of sand was overtopping the mouldboards indicating that the plough was operating at its maximum

depth. The use of larger movable mouldboards would prevent sand flowing around them but may not prevent overtopping and would undoubtedly increase the tow force.

The variation in trench profile with ploughing depth is shown in Figure 4-9. The trench profiles show that spoil sand falling into the trench from the heaps during deep ploughing tests causes a 'V' shaped trench trough whereas during shallow ploughing tests the box shape of the heel is better preserved in the trough. The angle of the side walls, α is sculpted by the share which slopes at 35º to the horizontal across its width. In the tests the angle of the side walls α_t ranges from 32º-34º with the critical angle of friction for HST50 equal to 34º (which is less than the share angle) defining the limiting angle for the side walls. Trenches with side walls of greater than φ'_{crit} (34º in HST50) are likely to have been subject to fall back of spoil from the heaps which sit at either side of the trench.

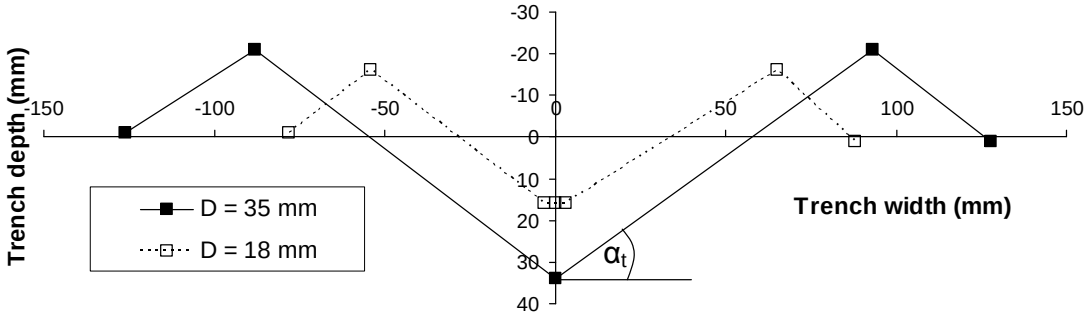

Figure 4-9: Trench profiles in dry HST50 at D_r = 25%

This information may be of use to industry as it shows that the closer the plough is pushed to the limits of its capability the less efficient it will be. It also shows that when trenching up to as deep as 35 mm model scale (1.75 m full scale) the plough is trenching efficiently as there is minimal fall back of spoil. This is confirmed by Machin (1995) who shows 1.8 m deep trench profiles created during a single pass by Coflexip Stena Offshore Ltd's Multipass Plough (MPP). It should be noted however, that the ratio of trench depth to plough depth would likely be considerably lower in the field when ploughing in more complex conditions. Non uniform bathymetry, such as sand waves would cause the plough's depth and pitch to constantly change and could consequently cause overtopping of the plough (Bransby *et al.*; 2010). Turbulence and eddies in the water flowing behind the plough may disturb spoil heaps and cause trench collapse. Both of these scenarios would serve to reduce the trench depth for a given plough depth and are likely situations when ploughing offshore.

4.2.3. Effect of forecutter on plough performance

Figure 4-10 plots steady state tow force against plough depth for ploughing tests both with and without a forecutter, in loose, dry sand (HST50). At plough depths below 26 mm the forecutter has no apparent affect on tow force as it is either fully disengaged (from 0 mm to around 12 mm plough depth for a pitch of 0º) or not significantly engaged (12-26 mm share depth, 0-14 mm forecutter depth) with the sand to have an affect on tow force. Use of the forecutter causes an increase in the tow force at depths of 26 mm and above. This may be due to shearing of some sand twice, firstly by the forecutter and secondly by the share as the forecutter does not push sand away from the share's path (see Figure 4-12b for relative positions of share and forecutter). At 30 mm plough depth the forecutter increases the tow force by 6% and at 40 mm this has increased to 10%.

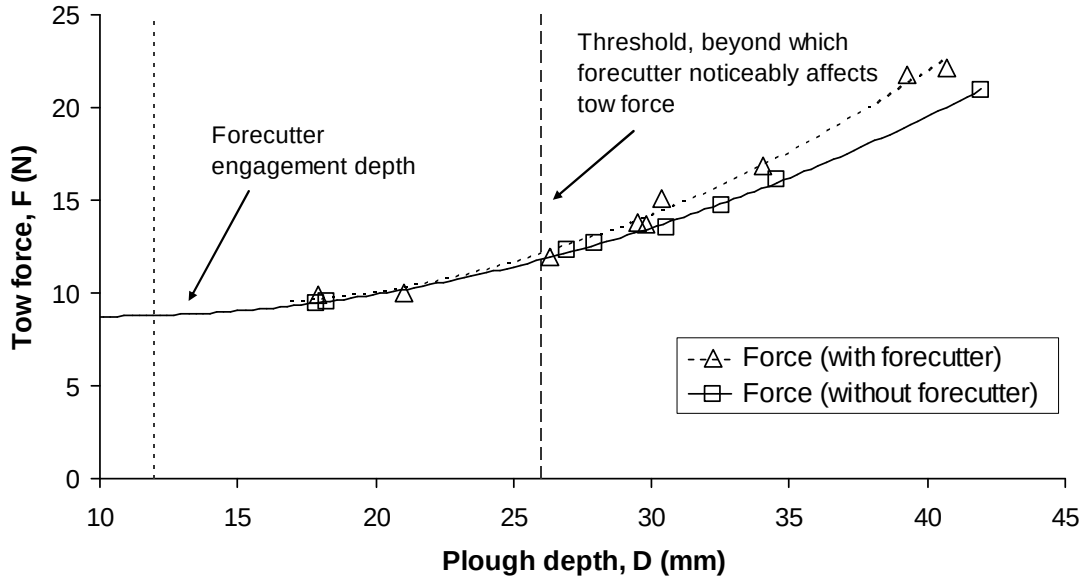

Figure 4-10: Effect of forecutter on tow force in dry HST50 at D_r = 25%

The forecutter also affects plough pitch and causes the pitch to reduce (pitch forwards) for depths where it is engaged significantly with the sand, i.e. $D > 26$ mm (see Figure 4-11). As plough depth decreases the pitch of the plough both with and without a forecutter converge to approximately 1º at around 26 mm. The forecutter may reduce pitch by altering the moment equilibrium of the plough as the resultant force from the sand above the share is pushed forwards towards the skids reducing its lever arm (see Figure 4-12).

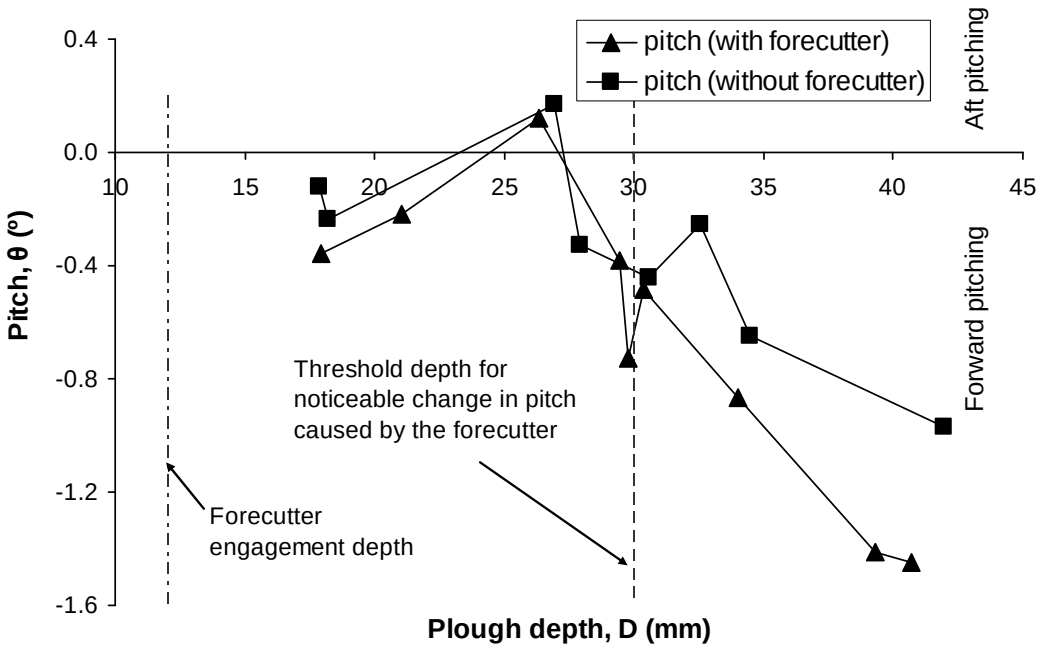

Figure 4-11: Effect of forecutter on pitch in dry HST50 at D_r = 25%

Figure 4-12 and Equation 4-6 illustrate that the depth of the plough is maintained by ensuring moment equilibrium about the pivot point *x*.

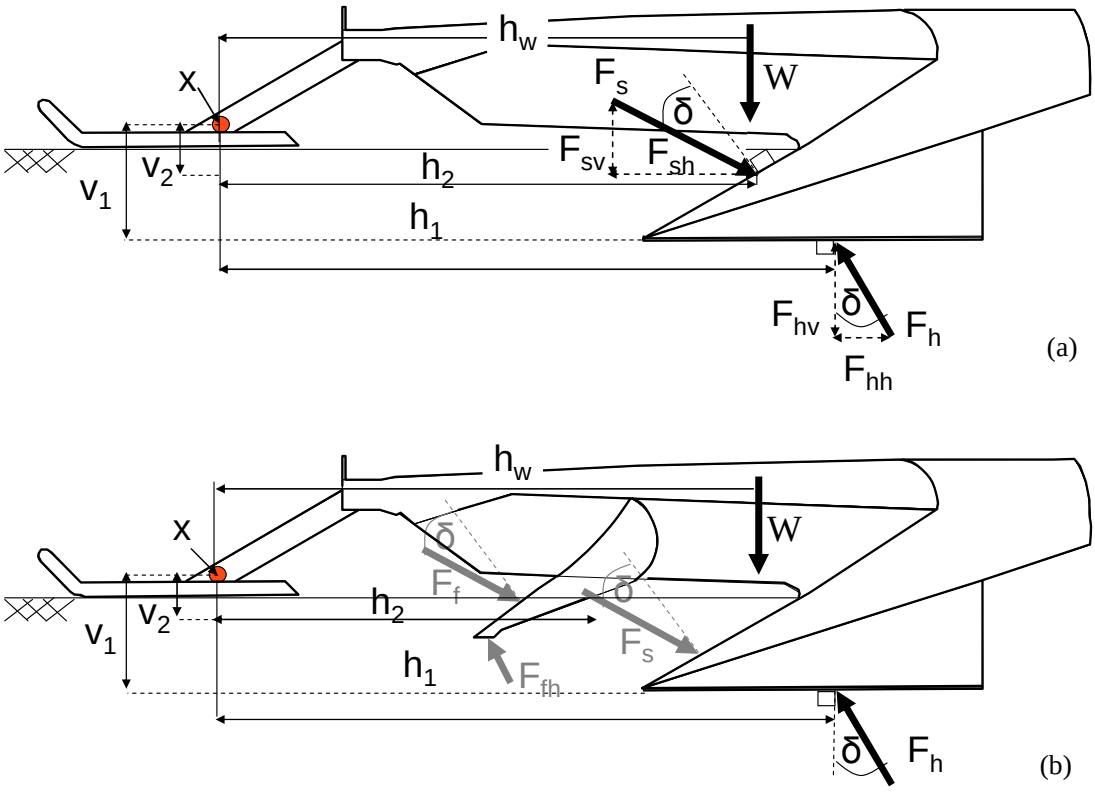

Figure 4-12: Depth control by moment equilibrium, (a) without a forecutter, (b) with a forecutter

$$Wh_w + F_{sv}h_2 - F_{hv}h_1 - F_{sh}v_2 + F_{hh}v_1 = 0 \quad (4\text{-}6)$$

The vertical component of the share force, F_s acting at horizontal distance, h_2 from x and the self weight of the plough, W acting at h_w from x are in opposition to the vertical component of the heel force, F_h acting at horizontal distance, h_1 from x and the horizontal components of F_s and F_h acting at vertical distances v_2 and v_1 respectively. For a more in depth description of plough kinematics and the long beam principle please refer to Chapter 2.

In Figure 4-12b the plough has a forecutter which is likely to reduce the magnitude of F_s but adds a forecutter reaction force F_f and effectively reduces the distance h_2, causing an overall reduction in the clockwise acting moment on the plough. The force F_{fh} is likely to be small due to the small size and shape of the under side of the forecutter. The forecutter therefore has the effect of causing the plough to forward pitch as less penetration is required by the heel to generate moment equilibrium through F_h and the trenching depth is reduced.

4.2.4. Influence of density on plough performance

Figure 4-13 illustrates the development of steady state depth, pitch and tow force in loose and very dense HST50 for the same skid setting which are typical for the whole test series. The plough was observed to trench deeper with a slightly greater pitch in loose sand compared to dense. The tow force in dense sand is greater for the deeper ploughing depths but only marginally so due to the plough depth reducing at the same skid settings in comparison to the loose sand tests. Plough depth and pitch reach constant values (steady state) by 350 mm plough displacement and tow force by 500 mm in loose sand, the lag in tow force development is presumably due to full formation of spoil heaps. In contrast, the spoil heaps develop simultaneously with plough depth and pitch for the very dense sand condition as greater plough displacement is required to reach steady state conditions which occur after approximately 600 mm of plough movement.

Trench cross sections have been measured at 250 mm intervals for some of the ploughing tests. However the resolution of this when considering the development of spoil heaps is very poor and formation of spoil heaps has only been considered qualitatively through observation during ploughing tests. In order to provide quantitative analysis of spoil heap formation the trench would require 3 dimensional mapping so that the volumes of sand excavated and deposited above original bed level could be found at any point along the trench.

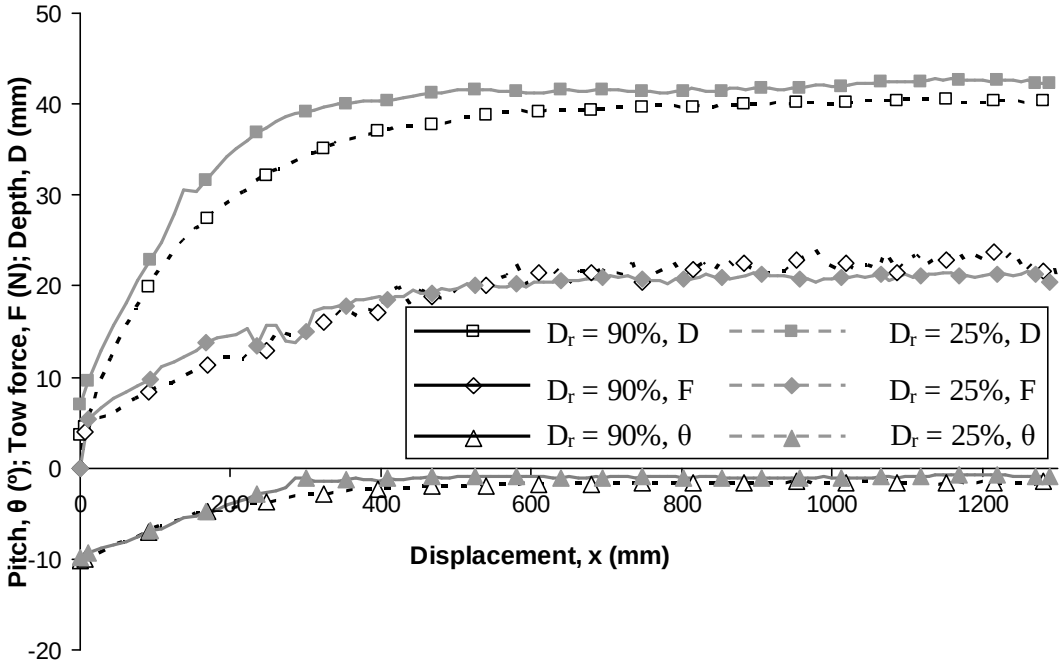

Figure 4-13: Development of steady state conditions in dry HST50 at two different relative densites (D_r = 25% and D_r = 90%)

Figure 4-14 compares the loose (D_r = 25%) tow force data previously shown in Figure 4-10 with ploughing tests conducted in very dense (D_r = 90%) HST50. The tow force is increased for the very dense tests when compared to the loose tests and this is most noticeable at the greatest plough depths. At 30 mm plough depth the very dense sand causes the plough to generate a 6% increase in tow force compared to the loose sand and at 40 mm plough depth this has risen to a 10% increase.The coefficient of passive pressure K_p, is for, loose and very dense HST50 11.55 and 13.25 respectively, where φ'_{crit} = 34° and φ'_{peak} = 41° were measured during direct shear tests of very dense HST50. If Equation 4-2 can be relied upon the increase in the passive component of

tow force should be around 15% when ploughing in very dense sand compared to loose.

Table 4-2 was constructed to compare the passive component of tow force between ploughing in loose and dense HST50. The loose test data are in fact interpolated between data points as the depths of the tests didn't quite match those of the very dense tests. The tests at 40 mm, 35 mm and 29 mm plough depth all show a 14-15% increase in the passive component of tow force for the very dense tests when compared with the loose tests. This may show that K_p is a good indicator of the passive component of tow force despite the inaccurate assumptions made during its calculation (a two dimensional, planar failure mechanism) and the transient nature of shear planes during ploughing since K_p is based on small strain φ'_{peak} values found during shear box tests. Table 4-2 shows a decrease in the passive component of tow force for the test at D = 18 mm in very dense sand compared with the loose test and is likely to be a result of experimental error. As plough depth reduces the absolute value of passive resistance reduces but the experimental variance stays the same, resulting in a larger percentage error and hence the results at the greatest plough depths can be taken with the most confidence.

Table 4-2: Comparison of passive resistance during ploughing in loose and very dense HST50

Plough depth, D (mm)	Passive resistance $F - W\tan\delta$ (N)		Percentage increase in passive resistance with increasing density from 25% – 90%
	D_r = 25%	D_r = 90%	
40	12.3	14.0	14.2
35	8.2	9.4	14.0
29	4.7	5.4	15.0
18	1.1	0.7	-40.4

Figure 4-14 shows that, as the plough depth reduces the loose and very dense data converge until there is no difference in tow force between them (approximately 25 mm plough depth and below). This is likely to be a result of interface friction accounting for the majority of the tow force generated during ploughing at shallow depths. The steel share is not rough enough to allow significant interlocking with sand

particles, therefore increasing the sand's relative density has only a minor effect on the interface friction angle. For further information refer to shear box interface tests results in Chapter 3.

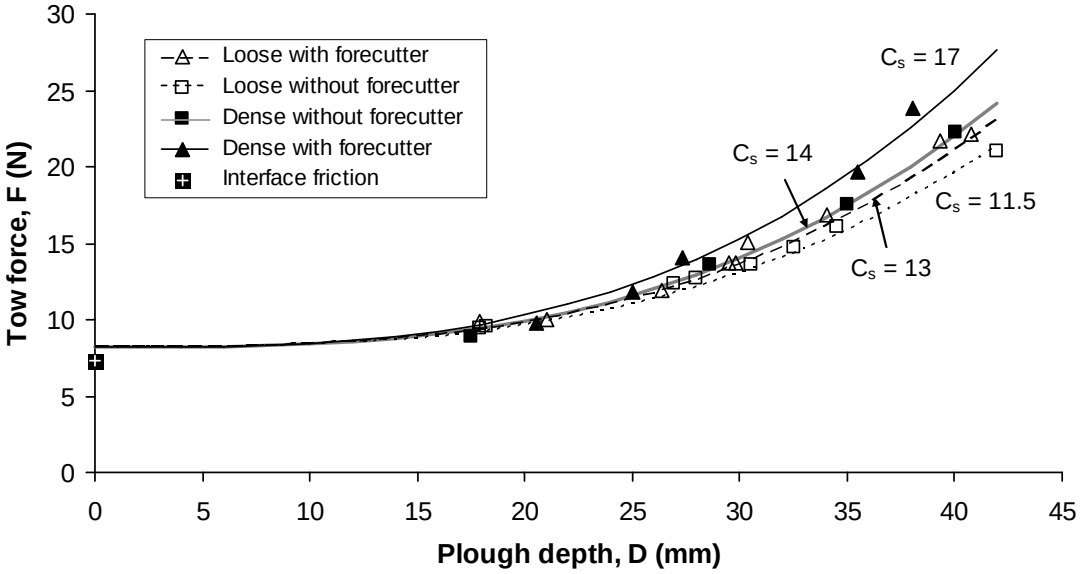

Figure 4-14: Effect of relative density and the forecutter on tow force generation in dry HST50

Figure 4-14 shows that the forecutter has a similar effect on the tow force in the very dense sand as it does in loose sand, whereby tow force is increased at the greater ploughing depths due to forecutter engagement with the sand. The forecutter is seen (Figure 4-15) to cause the plough to forward pitch more at depths greater than 30 mm but not affect the pitch at shallower depths.

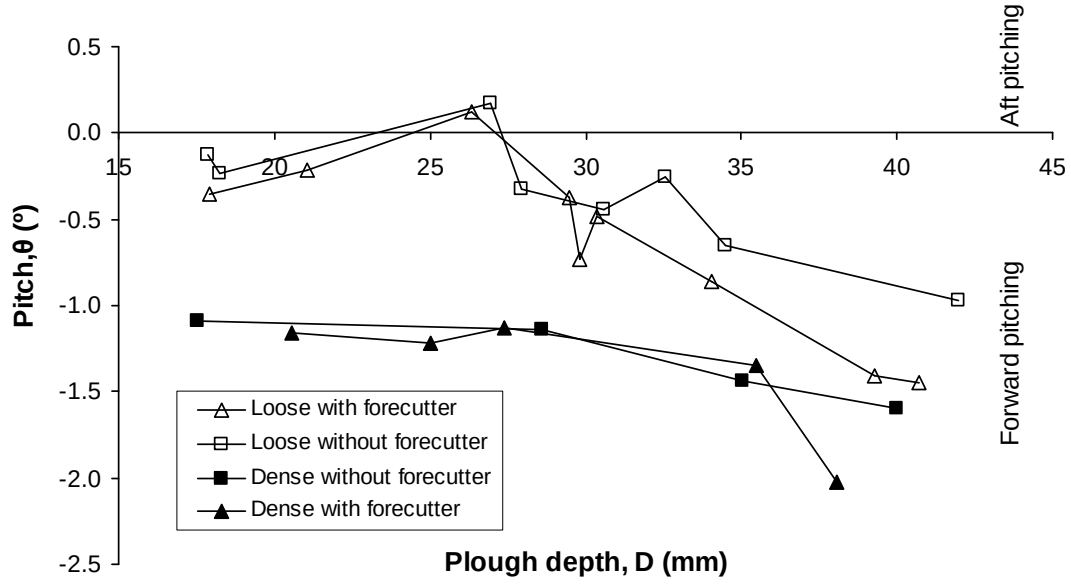

Figure 4-15: Effect of relative density and the forecutter on the plough pitch in dry HST50

Figure 4-15 shows the influence that relative density has on the plough's pitch. The pitch of the plough in both loose and very dense sand increases with reduction in plough depth. The plough tended to pitch between 0.5º and 1º less during very dense tests compared to loose tests which may have been due to increased bearing capacity of the very dense sand supporting the plough. Although they follow the same general trend, there also appears to be some convergence of pitch between loose and dense tests as ploughing depth increased as the pitch seems less affected by plough depth in very dense sand than in loose sand.

4.2.5. Effect of grain size on tow force generation

Figure 4-16 compares the steady state tow force against depth relationships in loose HST95 (fine Congleton) and loose HST50 (medium Congleton). The unit weight of both sands in the condition tested is 15.5 kPa. Due to e_{max} and e_{min} differences the relative densities of HST95 and HST50 are 17% and 25% respectively. At 25 mm plough depth, the forces appear the same but as depth increases there is a slight divergence as the tow force increases more rapidly in HST50 with depth than in HST95 resulting in a 1.5-2 N (7-10%) increase at the maximum ploughing depth of 41 mm.

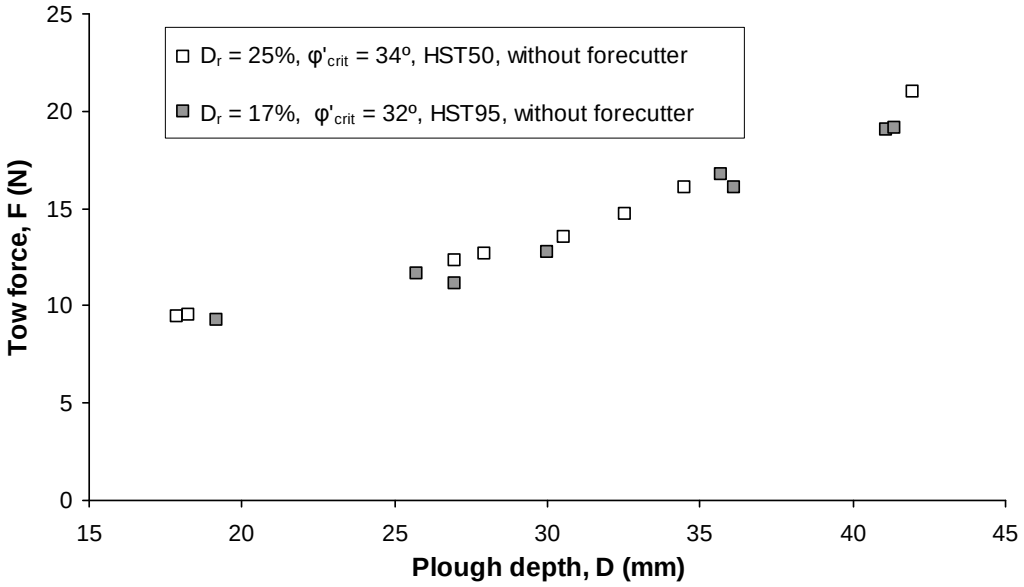

Figure 4-16: Comparison of steady state tow force when ploughing in HST95 and HST50

During shear box tests at low effective stresses, comparable to those experienced during 50th scale ploughing tests, both materials at this state showed measurable difference in their peak shear strength behaviour.

HST95: D_r = 17%, d_{50} = 0.1 mm, φ'_{crit} = 32º, φ'_{peak} = 36º, ψ_{max} = 4º, δ = 24º

HST50: D_r = 25%, d_{50} = 0.19 mm, φ'_{crit} = 34º, φ'_{peak} = 37º, ψ_{max} = 3º, δ = 27º

HST50 displays greater peak behaviour than HST95 possibly due to its larger relative density. The critical state angle of friction of HST50 is higher than that of HST95. These two points probably cause the higher measured tow forces in HST50 shown in Figure 4-16.

4.2.6. The effect of ploughing velocity on plough performance

Figure 4-17 presents steady state data from 6 ploughing tests in loose dry HST95. The effect of ploughing rate on: the required tow force, depth achieved and pitch during ploughing tests in dry sand are shown in Figure 4-17. There is very little difference between the data at 20 m/h and the data at 200 m/h and any difference is likely due to experimental error.

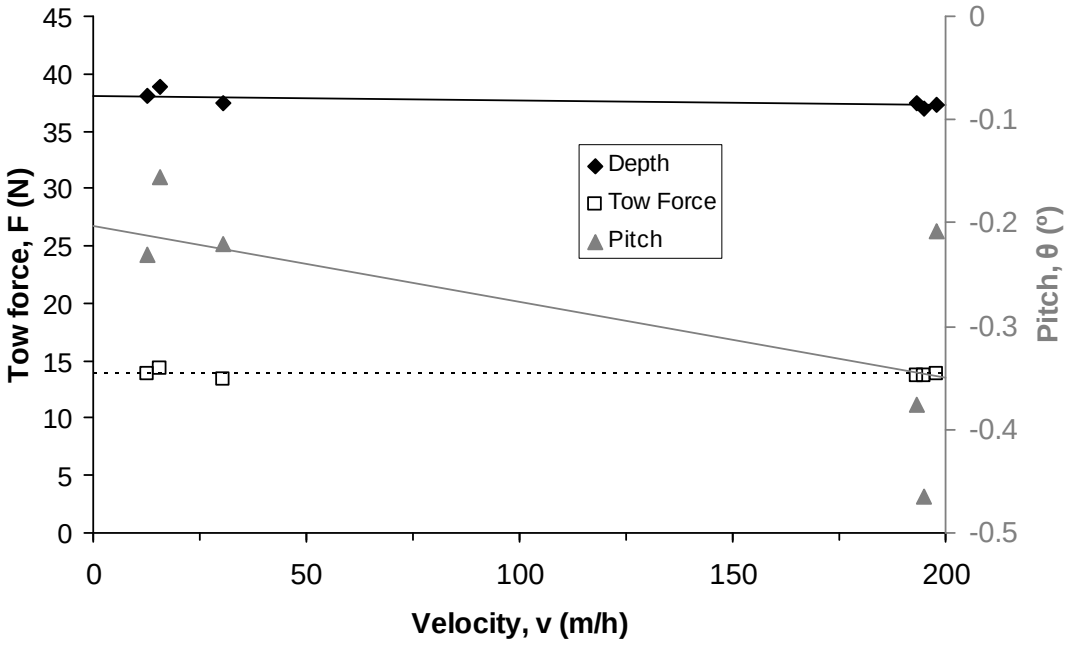

Figure 4-17: Effect of plough velocity on tow force and plough depth in dry HST95 at D_r = 17%

Making an informed estimate on the mass of sand at any time interval being accelerated ahead of the model plough and assuming the sand reaches plough velocity (unlikely worst case scenario) over the length of the share, Newton's Second Law (Equation 4-7) can be used to calculate the forces involved in ploughing which are due to inertia.

$$F = m \times a \tag{4-7}$$

Where m is the mass of the object being accelerated and a is its acceleration

The mass of sand in front of share, derived from measured volume of spoil heaps, known angle of failure plane in sand during ploughing and estimated unit weight of the sand, m = 0.6 kg.

Figure 4-18 shows a sand element initially at rest in front of the share tip at t_0. At some time t_2, the sand has reached its final position before leaving contact with the plough at which point it is assumed to have reached the same velocity as the plough. Figure 4-18 shows a worst case in terms inertial forces generated due to acceleration of sand. A more likely scenario is that the sand never reaches the plough's velocity and that its acceleration will occur over a greater length as it will start to accelerate before the plough comes in contact with it.

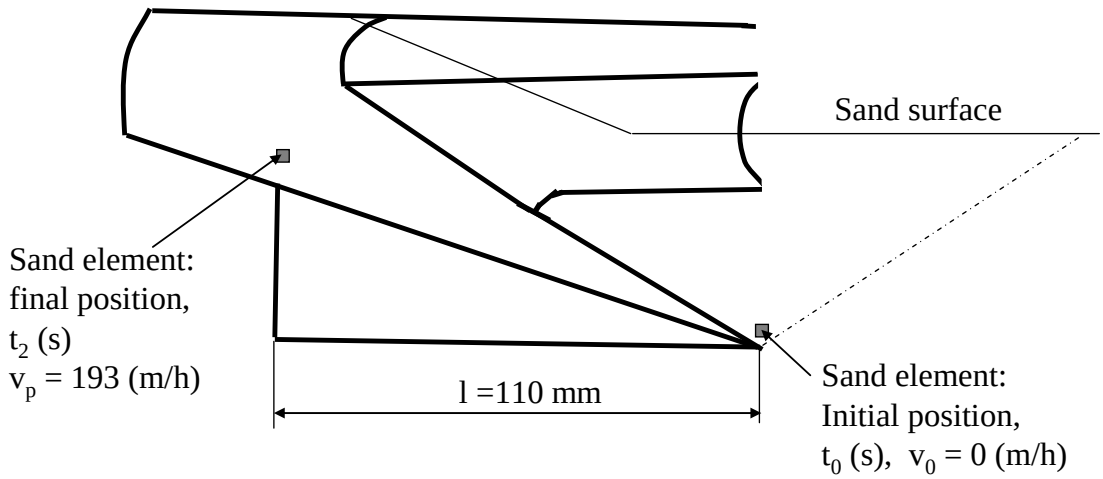

Figure 4-18: Acceleration of sand from stationary, v_0 to plough velocity, v_p

The acceleration of the sand was calculated by Equation 4-8

$$a = \frac{\Delta v}{\Delta t} = \frac{v_p - v_0}{t_2 - t_0} \tag{4-8}$$

where Δv is the change in velocity and Δt is the change in time over the duration of acceleration. v_p is the final velocity of the sand, v_0 is the initial velocity of the sand, t_2 is the time where v_p is reached and t_0 the initial time. For direct comparison to the tests shown in Figure 4-17, v_p was taken to be 193 m/h during the calculation of the expected force due to inertia.

The time interval over the acceleration of sand in front of the share takes place was calculated by Equation 4-9.

$$\Delta t = \frac{l}{v_p} \tag{4-9}$$

where, l is the length of the share

The acceleration of sand from stationary to plough velocity was calculated as 0.026 m/s^2, which allowed the calculation of the inertial force.

$F = m \times a = 0.6 \times 0.026 = 0.0156$ N

The calculation of the inertial force shows that it is ≈ 0.1% of the tow forces of the generated during ploughing at 193 m/h for the 50th scale plough and are likely to be negligible. This knowledge combined with the information in Figure 4-17 is of use in understanding the phenomena observed during saturated ploughing tests, discussed in Chapter 7.

4.3. *Comparison of 50th, 25th and 10th scale ploughing tests*

The majority of the ploughing tests were conducted using the 50th scale plough. This was because materials handling was most manageable using the smallest scale. In terms of a parametric study, 50th scale models seemed to strike an appropriate balance between practical issues and the reduced accuracy of data and measurements due to working at a small scale. In order to find out if and how reducing the scale of the

plough changed its behaviour tests were conducted using 25th and 10th scale ploughs and their results compared to those of the 50th scale plough.

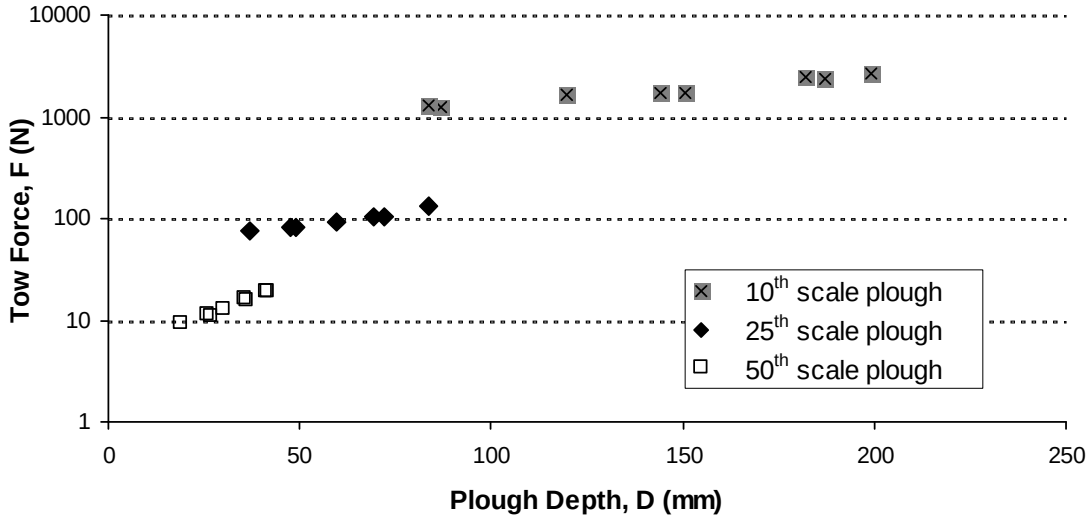

Figure 4-19: Comparison of 50th, 25th and 10th scale plough in dry HST95 at D_r = 17%

The steady state tow force for a range of plough depths is shown in Figure 4-19 for the 50th, 25th and 10th scale ploughs in loose dry HST95. In their current state the three data series cannot be compared and some form of manipulation must be carried out.

The steady state plough data shown in Figure 4-19 has been scaled up to full scale behaviour and is presented in Figure 4-20. The data was scaled simply by multiplying the tow force by the scale factor cubed (Equation 4-13) and the plough depth by the scale factor (Equation 4-11).

Forces are equivalent to the product of stress and area and stresses at model scale are inversely proportional to the scale factor.

$$\sigma_m = \frac{\sigma_p}{N} \tag{4-10}$$

where, N is the scale factor and σ_p and σ_m are stresses at prototype and model scale respectively.

Lengths and therefore plough depths at model scale are inversely proportional to the scale factor

$$D_m = \frac{D_p}{N} \tag{4-11}$$

where D_p and D_m are lengths at prototype and model scale respectively.

Therefore areas at model scale are inversely proportional to the square of the scale factor

$$A_m = \frac{A_p}{N^2} \tag{4-12}$$

where A_p and A_m are areas at prototype and model scale respectively.

Therefore forces at model scale are inversely proportional to

$$F_m = \frac{\sigma_p \times A_p}{N^3} \tag{4-13}$$

This does however ignore issues concerning how shear stresses should scale and the affect that particle size and shear band dimensions have on failure patterns and stresses which further complicate matters (discussed in Chapter 2).

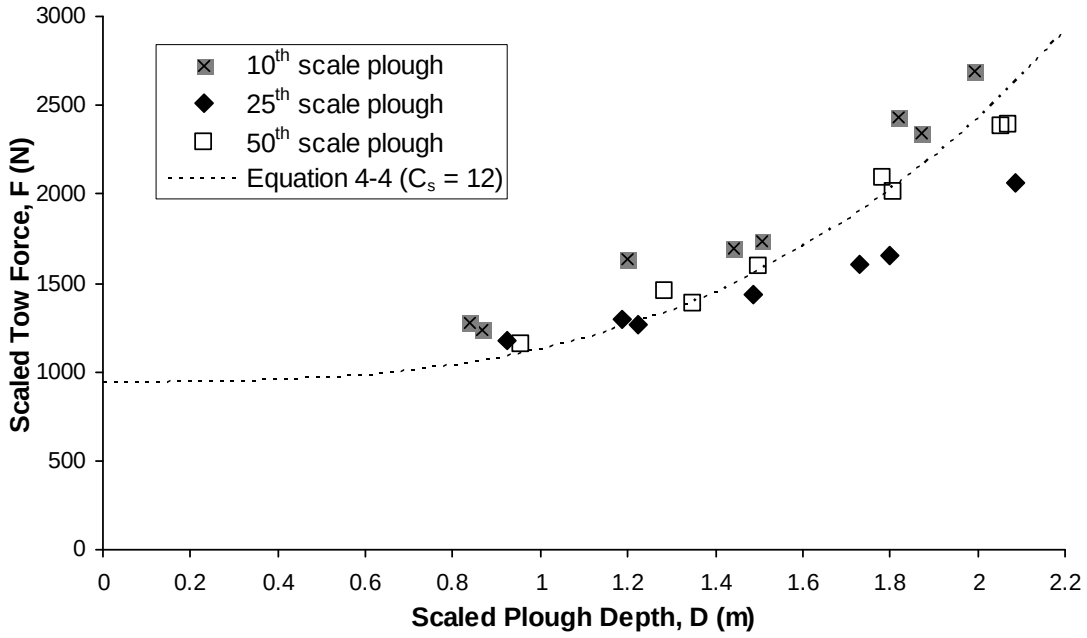

Figure 4-20: Scaling up of steady state data from ploughing tests in dry HST95 at D_r = 95% by Equation 4-10 and Equation 4-12

The scaled up data (Figure 4-20) from the ploughing tests at 50th, 25th and 10th scale compare fairly well. At shallow depths (≈ 1 m prototype scale) the data from the 50th and 25th scale ploughs agree very well. The data from the 10th scale test does however show higher tow forces than the 50th and 25th scale tests. As ploughing depth increases, the tow force increases at a similar rate for both the 10th and 50th scaled ploughs, while tow force for the 25th scale plough increases at a lesser rate.

The reason for repeating tests at three different scales was to see how scale effects affected the results. Figure 4-20 shows that there is no trend corresponding to scale factor in the data, which may prove that 50th scale ploughing tests can be used to directly represent prototype scale ploughs. Lack of a trend corresponding to scale could equally be due to the differences in scale between the models being too small to see an effect through experimental error. The test data fit the shape of the Cathie and Wintgens (2001) passive line, which was constructed using Equation 4-4 with $C_w = 0.45$ and $C_s = 12$ to get a best fit. The C_s value that causes the empirical equation to fit the test data is almost three times greater than the value suggested by Cathie and Wintgens (2001). Their equation would suggest that scale effects existed between model test data presented here and prototype scale, however it is equally possible that the values of C_s which they propose for use in loose sand are inaccurate.

To establish C_s for ploughing tests at 50th, 25th and 10th scale Equation 4-4 can be rearranged to solve for C_s to give Equation 4-14.

$$C_s = \frac{(F - C_w W)}{\gamma D^3} \tag{4-14}$$

Tow force and depth data taken from the model ploughing tests provide F and D whilst shear box test data provides C_wW is the plough weight, the unit weight of the sand is γ and both are known. Figure 4-21 depicts data from the 50th scale ploughing tests where, C_s is the slope of ($F - C_wW$) against (γD^3).

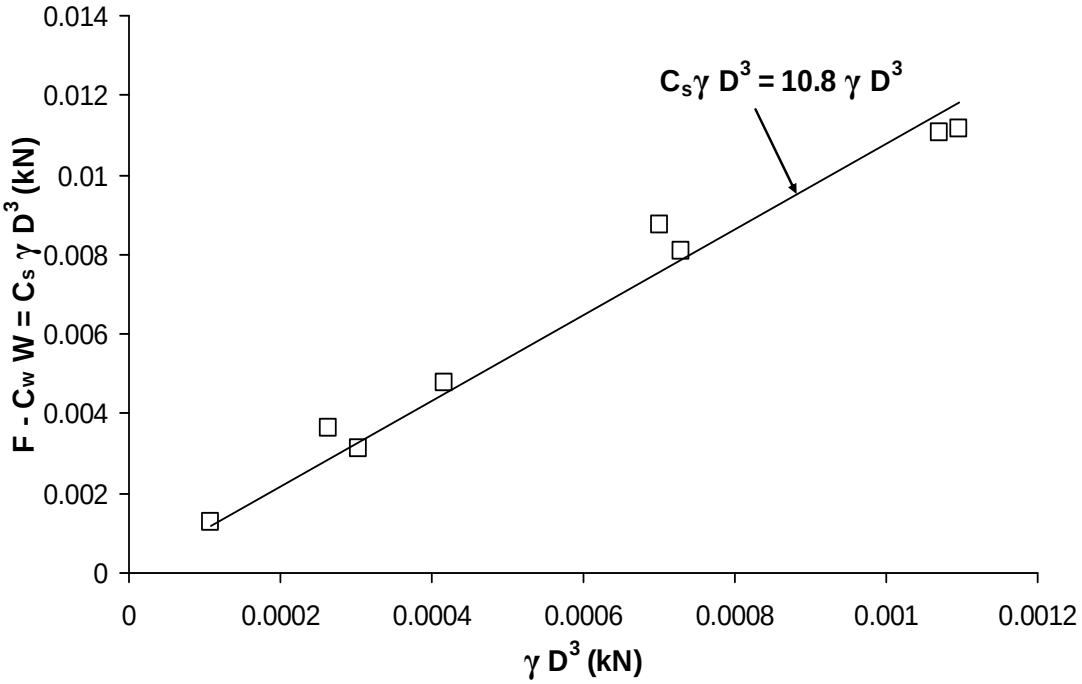

Figure 4-21: Extracting the passive pressure coefficient, C_s from steady state ploughing data in dry HST95 at D_r = 17%

Table 4-3: comparison of C_s values derived from scale model ploughing tests in dry HST95, D_r = 17% at 50th, 25th and 10th scale with the C_s value suggested by Cathie and Wintgens (2001) in loose sand

Scale	C_s values deduced from plough tests
1/50	10.8
1/25	8.6
1/10	14.5
1/1	5 (Cathie and Wintgens; 2001)

C_s is a parameter similar to the passive pressure coefficient, K_p and therefore varies with friction angle and dilation angle. Cathie and Wintgens (2001) suggest that C_s increases with relative density and present values of C_s for use in prediction of tow force depending on the relative density of the sand encountered. This is because φ'_{crit} is expected to spread over a small range of values for silicaceous sand and so variations in φ'_{peak} are expected to be largely due to variations in D_r. The value of C_s may be expected to increase with reduction in scale as this reduces the depth of ploughing and therefore the normal effective stresses, which may cause sand to dilate

more than it would at a higher stress state (see Bolton; 1986). The derived C_s values from the different scaled ploughing tests do not appear to agree with this logic (Table 4-3) as the C_s value for 10th scale ploughing is greater than for both 25th and 50th scale ploughing. This may because at the very low stresses considered during the model tests, φ'_{peak} and ψ_{max} are almost independent of stress (Bolton; 1987). The values in Table 4-3 reiterate what Figure 4-20 shows and highlight the difference amongst the C_s values at different scale model tests but also shows how much larger the C_s values are for all of the model tests in comparison to the Cathie and Wintgens (2001) data.

Due to the unsatisfactory nature of the scaling which was used in Figure 4-20 (possibly as a result of non-linearity of failure envelopes and shear band dimensions and progressive failure), another means of scaling the ploughing data has been investigated. The rationale behind this normalisation is that the share of the plough is relatively self similar especially at shallow depths before the mouldboards are engaged. Figure 4-22 illustrates that when the different scaled ploughs are at the same depth (D_{10}th = D_{25}th = D_{50}th) they affect the same volume of sand ahead of the share. The passive component of the tow force from tests using each scaled plough at the same depth might all be equal (Equation 4-15).

$$F_{10^{th}} - \tan\varphi.W_{10^{th}} = F_{25^{th}} - \tan\varphi.W_{25^{th}} = F_{50^{th}} - \tan\varphi.W_{50^{th}} \quad (4\text{-}15)$$

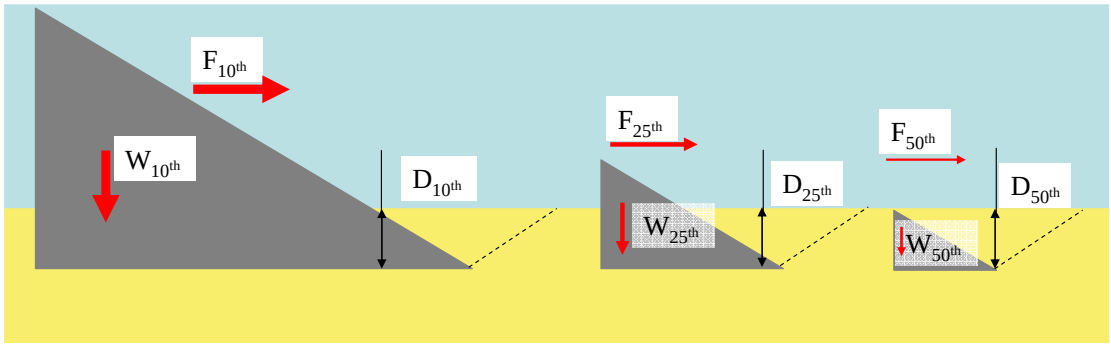

Figure 4-22: Depiction of rationale for modification. (assuming pitch = 0º for all cases)

The data shown in Figure 4-23 are the same as that in Figure 4-19 but the tow force has been modified by subtracting the interface friction component of force (i.e. W.tanδ) for the 50th and 25th scale tests and replacing them both with the interface friction component of force consistent with the 10th scale plough (Equation 4-16 and

Equation 4-17). Normalisation of the data in this way aligns the data from the 50th scale plough with that of the 25th scale plough quite well, however the force from the 10th scale plough sits slightly above the other two scales.

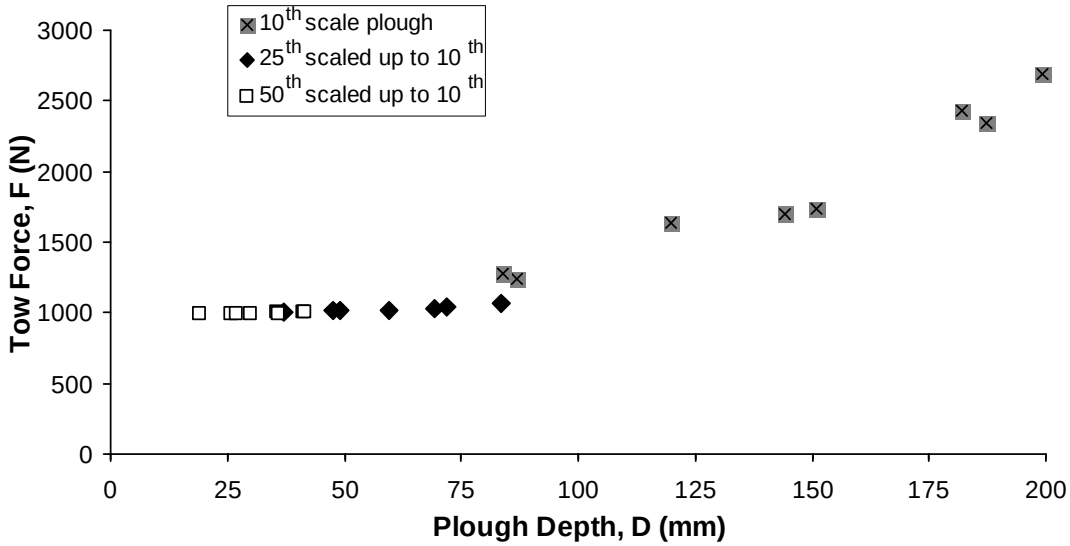

Figure 4-23: Comparison of 50th and 25th scale ploughing by modification of tow force to the 10th scale (W = 1962 N)

$$50^{th}\ scale\ tow\ force\ scaled\ up\ to\ 10^{th}\ scale = F_{50th} + (W_{10th} - W_{50th}).\tan\delta \qquad (4\text{-}16)$$

$$25^{th}\ scale\ tow\ force\ scaled\ up\ to\ 10^{th}\ scale = F_{25th} + (W_{10th} - W_{25th}).\tan\delta \qquad (4\text{-}17)$$

where, F_{50th} is the steady state tow force at 50th scale, F_{25th} is the steady state tow force at 25th scale, W_{50th} is the weight of the 50th scale plough, W_{25th} is weight of the 25th scale plough and W_{10th} is weight of the 10th scale plough.

The data in Figure 4-23 are scaled up to prototype scale by Equation 4-11 and Equation 4-13 but treating all of the data as if it were attained during 10th scale ploughing tests. The product of this manipulation is shown in Figure 4-24, the benefit being that the difference in dilation angle between average stresses involved during 10th scale and full scale ploughing is less than between 50th scale and full scale ploughing. The trade off with this approach is that the 50th scale plough can only be used to represent full scale depths of 10 times the depth tested at model scale and not 50 times the depth (in practice, 0.4 metres and below).

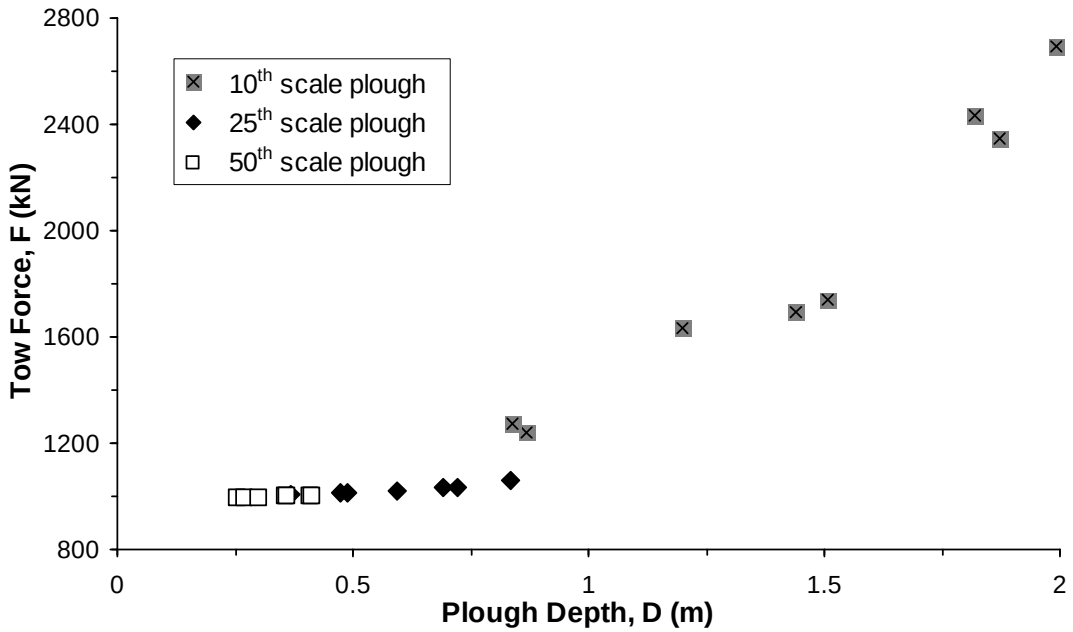

Figure 4-24: Scaling up the tow force by the difference in plough weight

It is not strictly true that the three scales of share are self similar as the ploughs are fitted with a shoe box (a rectangular prism) which runs the full length of the heel from tip to back and at 50th scale is 4 mm high by 9 mm wide. If the ploughs pitch positively so that the back of the heel defines the base of the trench then the self similarity is also reduced. Figure 4-25 shows that when the plough pitches at a positive angle the self similar shape of the different scaled shares does not hold and due to the different plough weights, different confining pressures are applied to the sand being sheared and their effect can not be decoupled from the passive pressure component of tow force.

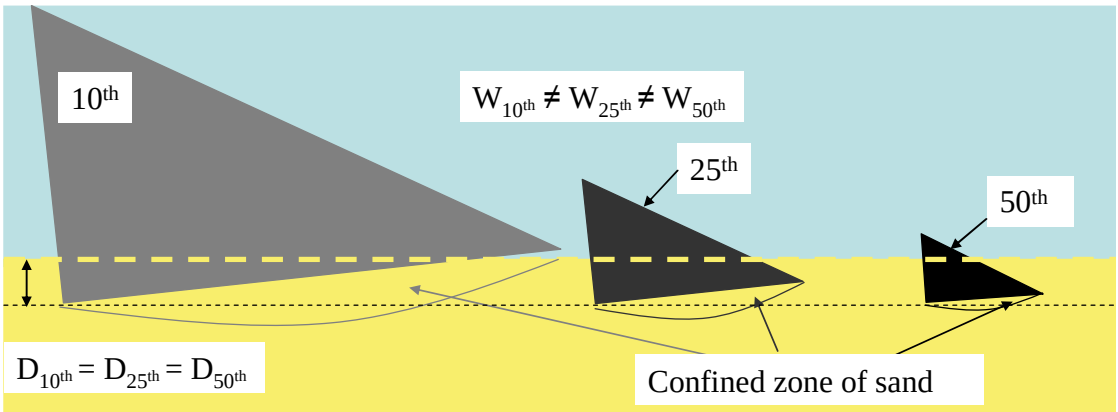

Figure 4-25: Disruption of self similarity

The complications with the self similarity approach to scaling (above) make it less attractive than at first glance. Since it is the plough's performance at deep trenching depths (around 2 m) that are of greatest commercial interest, scaling of results using the self similar approach may not be beneficial and Equation 4-11 and Equation 4-13 may prove to be more useful.

4.4. *Fixed ploughing tests*

The ploughing tests previously described within this thesis have all been setup in order to best replicate offshore ploughing operations. During these tests the plough was towed along a sand bed and was free to pitch and select its own trenching depth as dictated by the balance of the moments acting about the skids. During the fixed ploughing tests, the plough was forced through the sand whilst being held at a particular orientation and depth. Load cells measured the forces acting on the plough and were mounted so as to find the vertical force acting at the front of the plough and at the back of the plough and the horizontal force acting on the plough. A clinometer was mounted to the plough to ensure that the desired pitch was maintained throughout the each test.

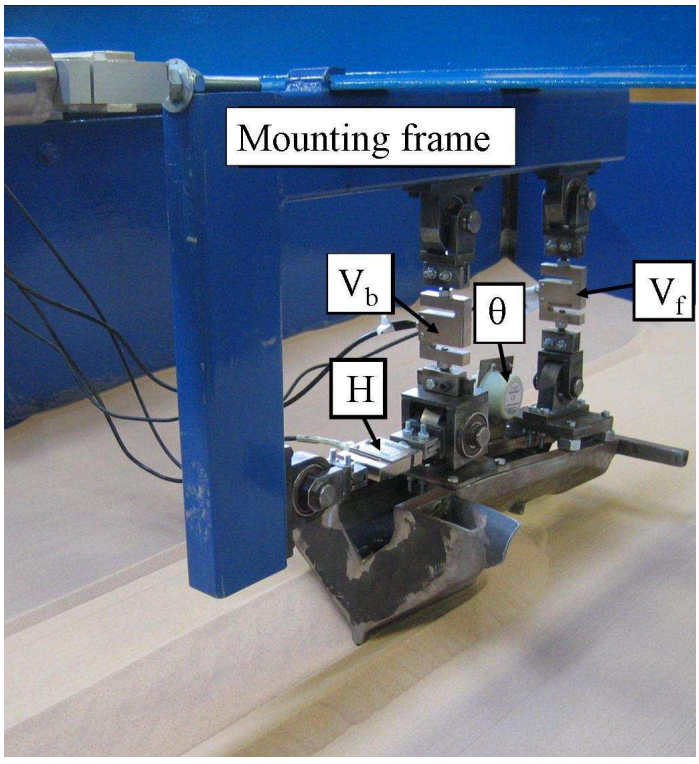

Figure 4-26: Fixed test setup

Figure 4-26 shows the load cell arrangement which was used fix the plough to the "L-shaped" mounting frame. V_f and V_b are forces measured by the load cells mounted vertically at the front of the plough and the back of the plough respectively. H is the force measured by the load cell mounted in the horizontal position at the back of the plough. The load cells are arranged to resist moments through coupled axial forces and the pinned connections at both the mounting frame and plough attachments to the load cells ensure this by preventing the individual load cells from carrying any bending moment.

Fixed tests provide the opportunity to try and break down the components of forces acting on the plough during testing. They allow pitch and depth changes to be isolated from each other which would not be practicable during conventional ploughing tests. A byproduct of fixed testing is that transition lengths are reduced which reduced the length of sand bed required and inturn reduced the mass of sand required for each test and allowing for larger scale model testing.

4.5. *Derivation of useful information from raw data*

The data gathered during the fixed ploughing tests consisted of three sets of load cell readings and Figure 4-27 shows an example of this from one of the fixed tests. Contrary to the conventional ploughing tests which require around 800 mm of transition to reach steady state values the fixed tests reach steady state almost instantly as shown in Figure 4-27. The data are averaged from 400 mm displacement to the end of the test to provide single values of force for each load cell for each test, in the same way as the steady state values for the conventional ploughing tests were arrived at. The sign convention shown in Figure 4-27 is that compression of the load cells is positive and tension negative.

The horizontal load cell is compressed as the plough moves forward and experiences resistance from the sand and for the test shown in Figure 4-27 this results in an average force of 38 N. The vertical load cells are loaded in tension due to the plough's self weight and are also under load from a combination of forces resulting from the sand reacting against the share. To extract the desired information from this data the proportion of the plough's self weight supported by each of the vertical load cells was

found by hanging the plough in space and recording the proportion of self weight supported by each load cell. As the self weight load caused tension (negative force) in the load cells it was then added onto the readings during testing.

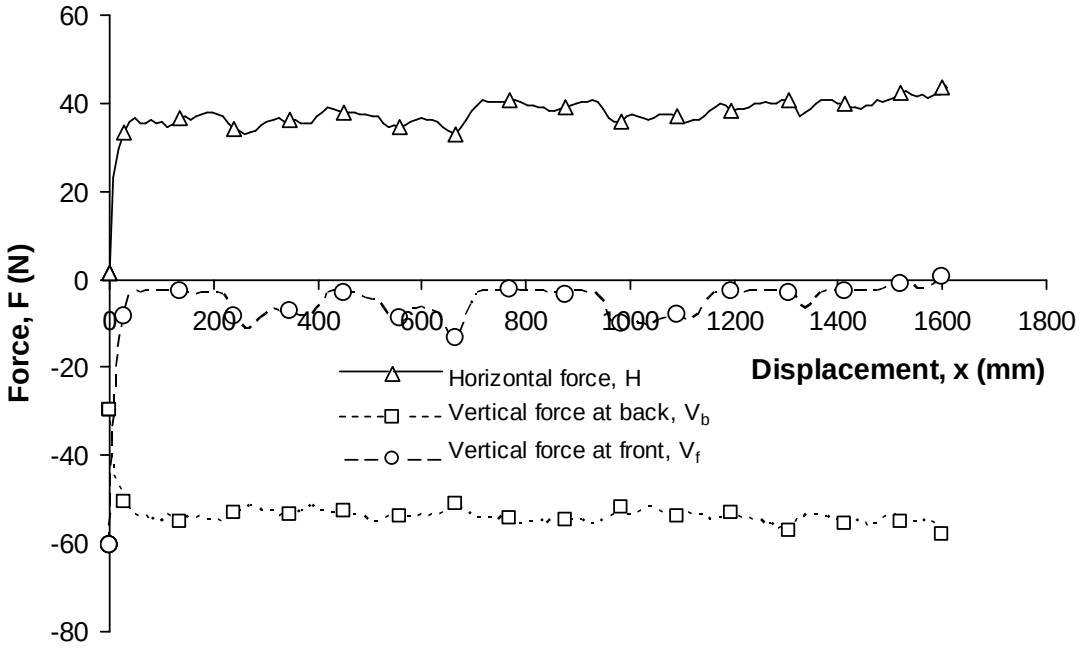

Figure 4-27: Fixed ploughing test using the 25th scale plough in loose, dry HST95 at D_r = 17%

The vertical loads measured during testing were therefore purely the sand reaction forces acting on the plough, which in Figure 4-27 are -3 N and -54 N for the load cell at the back and the front of the plough respectively.

The total vertical force and moment about the share tip are derived from the test data by means of Equation 4-18 and Equation 4-19 respectively.

$$V_{tot} = V_f + V_b \tag{4-18}$$

$$M = V_b \times l_b - V_f \times l_f - H \times l_h \tag{4-19}$$

Figure 4-28 shows the 25th scale plough during a test in its fixed setup and defines the symbols used in Equation 4-18 and Equation 4-19. The force measured by the load cell at the front of the plough is V_f, the vertical force at the back of the plough is V_b and the horizontal force is H. The distances from V_f, V_b and H to the share tip are

shown as l_f, l_b and l_h respectively. The total vertical force V_{tot} is defined as the sum V_f and l_b and moment about the share tip M is found by moment equilibrium. The share tip was taken as an arbitrary reference point for moment as the point of action for the sand reaction force could not be found with our current instrumentation.

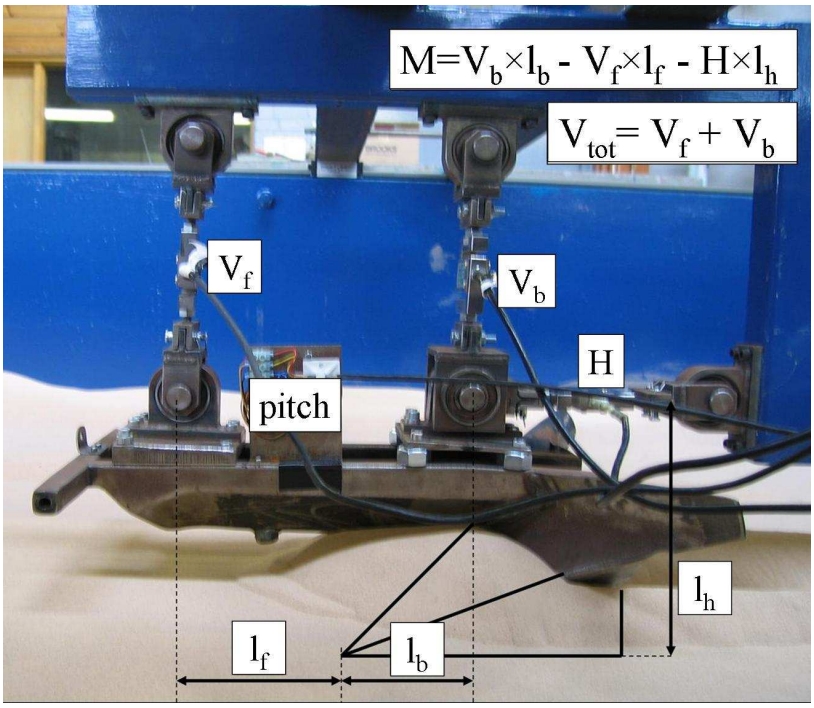

Figure 4-28: Photograph of the 25th scale plough in its fixed test setup showing the location of the load cells and the calculation of *M* and V_{tot}

4.6. *Sensitivity to ploughing depth and pitch*

25th scale fixed ploughing tests were conducted in loose, dry sand at various depths and at 3 pitches (one extreme aft pitch, one close to zero degree pitch and one extreme forward pitch) in order to investigate sensitivity to pitch. The pitch used during the fixed tests was selected to allow comparison with the pitch measured during model plough pull tests and to quantify how extreme aft and forward pitching affected the sand reaction forces acting on the plough.

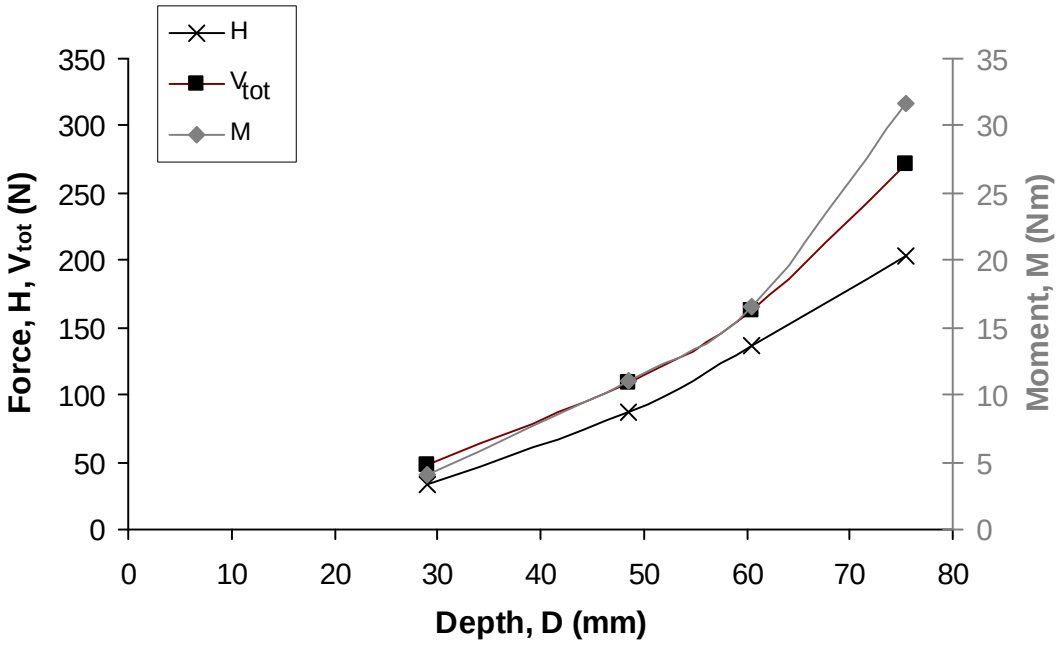

Figure 4-29: Influence of depth on V_{tot}, H and M during fixed tests with the 25th scale plough without forecutter at an aft pitch of 6º in dry HST95 at D_r = 17%

Figure 4-29 shows how V_{tot}, H and M vary with plough depth for 4 fixed tests where the plough was fixed at a 6º aft pitch. V_{tot}, H and M all appear to tend towards zero as the plough depth approaches zero. This is intuitive as there is no sand to react against the plough when its depth is zero.

The data shown in Figure 4-30 were gathered during fixed ploughing tests at an aft pitch of 0.5º which is more typical of the pitches measured during the conventional (drag) model ploughing tests, which tended to pitch between -1º and 1º during testing. The forces and moments are significantly lower in comparison to the test series conducted at an aft pitch of 6º. This may be due to the reduced degree of confined shearing taking place beneath the share as the pitch reduces.

At depths less than 45 mm $V_{tot} > H$ and M increases with depth. As the plough depth increases towards 45 mm the difference in force between V_{tot} and H reduces, as H increases at a greater rate and as a result M increases at a reduced rate with depth. Beyond 45 mm plough depth $H > V_{tot}$ and M starts to reduce.

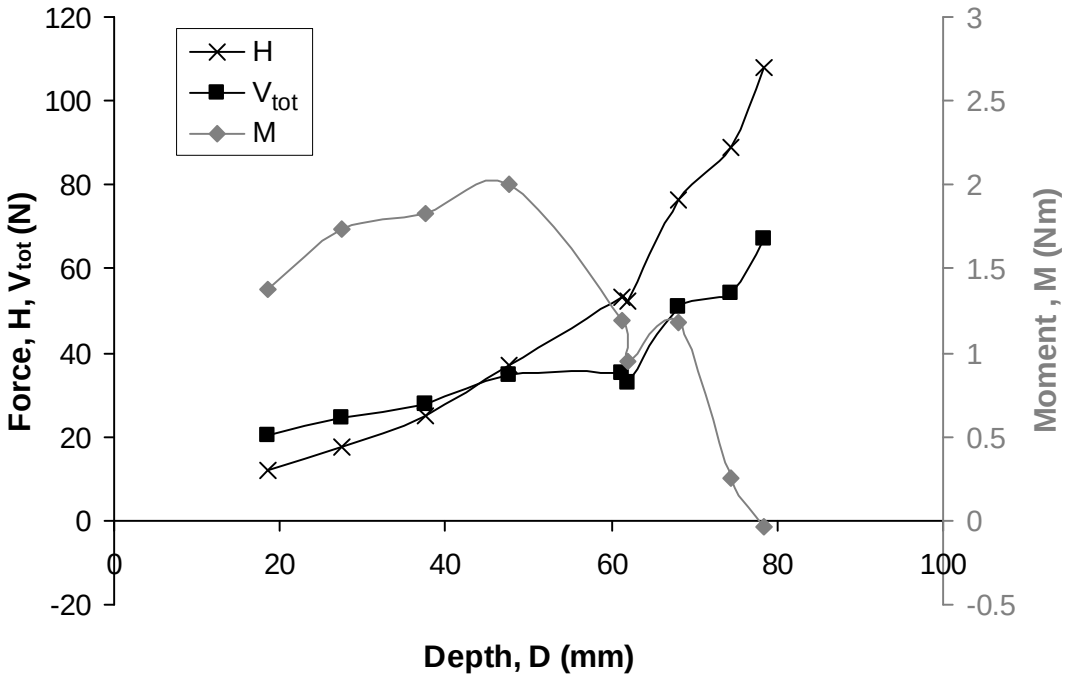

Figure 4-30: Influence of depth on V_{tot}, H and M during fixed tests with the 25th scale plough without forecutter at an aft pitch of 0.5º in dry HST95 at D_r = 17%

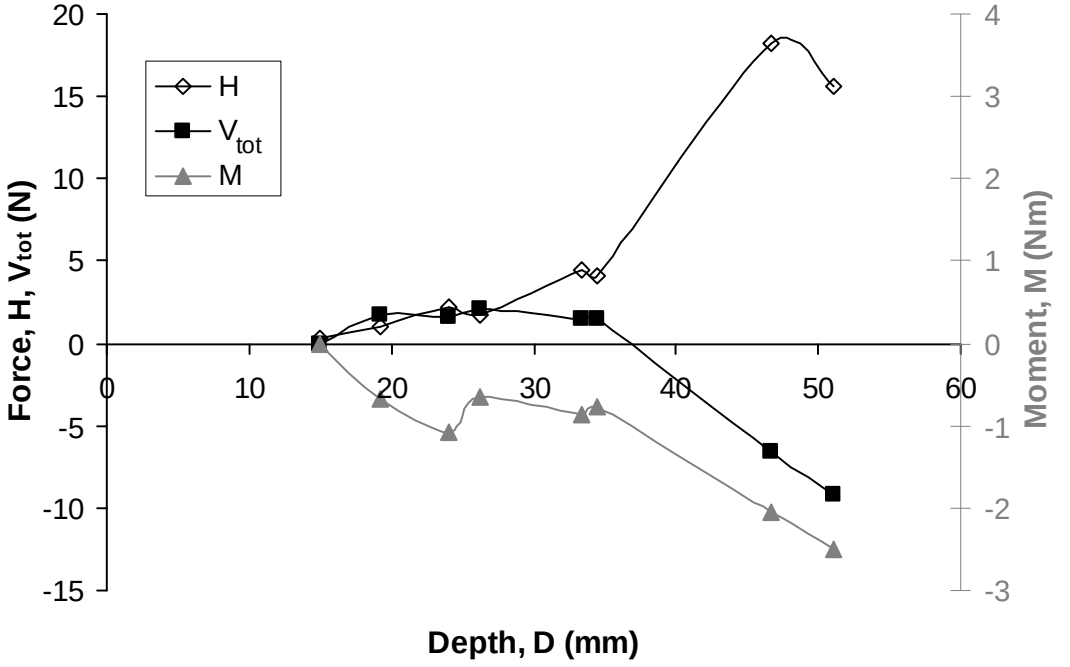

Figure 4-31: Influence of depth on V_{tot}, H and M during fixed tests with the 25th scale plough without forecutter at a forward pitch of -3º in dry HST95 at D_r = 17%

Figure 4-31 shows V_{tot}, H and M during a series of fixed tests over a range of depths where the plough was maintained at a 3º forward pitch. During this setup the

underside of the share is completely detached from the virgin sand as it is shielded by the topside but may contact the sand falling back into the trench. This results in a more simplified combination of forces acting on the share than for the aft pitching case. Plough depths were restricted to 50 mm to prevent the front of the beam making contact with the sand causing an increase in V_{tot} and an associated increase in H.

The forces and moments shown in Figure 4-31 are considerably smaller than for the tests shown in both Figure 4-29 and Figure 4-30 respectively and is likely due to the reduction in confinement as shear planes have a path to the surface of the sand. Forces are very small at low ploughing depths where both normal stresses and the projected area of the share are small and noise and errors will be higher in relation to the readings. V_{tot} appears to increase from close to 0 N to around 1.5 N from 15-19 mm plough depth and fall only very slightly as the plough depth is increased to around 35 mm and then becomes negative at greater ploughing depths.

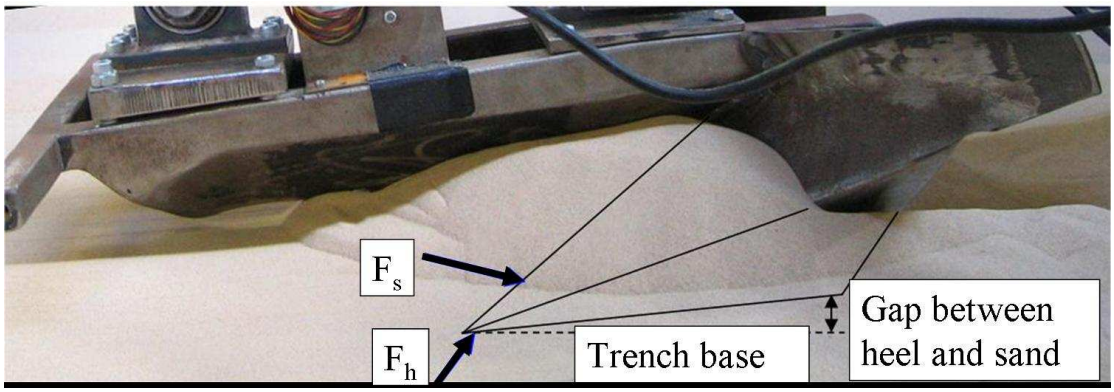

Figure 4-32: Assumed resultants of forces acting on the share and its heel for a forward pitching plough

Figure 4-32 shows assumed resultants of the forces acting on the share, F_s and its heel, F_h during a fixed test where the plough was maintained at a forward pitch. At shallow depths the vertical component of F_h may be greater than the vertical component of F_s which would result in a positive value for V_{tot} as F_h is pushing upwards against the plough and compressing the vertical load cells. As the plough's depth increases F_h increases in linear proportion due to normal effective stress increases but due to the majority of the heel being shielded from the virgin sand by the share, only a small portion of the heel, close to the tip remains in contact with the sand. F_h increases more rapidly with depth as the share widens from its tip up towards

the mouldboards and at a certain depth (possibly around 37 mm judging from Figure 4-31), the vertical component of F_s becomes grater than that of F_h resulting in V_{tot} becoming negative in value.

Figure 4-33 shows assumed resultants of forces acting on the share and its heel for an aft pitching plough. F_s is expected to be of similar magnitude to F_s during forward pitching tests of the same depth. The difference in V_{tot} and H between the forward pitching tests and aft pitching tests is expected to be due to difference in F_h. It should therefore be possible to provide values for F_s and F_h during the aft pitching tests by assuming that F_h is negligible during the forward pitching tests, which may only be true when ploughing at large depths. Subtracting H and V_{tot} established during the forward pitching tests from the aft pitching H and V_{tot} values should provide horizontal and vertical components of F_h during the aft pitching tests.

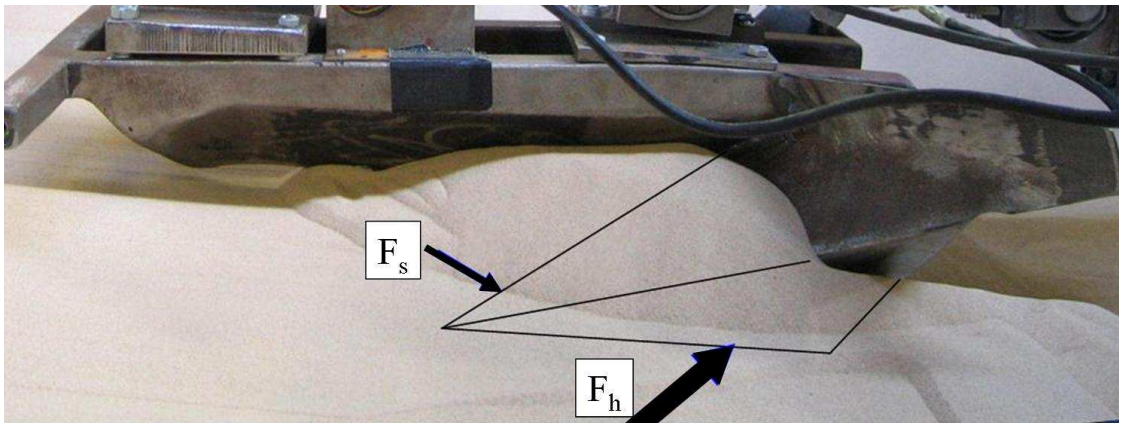

Figure 4-33: Assumed resultants of forces on the share and its heel for an aft pitching plough

The balance of the sum of the moments about V_f can be used to obtain the position of F_s during the forward pitch tests. Figure 4-34 shows how the horizontal position of V_{tot} can be found relative to V_f by simplifying the system two three vertical point loads. This method was employed using the data from the 51 mm and 46 mm deep ploughing tests at a forward pitch of 3º to find the position of F_s. The point of action of F_s for both tests was found to be in front of the share tip, which does not make any sense if the only forces acting on the plough are acting on the share. The most likely reason for this is that the forces acting against the beam are significant during these forward pitching tests where forces are low.

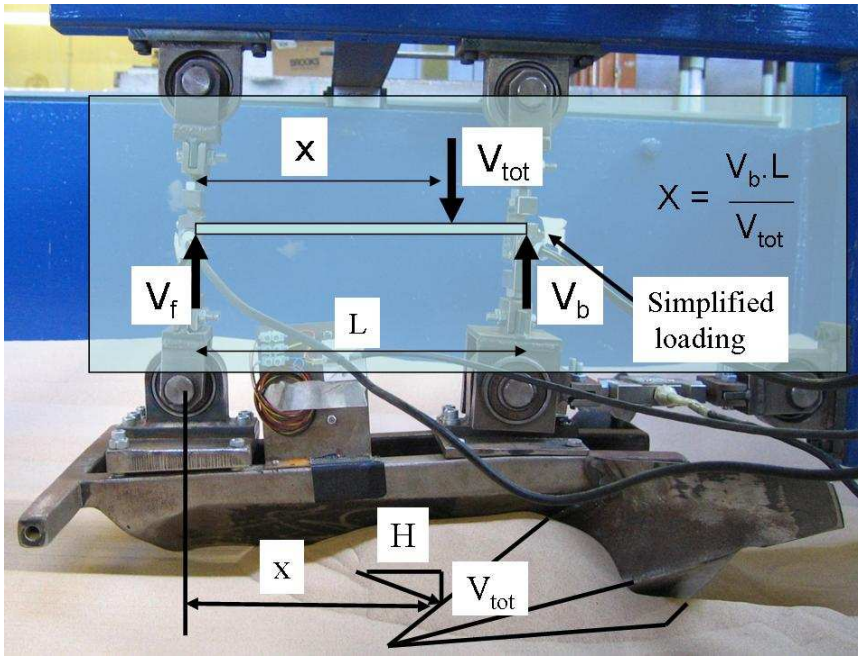

Figure 4-34: Finding the position of the resultant force acting on the share

4.7. *Comparison between fixed ploughing tests and conventional ploughing tests*

A direct comparison between the results of fixed ploughing tests and conventional ploughing tests is essential if fixed tests are to substitute conventional ploughing tests in order to study plough behaviour. During the conventional ploughing tests the plough finds its own depth and pitch which are dependent on skid position and the moments of the forces acting on the plough about the skids. During the fixed ploughing tests the plough is maintained at designated pitch and depth and the forces acting on the share were measured in the horizontal and vertical directions and the moment of resistance calculated from load cell readings.

4.7.1. Equivalent tow force from fixed test results

Figure 4-35 shows tow forces derived from 25th scale plough fixed tests by means of Equation 3-1 ($F = H + \tan\delta \times (W-V)$) and compares them to tow forces measured during pull tests with the 25th scale plough. The tow forces derived from fixed tests compare well with the tow forces measured during the pull tests.

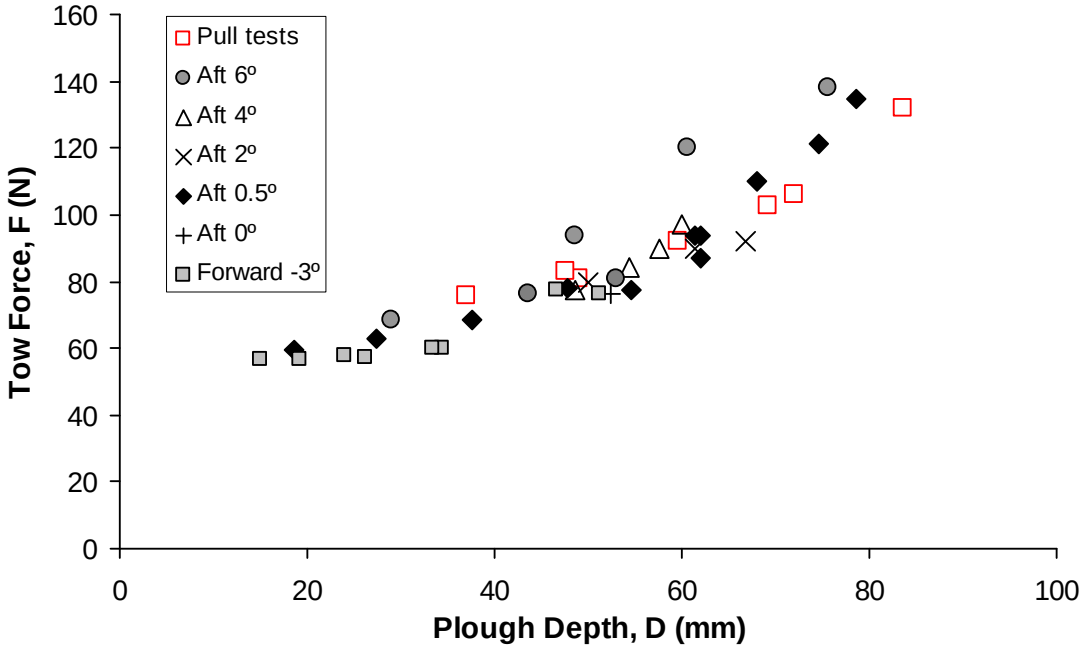

Figure 4-35: Comparison of tow forces measured during pull tests and tow forces calculated from fixed tests at 25th scale, in dry HST95 at D_r = 17% (all results are from tests without a forecutter)

The correction for the assumed difference between vertical forces during the fixed tests and pull tests draws the data together. The tow forces derived from the fixed tests do however tend to fall below the measured tow forces from the pull tests at depths less than 40 mm and are greater than the measured tow forces from the pull tests at depths greater than 60 mm. This might be because the correction for vertical force is not able to catch the sublety as to how plough pitch affects the whole deformation mechanism around the share of the plough which will consecutively influence tow forces generated. It would therefore appear that unless plough pitch measured during the pull tests, which changes with plough depth and the relative density of the sand, is matched during the fixed tests, the tests are not comparable. It would also be desirable to remove the interface friction correction from the comparison of the fixed and pull test results which, has lead to the comparison of moments acting on the plough during the two test types.

4.7.2. Comparison of the moments acting on the plough

The plough depth during the conventional (pull) tests is load controlled since it is dependant on the balance of moments about the skids and the plough stresses the sand directly by its self weight therefore causing strains in order for the plough to maintain its steady state depth. During the fixed tests the plough's weight is supported not by the sand but an external frame and the sand is strained by the plough displacement which generates stresses acting on the plough. The constitutive law between stresses and strains ensures that it does not matter whether an external force applied to the sand causes it to strain or whether displacement of the plough into the sand the same depth causes the sand to strain and in turn generate stresses. Comparison of the moment equilibrium about the skids between conventional ploughing tests and the fixed tests is used as a means of directly comparing tow force found during conventional plough tests to *V*, *H* and *M* found during the fixed tests.

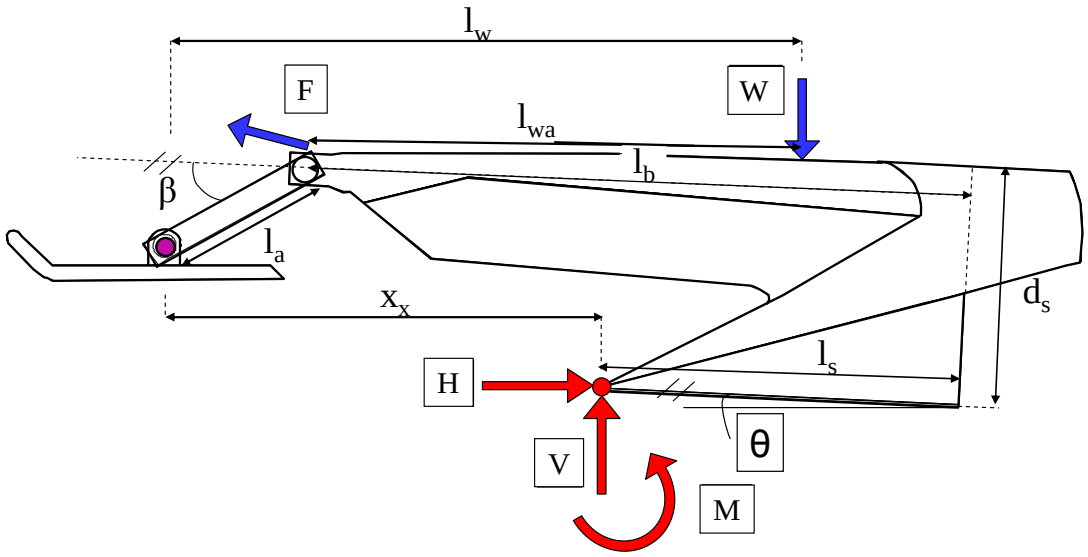

Figure 4-36: Forces acting on plough during trenching and *V*, *H* & *M* resolved about share tip

The external forces acting on the plough during trenching are those of tow force and self weight and are denoted by *F* and *W* respectively in Figure 4-36. The sand reaction forces in the horizontal and vertical planes and the moment reaction during the fixed ploughing tests are all taken at the share tip. As the reaction point for the sum of the stresses acting on the plough during trenching could not be found the share tip was therefore used as a reference point for V_{tot}, *H* & *M* during the comparison of fixed and tow test setups. The horizontal distance between the pivot point at the skids and the

centre of the plough's mass, l_w is calculated using Equation 4-20. The horizontal distance between the pivot point at the skids and the share tip, x_x is calculated by Equation 4-21. The vertical distance between the pivot point at the skids and the share tip, zx is calculated by Equation 4-22.

$$l_w = l_{wa}\cos\theta + l_a\cos(\beta-\theta) \tag{4-20}$$

$$x_x = l_a\cos(\beta-\theta) + l_b\cos\theta - d_s\sin\theta - l_s\cos\theta \tag{4-21}$$

$$z_x = d_s - l_a\sin(\beta-\theta) \tag{4-22}$$

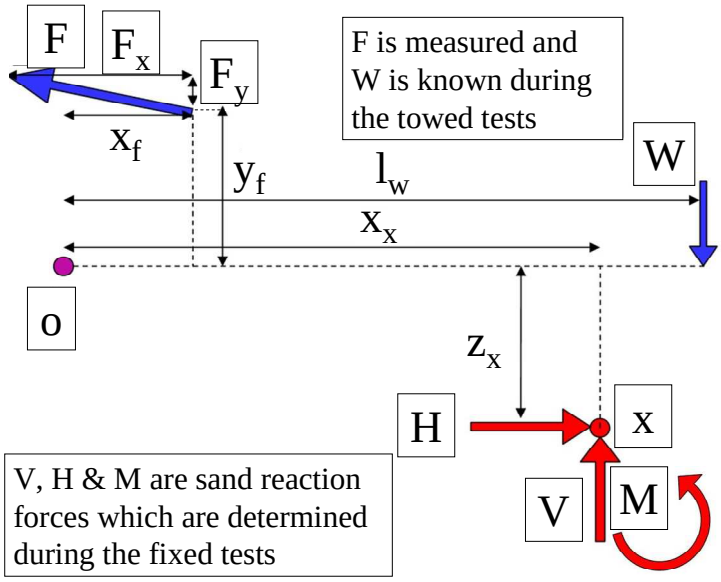

Figure 4-37: Free body diagram of plough

Figure 4-37 shows a free body diagram of the same forces in Figure 4-36 but with distances from every force to the free moment point at the skids, *O* added. For there to be equilibrium (constant velocity translation of the plough without any rotation) the external forces must equal the sand reaction forces during any ploughing test. Assuming that the same depth and pitch settings are replicated in the same sand conditions during a fixed test as for a standard ploughing test, then by moment equilibrium the moments about *O* should balance (Equation 4-23).

$$l_w W - F_y x_f - F_x y_f = H(x_x\sin\theta + z_x\sin\theta) + V(x_x\cos\theta + z_x\sin\theta) + M \tag{4-23}$$

where:

H	Force in horizontal plane
l_w	Length from moment release point at skids to centre of plough weight
M	Moment
F	Tow force
F_x	Horizontal component of tow force
F_y	Vertical component of tow force
V	Force in vertical plane
W	Self weight of plough
x_f	Horizontal distance from tow point on plough to moment release point at skids
x_x	Horizontal distance from moment release point at skids to share tip
y_f	Vertical distance from tow point on plough to moment release point at skids
z_x	Vertical distance between moment release point at skids and share tip
θ	Plough pitch

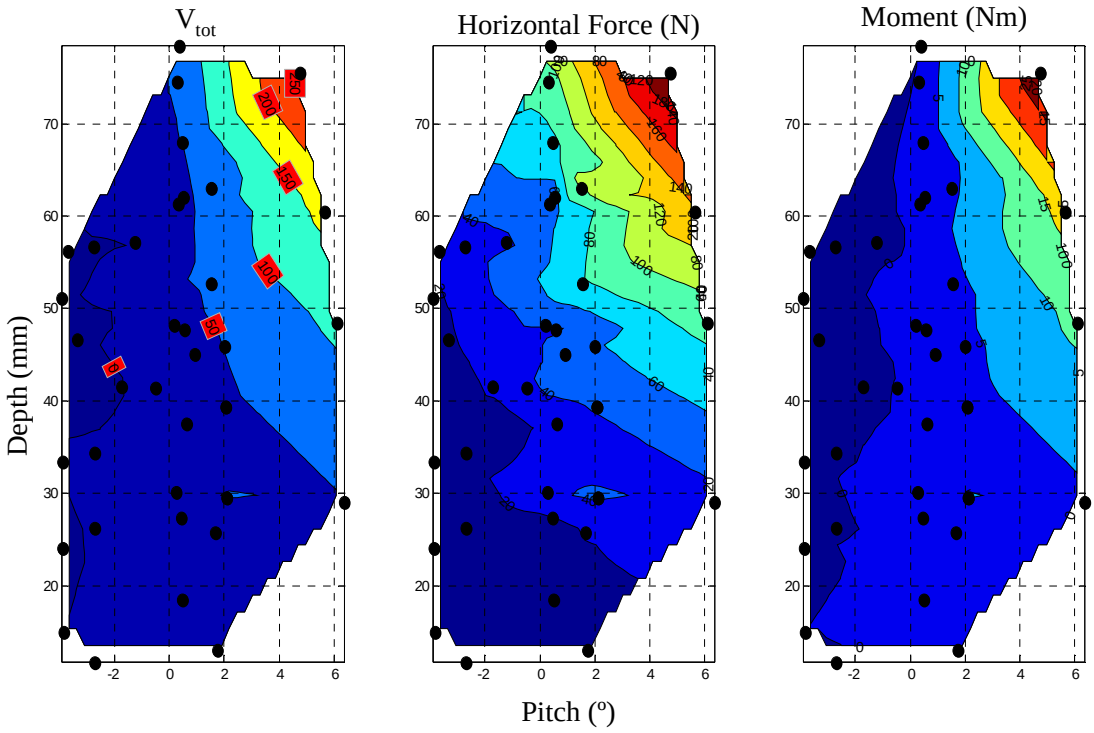

Figure 4-38: Interpolation of 25th scale fixed ploughing test results in dry HST95 at D_r = 17% to provide *V*, *H* and *M* data at specific *D* and θ which can be compared to conventional ploughing tests

Thirty-six fixed ploughing tests at depths ranging from 10 mm to 70 mm and pitches ranging from -4º to 6º were conducted in dry HST95 at a relative density of 17%. Figure 4-38 shows contour plots of *V*, *H* and *M* with respect to plough depth and pitch which were formed by interpolation of the thirty-six 25th scale fixed plough tests, where the black dots show the positions in *θ–D* space where tests were conducted. The spacing of the contours and their slope in *θ–D* space show the same trends as previously discussed in Figure 4-29, Figure 4-30 and Figure 4-31.

Figure 4-38 was used to provide *V*, *H* and *M* data at the appropriate plough depth and pitch which coincided exactly with the conventional ploughing tests shown in Figure 4-39.

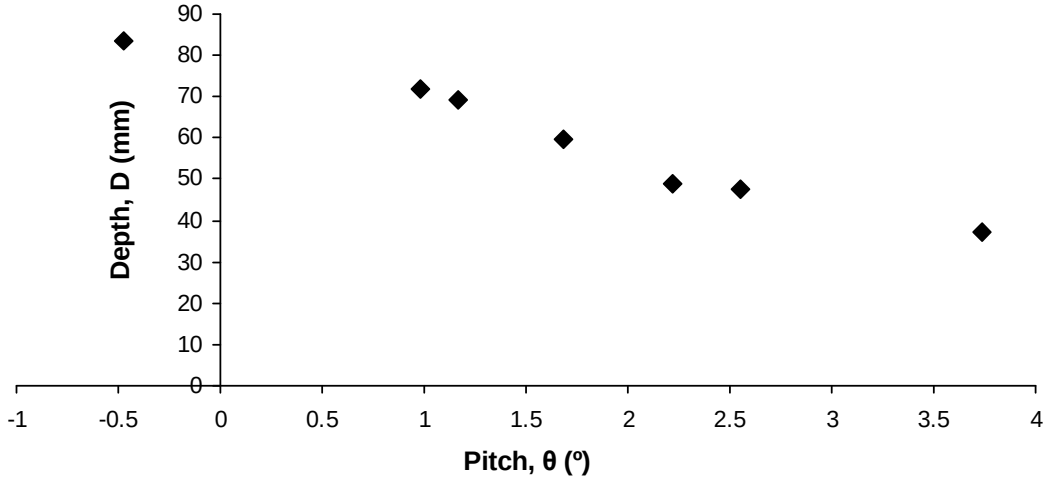

Figure 4-39: Depth and pitch values recorded during the towed ploughing tests at 25th sacle in dry HST95 at D_r = 17%, which were used as means of comparison to the fixed setup

Although there is a good amount of data which form the contour plot of Figure 4-38, much of the data is at depth and pitch combinations which do not correspond to those found during the conventional ploughing tests (see Figure 4-39) and is due in part to problems encountered in accurately setting up the tests. In the range of 0º to 2º pitch over the corresponding depth range of 70 mm to 50 mm there is a reasonable amount of fixed test data which can be used for comparison to the conventional plough tests. In the 2º to 4º pitch range there is a lack of test data and values are interpolated from tests at 2º and 6º pitch and may be a source of error in the comparison of the moments between the fixed tests and conventional tests.

Figure 4-40 compares moment equilibrium between the fixed tests and pull tests. The two data series should align on top of each other if the two test types can be directly compared and tow force can be reliably attained from fixed ploughing tests.

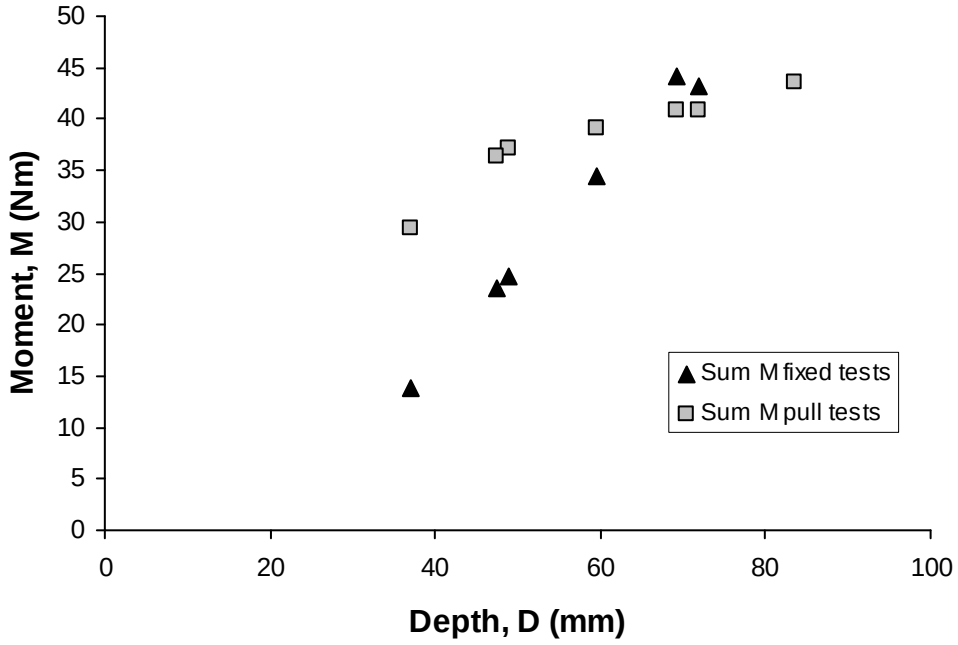

Figure 4-40: Comparison of moment equilibrium between the fixed tests and tow tests

The data does not compare very well although both test types show a similar trend whereby moment increases with depth. The length x_x depended on an arbitrary point at the share tip and was not likely to be the point at which the resultant forces act on the share and as a result various lengths of x_x were assumed for the calculations however this manipulation would not make the two data sets align. In conclusion, at present it would be unwise to use fixed ploughing test data as a means of predicting tow forces.

4.8. *Plane strain simple share tests*

Deformation of the sand in the vicinity of the plough and in particular the propagation of shear planes towards the sand's surface and emanating from the plough's share is of interest. The shear planes along which dilation occurs will no doubt affect the passive component of tow force and the rate effect. It would therefore be beneficial to know how pitch of the plough and possibly the shape of the share influence their behaviour.

A series of tests was conducted whereby a simple triangular prism was pushed through a prepared bed of sand, with the aim of observing the resulting sand deformations. The triangular prism extended the width of the sand box so that its ends could be seen pressed against the inside edges of the box's transparent side walls (see Figure 4-41). The triangular shape seen through the side walls of the box represents a slice through the centreline of the plough's share and during testing sand deformations could be viewed through the side wall as the prism advanced through the sand. Figure 4-41 shows load cells connecting to the prism however force data are not reported here as friction on the side walls of the box rendered the readings difficult to interpret. The alternate layers of natural coloured and blue coloured sand make it easier to observe a shear plane as it causes a discontinuity as it passes through a layer.

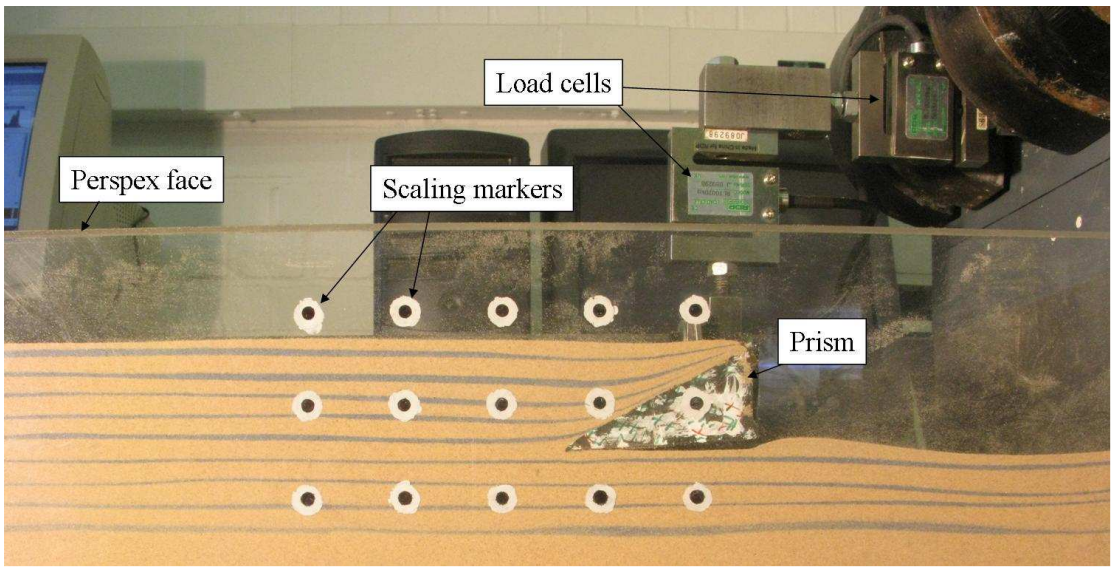

Figure 4-41: Plane strain test setup

Photographs of the advancing prism were taken through the side wall of the sand box at regular intervals. The photographs could be visually examined to map the progressing shear plane(s) and were also run through some software (GeoPIV8, White et al.; 2003) which could accurately map the sand displacements observed between successive photographs. The white circular markers with black centres which form a grid of 5×3 were used to scale displacements measured in pixels on the digital photographs to actual displacements in real space.

Figure 4-42 shows a close up of a test using the prism in dense HST95. The prism moves horizontally from the right with its leading tip at greater depth than its back

and is designed to simulate the share of the plough whilst forward pitching. The shear plane (highlighted by the dashed black line) is observed through the kinks (discontinuities) in the blue coloured sand and has just reached the sand's surface travelling 77 mm from the prism's tip in Figure 4-42 after 14 mm prism displacement.

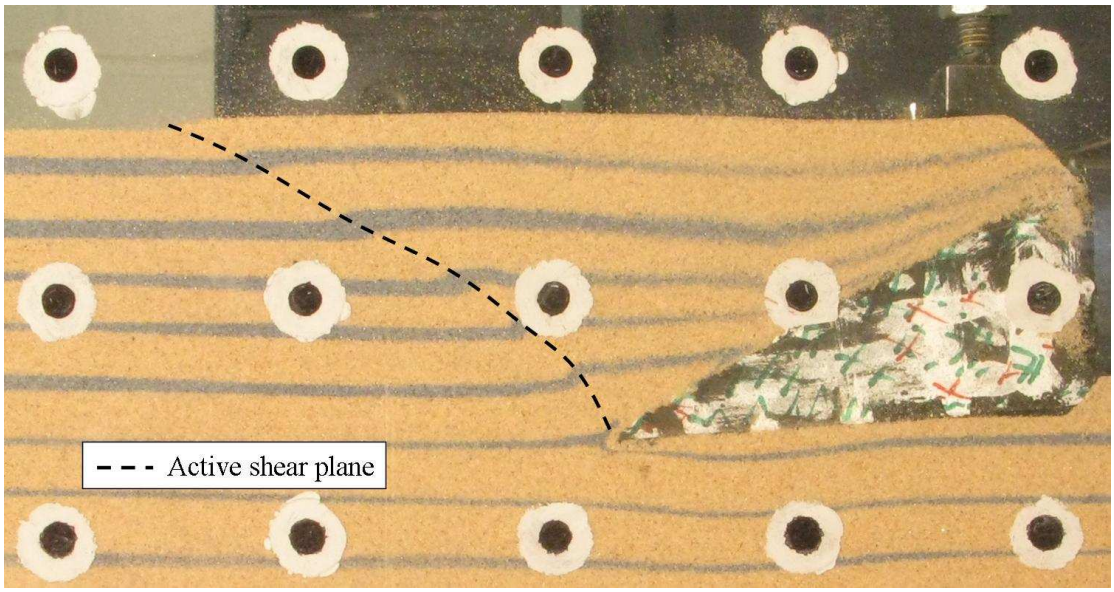

Figure 4-42: First shear plane fully mobilised during forward pitching test

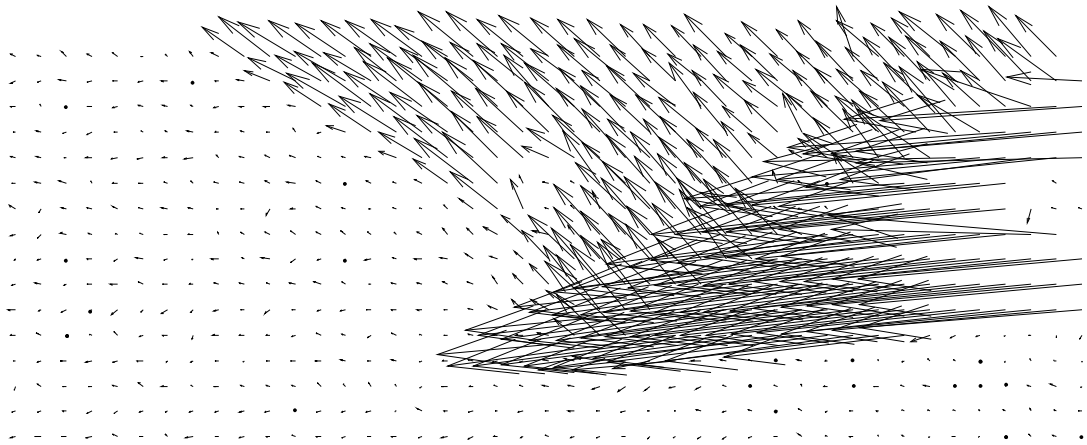

Figure 4-43: Cumulative sand and prism vector displacements from the start of the forward pitching test until full mobilisation of the first observed shear plane

Figure 4-43 shows the direction of vector displacements attained from particle image velocimetry (PIV) processing. The prism is shown by the triangular formation of vectors moving leftwards angled slightly below the horizontal from the right hand side of Figure 4-43. The wedge of sand above and in front of the prism is shown to move left and upwards away from the prism and the sand below the prism seems

unaffected by the prism. Shear strains were calculated from vector displacements using one of the subroutines supplied with the software.

Total maximum shear strains for the first 14 mm prism displacement are plotted in Figure 4-44. The lighter zones show areas where large shear strains are recorded. The interface between the sand and the prism shows as being the region of greatest shear strain. A shear plane is observed originating from the tip of the prism and extending to the surface of the sand. The shear plane is inclined at an angle of around 55º from the horizontal where it is close to the prism's tip and this angle reduces to roughly 40º from the horizontal as the shear plane reaches the surface. Note that the ring shaped zones of high shear strain are not real strains and have been caused by the way in which the strains were calculated. The rings of shear strain form due to the difference in velocity between the stationary scaling markers (painted on the Perspex face of the box) and the sand moving passed them.

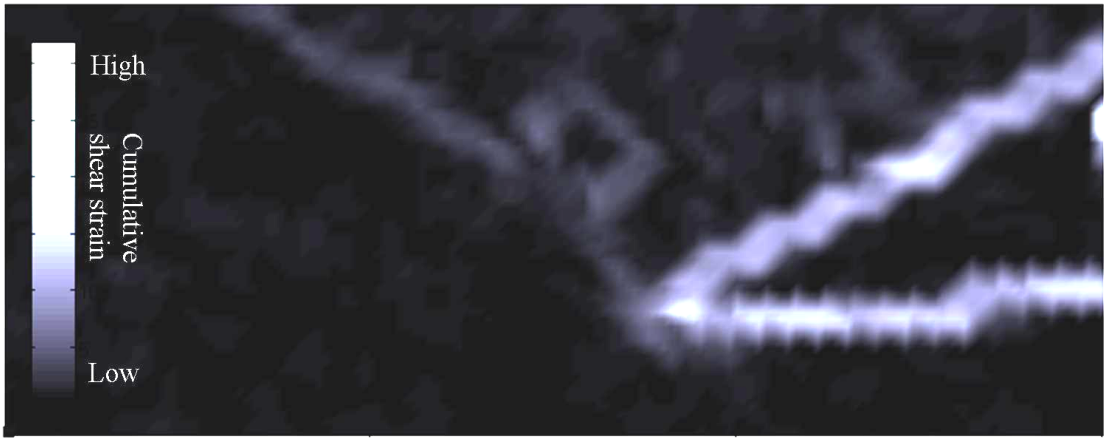

Figure 4-44: Cumulative shear strain after 14 mm prism displacement

The major principal stress in the passive Rankine state is horizontal and shear planes may be expected to rise at 45º-φ'_{peak}/2 to the horizontal. φ'_{peak} was found to be around 44º for dense HST95 over the range of effective stresses involved during the prism testing and therefore shear planes may be expected to project at 45º-44º/2 = 23.5º from the horizontal. This does not compare very well with the observed pattern of failure which results from the prism tests and may in part be due to friction acting on the interface between the prism and sand and the shape of the prism which causes the zone of sand bounded by the prism and shear plane in front to lift.

The prism tests are very similar to a raked retaining wall inducing passive failure upon the sand. It is known that if an upward force acts upon a rough retaining wall which is equal to the sum of the weight of the wall and the friction between the sand and the wall, a steepening of the shear plane close to the wall occurs which reduces to the Rankine case of 45^o-$\varphi'_{peak}/2$ as it extends beyond the wall's influence. This is similar to the shape of the shear plane observed in Figure 4-44 and the rake in the prism may induce the same effect as an upward force as sand is lifted over its front face. The shear planes in the small scale prism tests are fairly short ($\approx$ 80 mm in length) and may never extend far enough from the prism to be free of the uplift effects. Hettiaratchi and Reece (1975) conducted experiments during tests where a wide flat blade was translated horizontally through dry Leighton Buzzard sand at a variety of rake angles where depth was kept constant between tests. They found concave shaped failure planes similar to that shown in Figure 4-42 developed for tests where the rake angle was between 10^o and 60^o from the horizontal for a smooth surfaced blade and between 10^o and 40^o for a rough blade.

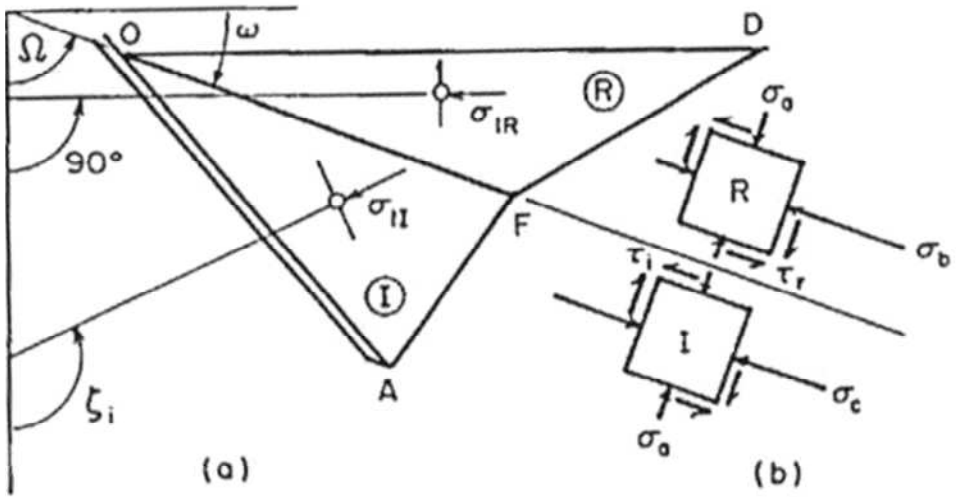

Figure 4-45: The slip-line field for small rake angles. (a) The plane of discontinuity *OF* separates the Interface *I* and Rankine *R* zones. (b) The stress conditions on either side of the stress discontinuity (Reece and Hettiaratchi; 1989)

Reece and Hettiaratchi (1989) present a slip-line method for estimating passive earth pressure. They present four types of slip-line field based on failure geometry which is dependent on rake angle, direction of translation, friction angle and interface angle. They found that for small rake angles and where $\delta < \varphi'$ (Figure 4-45) as is the case

for the prism in the plane strain tests discussed herein, the slip-line field comprised of an interface zone adjacent to the translating object and a Rankine zone extending to the soil's surface. The two zones are separated by a stress discontinuity and the slip-line field is shown in (Figure 4-45) bears resemblance to the failure planes observed during the prism tests.

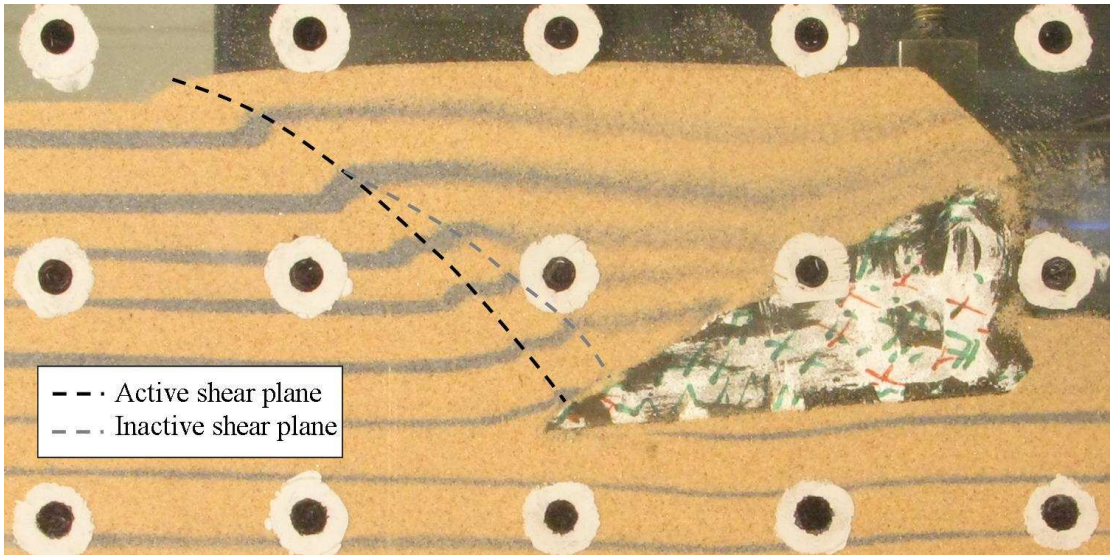

Figure 4-46: Forward pitching test after approximately 20 mm of prism displacement

Figure 4-46 shows the development of a second shear plane which supersedes the first shear plane as the main displacement discontinuity between the sand affected by the prism and the sand unaffected by the prism. The second shear plane formed around 7 mm ahead of the first one close to the prism's tip but converged towards the first one to join into it at around 50 mm from the share.

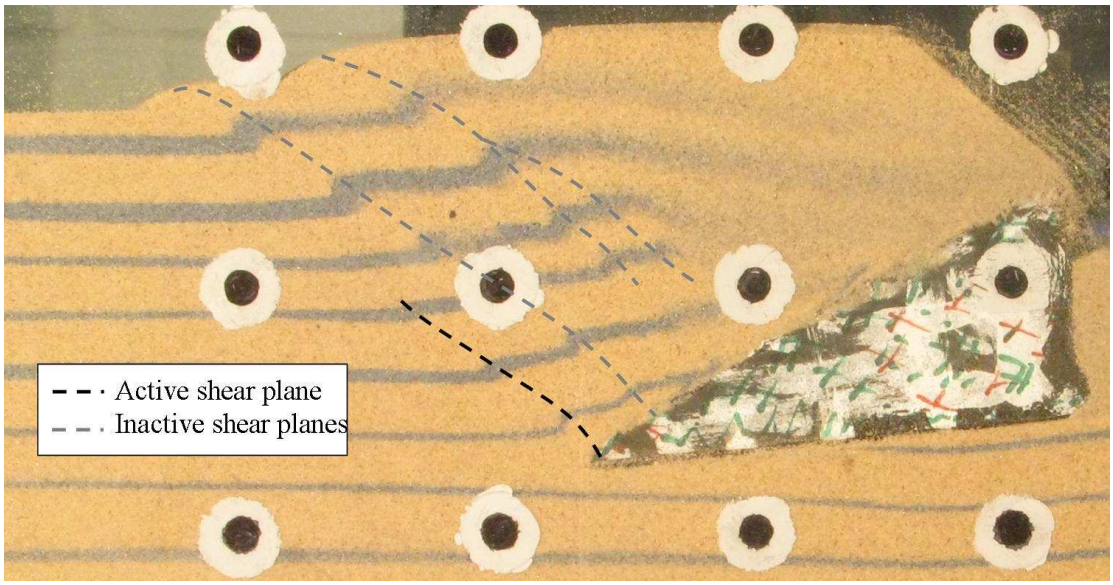

Figure 4-47: Forward pitching test after approximately 33 mm prism displacement

Figure 4-47 shows the pattern of inactive shear planes behind an active one after approximately 33 mm prism displacement. Shear planes were seen to form at spacing's of between 7 mm and 12 mm apart.

The initial prism and sand displacements during an aft pitching test in dense HST95 sand are plotted in Figure 4-48. The sand displacements above the prism look very much like those during the forward pitching prism. In contrast to the forward pitching test there are large sand displacements beneath the prism, which may extend down to the box base, which will inevitably influence the results. Unfortunately the test apparatus was not rigid enough to prevent the prism from rotating slightly so that its underside was parallel with the direction of displacement and it is not known how the shear planes would have progressed if the aft pitch had remained throughout the test.

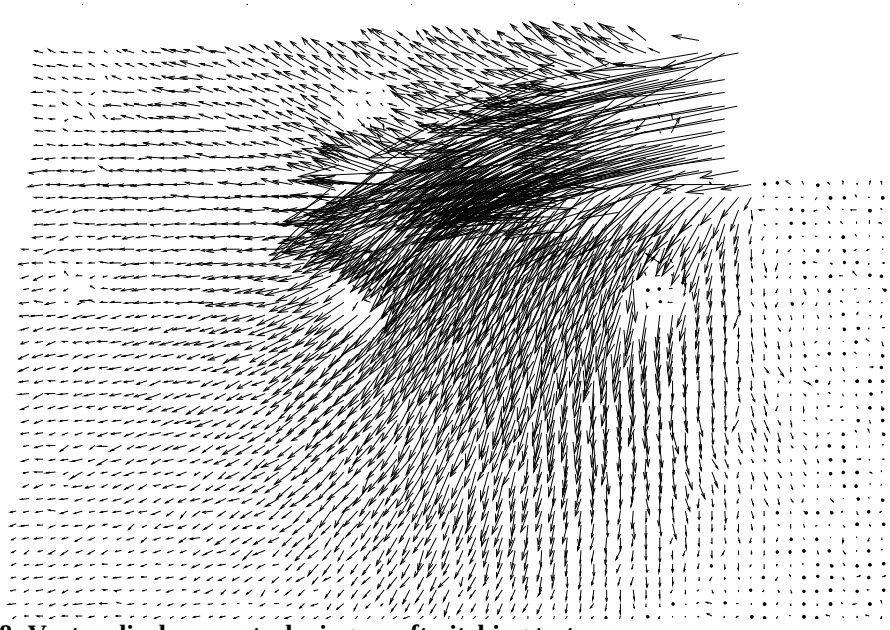

Figure 4-48: Vector displacements during an aft pitching test

4.9. *Comparison of ploughing test data to limit equilibrium analysis*

Limit equilibrium analysis has been performed on an assumed failure mechanism informed by soil mechanics principles and by observation of failure of sand during plane strain tests (see section 4.8). The purpose of this analysis was to try and produce a tow force prediction model which could be calibrated with the physical model test results.

4.9.1. Failure mechanism

The ploughing process has been simplified in the following failure mechanism as the process is not fully understood and it makes the maths more straightforward. The simple mode of failure shown in Figure 4-49 was assumed and Mohr-Coulomb failure criterion satisfied in limit equilibrium calculations as an attempt to predict tow force through statics. The angle θ, which defines the shear plane, was informed by the plane strain tests and taken as 40º from the horizontal. The forces R_3 and R_2 were assumed to act at the angle of interface friction, δ_{crit} from the normal to the share and heel faces respectively and R_1 at φ' from the normal to the shear plane. W_{plough} is the plough weight and W the weight of the sand wedge being moved by the plough.

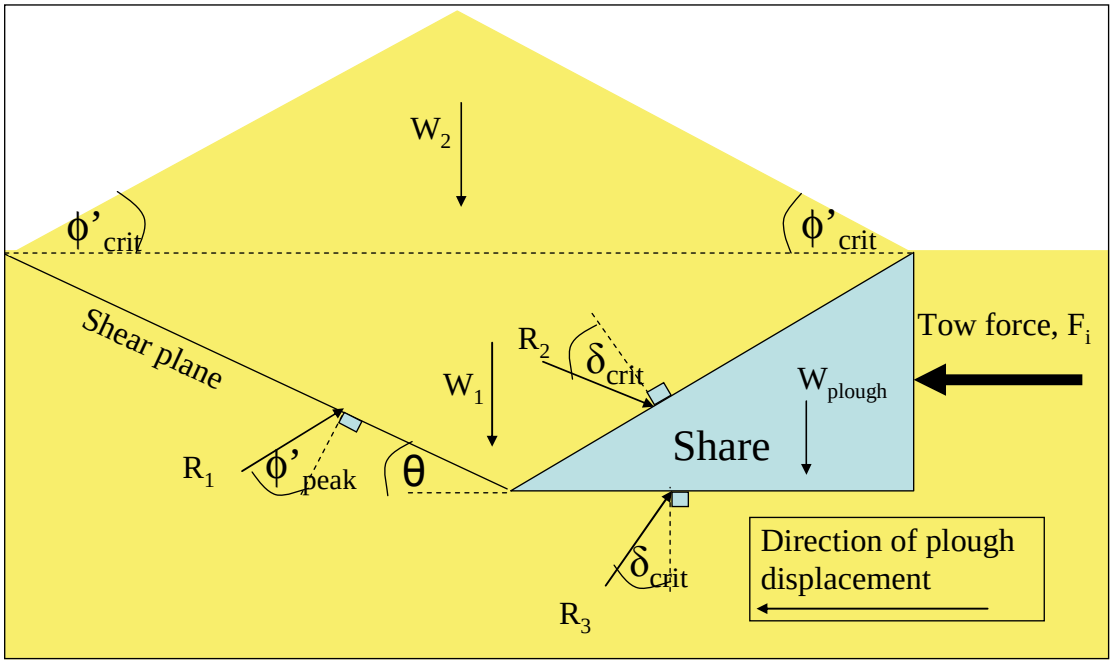

Figure 4-49: Plane strain simplification used for limit equilibrium analysis of ploughing

4.9.2. Limit Equilibrium Calculations

The weight of the wedge of sand is

$$W = 0.5\gamma w D^2 \times \left(\frac{1}{\tan\alpha} + \frac{1}{\tan\theta} \right) \quad (4\text{-}24)$$

For the wedge of sand, $\Sigma F_h = 0$

$$R_1 \sin(\theta + \phi'_{peak}) = R_2 \sin(\alpha + \delta_{crit}) \quad (4\text{-}25)$$

For the wedge of sand, $\Sigma F_v = 0$

$$W + W_2 = R_1 \cos(\theta + \phi'_{peak}) + R_2 \cos(\alpha + \delta_{crit})$$

(4-26)

Therefore R_2 is

$$R_2 = \frac{W + W_2}{\cos(\alpha + \delta_{crit}) + \frac{\sin(\alpha + \delta_{crit}) \times \cos(\theta + \phi'_{crit})}{\sin(\theta + \phi'_{crit})}} \quad (4\text{-}27)$$

For the share, $\Sigma F_v = 0$

$$R_3 = \frac{(R_2 \cos(\alpha + \delta_{crit}) + W_{plough})}{\cos \delta_{crit}} \quad (4\text{-}28)$$

Equation 4-29 gives the tow force, F_i required to pull the share through the sand and is found by the balance of forces in the horizontal direction, $\Sigma F_h = 0$

$$F_i = R_3 \sin \delta_{crit} + R_2 \sin(\alpha + \delta_{crit}) \quad (4\text{-}29)$$

where W_{plough} is the weight of the plough supported by the share per unit width. w is a characteristic width, d a characteristic depth and W is the weight of the sand wedge in front of the share per unit width. The weight of spoil heaps (W_2) was assumed to be the same as that of the wedge. R_1, R_2 and R_3 are sand reaction forces which oppose movement of the share. The share angle is denoted by α, γ is the unit weight of the sand, δ is the interface friction angle, φ'_{crit} is the critical state friction angle.

4.9.3. Compensating for the width of the share increasing with depth

Limit equilibrium calculations on the simplified failure mechanism shown in Figure 4-49 provide a force per unit width and in order to attain a representative cross section of the plough its width as split into five different strips as shown in Figure 4-50. If the plough is at maximum depth (40 mm at 50th scale) all five strips are used in limit equilibrium calculation of the tow force and as the plough depth is reduced so is the

number of strips in the limit equilibrium calculation. The limit equilibrium calculations were therefore performed on each strip separately and their individual tow forces summed to provide the tow force for the plough.

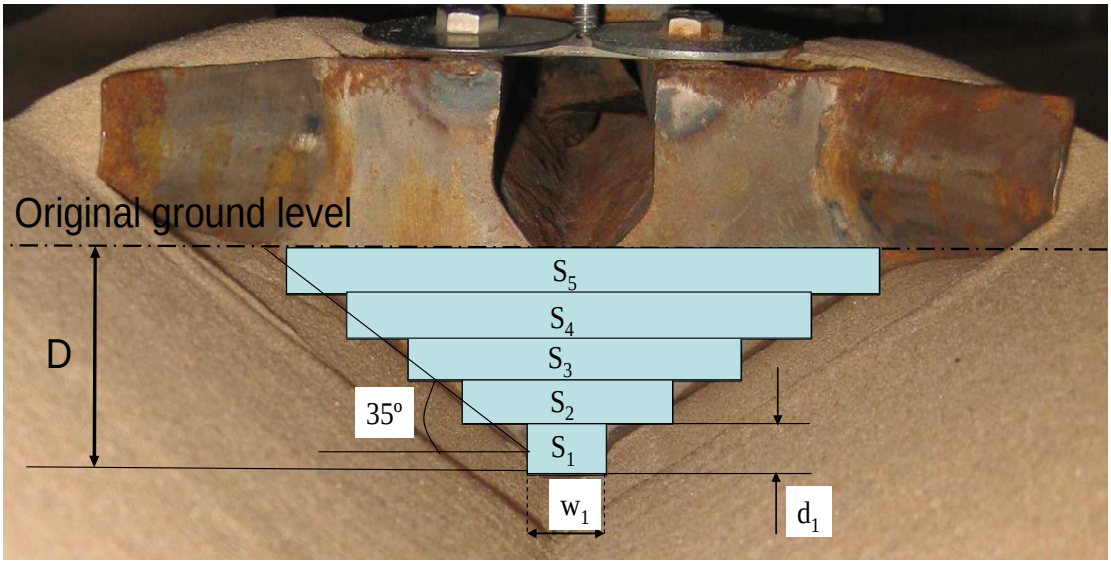

Figure 4-50: Section showing how the width of the plough was split for the limit equilibrium analysis

The weight of the wedge of sand in front of S_1 is given by Equation 4-30

$$W_1 = 0.5\gamma w_1 d_1^2 \left(\frac{1}{\tan\alpha} + \frac{1}{\tan\theta} \right) \quad (4\text{-}30)$$

The plough weight was assumed to be evenly distributed over each strip and therefore R_2, R_3 calculated and ultimately F_1 was calculated as the tow force due to strip S_1. The forces F_1-F_5 were then summed together and the total tow force F found.

4.9.4. Results

The limit equilibrium analysis outlined above was compared to 50th scale ploughing data and is shown in Figure 4-51. At shallow depths the limit equilibrium analysis compares well to the test data, however the tow force from the test data increase more rapidly with depth than the calculated tow force and the two data sets diverge with increasing depth. The calculated tow force at 40 mm plough depth is 11 N whereas the measured tow force during a 50th scale ploughing test at 41 mm is substantially larger at 19 N.

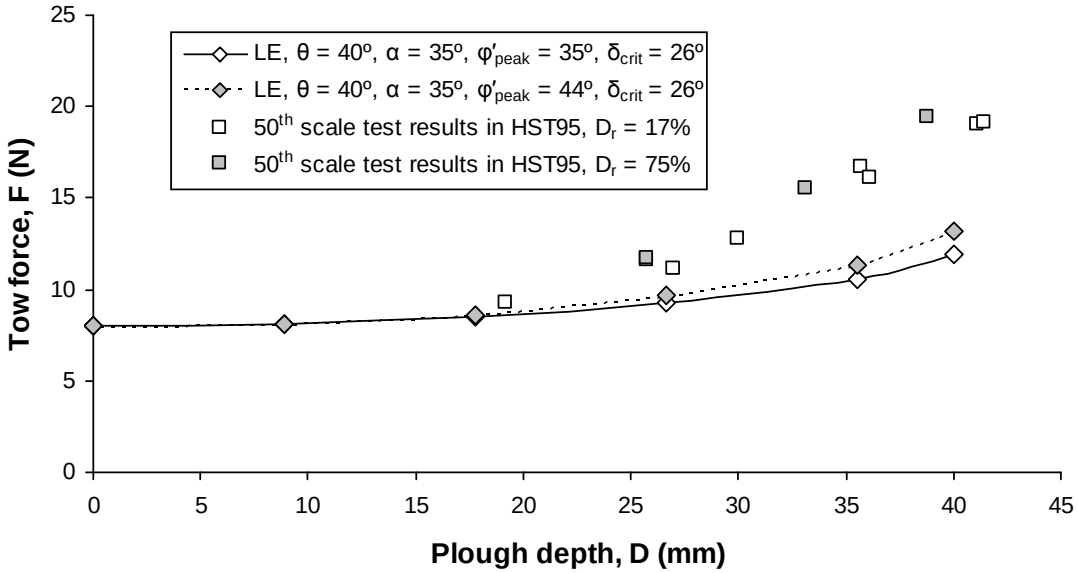

Figure 4-51: Comparison of limit equilibrium analysis (θ=40º, α=35º, δ_{crit}=26º) to 50th scale plough data in dry HST95 at D_r = 17% and D_r = 75%

The tow forces calculated by the limit equilibrium model are obviously dependent on the values of θ, α, δ and φ'_{peak} used. Increasing the friction angle of the sand to 65º (which was shown in Figure 3-23 to be the angle of friction of dense HST95 at a normal effective stress of 1kPa) causes the model to better fit the data. The validity of such high friction angles is however questionable.

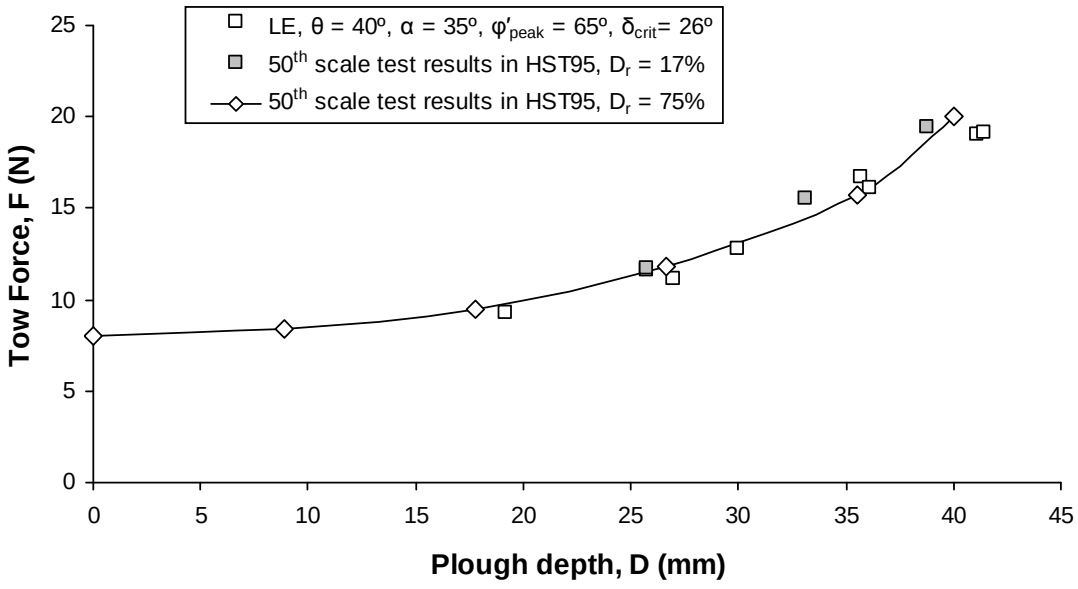

Figure 4-52: Comparison of limit equilibrium (LE) analysis (θ=40º, α=35º, δ_{crit}=26º, φ'_{peak}=65º) to 50th scale plough data in dry HST95 at D_r = 17% and D_r = 75%

The influence of both the rake angle (α) and the angle of failure plane (θ) on the tow force generated have been investigated through the limit equilibrium model. Tong & Moayad (2006) show through numerical simulations of a chisel plough in a clay loam ($\varphi' = 32^o$, $\delta = 23^o$) that the angle of failure plane is dependant on the rake angle. Figure 4-53 presents their data along with the angle of failure plane observed during the plane strain tests ($\varphi'_{peak} = 44^o$, $\delta_{crit} = 26^o$) discussed in section 4.8. Although the Tong & Moayad (2006) data does not match the angle of failure plane observed during the plane strain tests, their data (with trendline fitted to allow extrapolation beyond the rake angles which they tested) has been applied to the limit equilibrium analysis shown in Figure 4-54.

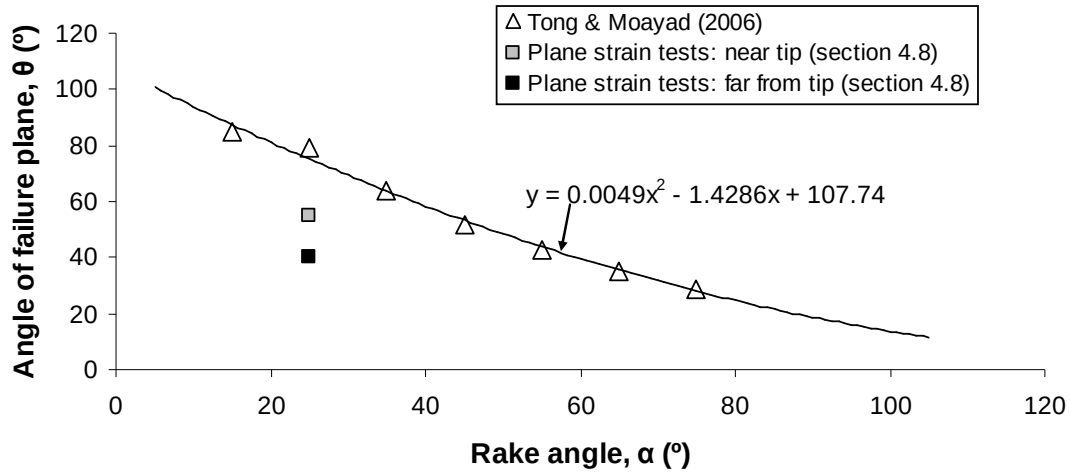

Figure 4-53: Influence of rake angle over the angle of failure plane

The relationship between rake angle and tow force has been investigated by means of the limit equilibrium model and results are shown in Figure 4-54. Limit equilibrium analysis where the angle of failure plane, θ was assumed independent of rake angle, α shows that the tow force is relatively unaffected by α over the range $25^o<\alpha<55^o$ and the minimum tow force occurs at $\alpha = 35^o$. The model gives reliable results only over the range $5^o<\alpha<75^o$ as there are vertical asymptotes at $\alpha = 0^o$, 80^o. The limit equilibrium anaysis whereby $\theta = f(\alpha)$ causes the minimum tow force to occur at a higher rake angle ($\alpha = 55^o$). Experimental work discussed in the literature review (section 2.5) found that the horizontal force required to translate a blade through sand reduced with rake angle from $20<^o\alpha<150^o$ and this does not agree with $\alpha = 35^o$ or 55^o found by the limit equilibrium model.

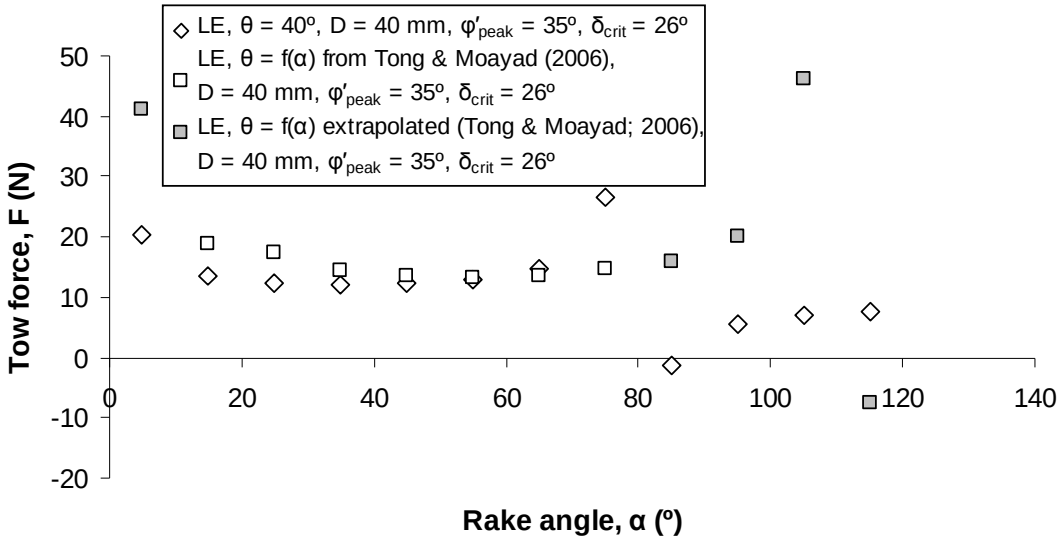

Figure 4-54: Influence of rake angle over the tow force generated, both with and without varying angle of shear plane

Note that in this analysis that no attempt has been made to account for sand interaction with the beam, or that of skid sinking. The three dimensional nature of soil movement has also been ignored. These important points may highlight why the limit calculations fail to replicate the tow force experienced during 50th scale model tests.

4.10. *Summary of test results in dry sand*

The bulk of the dry ploughing test results gathered during the course of this research have been presented in this chapter. The results have been presented with some explanation of factors which influence plough performance however the potential significance of the most important results are highlighted in Chapter 7. A summary of the observations made in this chapter is outlined below.

1. Increase in ploughing depth will result in a corresponding increase in tow force and a reduction in pitch. The tow force appears to have two separate components. The first component comes from base friction and the second component is a function of the cube of the depth giving $F = W\tan\delta$ + function (γD^3) as has been suggested by previous authors (e.g. Reece and Grinsted (1986) and Cathie and Wintgens (2001)).

2. The relative density of the sand being ploughed was found to affect plough performance. An increase in relative density results in an increase in tow force which is not insignificant at plough depths below 26 mm at 50th scale. The tow forces achieved during two ploughing tests at 35 mm depth, one in loose (Dr = 25%) HST50 the other in very dense (Dr = 90%) HST50 are 16.1 N and 17.6 N respectively. The increase in tow force from loose to dense HST50 at 35 mm depth is therefore only 9%. When ploughing at shallow depths the tow force was not observed to be influenced by the relative density of the sand. This was presumably due to the fact that the product of the interface angle (being unaffected by relative density) and the plough's weight provides the majority of the tow force when ploughing at shallow depths. The ploughs pitch was reduced (tended towards forwards pitching) with increasing relative density.

3. Ploughing tests were conducted in two fractions of silica sand from a single source, one fine and the other medium prepared at the same bulk density. The medium sand had a higher critical state friction angle than the fine sand and the difference in tow force achieved between these two sands was similar to ploughing in sand of two different relative densities. The medium sand being equivalent to a higher relative density than the fine sand.

4. Use of the forecutter increased the tow force during ploughing at depths great enough to allow forecutter engagement with the sand. The forecutter also caused the plough to forward pitch more than the plough without the forecutter which caused a reduction in plough depth for the same skid setting as the non forecutter case.

5. Tests were conducted using three scales of plough in the same sand conditions to find if the changes in effective stress altered the results. The scaled tow force data from the 10th, 25th and 50th scale ploughs does not appear to be substantially different (Figure 4-20) and may suggest that the increased dilation due to reduced effective stresses with reduction in scale is not an issue.

6. Fixed tests provide the opportunity to try and break down the components of forces acting on the plough during testing.

7. Transition lengths are reduced during the fixed tests which reduce the mass of sand required per test and allows larger (10^{th} scale) model testing to become practicable.

8. The forces acting upon the plough during fixed tests are extremely sensitive to the pitch of the plough. Forcing the plough through the sand while aft pitching increases both the horizontal and vertical forces applied to the plough significantly. This is probably due to confinement beneath the share increasing normal effective stresses.

9. The fixed test data could not be reliably compared to conventional plough test data preventing the use of fixed tests in the parametric study.

10. The plane strain tests provided a useful insight into strains around a share-like implement and the angle of shear planes provided a failure mechanism to be used in a limit equilibrium model for tow force prediction calculations.

11. Limit equilibrium analysis was conducted as a means of tow force prediction. It was not able to provide satisfactory predictions of tow force and substantially under predicted the increase in tow force due to increase in plough depth. This was likely due to simplifications made in the assumed failure mechanism as it was two dimensional and ploughing is a three dimensional process.

Chapter 5. Rate effects during ploughing

5.1. *Introduction*

The results and discussion up to this point have considered ploughing in fully drained conditions and therefore the normal effective stress in the sand is unaffected by the flow of pore fluid during shearing. Rate effects arise in saturated sand when during a shearing event there is insufficient time for pore fluid to freely drain into the dilating zone of sand which results in a reduction in the pressure of the pore fluid. This reduction in pore fluid pressure increases the normal effective stress of the sand ($\sigma_n' = \sigma_n - u$) thus increasing its resistance to shearing (see Chapter 2 for a more indepth description). These rate effects are central to offshore ploughing in sand and this chapter attempts to quantify the rate effect during different sand conditions. The findings should prove useful to ploughing contractors as a means of refining plough performance prediction.

5.2. *50th scale ploughing tests*

The majority of the saturated ploughing tests were conducted with the 50th scale plough as it was the easiest scale to work with and allowed a parametric study to be conducted rapidly. The variables involved in the parametric study were: velocity, permeability (altered through using different sand particle sizes), relative density, ploughing depth and the presence of a forecutter. The 25th scale ploughs were then used to look at scale effects during saturated ploughing as was done with the dry ploughing tests.

5.2.1. The effect of trenching rate on plough performance: typical results

Figure 5-1 presents steady state tow force data gathered during eight saturated ploughing tests, all of which were conducted in medium dense, medium sand (HST50) with ploughing velocities ranging from 17-187 m/h. There is a clear increase in tow force with ploughing velocity (known hereafter as the 'rate effect') which appears approximately linear in character. A straight line has been fitted through the

data and captures the trend reasonably well over the range of velocities shown. The offset of the straight line from the origin is the 'static' component of the tow force. The gradient of the line in Figure 5-1 effectively shows the rate effect to be an increase in tow force of 1.85 N for every 100 m/h increase in velocity for the particular conditions. The appropriateness of a linear relationship between tow force and velocity seems valid in other tests at velocity ranges up to 400 m/h. These were the maximum velocities ploughing tests were conducted at and therefore no comment on the form of the rate effect can be made outside this range.

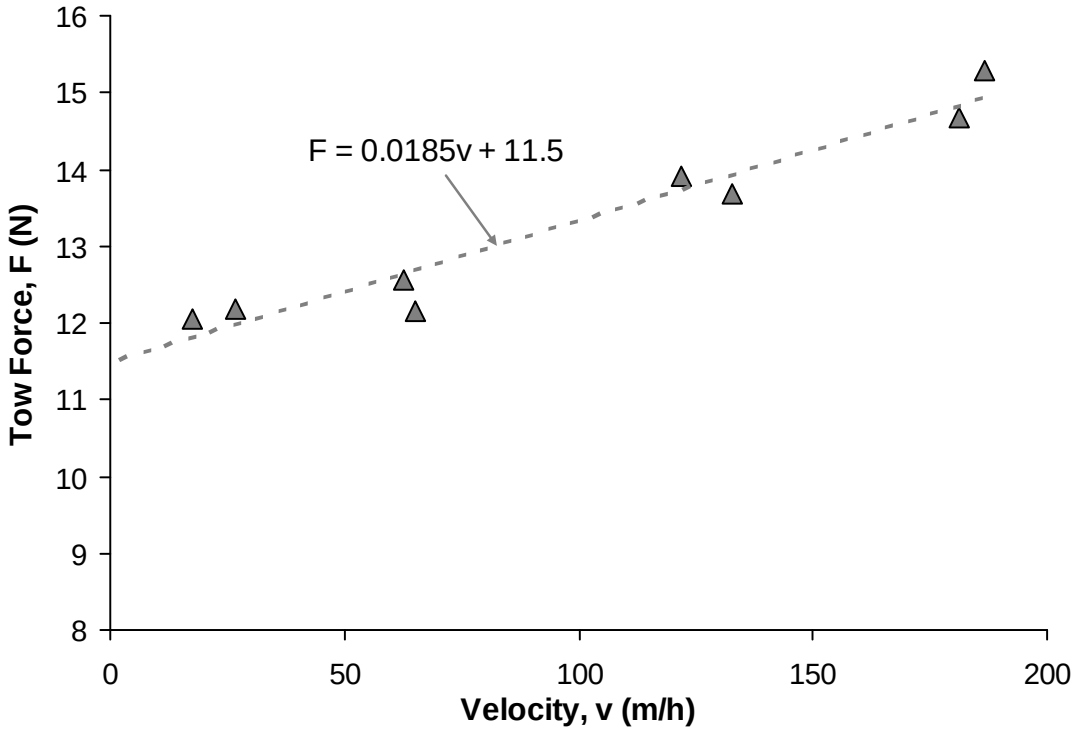

Figure 5-1: Tow force against plough velocity for the 50th scale model plough (W' = 14.3 N) in saturated HST50, D_r = 51%, γ' = 9.47 kN/m^3

Figure 5-2 shows plough pitch and depth plotted against velocity for the same tests shown in Figure 5-1. There appears to be a slight reduction in depth with increasing velocity of around 1 mm (3%) over the range of velocities tested. The plough's pitch might be expected to follow a similar trend to its depth, as it is the pitch, along with skid settings which define the vertical position of the share relative to the skids.

Figure 5-2 shows that there is no significant variation in either pitch or depth with velocity. This seems surprising as the rate effect (i.e. the increased share-soil reaction

with velocity) would be expected to cause a change in moment equilibrium which would alter the plough pitch and therefore its depth through the long-beam principle.

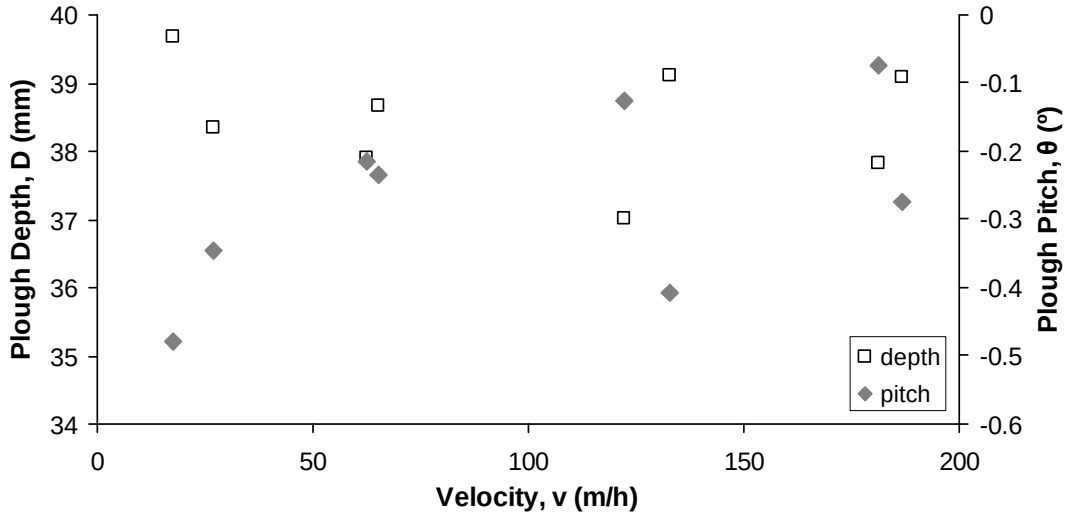

Figure 5-2: Effect of plough velocity on depth and pitch for the 50th scale plough in saturated HST50, D_r = 51%, γ' = 9.47 kN/m^3

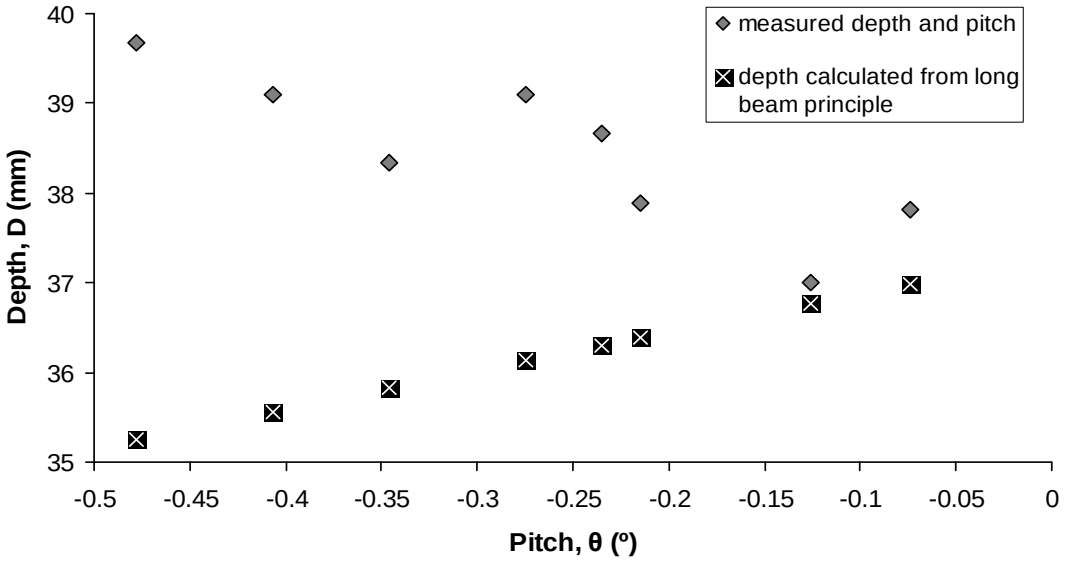

Figure 5-3: Relationship between pitch and depth for the 50th scale plough in saturated HST50, D_r = 51%, γ' = 9.47 kN/m^3

The relationship between plough pitch and plough depth is shown in Figure 5-3. The measured plough depth reduces with increasing pitch (a negative pitch signifies forward pitching and a positive pitch signifies aft pitching). Figure 5-4 shows the relative position of the skids and the back of the share, which are to define plough depth (assuming the skids sit on the surface of the sand) during the tests. Any

deviation from this depth during plough tests must be caused by changes in the plough's pitch which can be determined easily through use of basic trigonometry (Equation 5-1).

$$D = d_s + \sin\theta(l_a \cos\beta + l_b) - (d_s(1-\cos\theta)) - l_a \sin(\theta+\beta) - h_{sk} \quad (5\text{-}1)$$

where, D, d_s, l_a, l_b, h_{sk}, θ and β are all defined in Figure 5-4.

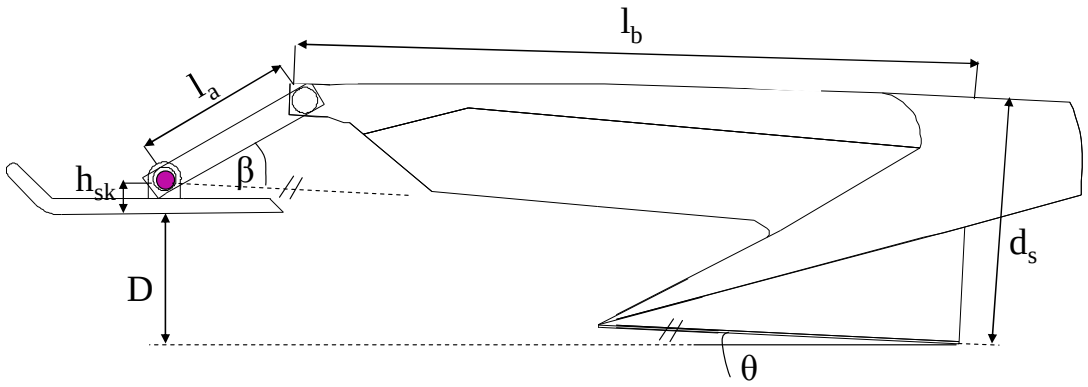

Figure 5-4: Skid position relative to the back of the share used during the tests

The depth calculated using trigonometric functions and plough depth settings shows that depth increases by around 1.5 mm with increasing pitch from 0.48º-0.07º. The discrepancy between the calculated depth (which follows the logical trend with pitch) and measured depth is likely due to skids sinking into the sand. It is entirely possible for the skids to dig into the sand by over 4 mm, which is the greatest difference between the measured depth and the calculated ploughing depth. This could be checked by putting an additional LVDT onto one of the skids of the plough, so that the depth of the skids relative to the sand throughout the test was measured. If this turns out to be the case then it shows that the skids sink less with increasing plough velocity and therefore rate effect. Perhaps interface shear between the skids and the sand causes reduction in pore pressure in the sand around the skids, therefore increasing its shear strength which prevents the skids from sinking.

The trends shown in Figure 5-1 are fairly typical of all the saturated ploughing tests conducted. Redhill 110 (silty sand) was found to be most sensitive to the rate effect

and HST50 (medium sand) least sensitive. The following data and analysis within this chapter explains why this is the case and its repercussions on ploughing.

The data of plough depth versus velocity shown in Figure 5-2 is typical of all tests in HST50, none of which showed much evidence of velocity affecting plough depth. Tests in HST95 and Redhill 110 showed that plough depth tended to reduce with velocity. The relationship between plough depth and pitch shown in Figure 5-3 is not representative of all tests. Some test series show almost no relationship between plough depth and pitch however others show plough depth and pitch to increase together.

5.2.2. Influence of sand particle size on the rate effect

Figure 5-5 plots tow force against velocity for ploughing in three different sands: medium sand (HST50), fine sand (HST95) and silty fine sand (Redhill 110). During the tests from which the data in Figure 5-5 was derived all three sands are of medium density and their respective permeability's, D_{10} and shear characteristics are shown in Table 5-1.

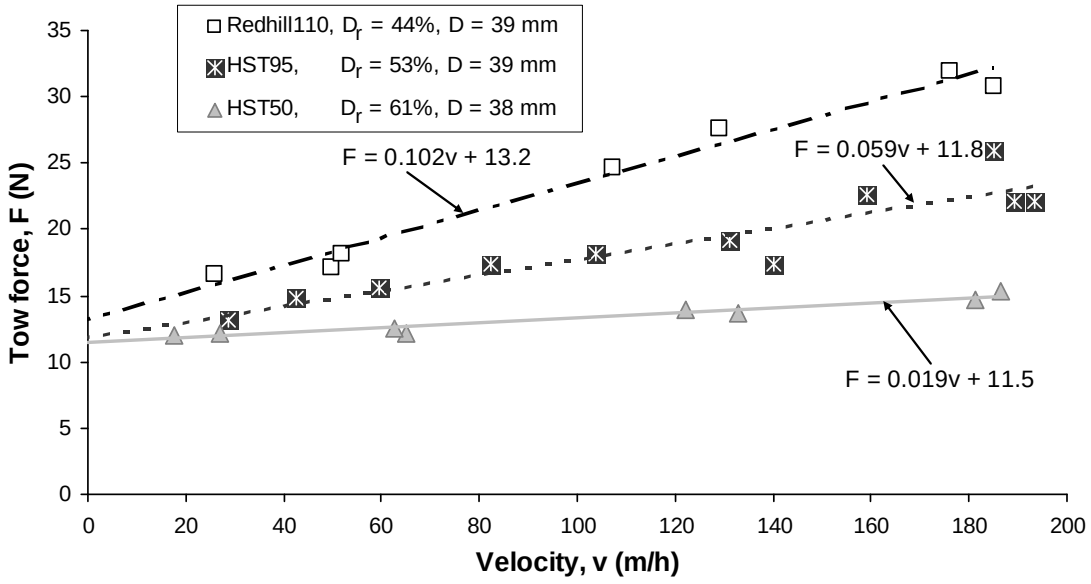

Figure 5-5: Steady state force against velocity for three different sands

Rate effects are displayed in all three sands in Figure 5-5. The zero velocity tow force is fairly similar for all three sands and is probably a result of them having similar

relative densities and frictional properties (see Table 5-1). The tow force achieved in the three sands diverges as ploughing velocity increases which is because the rate effect associated with each of the sands is different. The trend lines in Figure 5-5 are based on the least squares method and were used to attain a single value of dF/dv (the rate effect) in each of the test series. The rate effect is greatest in Redhill 110 and lowest in HST95 indicating that reducing permeability increases the rate effect.

Table 5-1: Physical attributes of the three sands in which ploughing tests were conducted

Sand type	Permeability, k (m/s)	D_{10} (mm)	Description	D_r (%)	φ'_{crit} (º)	φ'_{peak} (º)
HST50	0.000495	0.19	medium sand	61	34	39
HST95	0.000123	0.1	fine sand	53	32	38
Redhill 110	0.000101	0.08	silty sand	44	34	35

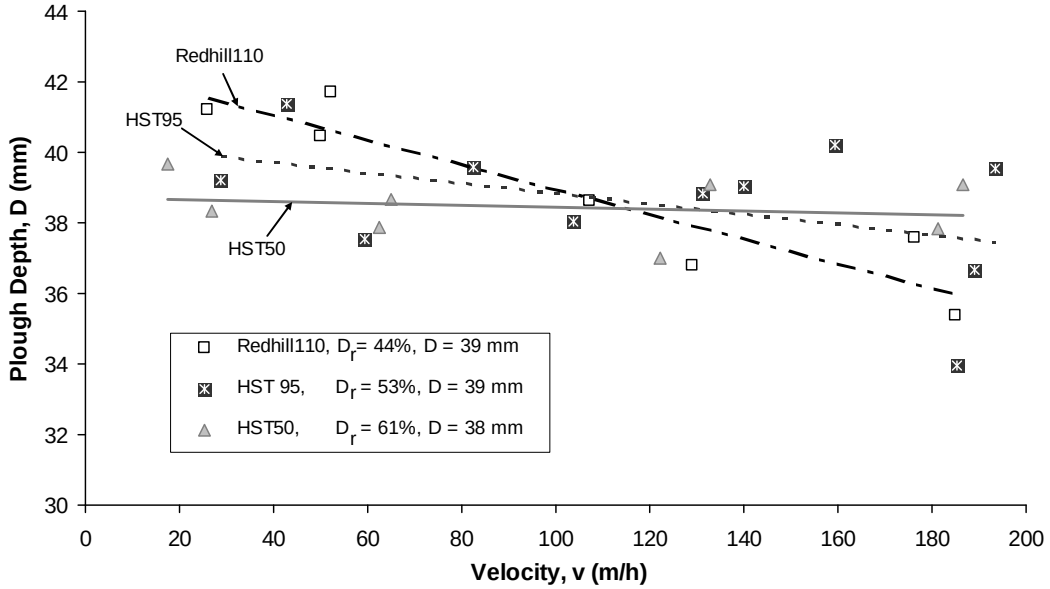

Figure 5-6: The influence of velocity on the plough's depth for three different sands

The variation of plough depth with ploughing velocity is shown in Figure 5-6. Although the average plough depth of each series is similar, the plough depth in HST50 is relatively unaffected by velocity. This was not the case in tests in HST95 and Redhill 110 whereby plough depth significantly reduced with velocity. In particular, the tests conducted in Redhill 110 ran at the greatest plough depth during slow ploughing rates and the shallowest depth during the fastest ploughing rates with

a difference of 13% (or 5 mm) for the range tested. The difference in plough depth at zero velocity is the probable cause in the difference in tow force at $v = 0$ between the three data series in Figure 5-5.

The rate effect increases with the depth of ploughing and is discussed in more detail in section 5.2.4. Therefore an apparent reduction in the rate effect may also be caused by the reduction in plough depth with increasing velocity in the Redhill 110 and HST95 data series i.e. the actual rate effect may be larger than indicated by the gradient of the lines in Figure 5-5 because faster tests are shallower.

The rate effect is thought to be a function of drainage during shearing and associated dilation of sand and therefore permeability and density state are expected to be two most important soil parameters. Although the relative densities of HST50, HST95 and Redhill 110 during the tests compared in Figure 5-5 are not the same, they are similar and are all classed as medium dense. The permeability of each sand (given in Table 5-1) was plotted against the rate effect in each sand (derived from the slope of the data shown Figure 5-5) and is plotted in Figure 5-7. Note however that this relationship may be skewed by respective differences in relative density between the three sands and the previously mentioned depth effects.

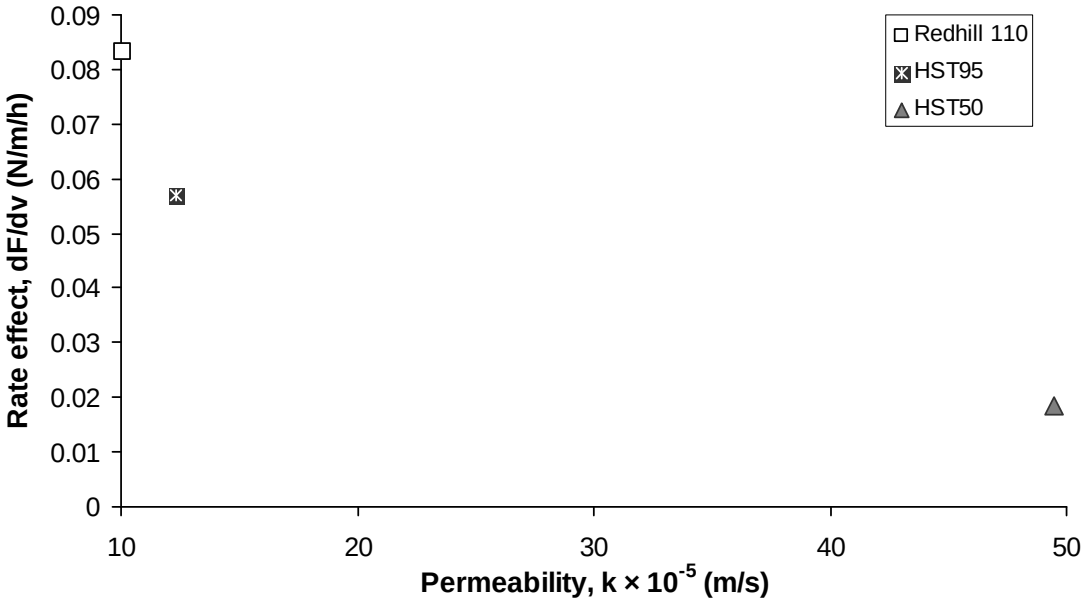

Figure 5-7: Relationship between the rate effect and permeability for three different sands

As there are only three data points in Figure 5-7 it is hard to draw any real conclusions from the data. That said as each data point was derived from numerous

tests (multiple ploughing tests to attain the rate effect and multiple permeability tests to attain the permeability) the error in the data is probably fairly low. The rate effect clearly increases with reduction in permeability over the range tested. However this cannot continue indefinitely as clay and silt contents would eventually become high enough to allow shearing without dilation.

5.2.3. Influence of relative density on the rate effect

To investigate the influence of relative density on the rate effect, ploughing tests were conducted at three different relative densities (D_r = 75%, D_r = 53% and D_r = 0%) in fine sand (HST95). The ploughing depth was considerably greater in loose sand than in medium and dense sand for the same skid settings. In order to find a tow force-velocity relationship in loose HST95 at a similar depth to the dense and medium tests, three tests were performed with the same skid setting as the dense and medium tests (setting 5) and three tests were performed with a shallower skid setting (setting 3). The results are plotted in Figure 5-8 with the depth of the plough during the test written beside the data. Linear interpolation was then used to find values of tow force and velocity for a plough trenching at 39.5 mm in loose sand and the 39.5 mm deep plough line in Figure 5-8 is an extrapolation of that data.

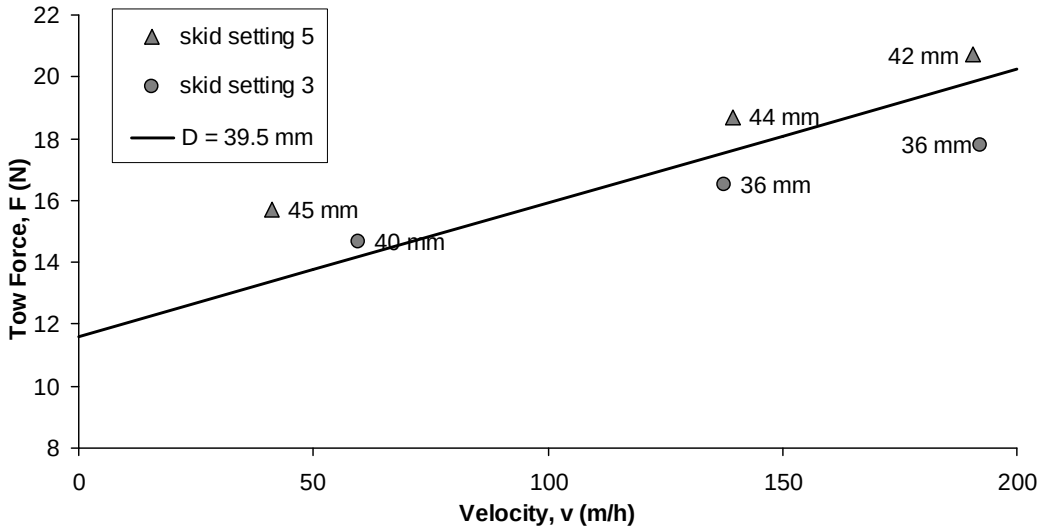

Figure 5-8: Tow force against depth results for ploughing in fine sand (HST95), D_r = 0%

Figure 5-9 presents tow force and velocity data for three series of ploughing tests in HST95 sand at relative densities of 75%, 53% and 0% respectively for D=39-40 mm.

The linear regression lines drawn have been fitted by the least squares method in order to provide a numeric value for the rate effect in each series. Although there is significant scatter in the data, there is a clear increase in the rate effect with relative density.

The rate effect would be expected to increase with relative density. This is because dense sand has a greater potential for dilation, which requires a greater volume of water per unit time to be sucked into the dilating zone of material during ploughing. This in turn requires greater pore water pressure reductions to drive the flow (e.g. Palmer; 1999). The permeability of the fine sand was measured in the permeameter for different densities. Permeability, *k* increased by 1.4 times from a dense state to a loose one. Consequently, a greater hydraulic gradient is required to drive the water through dense sand. However, it is not clear whether flow lines travel through disturbed or undisturbed sand and therefore this fact may be of little consequence.

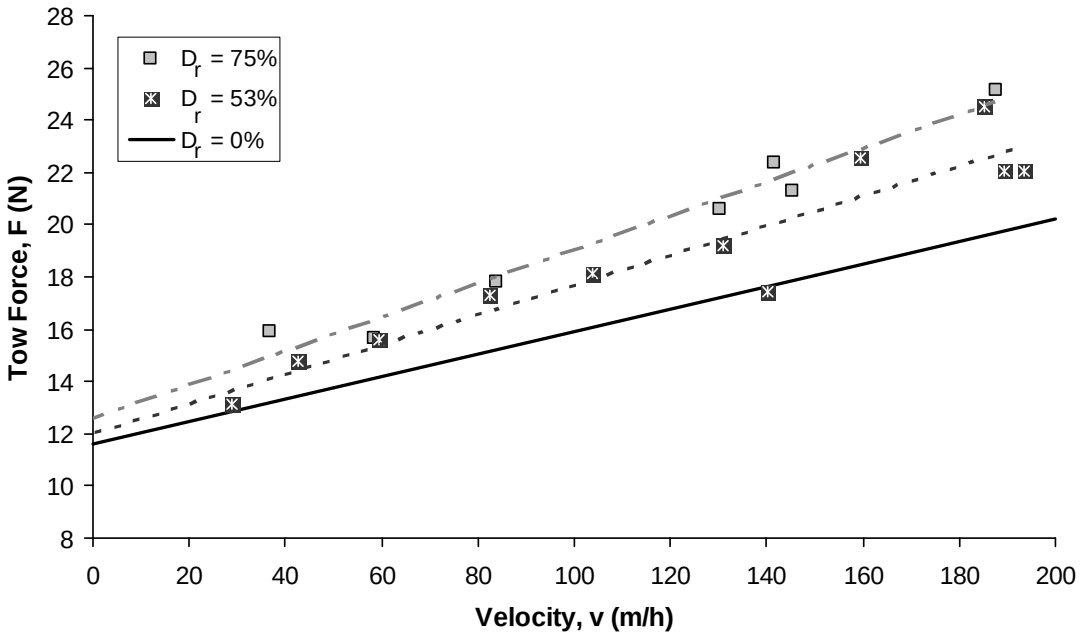

Figure 5-9: Influence of relative density on the rate effect in HST95 when ploughing without a forecutter at a depth of 39-40 mm

Figure 5-10 plots relative density against the rate effect, derived from the slope of the trend lines in Figure 5-9. The three data points indicate that the rate effect increases

by around 53% in a linear fashion from 0.043 N/m/h at 0% relative density to 0.065 N/m/h at 75% relative density.

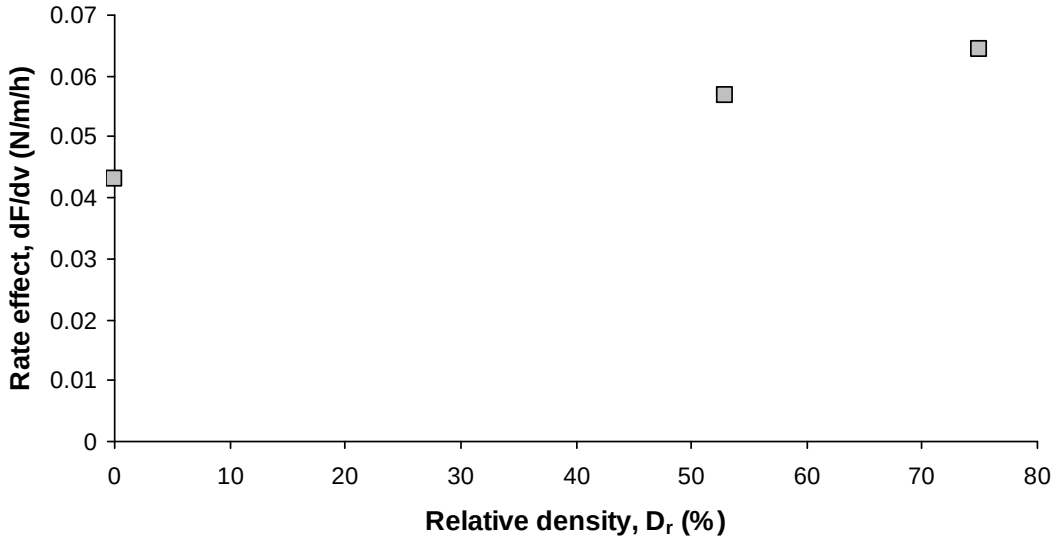

Figure 5-10: Rate effect plotted against relative density in HST95

Palmer (1999) suggested that in a very loose saturated sand a negative rate effect might be experienced where by as plough velocity increased, the corresponding tow force decreased, due to the reduction in volume of the shearing sand causing positive pore pressures and thus reducing the normal effective stress. Far from causing a negative rate effect, the 50th scale model tests show very loose HST95 to produce a strong positive rate effect. An explanation as to why this might be the case could be that the initially very loose sand is compressed in front of the share and in doing so reaches a denser than critical state and then further shearing and interface shearing on the share causes a positive rate effect.

The rate effect at each relative density has been normalised by the permeability of the sand at each respective relative density and is shown plotted against relative density in **Figure 5-11**. The normalised rate effect is shown to be around 6% greater at a relative density, D_r of 0% compared to a relative density, D_r of 75%. This suggests that the difference in rate effect between sand of different relative densities is solely a result of change in permeability and that dilation potential has no influence over the rate effect.

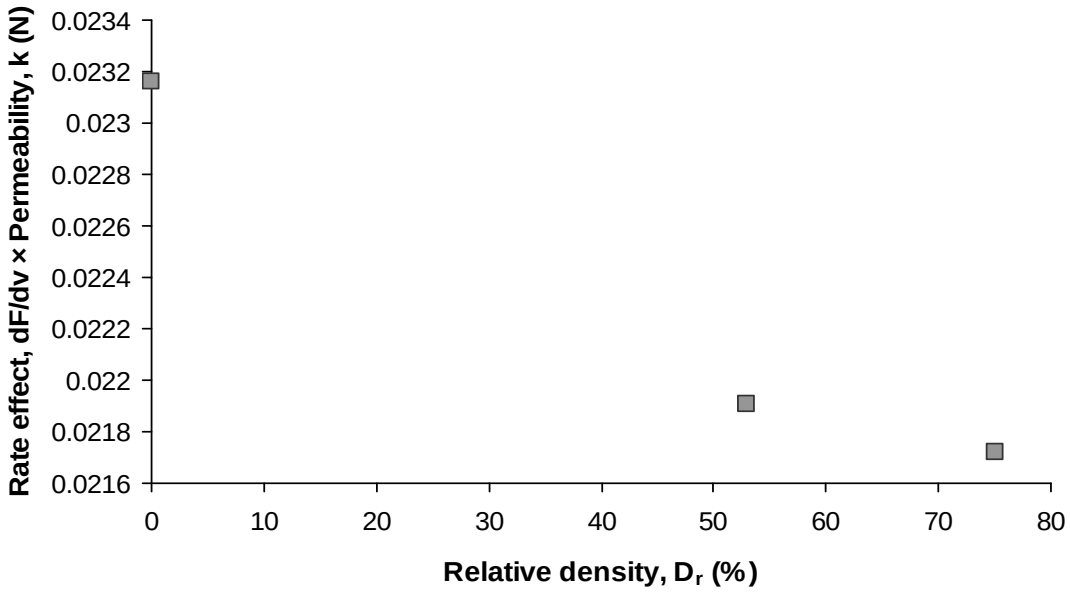

Figure 5-11: Rate effect modified by the permeability of the sand

5.2.4. Influence of plough depth on the rate effect

The static component of the tow force is shown to increase with plough depth and has been discussed in Chapter 4. Plough depth will also influence the rate effect as it is likely the controlling factor for the length of drainage paths.

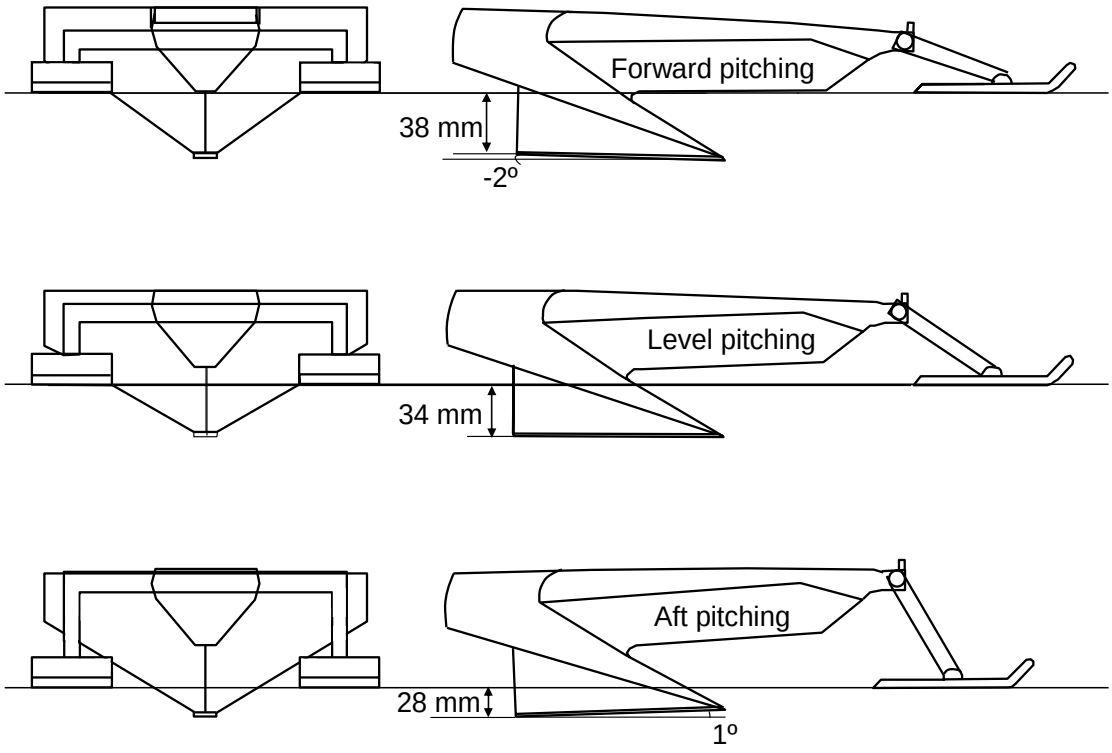

Figure 5-12: Schematic of plough position in the sand during steady state trenching at each of the three depth settings

Figure 5-12 shows the respective steady state pitches of the 50th scale plough during tests at three different skid settings (3, 4 and 5) resulting in plough depths of 28, 34 and 38 mm. As the skid settings change by rotation of the arm, the distance between the share and the skids changes with skid setting and therefore effectively changes the length of the beam, which will influence plough equilibrium. The plough pitches forward during the deep ploughing test series and aft during the shallow test series. This is consistent with the dry ploughing tests and is due to the change in the equilibrium of forces acting on the share and possibly also influenced by the bearing capacity of the sand. As a consequence the share tip defines the trench base during the deep test series and the heel defines the trench base during the shallow test series. When discussing plough depth it is in fact the heel depth that is being referred to as this is likely to have a greater correlation with tow force due to the width of share being far greater at the heel.

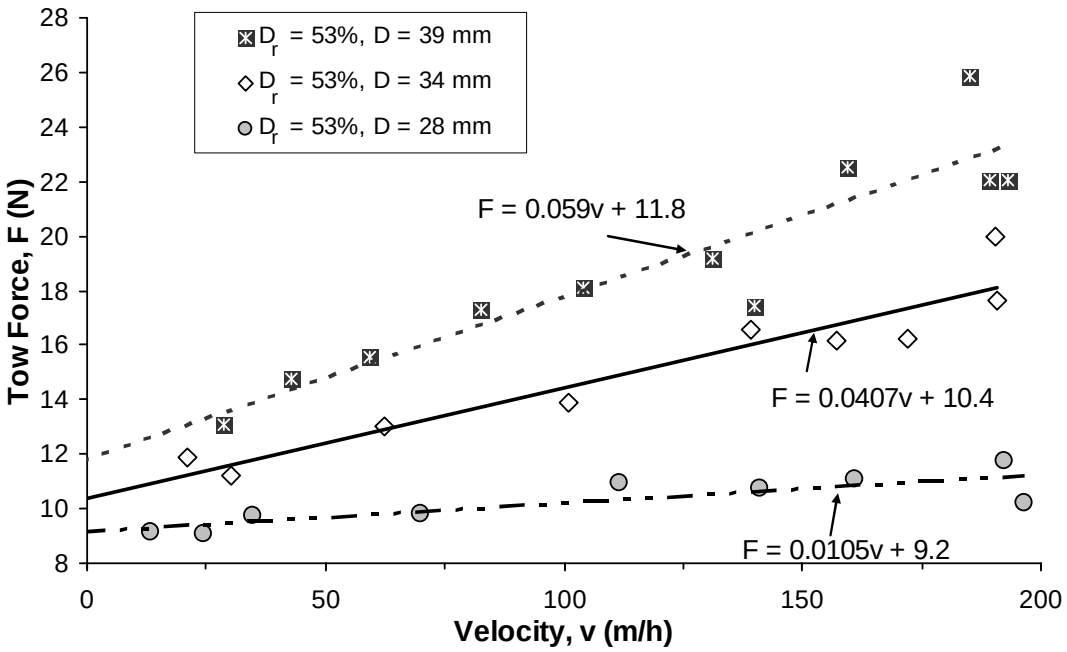

Figure 5-13: Influence of plough depth over the rate effect in HST95, D_r = 53% during tests without a forecutter

Figure 5-13 presents tow force and velocity data for three series of ploughing tests in fine sand (HST95) at average plough depths of 28, 34 and 39 mm respectively. The trend lines are numerically fitted the using least squares method and are not defined by any physical parameters. The rate dependant component of the tow force increases with plough depth and is shown by the gradients of the fitted lines. This may be due to

a combination of an increase in drainage path lengths (which reduce the amount of drainage occurring at the same velocity) and the shape of share. The end elevation diagrams in Figure 5-12 show that the width of the share increases with the depth during ploughing so that the projected area is proportional to D^2.

Figure 5-14 plots the tow force at zero velocity derived from the trend lines in Figure 5-13 minus the base friction force, to give the passive resistance component of ploughing against the cube of the plough's depth. The passive resistance during ploughing is shown to be proportional to D^3 as shown previously by the results from tests in dry sand.

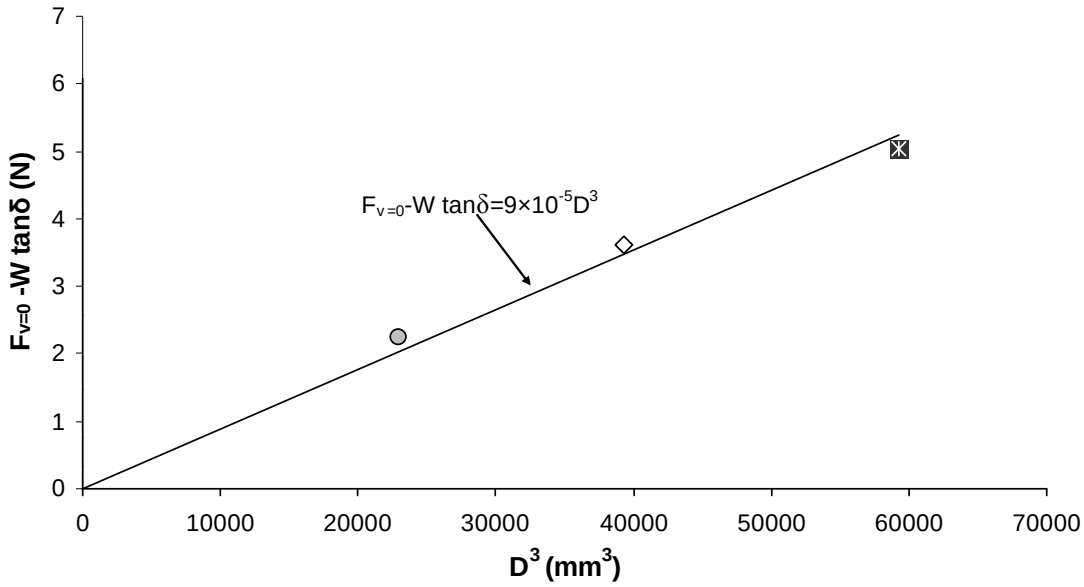

Figure 5-14: Passive component of tow force against the cube of the plough's depth in HST95, D_r = 53% during tests without a forecutter

The data in Figure 5-15 was constructed using the slope of the rate effect defined by the trend lines in Figure 5-13. D^2 and D^3 relationships are also shown and linear least squares regression analysis was used to define the fitting constants for both lines. The D^3 line provides the most convincing fit to the limited data set, although more data is required to make a better prediction of the relationship. Cathie and Wintgens (2001) show that the rate effect varies with D^2 rather than D^3 however part of their reasoning for this was that the ploughs they were considering had forecutters which effectively reduce the length of drainage path from the share tip to the surface. The data shown in

Figure 5-15 is for a plough without a forecutter and a reason for the disagreement with Cathie and Wintgens (2001).

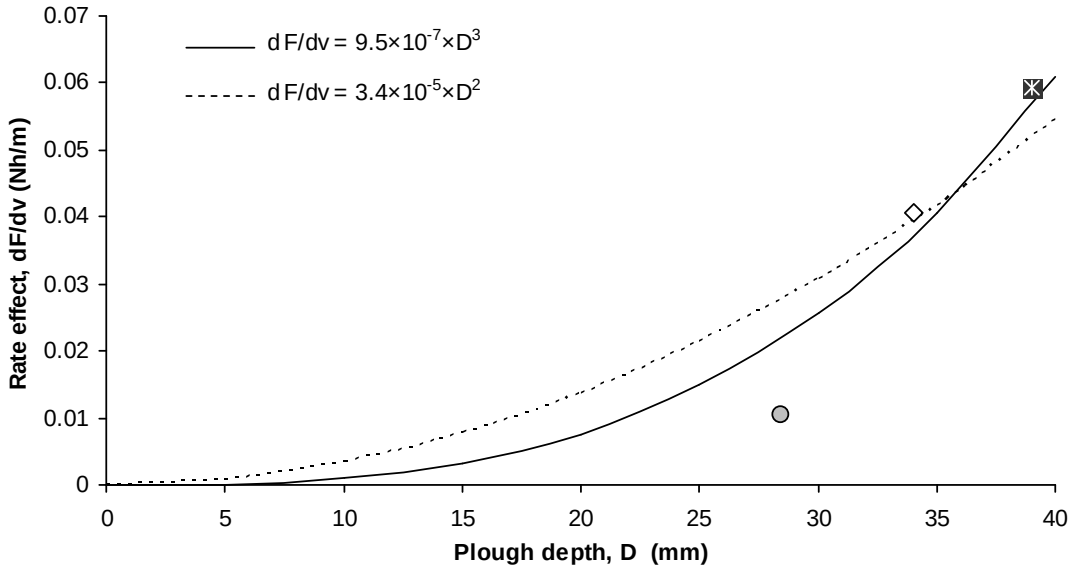

Figure 5-15: The rate effect with respect to plough depth in HST95, D_r = 53% during tests without a forecutter

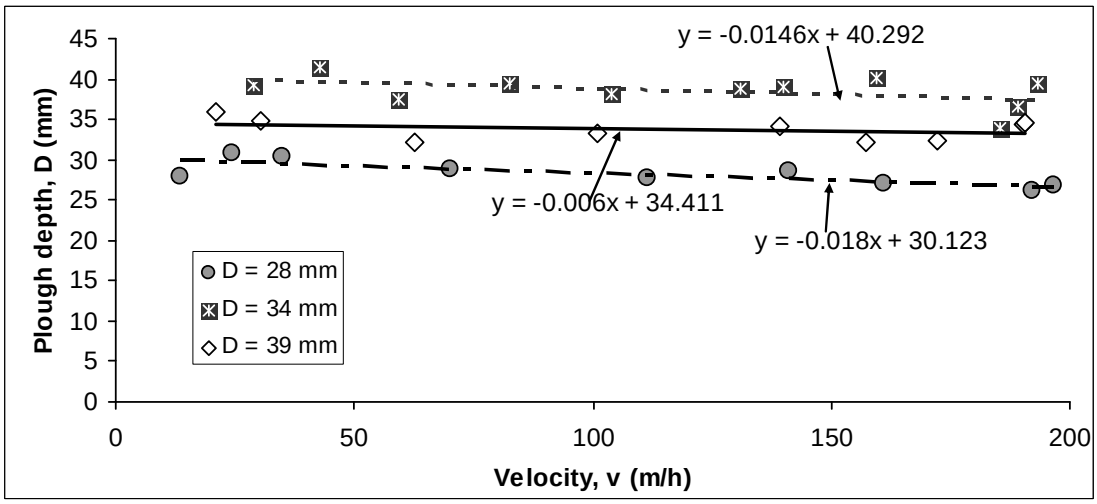

Figure 5-16: The reduction in plough depth with increasing velocity when ploughing without a forecutter in HST95, D_r = 53%

It has previously been discussed that plough depth is influenced by velocity. The plough depths shown in Figure 5-15 are average depths for each series of tests. Figure 5-16 shows the depth of each test conducted for each of the three series. The depth during a test at 200 m/h is found to be 12% smaller than a test at close to 0 m/h during

the D = 28 mm series. The percentage depth differences between tests at 200m/h and tests close to 0 m/h found during the D = 39 mm and D = 34 mm series are 7% and 4% respectively. This shows that the rate effect found during the shallowest test series (D = 28 mm) will have been reduced the greatest amount due to the plough depth reducing with increasing velocity. The result of this is that the rate effect for the D = 28 mm series shown in Figure 5-15 is likely to be smaller than it should be.

5.2.5. The influence of the forecutter on the rate effect

A forecutter can be mounted onto the beam in front of the share with the aim of reducing the rate effect. The forecutter is smaller than the share and will produce a shallow trench in the sand which the share then deepens and opens up. It is thought that the forecutter reduces the rate effect by splitting the depth of cut into two and effectively reducing the drainage path length. However there is currently little evidence to support this assumption.

Tests were conducted using the 50^{th} scale model plough with its forecutter attached and then repeated under the same conditions with the forecutter removed. This allowed the forecutter's influence over the plough's performance to be studied. Figure 5-17 shows steady state tow force data at a range of velocities from 25-190 m/h in both HST95 and HST50 sand. The forecutter appears to cause an increase in tow force at low plough velocities in both sands. This is not a $W\times\tan\delta$ effect as extra weight was added to the plough during tests without the forecutter to compensate for the change in weight and is likely to be due to an increase in passive pressure, as discussed in detail in Chapter 4. The forecutter clearly reduces the rate effect in both HST95 and HST50.

Figure 5-17 shows that during tests at velocities greater than 60 m/h in HST95 the tow force has been reduced where a forecutter has been used in comparison to tests when it was absent. The tests in HST50 have a rate effect that is relatively small in comparison to the tests in HST95 and although the forecutter reduces the rate effect in HST50, tests with a forecutter always displayed higher tow forces than those without over the range of velocities tested. This is because the increase in the static component of tow force is larger than the reduction of the rate effect even at the highest velocities tested.

At first glance this seems a mixed result. However, the overall tow force in the medium sand was lower than in the fine sand at all velocities tested regardless of whether a forecutter is present or not. The tests reveal what is already known in practice, that ploughing in medium sized sand is not problematic and therefore increasing the tow force slightly by use of a forecutter is likely to make little difference to trenching progress. This would indicate that a forecutter should have a positive influence on a plough's overall performance as it is the hard ploughing conditions (fine sands or silty sands) that are important.

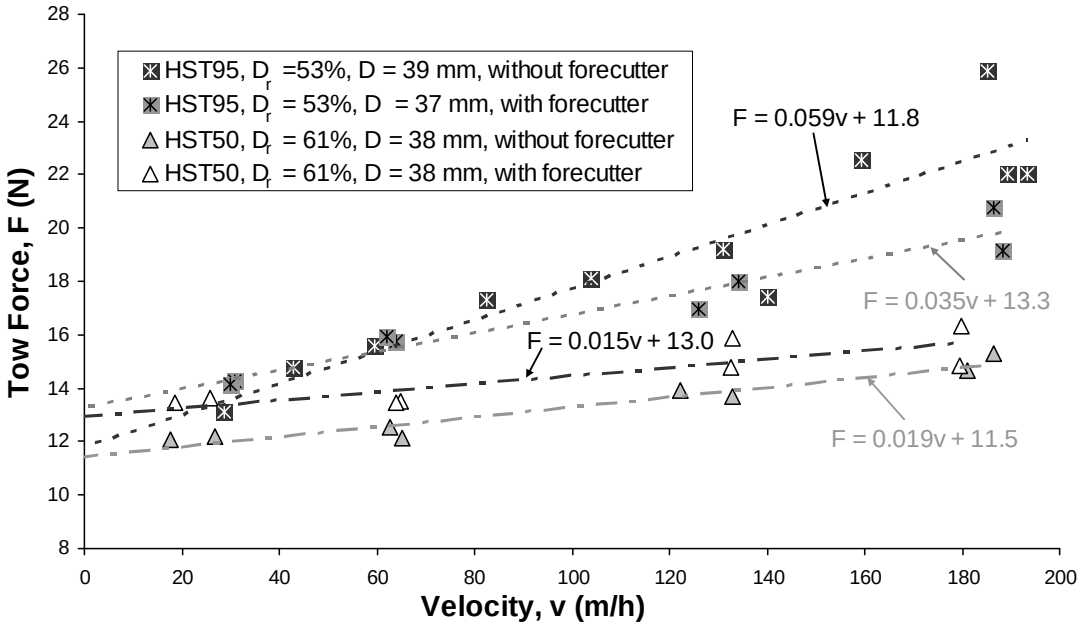

Figure 5-17: Comparison of a ploughs performance in HST95 (D_r = 53%) and HST50 (D_r = 61%) both with and without a forecutter

Although the forecutter does reduce the rate effect, it also causes a reduction in ploughing depth by causing the plough to pitch forward. Figure 5-18 plots plough depth against velocity and shows that over the range of velocities tested the plough depth reduces slightly with increasing velocity. The forecutter reduces plough depth by around 2 mm when ploughing in HST95 but only 0.4 mm in HST50. A fairer comparison between ploughing tests with and without a forecutter in HST95 would involve normalisation by depth.

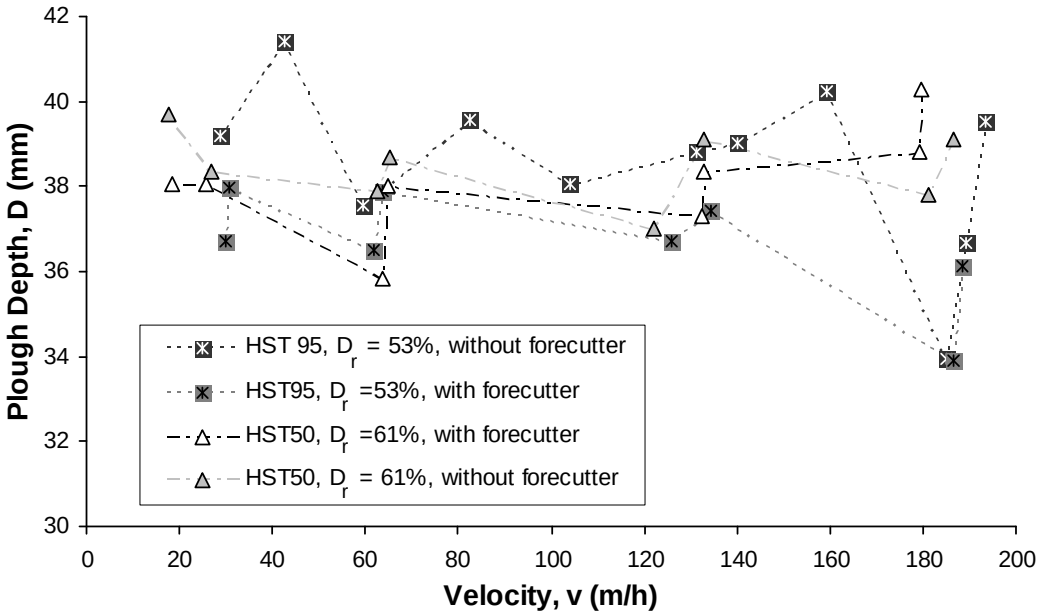

Figure 5-18: The relationship between plough depth and velocity in medium dense HST50 and medium dense HST95

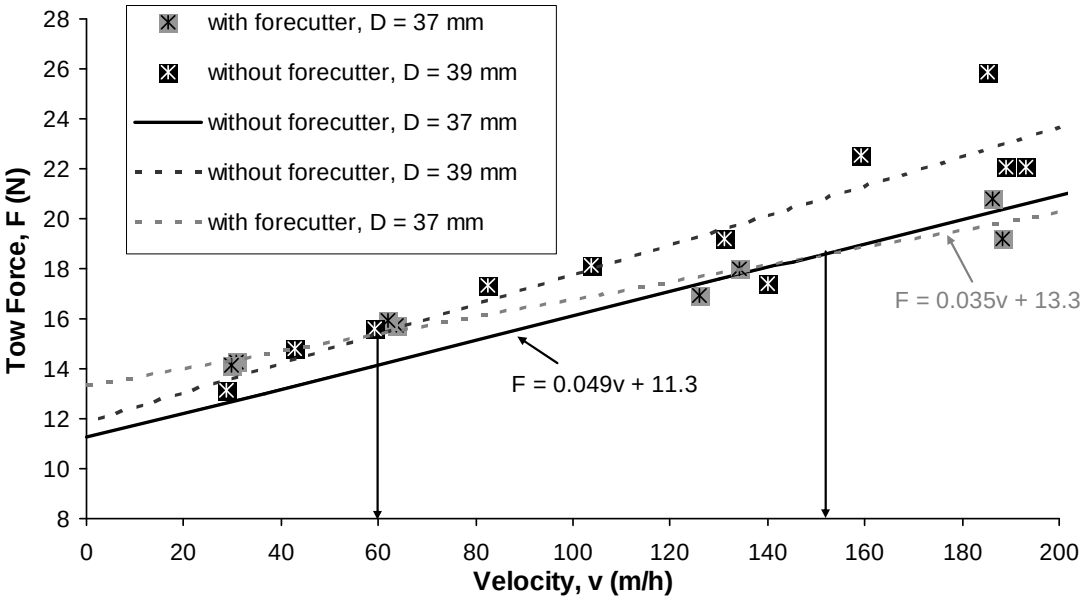

Figure 5-19: Effect of forecutter on tow force in HST95 (D_r = 53%) with plough depth correction

Figure 5-19 was constructed in order to find out if the 2 mm difference in average plough depth between tests in HST95 with a forecutter and those without had a significant effect on the data. The dashed line was constructed by interpolating both the static component of tow force and the rate effect for a plough trenching without a forecutter at 37 mm deep in HST95 sand from between 34 mm and 39 mm plough

depth data series. This allows the effect of the forecutter on the tow force to be isolated from depth. Figure 5-19 shows that the forecutter does reduce the rate effect but that its influence is less dramatic than shown in Figure 5-17, resulting in the velocity at which it becomes beneficial in reducing the tow force to be higher than previously shown (60 m/h) and is in fact around 150 m/h.

5.2.6. Scaling of rate effects

Chapter 5 has up until now has compared 50th scale model test results in different sand conditions to find out which parameters influence the rate effect. It is important for industry to know if the rate effects displayed within this chapter can be used directly to inform full scale plough behaviour. There was some conflict in the literature as to whether rate effects found during reduced scale model tests would be the same as those found at prototype scale and clearing this up would be beneficial.

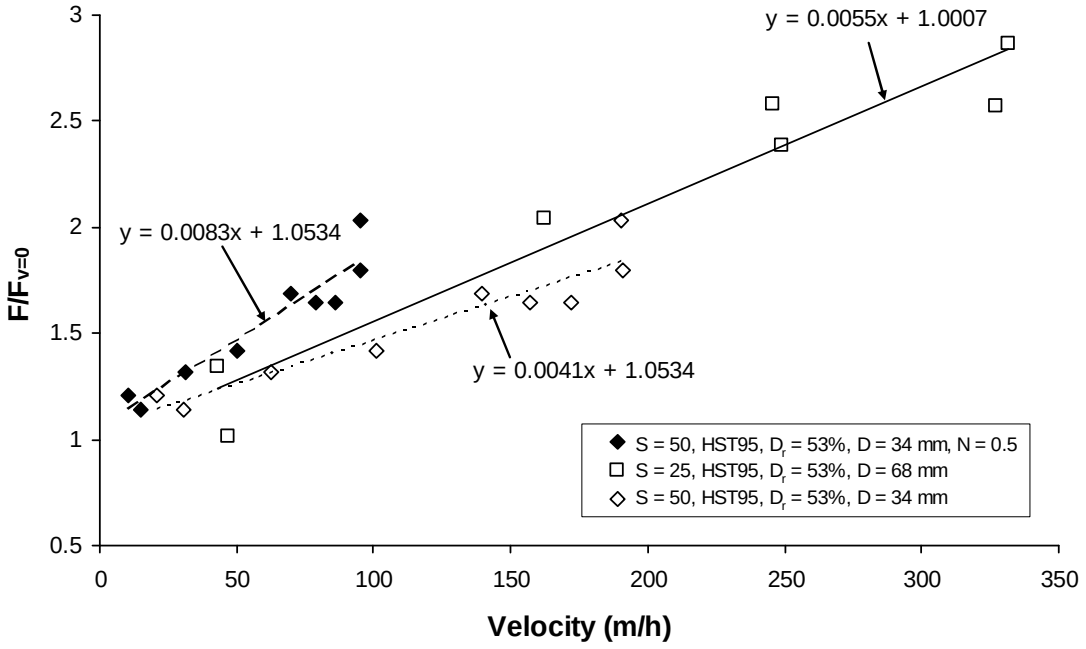

Figure 5-20: Comparison of normalised steady state tow forces found during 50th and 25th scale ploughing tests without a forecutter in HST95, D_r = 53%

Figure 5-20 presents normalised tow forces found during 50th scale (S = 50) and 25th scale (S = 25) ploughing tests in HST95 at a reative density of 53%. The normalised tow force is the steady state tow force found during each test normalised by the 'static' tow force ($F_{v=0}$) of the series. The tow force of each data set was normalised

by first plotting the data in force velocity space and then using the least squares method to pass a best fit line through the data. The 'static' tow force is the tow force where the best fit line intersects with the y-axis at zero velocity.

The 50th scale data has been plotted twice: once with the real test velocity and once where the test velocity has been reduced by a factor of two. The reason for plotting reduced velocities from the 50th tests is that comparing these to the 25th scale test velocities satisfies the Pamler (1999) approach where the product of v and D must be the same for all scales of test in order to achieve comparable rate effects. The results are inconclusive as the rate effect found during the 25th scale tests is greater than the rate effect found during the 50th scale tests but less than that of the 50th scale tests where vD is matched to the 25th scale tests.

5.2.7. Nondimensionalization of rate effects

The results from saturated ploughing tests have up until now been plotted in numerous simple graphs, each showing how the rate effect is affected by a particular parameter. Presenting the data in this manner is likely to be of limited use to the trenching contractor and grouping the data together in fewer charts or describing it by a simple equation would be desirable. Rate effects have been normalised in order to find the physical properties, for example: the length of drainage paths and soil permeability which govern or influence rate effects. This allows data of different test series to be grouped together and may provide more useful relationships. Nondimensionalization allows full scale predictions to be made from model scale tests.

A non-dimensional loading rate, (Equation 5-2) was proposed by Finnie (1993) during analysis of the reaction of shallow foundations subjected to vertical displacements. This approach has since been extended to examine drainage effects for other penetrating objects such as T-bar and piezocone tests e.g. Finnie and Randolph (1994), House *et al*. (2001), Randolph and Hope (2004) and Silva and Bolton (2005).

$$V = vD / c_v \qquad (5\text{-}2)$$

Where V is the normalised velocity, v is the velocity of the object penetrating the soil, D is the diameter or width of the penetrating object (plough depth is used here) and c_v is the coefficient of consolidation.

In order to apply Equation 5-2 to the rate effects discussed herein c_v was attained by the following relationship (Equation 5-3) as it is not a commonly measured property for sand.

$$c_v = E_0' k/\gamma_w \quad (5\text{-}3)$$

where the confined modulus, E_0' (see Table 5-2) and permeability, k (see Table 5-3) were measured for HST95 and HST50 at both medium and dense states during standard laboratory tests.

Table 5-2: Confined modulus attained over the stress range 5-10 kPa in an odeometer cell

	Values of confined modulus, E_0 (kN/m^2)		
Condition	HST50	HST95	Redhill 110
Medium	6500	5000	1700
Dense	11500	8000	-

Table 5-3: Permeability of HST50, HST95 and Redhill 110 from permeameter tests

	Values of permeability, $k \times 10^{-5}$ (m/s)		
Condition	HST50	HST95	Redhill 110
Medium	49.5	12.3	10.0
Dense	38.4	8.6	-

Figure 5-21 presents data from test series in medium dense HST95 and HST50, where the normalised velocity is plotted against the tow force normalised by the static tow force ($F_{v=0}$). The tow force of each data set was normalised by first plotting the data in the force-velocity plane and then using the least squares method to pass a best fit line through the data where its intersection with the y-axis at zero velocity was used as a 'static equivalent' tow force. The normalisation has aligned the two data series with HST50 having lower normalised velocities than HST95 due to its increased

permeability. Finne and Randolph (1994) report values of normalised velocity, V of around 0.01 and 30 which equate to limits of drained and undrained behaviour respectively found during vertical displacement tests of circular footings in calcareous sands and silts.

Figure 5-21 shows that all of ploughing tests in HST50 were conducted at normalised velocities where fully drained behaviour should be expected. If this was the case rate effects should not be displayed during the tests at $V < 0.01$, however a clear rate effect exists. One possible explanation for this is that the normalised velocities reported here are incorrect. The E_0' values used to define c_v describe the soil response at stresses higher than those experienced during the scale model ploughing and therefore may be unrealistically high. This would increase c_v above its correct value for the ploughing tests and hence reduce V.

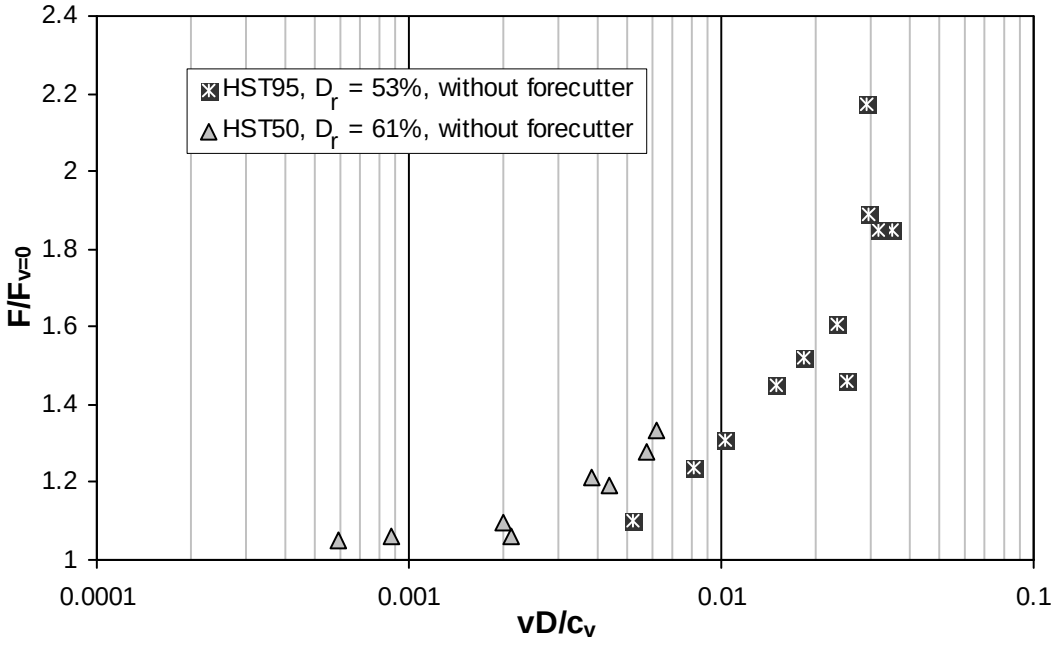

Figure 5-21: Rate effects normalised by vD/c_v

At present most of the use of the normalised velocity, V has been to describe objects which are vertically penetrating the soil whereas the ploughing tests described here are near surface horizontal translation which complicates the selection of an appropriate D to use in the calculation of the normalised velocity. The use of another length other than the plough depth may be more appropriate for defining D. Bransby and Ireland (2009) report values of V which provoke drained and undrained soil

response during pipeline uplift tests in sand as 0.00001 and 0.01 respectively where they used the pipeline diameter as the appropriate length scale for *D*. Bransby and Ireland (2009) note the difference between their values and those of other researchers and suggest one reason for this might be the difference in failure mechanism between the pipeline uplift problem and for example shallow foundation tests where limits of *V* were originally found. They state that localisation of shear failure above the pipeline during uplift may cause preferential drainage and therefore *D* should be reduced to a value less than the pipeline diameter.

The ploughing tests reported here and also during offshore ploughing operations in general may occur over a very limited range of velocities within partially drained soil behaviour. This may be one reason why rate effects appear to increase linearly with velocity whereas this should not be the case as they cannot continue indefinitely like this since they are a response to partial drainage.

This normalisation may not be valid for ploughing at different depths or for ploughs of different weights. If we consider $F/F_{v=0}$ in terms of Cathie and Wintgens (2001) model for cohesionless soil (Equation 2-3), Equation 5-4 is derived. Equation 5-4 shows that if either *W* or *D* for example are changed then the ratio $F/F_{v=0}$ of changes. This may invalidate comparison of tests conducted at different depths or between ploughs of different mass.

$$\frac{C_w W' + C_s \gamma' D^3 + C_d v D^2}{C_w W' + C_s \gamma' D^3} \tag{5-4}$$

If however rate effects are considered to affect the weight of the plough and are proportional to D^3 (see, Figure 5-15) this adds some value to $F/F_{v=0}$. If rate effects act on the plough as shown in Equation 5-5 and the effect is of similar magnitude on the friction component as on the passive pressure component the normalisation should allow for different conditions to be directly compared.

$$\frac{C_w (W' + A\Delta u) + C_s \frac{v}{r} \gamma' D^3}{C_w W' + C_s \gamma' D^3} \tag{5-5}$$

where, A is the area beneath the share, Δu is the change in pore water pressure and r is a coefficient which allows C_s to increase by the correct proportion with velocity and will be influenced by permeability and relative density as is the case for C_d.

The data in Figure 5-22 shows comparison of plough tests at different depths using the same normalisation as in Figure 5-21. The data from the tests conducted at plough depths of 38 mm and 34 mm align well and form a distinct trend. The data from the tests conducted at a depth of 28 mm show a fair degree of scatter which is largely due to the normalisation of the tow force.

The depth of each test within each test series varies and generally reduces with increasing velocity which causes an apparent reduction in the rate effect. This is probably due to the plough relying on maintaining its trenching depth by moment equilibrium about the skids which is affected by changes in tow force due to the rate effect. Normalising the tow force of each test by a single static value at a depth which is average to the series causes the data to scatter as some of the tests are normalised by static values which are too high and some by values which are too low since the depth is not constant within the series. In most of the test series this has only a minor affect, however the total depth being the smallest of test series and the depth difference within the series the highest, the error is amplified. The data from the series at D = 28 mm has also been plotted in Figure 5-22 where the tow force has been normalised by Equation 4-4 ($F_{v=0} = C_w W' + C_s \gamma D^3$) which gives the static tow force generated when ploughing in sand.

The advantage of using this equation is that it eliminates the scatter in the data caused by the differences in plough depth within the test series. The value of C_w used in the normalisation is 0.45 and was derived from interface friction tests conducted in a shear box. A value of 13.5 was taken for C_s, which was found during the dry ploughing tests. The grouping of the data series is improved when the tow force is normalised by Equation 4-4, however the series does sit noticeably below the other two test series.

A second approach in reducing the scatter of the data is to take the slope of the rate effect found using least squares method for the entire data series and back calculate

the static tow force for each data point in the series using its own unique tow force. The tow force normalised in this manner sits very close to the normalisation by Equation 4-4. At low velocities the data for D = 28 mm match well with other series but as the velocity increases the data diverges from the other series and is probably a result of the plough depth reducing with increasing velocity for the D = 28 mm series.

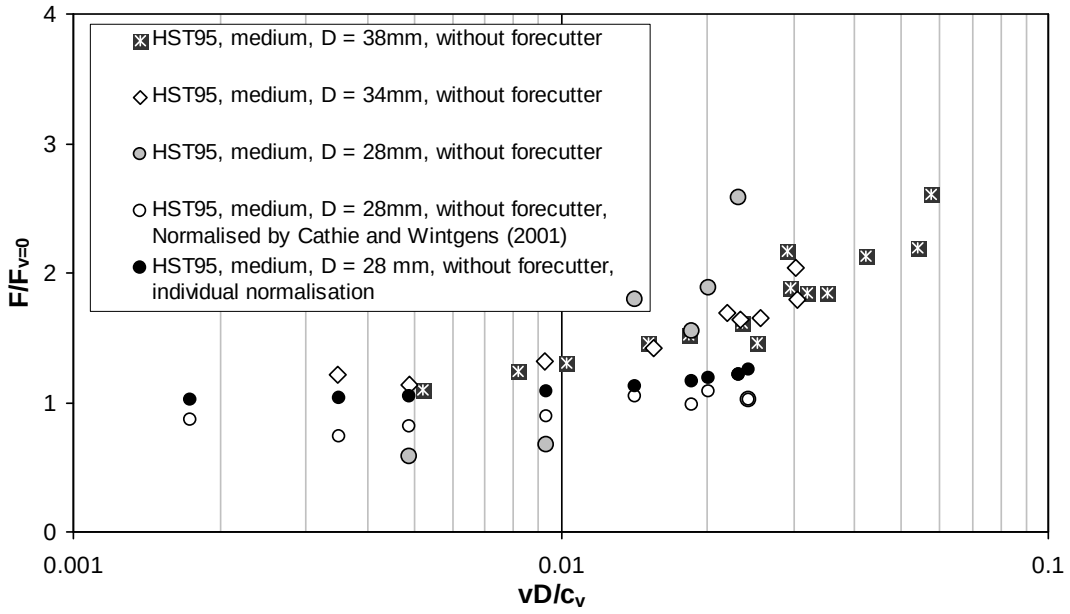

Figure 5-22: Grouping together data from tests at different depths of ploughing by normalising the tow force by its static component

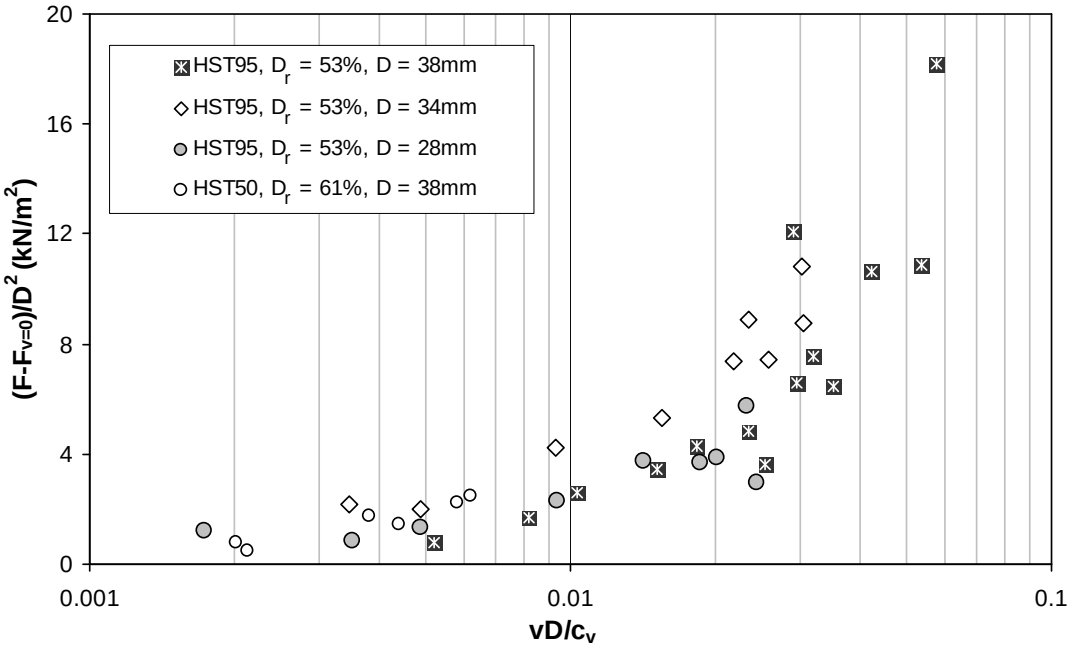

Figure 5-23: Comparison of data using the rate dependant component of force normalised by D^2

Separation of the rate effect from the static tow force as prepared by Cathie and Wintgens (2001) does not rely on conjecture as to how the rate effect affects the individual components of tow force. This method will also prevent the scatter caused by the normalisation in Figure 5-22 where data series of low rate effects are analysed. The plough depth and tow force were scaled up (in the same way as was done in the previous chapter) to give the rate effect in kN/m^2. The data series in Figure 5-23 align reasonably well with the exception of the 34 mm deep tests in HST95 which sits noticeably above the rest of the data. It was previously shown that the rate effect may vary with the cube of the plough depth and therefore D^3 may be a more appropriate normalisation of the rate effect than D^2. Figure 5-24 shows comparison of rate effect normalised by D^3 and the various series align reasonably well however the series at 38 mm in HST95 sits below the rest of the data.

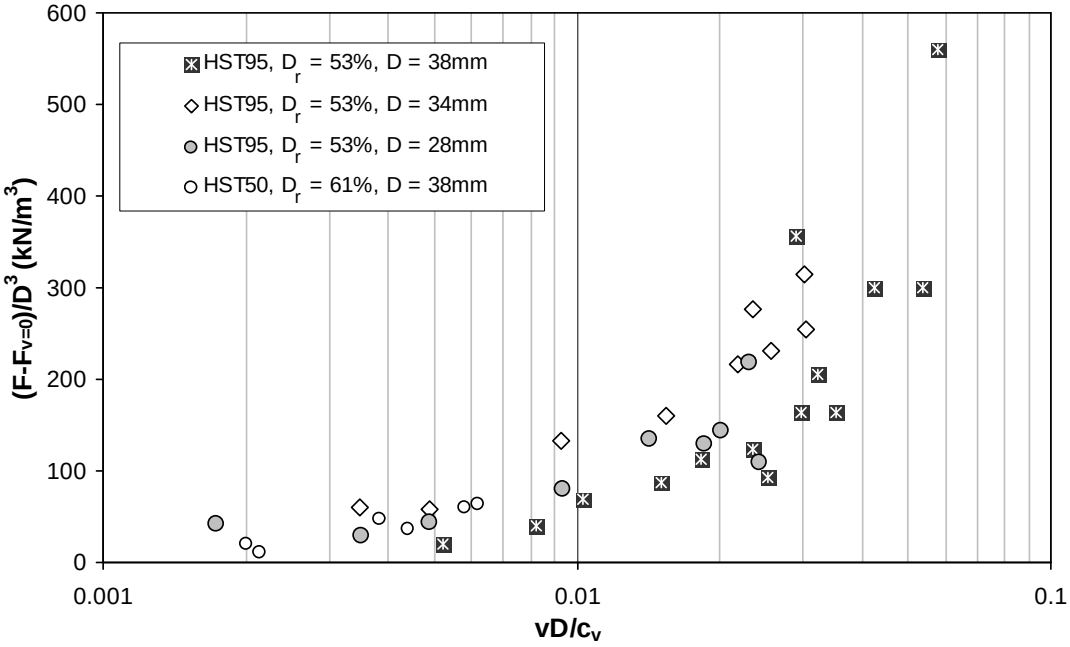

Figure 5-24: Comparison of data using the rate dependant component of force normalised by D^3

Palmer (1999) conducted an analytical analysis of the ploughing process and found that the reduction in pore water pressure during ploughing was proportional to $VD[\Delta e/(1+e)]/k$. Effective stress increases are proportional to pore water pressure reductions and the area of the shear zone during ploughing is proportional to the square of the plough's depth. Therefore, the increase in tow force, ΔF, due to pore water pressure reductions was represented by Palmer (1999) as:

$$\Delta F \propto \frac{vD^3\left(\frac{\Delta e}{1+e}\right)}{k} \tag{5-6}$$

where, v is the plough's velocity, D is the plough's depth, e is voids ratio and k is the permeability of the soil.

The data from the same four test series as shown in Figure 5-24 has been normalised using analysis from Palmer (1999) and plotted on Figure 5-25. The data show that the rate effect increases with D^3/k.

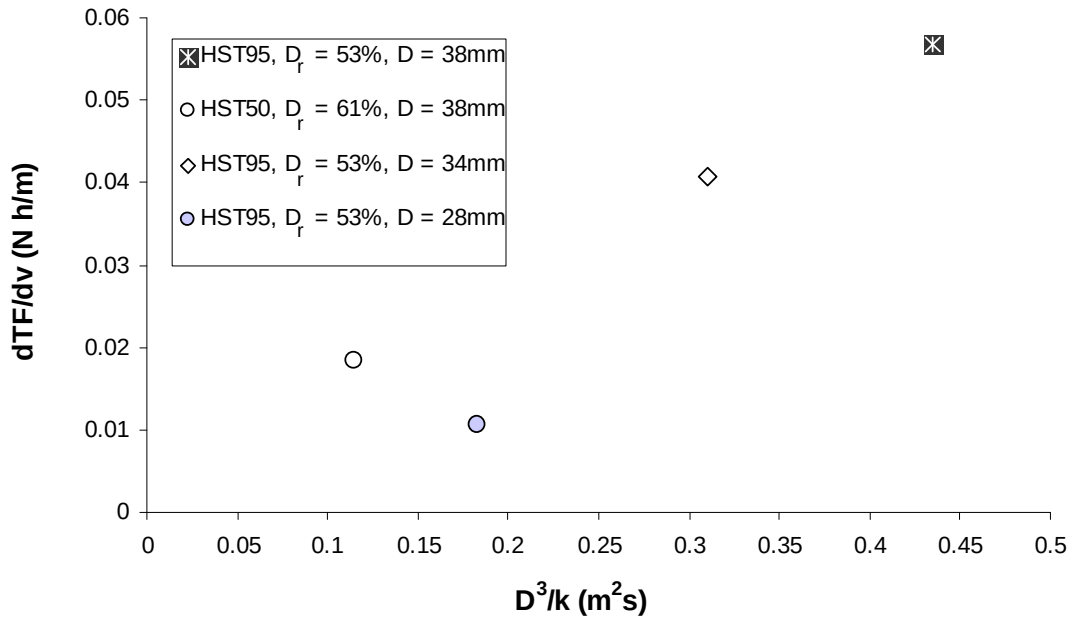

Figure 5-25: Comparison of rate effects by D^3/k

By considering phase relationships, Palmer (1999) describes the net inflow of water into the shear plane per unit volume of soil as the change in void ratio divided by the specific volume. The data shown in Figure 5-25 has been further normalised by what Cathie and Wintgens (2001) describe as the dilation potential, S (see Equation 5-7) and is shown in Figure 5-26 along with data sets from ploughing tests in dense HST50 and dense HST95.

$$S = \Delta e/(1+e) \tag{5-7}$$

Where, Δe is the change in voids ratio to critical state conditions and e is the initial voids ratio. The critical state void ratio was assumed to be that obtained through dry stirring of the sand as the sand was effectively being sheared repeatedly, hopefully to the point of constant volume shearing. This showed e_{crit} to occur at D_r = 17% in HST95, at D_r = 25% in HST50 and at D_r = 26% in Redhill 110 over the range of stresses experienced during the model plough tests.

Normalising in this manner may not be appropriate in describing densities less than critical state as this would result in negative S values and therefore negative normalised velocities. It is however, rare to find loose sands on the sea bed due to the method of deposition so this shouldn't cause a problem for trenching contractors using this normalisation to predict tow forces.

Figure 5-26 shows the rate effect normalised by SD^3/k. A linear trend in the data is apparent and a straight line has been fitted and forced through the origin. The data from the test series in dense HST95 does not agree with the rest of the data.

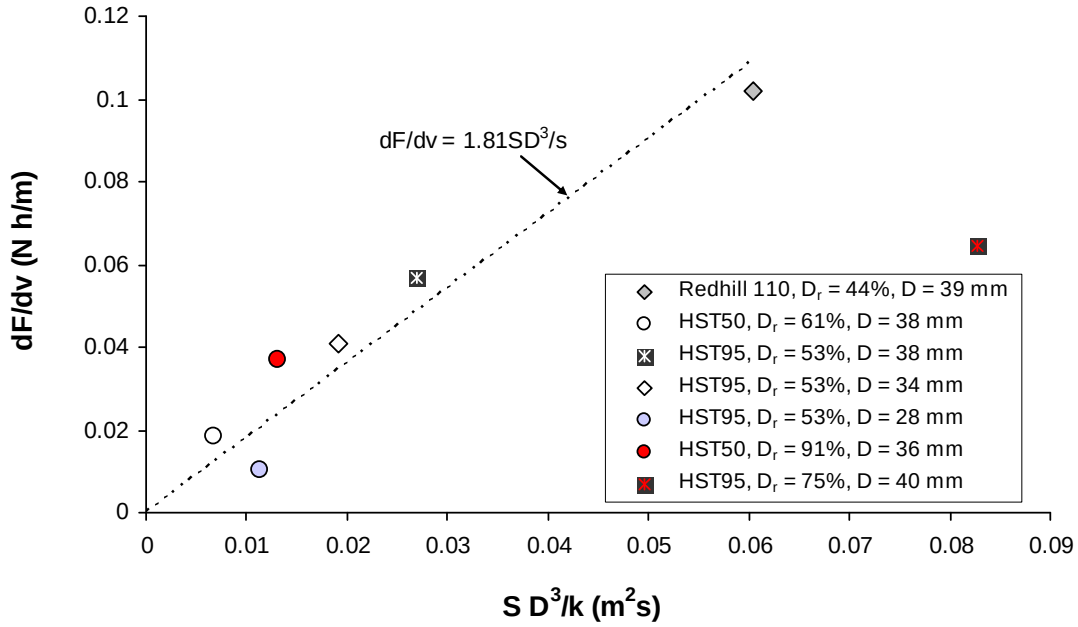

Figure 5-26: Rate effect normalised by SD^3/k to compare of sands at different relative density

Figure 5-27 shows the rate dependant component of tow force normalised by the square of the plough depth against the product of the non-dimensional velocity and the dilation potential. Normalising by the dilation potential accounts for the increase in volume of pore fluid required within the sand during shearing of the sand. The

coefficient of consolidation takes into account the increase in stiffness and reduction in permeability which results from increasing the density of sand. The normalisation on the x-axis therefore brings together data from ploughing tests in sands of different permeability and of different relative density reasonably well. There is some uncertainty as whether to normalise the y-axis by D^2 or D^3 however a fairly good prediction of rate effects dependant on the permeability, stiffness and density of the sand and the depth of the plough can be made using Figure 5-27.

The fitted line through the data provides Equation 5-8 which can be used to estimate rate effects in sands of relative density above critical state.

$$\frac{(F - F_{v=0})}{D^2} = 6000 \times vDS / c_v \qquad (5\text{-}8)$$

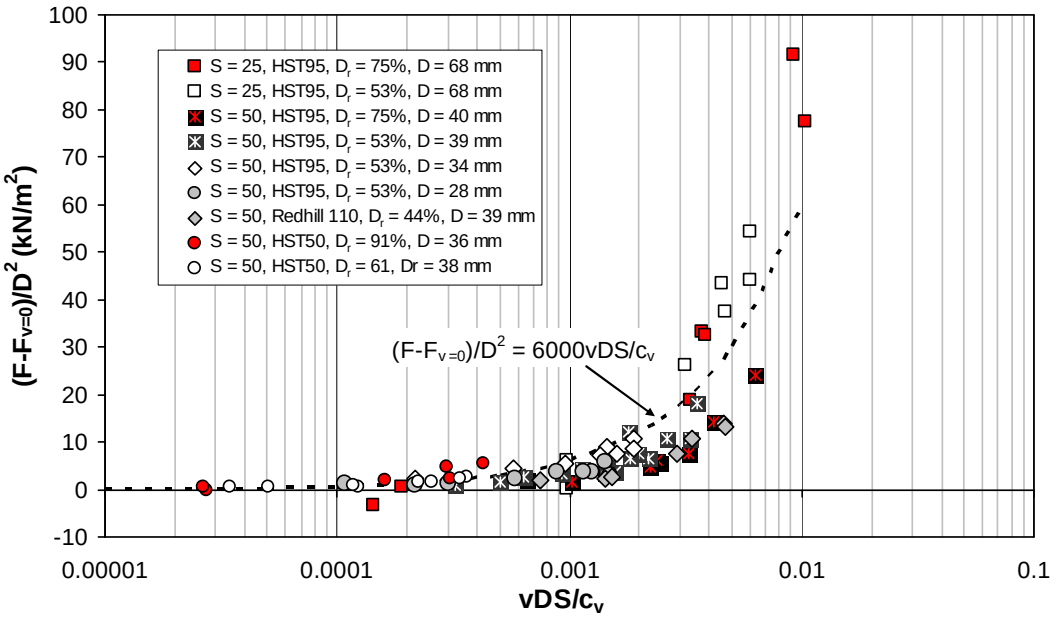

Figure 5-27: $(F\text{-}F_{v=0})/D^2$ against vDS/c_v

The rate effect is assumed to be controlled by the amout of drainage that occurs during ploughing. Equation 5-8 which defines the rate effect shown in Figure 5-27 is therefore only valid over a range of normalised velocities which provoke a partially drained soil response to ploughing. It is therefore beneficial to define the limits of partially drained soil response to ploughing in terms of normalised velocity as Finnie and Randolph (1994) did for vertical loading of shallow foundations. Figure 5-27 shows that $F\text{-}F_{v=0}$ tends towards zero at around vDS/c_v = 0.00002 which defines the

upper limit of drained behaviour. Since Figure 5-27 shows no sign of the rate effect reducing with increasing velocity the transition between partially drained and undrained soil response can not be defined, however at some value of vDS/c_v greater than shown in Figure 5-27 $(F-F_{v=0})/D^2$ is expected to cease to increase.

5.2.8. Measurement of pore water pressures during 50th scale ploughing tests

To investigate and quantify the changes in pore water pressure during 50th scale ploughing tests, two pore water pressure transducers were inserted into the bed of saturated sand prior to ploughing. The two transducers were placed on the centreline of the plough trench, 1000 mm from the edge of the box at depths 70 mm and 100 mm respectively below the surface of the sand (see Figure 5-28).

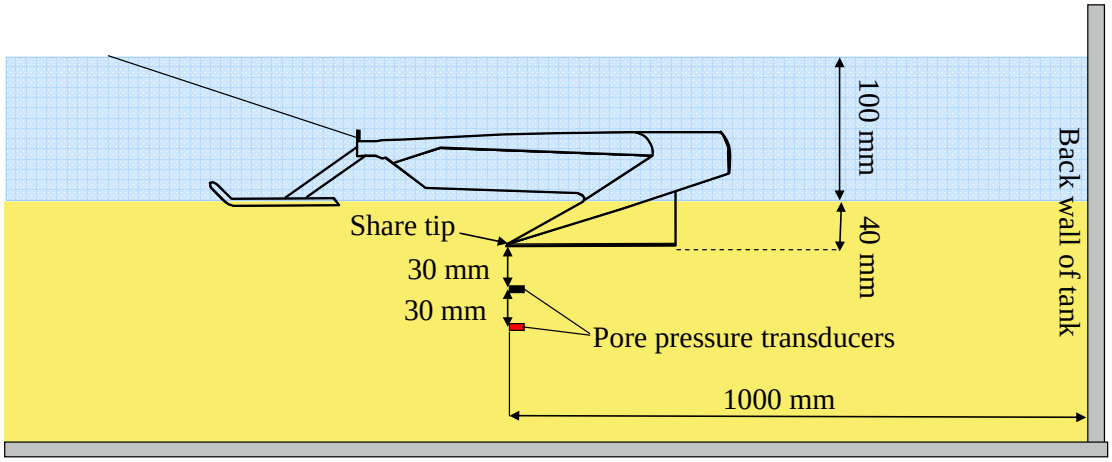

Figure 5-28: Schematic showing the positions of the pore pressure transducers

Figure 5-29 shows how the pore water pressure changed with position of the plough during two different ploughing tests in medium dense (D_r = 44%) Redhill 110 sand at velocities of 25 m/h and 187 m/h and ploughing depth of 39 mm. The initial readings on the x-axis start at around 140 mm, which was the measured distance from the edge of the sand tank to the share tip at the start of each test. The pressure head readings on the y-axis are at 0.2 m and 0.17 m respectively at the start of each test and correspond to the head of water above the transducers (i.e. giving 2 kPa and 1.7 kPa of positive pore pressure respectively). As the plough advanced towards the transducers embedded in the sand, they did not record any change in pore pressure until the plough was between 150-200 mm behind them at which point the pressure drops (i.e.

there is a reduction in positive head and so a relative suction is measured). The pressure only re-stabilises again after around 300-400 mm of further plough displacement from the initial drop i.e. once the full length of the share has passed the transducers. This may be evidence that both the shearing of sand ahead of the share and the sand in direct contact with the share contribute to the rate effect in which case supports the $F/F_{v=0}$ normalisation in Figure 5-22.

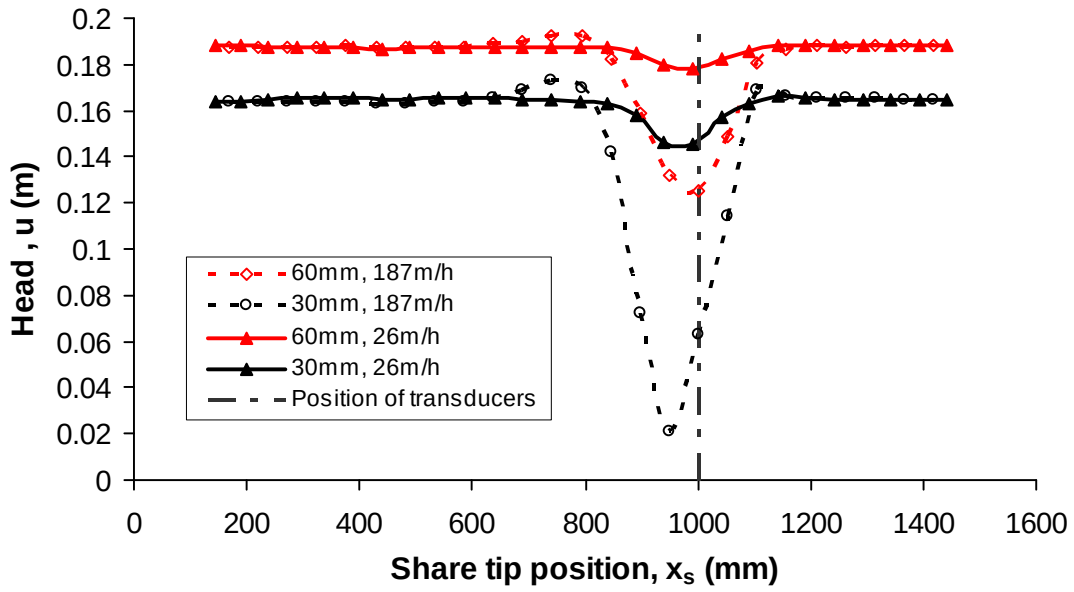

Figure 5-29: The change in pore pressure below the share as the plough (without forecutter) shears sand (medium dense, Redhill 110) above

The ploughing test conducted at 187 m/h causes greater pore water pressure reductions than the test at 26 m/h. During the 26 m/h test there is more time for pore water to flow into the dilating zone of sand being sheared by the share. Consequently a lower pressure differential is required to drive the flow of pore fluid into the dilating zone of sand than during the 187 m/h test (see Van Leussen & Nieuwenhuis, 1984). The measured pore pressure reductions are greater at the transducer closest to the plough, which is likely to be a result of the flow rate reducing with distance from the shearing zone in order to drive flow.

Finite element modelling conducted at Cathie Associates (Cathie and White; 2010) has shown suction pressures to be greater around the share than ahead of the share, which they attribute to increase in mean stresses due to the advancing share. In contrast Figure 5-29 shows the minimum pore pressure to occur between 0 mm and

50 mm ahead of the share at 50th scale which is roughly equivalent to 0-0.5 sharelengths. The minimum pressure recorded in the transducer 30 mm below the share seems to occur slightly before the minimum pressure recorded by the transducer 60 mm below the share.

The maximum reduction in pore water pressure for each test is plotted against plough velocity in Figure 5-30. The pressure drop appears to increase linearly with velocity. Tests where the forecutter was attached to the plough reveal that the forecutter strongly reduces the pressure drop at 30 mm below the share and noticeably reduces the pressure drop in pore water 60 mm below the share.

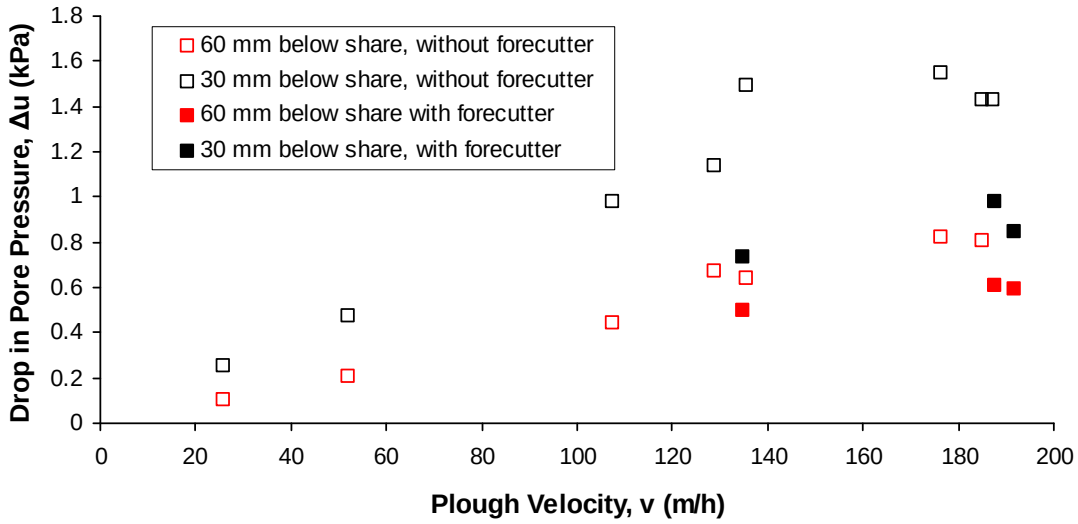

Figure 5-30: Maximum reduction in pore water pressure measured during ploughing tests in Redhill 110 (D_r = 41%) by pore water transducers at 30 mm and 60 mm below the share

The change in pore pressure during ploughing can be thought of in terms of Darcy's Law rearranged to find ΔP (Equation 5-9).

$$\Delta P = \frac{v_f \gamma_w l}{k} \tag{5-9}$$

where, v_f is the velocity of pore fluid driven by the dilating sand and for a particular sand at a particular density v_f is proportional to the velocity of the plough, v. k is the coefficient of permeability, γ_w is the unit weight of water, l is the length of drainage path and ΔP is the change in pressure required to drive the flow.

Darcy's law can be used to show that tests conducted at 50 scale will cause pressure changes within the pore water that are 50 times smaller than at prototype scale. v_f is dependent on v for which the scale factor is 1 (Table 2-3) and the respective scale factors for k and γ_w are both also 1. The length of drainage path, l is proportional to plough depth and is therefore 50 times greater at prototype scale than at 50th scale. This causes ΔP to be 50 times greater at full scale than at 50th scale. For instance the pressure reductions shown in Figure 5-30 from tests at 50th scale measured at 30 mm and 60 mm below the share would be expected to be 50 times greater at prototype scale when measured at 1500 mm and 3000 mm beneath the share.

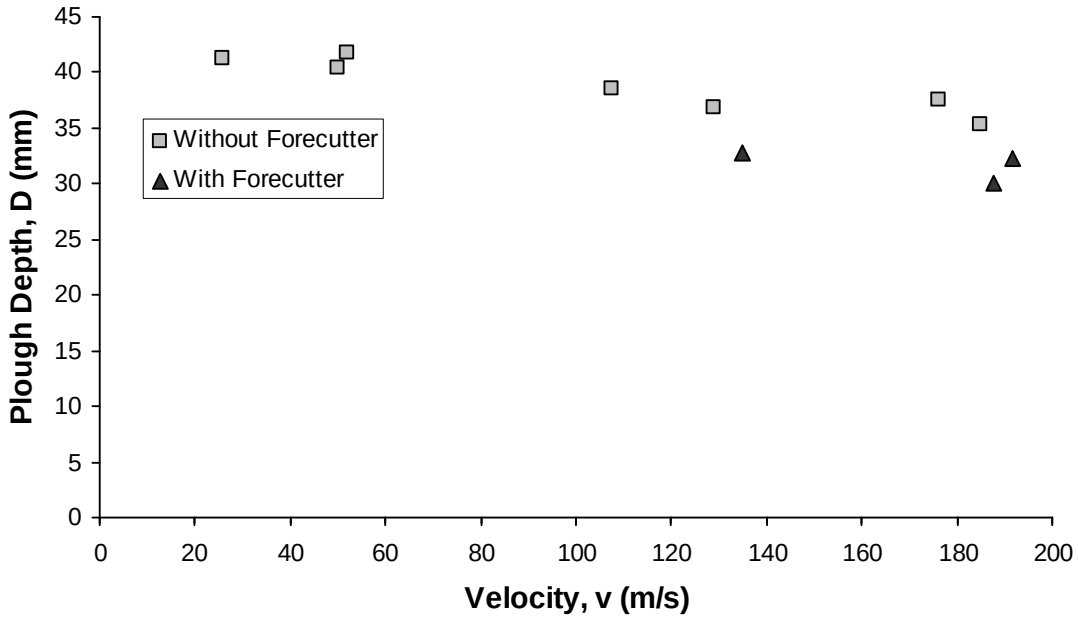

Figure 5-31: Change in plough depth with velocity in Redhill 110 (D_r = 41%)

The share depth reduced with increasing plough velocity (see Figure 5-31) and the transducers were placed at 70 mm and 100 mm below the sand respectively for all tests. The tests with the forecutter attached also caused the plough to trench at a shallower depth and also skews results. The transducers are therefore at somewhat different depths relative to the plough during different tests and will affect results. The reduction in plough depth due to the forecutter is however only around 3 mm and the pressure drop at ≈30 mm below the share when the forecutter is present is similar to that ≈60 mm beneath the share when it is absent. Therefore the diminishing pore pressure reductions due to the forecutter is a real effect and not just a product of comparing two slightly different depth test series.

Figure 5-32 shows the tow force in Redhill 110 sand is reduced for tests where a forecutter was used. The pore pressure reductions shown in Figure 5-30 will increase normal effective stresses ($\sigma_n' = \sigma_n - u$) and in turn increase the shear stresses required to cause failure in the sand and provide an answer to how the forecutter reduces tow forces.

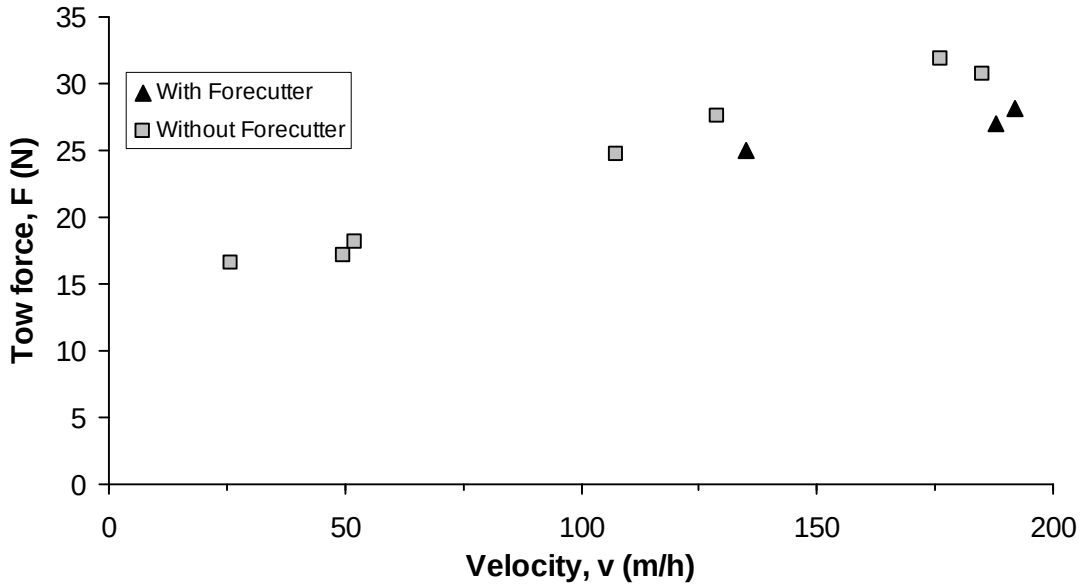

Figure 5-32: Tow force – velocity relationship for ploughing tests with and without a forecutter in silty sand (Redhill 110)

5.2.8.1. Use of pore pressure measurements to predict the tow force

The pore pressure measurements have been used to calculate normal effective stresses around the share during dilation. The corresponding shear stresses have been calculated by Coulomb's equation and the expected tow force calculated based on the observed failure plane geometry.

Figure 5-33 shows an oblique view of half of the plough during trenching. The picture shows the head of spoil heap in front of the right side of the share and a small section of the heap behind the plough at the right side of the trench. A shear plane which has emerged at the surface of the sand is highlighted ahead of the spoil heap. As the plough advances the spoil heap does so at the same rate and another shear plane will form in roughly the same position relative to the plough as the current one. The line referred to as 'the assumed profile of shear plane at surface' shows a simplified

version of the observed failure plane (and assumed failure plane at either side of the plough which is masked by the spoil heaps) and the 'assumed profile of shear plane at share depth' is dictated by the shape of the share. The area of the shear plane in the following calculations is the area bounded by these two assumed lines, one at share depth and the other at the surface of the sand.

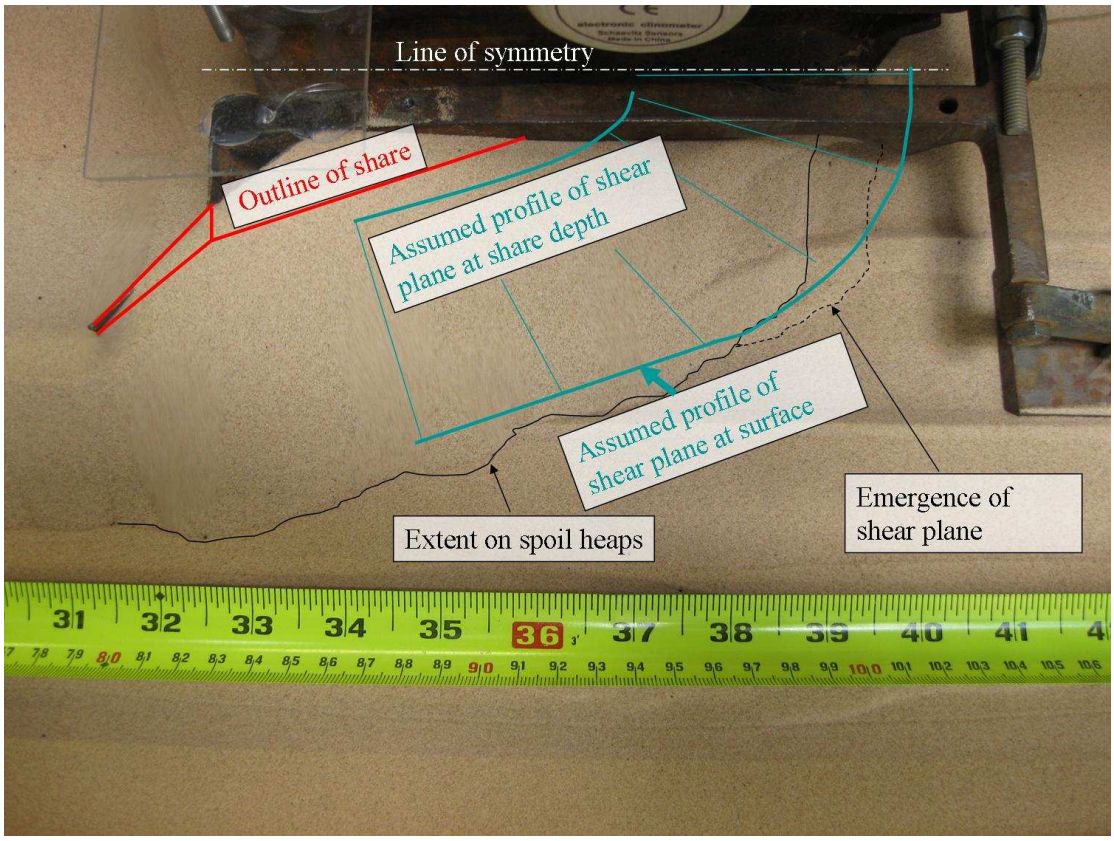

Figure 5-33: Assumed shape of failure plane used in tow force prediction calculations

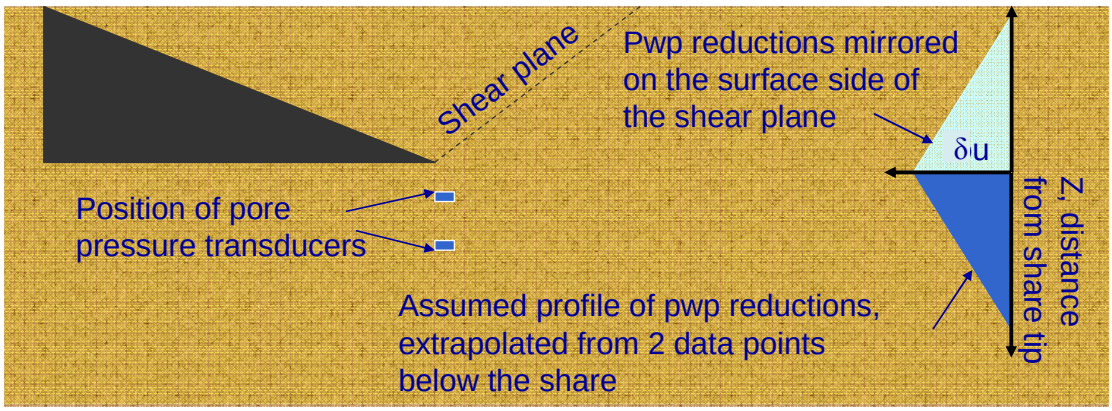

Figure 5-34: Pore pressure reduction assumptions

Rate effects are believed to result from pore pressure reductions as the sand nearby the share dilates and draws in water. Pore water pressures were measured at two

discrete points (Figure 5-34) below the shear plane and these measurements have been extrapolated to provide an assumed pore pressure profile below the share. The assumed profile varies linearly with depth, which being based on only two data points was considered the most appropriate shape even if unlikely in reality. It was then assumed that the pore pressure profile below the share base was mirrored above as water is drawn into the shear plane from all directions.

Figure 5-35 shows pore water pressure distributions attained from 3D finite element modelling conducted at Cathie Associates (White and Cathie; 2010). The pore pressure distribution is shown to be similar both above and below at close to the share tip where the depth is great enough for the surface of the sand not to have an effect on drainage (Figure 5-35a). This supports the assumption that pore pressures are mirrored above and below the share, made in Figure 5-34. Figure 5-35b shows that the assumption does not hold further back the share, however the finite element model does not appear to consider the effect of spoil heaps which would provide a layer of cover over the share and potentially provide a pore pressure profile more akin to Figure 5-35a.

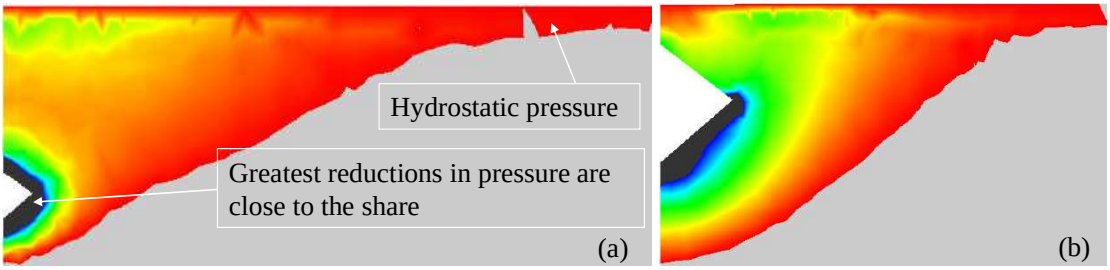

Figure 5-35: Front view of one half of an advancing share showing the pore pressure distribution around (a) the share tip and (b) towards its back during ploughing (White and Cathie; 2010)

The predicted force to cause failure along the shear plane was calculated by splitting the shear plane into small sections and using the assumed change in pore pressure profile to find the average normal effective stress for each section (Equation 5-10 and Figure 5-36). The shear stress required to induce failure on the shear plane for each section was then found by using Coulomb's equation and finally the shear stresses are summed together over the entire depth of the shear plane and the force required to cause failure over the entire shear plane, F_s was found (Equation 5-11).

$$\tau = (\sigma' + \Delta u) \times \tan\phi \qquad (5\text{-}10)$$

$$F_s = w\sum_0^z \tau_s \qquad (5\text{-}11)$$

where, z is the depth of the share and w is the width of the shear plane

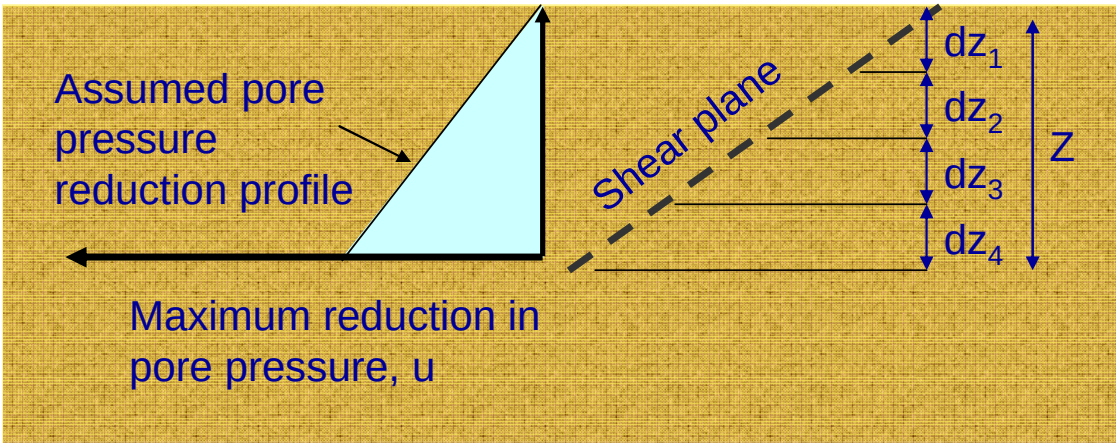

Figure 5-36: Calculation of force acting along shear plane

Rate effects were assumed to affect the base friction component of the tow force as shown in Equation 5-12.

$$(W + A\times\Delta u)\times\tan\delta \qquad (5\text{-}12)$$

where, A is the area beneath the share

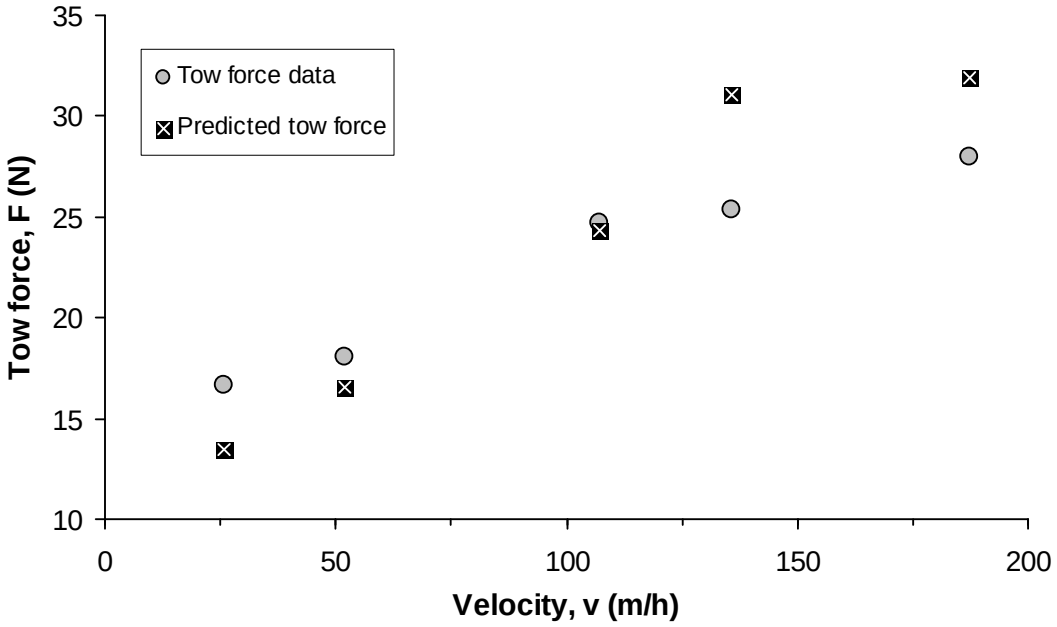

Figure 5-37: Comparison of the tow force achieved during scale model testing with the tow force calculated based on measured pore pressure reductions in Redhill 110 at D_r = 41%

The force required to cause failure over the shear plane was then added to the force due to interface friction to give the predicted tow force. Figure 5-37 compares tow forces measured during 50^{th} scale ploughing tests in silty sand with those predicted by the above method. The predicted tow forces compare fairly well with the measured tow forces but tend to over predict the rate effect. This is likely to be caused by error in the assumptions made (pore pressure profile and shear plane geometry) in order to validate the calculations.

5.3. *Summary of saturated ploughing results*

1. The reduction in permeability associated with reducing the particle size increases the magnitude of the rate effect

2. Increasing the relative density of the sand increases the rate effect and is caused by the associated reduction in permeability. The volume of water required to fill the increased pore space during dilation is either somehow unaffected by relative density or more likely does not influence the rate effect.

3. The rate effect was found to increase with the cube of the plough depth and is presumably a result of increased drainage path lengths.

4. The forecutter was found to reduce the rate effect possibly by creating a two stage cutting process whereby drainage path lengths are effectively reduced. The forecutter also had a negative effect on the static resistance of the plough compromising its effectiveness in reducing the tow force during ploughing. Therefore, refinement of forecutter design may prove useful in reducing forces during ploughing.

5. Normalisation of the ploughing data has proved a useful tool in finding how certain parameters affect results and allows data from different series to be grouped together, providing it in a more useful format to the trenching contractor. Finnie (1993) normalisation (vD/c_v) seems to fit the data better than that of Palmer (1999). An empirical relationship

($\frac{(F - F_{v=0})}{D^2} = 6000 \times vDS / c_v$) has been proposed to determine rate effects in sands.

6. Direct measurement of pore water pressure changes during tests provided data to back up theory about the cause of the rate effect. The pore pressure data has also been used successfully in an attempt to predict tow forces. The pore water pressures also provide the effective stresses in the soil around the plough which are important in determining the expected dilation angle of the sand.

Chapter 6. Implications for industrial practice

Cathie and Wintgens (2001) was previously identified as an important paper within the ploughing industry. Their work laid down a framework by which pipeline plough velocities could be quickly and easily calculated for a specific trenching depth in specific soil conditions with a support vessel of particular bollard pull. Equation 2-3 ($F = C_w W' + C_s \gamma' D^3 + C_d v D^2$) is the relationship they developed for plough performance prediction in sand and was shown previously in Chapter 2.

As discussed in the literature review, there is some uncertainty regarding the three coefficients, especially C_s and C_d. This is a result of both the stepwise manner by which the coefficients were determined (i.e. the value of C_s is dependant on C_w and the value of C_d is dependant on the values of both C_s and C_w.) and the lack of accurate information regarding soil characterisation and state.

6.1. *Determination of C_w and C_s*

Table 6-1 shows the respective values of C_w and C_s dependant on relative density, which Cathie and Wintgens (2001) proposed for cohesionless soils.

Table 6-1: Tow force coefficients C_w and C_s for cohesionless soils (Cathie and Wintgens; 2001)

Tow force coefficient	Relative density, D_r (%)	Value
C_w	All	0.4
C_s	Loose	5
	Medium Dense	10
	Dense	15
	Very Dense	20

Table 6-2 shows interface angles determined for this study during modified shearbox tests, where a steel plate was used in the bottom of the box in place of sand to simulate plough-soil interface shearing. The critical state interface angles are used to calculate the friction coefficient during tests in both HST95 (fine sand) and HST50 (medium sand) over a range of normal effective stresses from 8-35 kPa. The results

are comparable to Cathie and Wintgens (2001) suggested value which corroborates its use.

Table 6-2: Friction coefficient C_w in fine and medium sand

	Interface angle, δ (°)	Friction coefficient, $C_w = \tan^{-1}\delta$
HST95	24	0.39
HST50	27	0.44

Values of C_s were determined from ploughing tests conducted in dry HST95 and HST50. Use of dry sand prevented any rate effects from occurring and allowed greater accuracy in the determination of C_s values than is possible in the field. In determining their proposed values of C_s, Cathie and Wintgens (2001) had the task of examining data from previous ploughing projects to identify data where the plough velocity was thought to be low enough for rate effects to be negligible. The C_s values presented in Table 6-3 were derived in controlled laboratory conditions and should contain less uncertainty than the Cathie and Wintgens (2001) values. The values of C_s derived from the laboratory test results were however attained at significantly lower effective stresses than exist in the field which will affect φ'_{peak} (Bolton; 1986).

Table 6-3: Passive pressure coefficient, C_s values in loose, dense and very dense dry sand for plough's with and without a forecutter

Sand type	Scale	Forecutter	Very Dense	Dense	Loose
HST50	1/50	yes	15.5	-	13.9
HST95	1/50	yes	-	15.4	14.1
HST50	1/50	no	13	-	13
HST95	1/50	no	-	13.6	13.4
HST95	1/25	no	-	10.3	6.9
HST95	1/10	no	-	13.3	-

C_s values were determined for each individual test in dry sand in the following way:

1. The passive force, F_p was calculated by subtracting the interface friction component from the measured tow force.

$$F_p = F - C_w \times W \tag{6-1}$$

2. C_s was determined from the passive force

$$C_s = \frac{F_p}{\gamma \times D^3} \tag{6-2}$$

3. The C_s values for ploughing tests at different depths but grouped by sand type, density and presence of forecutter were averaged to give the values shown in Table 6-3.

C_s values calculated at very shallow depths were not as consistent as the rest of the data. It was assumed that because at shallow depths the passive force was low that the error to force ratio was comparatively high and these values were ignored. The full range of C_s values can be found in Appendix A for transparency. The C_s values shown in Table 6-3 are of similar magnitude to the Cathie and Wintgens (2001) values (Table 6-1) however they do not show the strong trend with relative density which Cathie and Wintgens (2001) found. Table 6-3 shows density to have only a minor affect in increasing the C_s value. C_s values are slightly higher in HST95 than HST50 but again this is such a minor effect, it is of no consequence and may just be experimental scatter. The effect of the forecutter is to increase the C_s value by around 6% in loose sand and 12% in dense sand, which indicates relative density may in fact have some influence over C_s. This cannot be compared to Cathie and Wintgens (2001) data as they do not examine the effect of the forecutter on tow force.

Table 6-4 compares the variation of C_s (derived from model tests) and K_p (based on φ'_{peak}) with relative density. K_p increases by 55% from loose to dense state in HST95 whereas C_s only increases by around 10%. In HST50, K_p increases by 36% from loose to dense state however C_s remains constant. This may imply that C_s is controlled by φ'_{crit} rather than φ'_{peak} however φ'_{crit} in HST95 is lower than for HST50 but HST95 shows the higher C_s value in a loose state which makes it hard to draw conclusions on what soil parameter most heavily influences C_s.

Table 6-4: Comparison between C_s and K_p at different relative densities

	D_r (%)	φ'_{peak} (°)	K_p	C_s
HST95	17	32	3.3	12.2
	75	42	5.0	13.6
HST50	25	34	3.5	13
	90	41	4.8	13

Table 6-5: C_s values derived from saturated ploughing tests

Sand	C_s	Density	Forecutter
HST95	10.1	Dense	No
	10.7	Medium	No
	10.1	Loose	No
HST50	9.9	Dense	No
	10.2	Medium	No
Redhill 110	13.1	Medium	No
HST95	14.7	Dense	Yes
	15.5	Medium	Yes
HST50	14.5	Dense	Yes
	12.8	Medium	Yes

C_s values determined from saturated ploughing tests are shown in Table 6-5 and values ranging from 9.9 to 15.5 were found. The forecutter was again found to increase C_s and relative density, D_r was found to have no influence over C_s. The values compare well with those found during the dry tests.

Figure 6-1 compares the C_s values determined by 50th scale ploughing tests in HST95 with the Cathie and Wintgens (2001) values. The relative densities used for the Cathie and Wintgens (2001) data are mid range values for the respective state that each of their C_s values relates. Tests where a forecutter was used are shown in the legend with an *F* and tests without shown with an *N*. Cathie and Wintgens (2001) values of C_s increase linearly with relative density whereas the model test values are fairly independent of relative density. If the model test values can be relied upon to provide accurate values of C_s then loose and medium C_s values given by Cathie and Wintgens (2001) may cause underestimation of tow forces. A C_s value of around 10 is

appropriate for ploughing without a forecutter wheras a C_s value of around 15 should be used for performance predictions of ploughs with a forecutter.

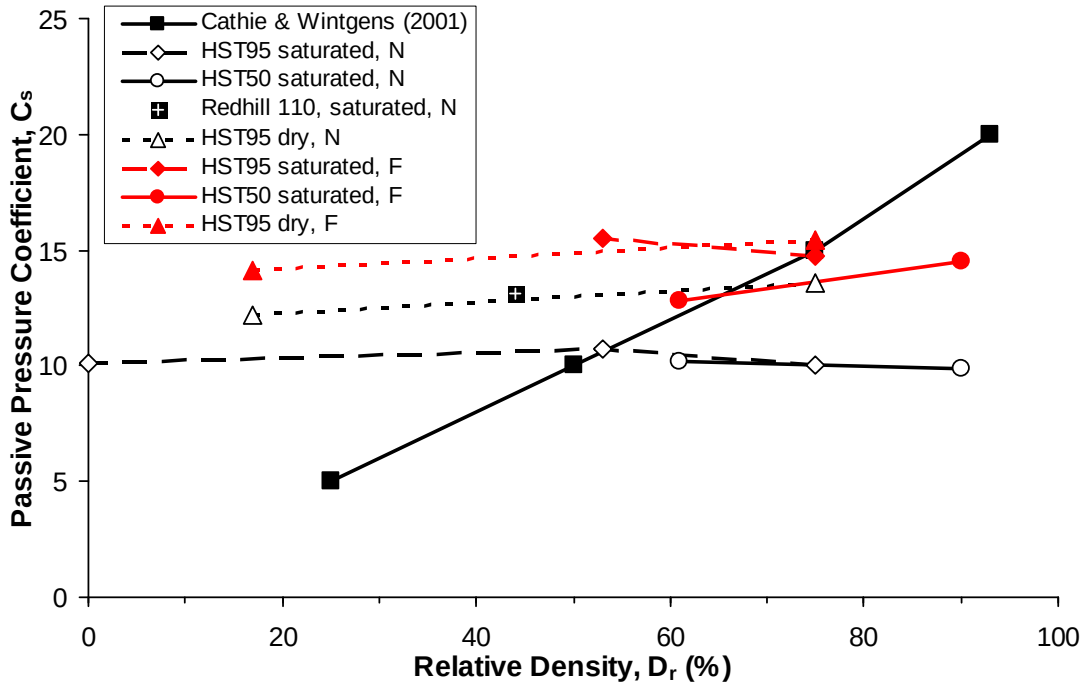

Figure 6-1: Comparison of C_s values attained through 50th scale model ploughing tests in sand with the Cathie and Wintgens (2001) values

6.1.1. Determination of the dynamic tow force coefficient, C_d

Cathie and Wintgens (2001) chart for determining the dynamic ploughing resistance coefficient is shown in Figure 6-2. The chart shows their data collected from numerous ploughing projects. The data show an increase in dynamic resistance coefficient, C_d with reduction in the maximum size of the finest 10% of particles in the sand, D_{10}, from which permeability is inferred. The relative density state is marked on the data and it is hard to come to a conclusion from the data as to influence of relative density over C_d. The trend lines are Cathie & Wintgens (2001) interpretation of the data which show C_d to increase with both increasing relative density and with reducing D_{10}.

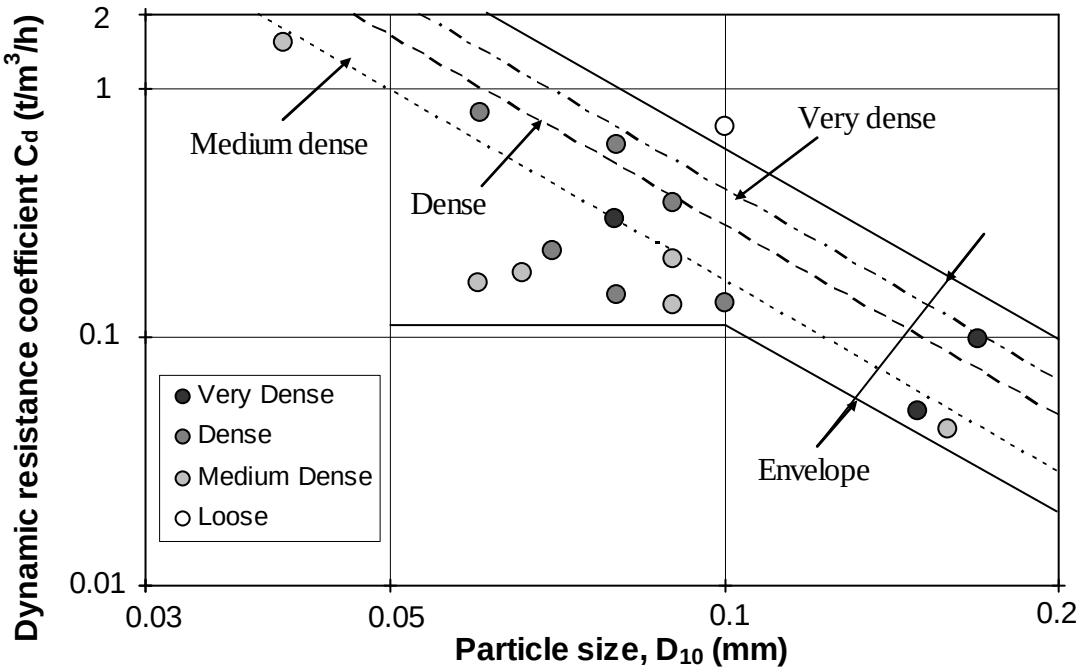

Figure 6-2: Determination of C_d (Cathie and Wintgens; 2001)

In this study, C_d was determined during numerous saturated ploughing tests in 3 different sands at different relative densities. This was achieved by the following procedure:

1. The forces and depths found during the model tests were scaled up to prototype scale. This was necessary as velocity was found not to require scaling (Brown & Bransby; 2006, Lauder *et al*.; 2010) and therefore to achieve a rate effect comparable to Cathie and Wintgens (2001) the forces and depths had to be scaled. This was conducted using scaling laws found in Wood (2005) which gave Equation 4-11 and Equation 4-13.

2. The static component of resistance, $F_{v=0}$ was determined for each test series as shown in Figure 6-3.

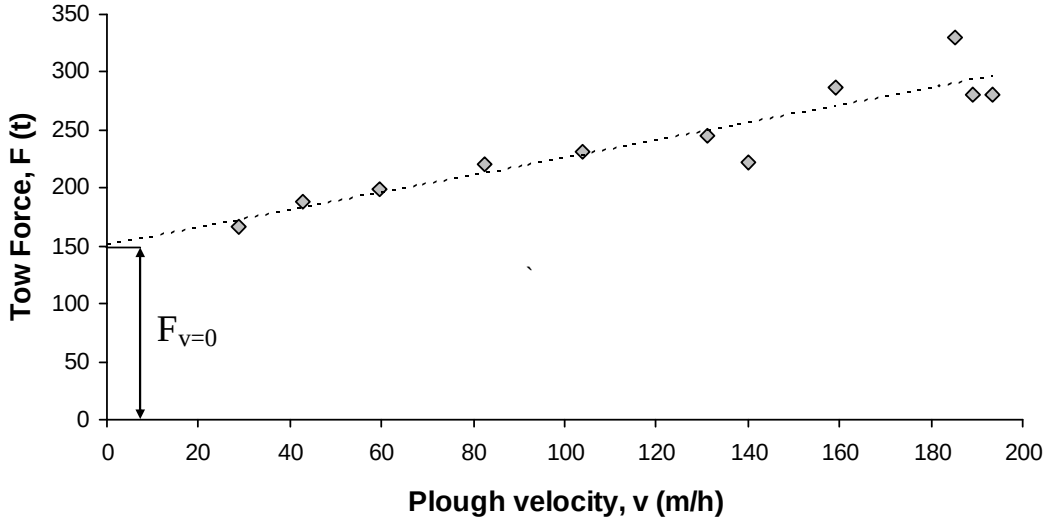

Figure 6-3: Determination of static component, $F_{v=0}$ of ploughing during a saturated ploughing test series without a forecutter in medium dense HST95 at a scaled depth of 1.9 m

C_d is then calculated for each data point within the series, using a common static component of tow force from Equation 6-3, where: v is the plough velocity, D is the plough depth, F is the tow force and $F_{v=0}$ is the static component of tow force.

$$C_d = \frac{(F - F_{v=0})}{v \times D^2} \tag{6-3}$$

The C_d values calculated from the saturated ploughing tests are compared to those of Cathie and Wintgens (2001) in Figure 6-4. The legend denotes the data series from this study by a letter, either: *L*, *M* or *D*, which indicates the relative density and a number indicating the scale factor. The Cathie and Wintgens (2001) data is denoted by, *VD*, *D*, *M*, *L* which denotes relative density followed by *CW*. All tests shown in Figure 6-4 were conducted without a forecutter.

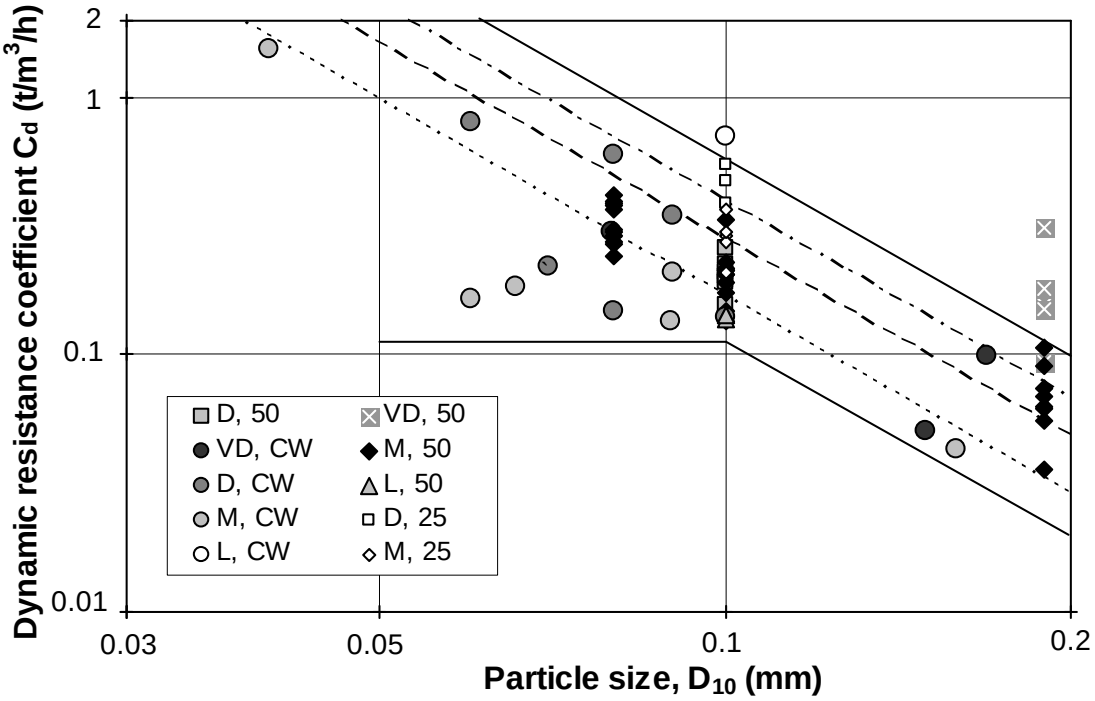

Figure 6-4: Determination of C_d, comparison of the data within this study with the Cathie and Wintgens (2001) data

The laboratory data and the Cathie and Wintgens (2001) data loosely agree and both show that reducing particle size increases C_d. The Cathie and Wintgens (2001) data has been reproduced with the relative density of their data also shown. Cathie and Wintgens (2001) data shows only a very loose relationship between relative density and C_d and their prediction lines which increase with relative density are possibly based on soil mechanics principles rather than their solely based on their data. Most of the scale model laboratory test data shows a clear increase in C_d with increasing relative density. The exception is the tests at 50th scale in HST95 where D_r does not show any affect on C_d although this is possibly due to experimental error. Many of the dense data points derived from the model tests fall above the Cathie and Wintgens (2001) envelope. This could however be a result of increased dilation at model scale due to lower effective stresses.

A possible reason for the Cathie and Wintgens (2001) data not showing a clear relationship between the relative density and C_d could be due to inaccurate characterisation. The literature review has highlighted the problems associated with determining D_r and φ' at shallow depth from CPT results. The use of D_{10} as a measure

of permeability also introduces error as Hazens law is affected by the whole grading curve. Determination of C_d is dependant on D^2 and since plough depth may be hard to measure accurately in the field the resulting error in C_d could be enough to mask the affect of D_r on C_d.

Figure 6-5 shows the average dynamic coefficient C_d plotted for 50th scale ploughing tests both with a forecutter (F) and without (N) in HST95 and HST50. The forecutter is shown to reduce the value of C_d which is particularly evident in the fine sand (HST95).

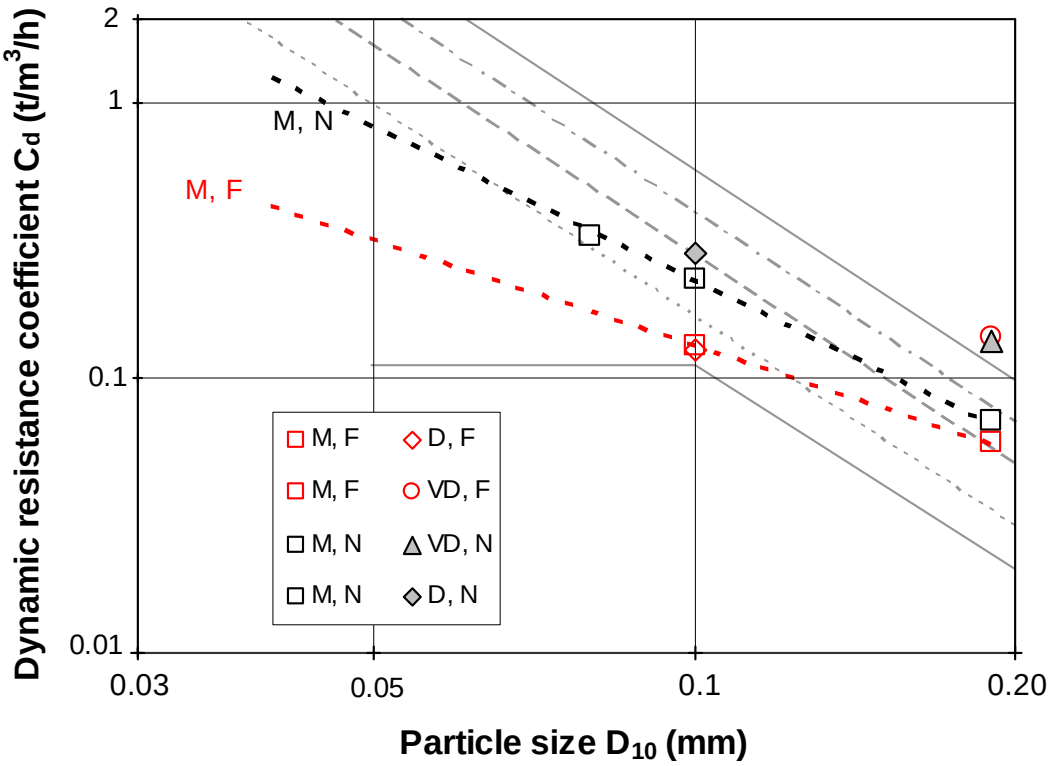

Figure 6-5: Average C_d values from tests at various relative densities both with a forcutter (F) and without (N) to find its influence over C_d

When ploughing without a forecutter through medium dense sand the dynamic resistance coefficient, C_d can be found by Equation 6-4.

$$C_d = 0.03 \times D_{10}^{-1.873} \tag{6-4}$$

When ploughing with a forecutter through medium dense sand the dynamic resistance coefficient, C_d can be found by Equation 6-5.

$$C_d = 0.007 \times D_{10}^{-1.277} \quad (6\text{-}5)$$

6.1.2. Summary

The comparison between laboratory test data and the Cathie and Wintgens (2001) model has been made by means of the coefficients for Equation 2-3. C_w attained through interface friction shear box test data (tanδ) compared well with Cathie and Wintgens (2001) values. C_s was found during 50th scale model plough test results in both dry and saturated sand which gave values of similar magnitude to Cathie and Wintgens (2001). C_s values derived from the model tests did not show the trend with relative density which the Cathie and Wintgens (2001) values show. The C_s values derived from ploughing test results in saturated sand are about 30% higher than those derived from dry sand test results. C_d values have been back calculated from saturated model test results and give values which generally sit around the values suggested by Cathie and Wintgens (2001). Equations for the calculation of C_d when ploughing in medium dense sand have been proposed for ploughs both with and without a forecutter. Data for dense and very dense sand is not as complete but sits slightly above the Cathie data.

Chapter 7. Conclusions and Future Recommendations

7.1. *Introduction*

Offshore pipeline ploughs are currently used as a means of forming a trench in the seabed for the protection of pipelines. Ploughs have been used for this purpose for the past 20 years and their use is now widespread. In spite of the experience gained during these operations, accurate prediction of plough performance remains difficult especially in sandy soils. Scale model ploughing tests have been conducted in controlled laboratory conditions and their results analysed to improve the prediction of plough performance in sands. Conclusions drawn from the analysis of the test results are presented in this chapter along with recommendations for future research in the field of offshore pipeline ploughing.

7.2. *Dry sand ploughing tests*

The following conclusions have been made from the towed ploughing tests, fixed ploughing tests and plane strain tests which were conducted in dry sand.

1. Increasing the ploughing depth during ploughing will result in a corresponding increase in tow force and reduce the pitch (i.e. rotate the plough forward). The tow force appears to have two separate components. The components of the tow force may be represented by interface friction and passive pressure terms giving $F = W\tan\delta + f(\gamma D^3)$ where, W is the weight of the plough, δ is the interface angle between the plough and the sand, γ is the unit weight of the sand, D is the depth of the plough and f is a fitting constant dependant on the friction angle of the sand and the shape of the plough's share. This form is in agreement with research by previous authors i.e. Reece and Grinsted (1986) and Cathie and Wintgens (2001).

2. The relative density of the sand being ploughed was found to affect plough performance. When ploughing at depths greater than 28 mm at 50^{th} scale (1.4 m prototype) an increase in relative density results in a relatively small (14%) increase in tow force. When ploughing at shallow depths (less than

28 mm at 50th scale) the tow force was not observed to be influenced by the relative density of the sand. This was presumably due to the fact that the product of the interface angle (being relatively unaffected by relative density) and the plough's self weight provide the majority of the tow force when ploughing at shallow depths. The plough's pitch was also reduced (tended towards forwards pitching) with increasing relative density. For example the 50th scale model plough tended to forward pitch by 1^{o} when ploughing at 40 mm in loose sand whereas in dense sand at the same depth the plough would forward pitch by around 1.5^{o}.

3. Ploughing tests were conducted in two fractions (particle size distributions) of silica sand, one fine and the other medium. The medium sized sand (HST50) had a higher critical state friction angle than the fine sand (HST95). The two fractions were prepared at a similar relative density. The difference in tow force between ploughing in these two sands was similar to ploughing in sand of two different relative densities (9% greater tow force at 40 mm plough depth for HST50 compared to HST95) with the medium sand equivalent to a higher relative density than the fine sand. This was attributed to its larger friction angle.

4. Use of the forecutter increased the tow force during ploughing at depths great enough to allow significant forecutter engagement with the sand (around 26 mm at 50th scale). The forecutter also caused the plough to forward pitch more than the plough without the forecutter. This resulted in a reduction in plough depth where the same skid setting was used in tests where the forecutter was absent. Implications are that any benefit the forecutter provides in terms of reducing the rate effect by reducing drainage path lengths will be offset by its increase in the passive component of tow force.

5. To study stress related scale effects, tests were conducted over a range of depths using three different scales of plough (10th, 25th and 50th scale) in the same sand (HST95) and the same relative density (D_r = 17%). Tests were also conducted using the 25th and 50th scale ploughs in dense (D_r = 75%) HST95. The scaled tow force data from the 10th, 25th and 50th scale ploughs did not

appear to be substantially different. The lack of change in tow force with plough scale and therefore normal effective stress may suggest that stress related scale effects are not an issue.

6. The idea of fixed setup ploughing tests initially appeared promising as it allowed transition lengths to be reduced compared to the pulled tests. Fixed setup ploughing tests therefore made larger scale model plough testing more practical as materials handling was reduced. Depth and pitch were more accurately controlled during the fixed ploughing tests which prevented the reduction in depth with increasing velocity observed in the saturated pull tests. The fixed tests also offered the opportunity to break down the components of the total force acting on a plough during ploughing, however reliable comparison to the pull ploughing tests was not achieved and an extensive study using the fixed ploughing test setup was therefore not completed.

7. Plane strain tests allowed the deformation of sand around a simplified share to be viewed during forward translation. This provided an insight into the failure mechanism of the soil during ploughing which was in agreement with early work by Reece and Grinsted (1986) in which a wedge of sand ahead of the share slid along a failure plane until the plane became kinematically inadmissible and another plane formed slightly ahead. The failure plane was found to incline at around 55^{o} to the horizontal near the tip of the share which reduced to around 40^{o} to the horizontal as it neared the surface of the sand. The test's apparatus was found to be too flexible to hold the model share at the desired inclination during testing. Accordingly, equipment modification is required to allow a further, more comprehensive study to be completed.

7.3. *Ploughing tests in saturated sand*

The following conclusions have been made from the analysis of scale model ploughing tests in saturated sand:

7. The decrease in permeability associated with reducing the particle size over the range studied ($0.08<D_{10}<0.18$) increases the magnitude of the rate effect associated with ploughing at increased rates. This agrees with the work of Grinsted (1985) and Cathie & Wintgens (2001).

8. Increasing the relative density of the sand resulted in an increase in the rate effect. Increasing the density of the sand causes an associated reduction in permeability and seems to be the main reason relative density influences the rate effect. Since volumetric strains associated with shear strain increase with relative density there is a requirement for larger volume of pore water to fill the increased void space as relative density is increased. This should cause an increase in flow rate which will require an associated pressure drop, increasing effective stresses for a given plough velocity. The data show this to have a negligible effect on tow forces, however, volumetric strains are not measured during ploughing tests and perhaps the temporary increase in normal effective stresses reduces the critical state void ratio. This could result in there being little difference between initial void ratio, e_i and critical state void ratio, e_{crit} for sands of different e_i above e_{crit}. Reece & Grinsted (1986) and Kutter & Voss (1995) theorise that as ploughing rates increase the magnitude of the rate effect may increase due to this effect of dilation suppression with increasing normal effective stresses and it is entirely possible for an increase in relative density to cause a similar effect.

9. The rate effect was found to increase with either the plough depth squared or cubed. This is interpreted as a combination of increased drainage path lengths as plough depth is increased and plough geometry whereby share width increases with depth.

10. The forecutter was found to reduce the rate effect and for example, during 50^{th} scale ploughing tests in medium dense fine sand at a plough depth of 37 mm roughly a 30% reduction in the rate effect was found. It is suggested that this may result from the forecutter creating a two stage cutting process in which drainage path lengths are reduced. The forecutter was however observed to increase the static resistance of the plough, compromising its effectiveness in

reducing the tow force. Therefore, refinement of forecutter design (geometry and positioning) may prove useful in reducing forces during ploughing.

11. Normalisation of the ploughing data has allowed analysis of the influence of permeability, relative density and plough depth over tow force and grouped different test data together. This has an important practical application in providing a useful format to the trenching contractor where a single chart or equation can be used to determine rate effects during ploughing in different sand conditions. Finnie's (1993) normalisation (vD/c_v) seems to fit the data better than the normalisation suggested by Palmer (1999). An empirical relationship $\frac{(F - F_{v=0})}{D^2} = 3400 \times vDS / C_v$ has been proposed to determine rate effects in sands.

12. Direct measurement of pore water pressure changes below and in advance of the share during ploughing tests show that pore pressures reduce ahead of the share. This is consistent with the theory that soil is shearing ahead of the share and therefore dilating, reducing pore pressures which in turn increases normal effective stresses. The pore pressure data has been used successfully to predict tow forces. The pore water pressures are also necessary in determining the effective stresses in the soil around the plough. Since the dilation angle, ψ is stress dependant normal stresses are required in the interpretation of tow forces using soil strength characteristics.

7.4. *Implications of findings for current prediction techniques*

1. An agreement with the Cathie and Wintgens (2001) value of friction coefficient C_w was found. The friction coefficient determined from modified shear box tests was between 0.4 and 0.45 whereas back calculated values from model ploughing tests were around 0.5.

2. The passive pressure coefficient, C_s has been found to be almost independent of relative density. As a result, the Cathie and Wintgens (2001) values for C_s in loose sand are likely to cause underestimations of expected tow forces.

Therefore it is not recommended that the C_s value of 5 for ploughing in loose sand published in Caithie and Wintgens (2001) is used for performance predictions. A C_s value of 10 is recommended for use when ploughing without a forecutter. The forecutter was found to increase C_s and a value of 15 would be appropriate for use in performance predictions when a forecutter is used.

3. The dynamic coefficient, C_d has been shown to increase with reducing D_{10} (permeability) and increasing relative density, D_r. The forecutter was found to reduce C_d. The upper bound limit for C_d, shown in the Cathie and Wintgens (2001) model could be increased to include higher values. A better fit to the data collected during the course of this research has been presented.

   When ploughing without a forecutter through medium dense sand the dynamic resistance coefficient, C_d can be found by Equation 6-5

$$C_d = 0.03 \times D_{10}^{-1.873} \tag{6-5}$$

   where, D_{10} is the size of the largest particles in the finest 10% of the sand.

   When ploughing with a forecutter through medium dense sand the dynamic resistance coefficient, C_d can be found by Equation 6-6.

$$C_d = 0.007 \times D_{10}^{-1.277} \tag{6-6}$$

   where, D_{10} is the size of the largest particles in the finest 10% of the sand.

   More data is required to provide C_d relationships in dense and very dense sand although the data presented shows that C_d increases with relative density.

7.5. *Recommendations for future research*

The following recommendations have been highlighted during the course of the research described within this document. Recommendations have been focussed around ideas for research which may be of use to the offshore industry however

suggestions have also been made for the modification of the equipment which was developed as part of this research in order to improve any future testing.

1. It is suggested that a potential area for further research using scale model plough tests is the prediction of plough performance in on silts and sands with higher silt contents. Such a series of tests would allow the characterisation of the rate effect over a larger range of particle size distributions and show where the large rate effects experienced in fine sands over typical ploughing rates begin to transition into the more modest rate effects observed when ploughing in clays.

2. Scale effects have been discussed within this thesis, however, for the reduced scale plough test data to be accepted in a quantitative manner by the offshore industry, unresolved scaling issues may need to be addressed. This could be achieved by a test programme encompassing 50^{th} scale ploughing tests conducted within a centrifuge at increased gravity, which would account for stress related scale effects. An extension of the test series at 25^{th} and 10^{th} scale would also be of benefit as scaling issues due to particle size effects and post peak strain softening can be addressed. If results from 50^{th} scale tests conducted at elevated gravity equal to the stresses at 10^{th} scale are compared to 10^{th} scale test results the changes to tow force resulting from strain softening along shear bands can investigated.

3. The interface friction component of tow force ($W \times \tan\delta$) can be decreased by reducing either the plough weight or by reducing the interface friction angle. At present trenching contractors can reduce the plough weight by way of buoyancy tanks primarily to prevent the plough from sinking in soft clay rather than reduce tow forces. However, there are stability issues associated with the use of buoyancy tanks and it would be necessary to overcome these before the use of large buoyancy forces could become beneficial during ploughing. Use of low friction materials on the underside of the skids and the share could be used to reduce the interface angle although wear of this material may be an issue. Some ploughs have a hydraulically driven share track which runs along the underside of the share which can be used to drive

the plough forward (or left to run free when not in use). The technology is far from proven, however there would appear to be merit in using the share track or something similar as an interface between the plough and sand. Since rolling friction rather than sliding friction is associated with the share track, this could lead to large potential reductions in tow forces generated during ploughing.

4. At present a single term $W \times \tan\delta$ is used to define the interface friction between the plough and the soil. Although this works well in uniform soils in the laboratory, in most cases the stratigraphy of offshore soils is more complex. In the North Sea for example, a thin sand layer often overlays clay. Cathie and Wintgens (2001) state that in this situation the portion of the plough's weight on the skids would be treated as a frictional resistance term and the weight supported by the share would cause resistance due to adhesion. In practice defining the proportion of the plough's weight acting on the skids is complicated by forces acting on the plough for which only an overall tow force is actually known. If load cells were used to connect the skids to the plough during model tests then it may be possible to gain insights into how the plough's weight is supported. This could be done during model tests and would also give the bearing pressure beneath the skids which may be important in soft soil conditions. Low friction material such as Teflon could be attached to the underside of the skids to investigate the potential applicability of reducing interface friction and hence, tow force by changing the interface properties of the skids.

5. In difficult soil conditions it is often necessary for the plough to form a trench to a desired depth by running over the line of the trench more than once in a process known as multi-pass ploughing. In this technique drainage paths and soils are altered more compared to a single pass. Therefore, there is potential for characterising the forces during this type of operation using scale model ploughs, which could allow for the optimisation of the depth of each pass. This would require more accurate mapping of trench profiles between passes in order to allow analysis of results than has been used within this research.

6. The limited number of tests where pore pressure measurements made during this study have provided a useful insight into the rate effect which has been discussed within this thesis. To improve the understanding of the rate effect and how to reduce it, a better understanding of the pore pressure distribution around the share during ploughing is required. Mounting pore pressure transducers on the share as well as seeding the soil with pore pressure transducers would allow further investigation of pore pressure distribution around the plough during trenching.

7. Element testing designed to observe rate effects could prove useful in the characterisation of rate effects during ploughing. It was shown in Chapter 5 that it is useful to be able to estimate the degree of drainage anticipated if soil response to loading is to be predicted.

8. It was highlighted in the literature review that share geometry design is a viable avenue of future research. This was beyond the scope of this thesis but has the potential to lead to the design and manufacture of more efficient ploughs with associated financial benefits. Forecutter design, sizing and positioning relative to the main share is another opportunity for refinement of plough design. Some ploughs, such as the VMP 500 have jetting nozzles built into the share to reduce rate effects by increasing pore pressures around the share. However, their effectiveness is yet to be proven and is worth investigation. The idea of vibrating the plough or its share to increase pore water pressures and therefore reduce effective stresses has been mooted in communication with an offshore contractor and is also worth future exploration.

9. Accurate characterisation of relative density and permeability are essential for optimal plough performance prediction. The literature review found that cone penetration testing (CPT) at shallow depths in complex soil conditions does not allow accurate interpretation of the relative density of the soil. This indicates that the current practice of site investigation (i.e. CPT at 0.5 km intervals) needs to be improved if plough performance predictions are to be made more accurate. Therefore, there is potential for research into

investigating more accurate methods of interpreting CPT data at shallow depths or devising new site investigation methods/strategies.

10. Modification of the trolley system on the large (2.5 m×1.5 m×0.75 m) tank developed for sand preparation and model testing would be beneficial to future researchers working on this equipment. At present the trolley can accommodate four carriages, two at each side running on parallel tracks sitting above the side walls of the tank. The trolley is prone to jamming, causing a number of tests to be stopped prematurely. A monorail system would be a simple but efficient solution to this problem although this would not have the extra stability of a dual rail which is desirable during fixed tests.

References

Albuquerque, J.C.D. & Hettiaratchi, D.R.P. (1980) “Theoretical mechanics of sub-surface cutting blades and buried anchors” *Journal of Agricultural Engineering Research* **25**(2), 121-144.

Atkinson, J.H. (1993). *The Mechanics of Soils and Foundations*, London: McGraw-Hill International series in Civil Engineering.

Bareither, C.A., Tuncer, B.E., Benson, C.H. & Mickelson, D.M. (2008). “Geological and physical factors affecting the friction angle of compacted sands” *ASCE Journal of Geotechnical and Environmental Engineering* **134**(10), 1476-1489

Bolton, M.D. (1986). “The strength and dilatancy of sands” *Geotechnique* **36**(1), 65-78

Bolton, M.D. (1987). “Discussion on the strength and dilatancy of sands” *Geotechnique* **37**(2), 219-226

Bolton, M.D. & Lau, C.K. (1988) “Scale effects arising from particle size” *Proceedings of International Conference on Geotechnical Centrifugal Modelling*, Paris, France 127 - 131

Bolton, M.D. & Lau, C.K. (1989). “Scale effects in the bearing capacity of granular soils” *Proceedings 12th International Conference on Soil Mechanics and Foundation Engineering*, Rio de Janeiro, 2, pp. 895-898, Balkema, Rotterdam.

Bransby, M.F., Brown, M.J., Hatherley, A.J., & Lauder, K.D. (2010). “Pipeline plough performance in sand waves. Part 1: model testing” *Canadian Geotechnical Journal* **47**(1), 49-64

Bransby, M.F., Brown, M.J., Lauder, K.D. and Hatherley, A.J. 2010. “Pipeline plough performance in sand waves. Part 2: kinematic calculation method” *Canadian Geotechnical Journal* **47**(1), 65-77.

Bransby, M.F. & Ireland, J. (2009). "Rate effects during pipeline upheaval buckling in sand" *Proceedings of the Institution of Civil Engineers, Geotechnical Engineering*, **162** (5) 247-256.

Bransby, M.F., Yun, G., Morrow, D.R. & Brunning, P. (2005). The performance of pipeline ploughs in layered soils. *Frontiers in Offshore Geotechnics*, pp. 597-606 Gourvenec & Cassidy (Eds).

Brown, M.J., Bransby, M.F. & Simon Soberon, F. (2006). "The influence of soil properties on ploughing speed for offshore pipeline installation" *International Conference on Physical Modelling in Geotechnics*, Hong Kong, China, 4-6th August, pp. 709-714 CRC Press, Boca Raton, Fla.

Cable, S.B., Carlisle, H., Skyers, B. and Taylor, R. (1993). "Hydrostatic pressure effects on thin blade plow resistence in dense, saturated, cohesionless soil", Report No. TM-42-93-06, Naval Civil Engineering Laboratory, Port Hueneme, CA.

Cathie Associates (2006) "Plough stability on soft clays, AMP500 and BFP" Report Number G0131R01-01 for CTC Marine projects Ltd

Cathie, D., Barras, S. & Machin, J. (1998). "Backfilling pipelines: state of the art. 21st Annual Offshore Pipeline Technology Conference" Oslo, February, pp. 1-29

Cathie, D., Morgan, N., Pyrah, J. & Steward, J. (2007). "Pipeline and cable plough stability in soft clays" *Offshore site investigation and geotechnics, confronting new challenges and sharing knowledge*, London, September 11-13, pp. 485-490

Cathie, D.N. & Wintgens, J.F. (2001). "Pipeline Trenching Using Plows: Performance and Geotechnical Hazards" *Proceedings of the Thirty-third Annual Offshore Technology Conference*, Houston April/May 2001, pp. 1-14 (13145)

Charles, J.A. (1982). "An appraisal of the influence of a curved failure envelope on slope stability" *Geotechnique* **32**(4), 389-392

Chen, J., Lin, C. & Lee, W. (2003). "Dilative behaviour of granular materials" *International Journal of Offshore and Polar Engineering* **13**(4) 301-307

Chen, Z., Liu, Y., Liu, P. & Bijker, R (2001). "An integrated approach to pipeline design through sandwave fields: Dongfang Pipeline" *Proceedings of OMAE 2001: 20th International Conference on Offshore Mechanics and Arctic Engineering*, Rio de Janeiro. June 3-8, 2001. Ocean, Offshore, and Arctic Engineering Division of the American Society of Mechanical Engineers (ASME), New York, paper no. OMAE01-PIPE4031

Cho, G.C., Dodds, J. & Santamarina, C. (2006). "Particle shape effects on packing density, stiffness and strength: natural and crushed sands" *ASCE Journal of Geotechnical and Environmental Engineering* **132**(5), 591-603

Fannin, R.J., Eliadorani, A. & Wilkinson, J.M.T. (2005). "Shear strength of cohesionless soils at low stress" *Geotechnique* **55**(6), 467–478

Fannin, R.J., Eliadorani, A. & Wilkinson, J.M.T. (2006). "Discussion on shear strength of cohesionless soils at low stress" *Geotechnique* **56**(6), 439–441

Featherstone, J., Cronin, A., Kordahi, M. & Shapiro, S. (2001). "Recent trends in submarine cable system faults" *SubOptic 2001 International Convention*, Kyoto, May 20-24, 5 pp, accessed from www.scig.net

Finch, M., Fisher, R., Palmer, A. & Viggiani, G. (2000). "An integrated approach to pipeline burial in the 21st Centuary" *Deep Offshore Technology 2000*

Finch, M. & Machin, J.B. (2001) "Meeting the challenges of deepwater cable and pipeline burial" *Proceedings Thirty-third Annual Offshore Technology Conference*, Houston (13141) April/May 2001, pp 1-14

Finnie, I.M.S. (1993). “Performance of shallow foundations in calcareous soils” PhD Thesis. University of Western Australia, Perth. November.

Finnie, I.M.S. & Randolph, M.F. (1994) “Punch-through liquefaction induced failure of shallow foundations on calcareous sediments” Research Report No. G1126, accessed from www.cofs.uwa.edu.au/publications

Finno, R.J., Harris, W.W., Mooney, M.A. & Viggiani G. (1997). “Shear bands in plane strain compression of loose sand” *Geotechnique* **47**(1), 149-165

Fugro Report (2005) “AMP500 Performance assessment atlantic cromarty pipeline north sea” Report number C312-78-02, for CTC Marine Ltd.

Girard, J. & Taylor, R. (1994). “Blade geometry and soil permeability effects in thin blade plow resistance in dense, cohesionless soils” Naval Facilities Engineering Service Center, Phase II Report, TM-2026-OCN

Grinsted, T.W. (1985). “Earthmoving in submerged sands” Unpublished Ph.D. thesis, University of Newcastle upon Tyne

Gudehus, G. & Nubel, K. (2004). “Evolution of shear bands in sand” *Geotechnique* **54**(3), 187-201

Hata, S. (1979). “Submarine cable: multi-blade plough” *Geotechnique* **29**(1), 73-90

Hettiaratchi, D.R.P. & Reece, A.R. (1975). Boundary wedges in two-dimensional passive soil failure. *Geotechnique* **25**, No.2, 197-220

Hettiaratchi, D.R.P. and Reece, A.R. (1989). “A slip-line method for estimating passive earth pressure” *Journal of Agricultural Engineering Research* **42**(1), 27-41

Hoshina R. & Featherstone, J. (2001). “Improvements in submarine cable system protection” *SubOptic 2001 International Convention*, Kyoto, May 20 – May 24, Paper 6.7, 4 pp, accessed from www.scig.net

House, A.R., Oliveira, J.R.M.S. & Randolph, M.F. (2001). “Evaluating the coefficient of consolidation using penetration tests” *International Journal of Physical Modelling in Geotechnics* **1**(3), 17-26

Kutter, B.L. & Voss, T. (1995). “Analysis of data on plough resistance in dense, saturated, cohesionless soil” Naval Facilities Engineering Service Center, Contract Report CR 95.004

Lauder, K.D., Bransby, M.F. &Brown, M.J. (2008) “Experimental testing of the performance of pipeline ploughs” Proceedings of the Eighteenth International Offshore and Polar Engineering Conference, July 2008, Vancouver, Canada

Lauder, K.D., Brown, M.J. Bransby, M.F. & Pyrah, J. (2010) “Investigation into the effect of a forecutter on plough performance” Second International Symposium on Frontiers in Offshore Geotechnics, November 2010, Perth, Australia

Machin, J.B. (1995). “Operational experience of multipass and backfill ploughs” *Subtech '95: Addressing the Subsea Challenge, Aberdeen*. (ST-95-237) November 7-9, pp. 237-248.

Maksimovic, M. (1996). “A family of nonlinear failure envelopes for non-cemented soils and rock discontinuities” *The Electronic Journal of Geotechnical Engineering*, 1-67.

Miedema, S.A. & Yi, Z. (2001) “An analytical method of pore pressure calculations when cutting water saturated sand” *Texas A&M 33nd Annual Dredging Seminar*, Houston, June 2001.

Mitchell, J.K. & Soga, K. (2005). *Fundamentals of soil behaviour*. Third edition, John Wiley & Sons, New Jersey

Mühlhaus, H.B. & Vardoulakis, I. (1987). “The thickness of shear bands in granular materials” *Geotechnique* **37**(3), 271-283

Ochtman, J.A. & der Boer, A.S. (1980). "Post ploughing for rigid lines – Controlled trench depth and high progress rate" *Proceedings of the Twelfth Annual Offshore Technology Conference*, Houston (3738) May 1980, 27-34

Oda, M & Kazama, H. (1998). "Microstructure of shear bands and its relation to the mechanisms of dilatency and failure of dense granular soils" *Geotechnique* **48**(4), 465-481

Offshore soil investigation forum (2004). "Guidance notes on geotechnical investigations for marine pipelines" *Offshore site investigation and geotechnics* www.sut.org.uk

Palmer, A.C. (1999). "Speed effects in cutting and ploughing" *Geotechnique* **49**(3), 285-294

Palmer, A.C., Kenny, J.P., Perera, M.R. & Reece A.R. (1979). "Design and operation of an underwater pipeline trenching plough" *Geotechnique* **29**(3), 305-322

Ponce, V.M. & Bell, J.M. (1971). "Shear strength of sand at extremely low pressures" ASCE, Journal of the soil mechanics and foundations division **97**(4) 625-637

Puech, A., Cour, F., Meunier, J., Michel, J.L. & Dubois, J.C. (1994). "SHRIMP: An investigation tool for pipeline and cable burial" *OCEANS '94. Proc. 'Oceans Engineering for Today's Technology and Tomorrow's Preservation.* Brest, France. Sep 1994, Vol. 2 pp. 667-682

Puech, A. and Foray, P. (2002) "Refined Model for Shallow Penetration CPTs in Sands" *Proceedings of the Offshore Technology Conference*, Houston (14275) May 2002, pp. 1-9

Randolph, M.F. & Hope, S. (2004). "Effect of cone velocity on cone resistance and excess pore pressures" Proceedings of the international symposium on engineering practice and performance of soft deposits, Osaka, pp. 147-152.

Reece, A.R. (1965). "The fundamental equation of earth-moving mechanics" *Proceedings of the Institution of Mechanical Engineers* **179**(3F), 16-22

Reece, A.R. and Grinsted, T.W. (1986). "Soil Mechanics of Submarine Ploughs" *Proceedings of the Eighteenth Annual Offshore Technology Conference*, Houston (5341) May 1986, *pp.* 453-461

Reece, A.R. and Hettiaratchi, D.R.P. (1989) "A slip-line method for estimating passive earch pressure" *Journal of agricultural engineering research* **42**(1), 27-41

Rockwell, P.K. (1981). Water jet trenching in submerged clays. *Proceedings of the First U.S. Water Jet Symposium*, Colorado April 1981, pp. 195-206.

Rosa, U.A. (1997). "Performance of narrow tillage tools with internal and strain rate effects" Ph. D. thesis, University of Saskatchewan.

Roscoe, K.H. (1970). "The influence of strains in soil mechanics (10^{th} Rankine Lecture)" *Geotechnique* **20**(2), 129-170

Rouse, P.C., Fannin, R.J. & Shuttle, D.A. (2008). "Influence of roundness on the void ratio and strength of uniform sand" Geotechnique **58** (3) 227-231

Silva, F.M. & Bolton, M.D. (2005). Interpretation of centrifuge piezocone tests in dilatant, low plasticity silts. *Proceedings of International Conference on Problematic Soils*. May 2005. Famagusta N. Cyprus

Stamatopoulous, A.C. & Kotzias, P.C. (1978). "Soil compressibility as measured in the oedometer" *Geotechnique* **28**(4), 363-375

Stone, K.J.L. & Wood, D.M. (1992). "Effects of dilatancy and particle size observed in model tests on sand" *Soils and Foundations* **32**(4), 43-57

Sture, S., Costes, N.C., Batiste, S.N., Lankton, M.R., AlShibli, K.A., Jeremic, B., Swanson, R.A. & Frank, M. (1998). "Mechanics of granular materials at low effective stresses" *ASCE Journal of Aerospace Engineering* **11**(3), 67-72.

Tanner, D.W. (1960). "Further work on the relationship between the rake angle and the performance of simple cultivation implements" *Journal of Agricultural Engineering Research* **5,** 307-315

Terzaghi, K., Peck, R.B. & Mesri, G. (1996). *Soil mechanics in engineering practice*. John Wiley & Sons, Inc

Tong, J. & Moayad, B. Z. (2006). "Effects of rake angle of chisel plough on soil cutting factors and power requirements: A computer simulation," *Soil and Tillage Research* **88**, 55-64

Tufenkjian, M.R. & Thompson, D., (2005). (b), "Friction Angle of Sand from Minicone Soundings at Shallow Depth," *Proceedings of Oceans 2005 MTS/IEEE*, September 18-23, Washington D.C.

Van Leussen, W. & Nieuwenhuis, J.D. (1984). "Soil mechanics aspects of dredging" *Geotechnique* **34**(3), 359-381

Van Os, A.G. & Van Leussen, W. (1987). "Basic Research on Cutting Forces in Saturated Sand" *ASCE Journal of Geotechnical Engineering* **113**(12), 1501-1517

Vardoulakis, I., Graf, B. & Gudehus, G. (1981). "Trap-door problem with dry sand: A statical approach based upon model test kinematics" *International journal for numerical and analytical methods in geomechanics.* **5**, 57-78

Vesic, A.S. & Clough, G.W. (1968). "Behaviour of granular materials under high stresses" ASCE, Journal of the soil mechanics and foundations division **94**(3) 661-687

Villalobos, F. (2007). "Installation of suction caissons in sand" VI Congreso chileno de geotecnia. http://web2.ucsc.cl/~avillalobos/articulos/Valparaiso1.pdf

White, D.J. (2002). “An investigation into the behaviour of pressed-in piles” Ph. D Thesis, University of Cambridge

White, D.J. & Cathie, D.N. (2010). “Geotechnics for subsea pipelines”, *2nd International Symposium on Frontiers in Offshore Geotechnics (ISFOG)*, Perth, November.

White, D.J., Take, W.A. & Bolton, M.D. (2003) “Soil deformation measurement using particle image velocimetry (PIV) and photogrammetry” *Geotechnique* **53**(7), 619-631

Whitlow, R. (2001). *Basic Soil Mechanics*. Pearson Education Limited. London.

Wood, D.M. (2002). “Some observations of volumetric instabilities in soils” *International Journal of Solids and Structures* **39**, 3429-3449.

Wood, D.M. (2005). Geotechnical modelling. Spon Press, Oxfordshire

http://tugster.wordpress.com/

www.ag.ndsu.nodak.edu

www.tricomarine.com

APPENDIX A Full list of C_s values derived from ploughing tests at 50th scale

HST50	D_r = 25%						
C_s	Passive force, N	velocity, m/h	trench depth, mm	plough depth, mm	tow force N	pitch, ^{o}	forecutter
13.4	14.0	51.4	35.4	40.7	22.2	-1.5	yes
14.5	13.6	48.1	35.8	39.3	21.7	-1.4	yes
14.3	8.7	50.8	33.9	34.0	16.9	-0.9	yes
16.0	6.9	48.2	30.8	30.4	15.1	-0.5	yes
13.6	5.6	50.6	28.9	29.8	13.7	-0.7	yes
14.1	5.6	53.9	28.4	29.5	13.8	-0.4	yes
13.3	3.7	53.7	25.9	26.3	11.9	0.1	yes
12.5	1.8	54.9	20.2	21.0	10.0	-0.2	yes
19.7	1.8	60.5	18.2	17.9	9.9	-0.4	yes
13.9							

11.2	12.8	38.1	35.2	42.0	21.0	-1.0	no
12.5	7.9	48.6	33.6	34.5	16.1	-0.7	no
12.2	6.5	51.0	32.2	32.5	14.7	-0.3	no
12.2	5.4	53.4	30.8	30.6	13.6	-0.4	no
13.2	4.5	54.3	26.6	28.0	12.6	-0.3	no
13.7	4.2	57.0	26.8	27.0	12.3	0.2	no
14.3	1.3	61.1	18.8	18.2	9.5	-0.2	no
14.6	1.3	53.3	17.5	17.9	9.5	-0.1	no
13.0							

HST50	D_r = 90%						
C_s	Passive force, N	velocity, m/h	trench depth, mm	plough depth, mm	tow force N	pitch, ^{o}	forecutter
12.8	14.0	48.4	33.7	40.0	22.2	-1.6	no
12.8	9.4	45.0	31.3	35.0	17.6	-1.4	no
13.5	5.4	56.6	27.6	28.6	13.6	-1.1	no
7.2	0.7	55.3	17.5	17.5	8.8	-1.1	no
13.0							

16.6	15.6	46.6	32.7	38.0	23.8	-2.0	yes
15.0	11.5	45.7	32.4	35.5	19.6	-1.3	yes
16.9	5.9	54.3	26.8	27.4	14.1	-1.1	yes
13.5	3.6	50.0	24.1	25.0	11.8	-1.2	yes
10.7	1.6	54.6	20.0	20.6	9.8	-1.2	yes
15.5							

HST95	D_r = 17%						
C_s	Passive force, N	velocity, m/h	trench depth, mm	plough depth, mm	tow force N	pitch, ^{o}	forecutter
19.1	4.9	52.3	22.7	25.8	12.4	-0.5	yes
15.0	5.9	51.7	27.4	29.6	13.3	-0.6	yes
15.3	10.1	51.6	32.1	35.3	17.5	-0.8	yes
13.0	13.4	124.2	33.0	41.0	20.9	-1.2	yes

13.0	12.9	48.7	33.7	40.3	20.3	-1.3	yes
14.1							

17.1	1.8	52.7	18.3	19.1	9.3	0.1	no
16.3	4.2	46.5	24.4	25.7	11.6	-0.4	no
12.4	3.7	51.6	24.7	27.0	11.1	-0.3	no
13.1	5.3	50.9	28.7	30.0	12.8	-0.6	no
13.6	9.3	51.6	31.8	35.7	16.7	-0.9	no
12.2	8.6	52.1	32.1	36.1	16.1	-0.8	no
11.1	11.6	46.6	34.3	41.1	19.1	-1.1	no
11.0	11.7	43.4	34.6	41.4	19.2	-1.1	no
12.2							

HST95	D_r = 75%						
C_s	Passive force, N	velocity, m/h	trench depth, mm	plough depth, mm	tow force N	pitch, °	forecutter
16.9	4.6	52.2	22.7	25.3	12.0	-1.2	yes
15.2	10.0	48.8	31.4	34.0	17.5	-1.3	yes
14.0	14.4	48.2	32.9	39.5	21.8	-1.4	yes
15.4							

15.0	4.3	53.0	25.0	25.7	11.7	-1.2	no
13.4	8.1	47.1	30.7	33.1	15.5	-1.4	no
12.3	11.9	46.3	32.6	38.7	19.4	-1.4	no
13.55264							